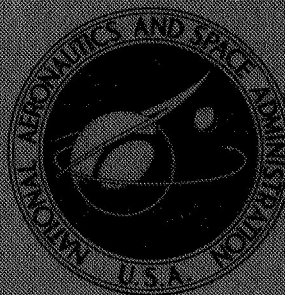


NASA CONTRACTOR REPORT



NASA CR-962

NASA CR-962

GPO PRICE \$ _____

CFSTI PRICE(S) \$ _____

Hard copy (HC) 3.00

Microfiche (MF) .65

ff 653 July 65

FACILITY FORM 602

N 68-18144

(ACCESSION NUMBER)

(THRU)

211
(PAGES)

1
(CODE)

(NASA CR OR TMX OR AD NUMBER)

08
(CATEGORY)

INVESTIGATION OF THE DYNAMIC CHARACTERISTICS OF A V ANTENNA FOR THE RAE SATELLITE

Final Report for Phase A

Prepared by

AVCO CORPORATION

Wilmington, Mass.

for Goddard Space Flight Center

NATIONAL AERONAUTICS AND SPACE ADMINISTRATION • WASHINGTON, D. C. • MARCH 1968

INVESTIGATION OF THE DYNAMIC CHARACTERISTICS
OF A V ANTENNA FOR THE RAE SATELLITE

Final Report for Phase A

Distribution of this report is provided in the interest of information exchange. Responsibility for the contents resides in the author or organization that prepared it.

Issued by Originator as AVCO RAD-TR-65-28

Prepared under Contract No. NAS 5-9179 by
AVCO CORPORATION
Wilmington, Mass.

for Goddard Space Flight Center

NATIONAL AERONAUTICS AND SPACE ADMINISTRATION

For sale by the Clearinghouse for Federal Scientific and Technical Information
Springfield, Virginia 22151 - CFSTI price \$3.00

PRECEDING PAGE BLANK NOT FILMED.

ABSTRACT

This report presents the results of the first phase of an investigation of the dynamic characteristics of the Radio Astronomy Explorer (RAE) satellite equipped with a double-V antenna. During this first phase, computer programs which will provide the analytical tools necessary for continued study of the satellite dynamic performance have been prepared. For this purpose, a flexible-body analog computer program, a rigid-body digital computer program, and a flexible-body digital computer program were developed. The first two programs have been checked out and are fully described and included in this report, together with results of checkout runs. The flexible-body computer program is being checked out; the detailed derivation and description of the simulation is contained in this report. It is recommended that the next phase of the study provide for improvement in the accuracy and capability of the computer simulations and evaluation of satellite and control system dynamics, damping requirements, and overall satellite design.

PRECEDING PAGE BLANK NOT FILMED.

PREFACE

This report is the first of two volumes to be published on the development of formulations and computer simulations to describe the dynamics of the Radio Astronomy Explorer Satellite (RAE). The first volume contains most of the formulation of the study, and descriptions of rigid body digital and flexible-body analog simulations. The second volume will review the formulation and describe a flexible-body digital program and parametric study used to design a libration damper. There are instances where the information contained in the first document will be updated in the second volume, and some of the assumptions in the math formulation will be modified.

The objective of the RAE satellite project is to measure, with modest directivity, the intensity of radio signals from celestial sources as a function of frequency, direction, and time. To achieve this objective, the spacecraft will employ a pair of long "V" antennas back to back; thus forming a large "X" with a central body (core) of instrumentation at the juncture of the antennas. The antennas are tubular structures, which are deployed from the central body once the spacecraft is in a 6000 Km circular orbit. The tubes are about 0.6 inches in diameter and 750 feet long from central body to tip. Gravity-gradient attitude stabilization is to be used so that one set of "V" antennas will always point toward the earth, the other away. The dimensions and material characteristics of the long antennas pose a flexible-body dynamics problem.

The prime purpose of this study was to develop a formulation and computer simulation to accurately describe the dynamic behavior of the RAE spacecraft. This computer simulation was then to be used to study:

- a. The general spacecraft stability
- b. Deployment and capture techniques.

- c. Design parameters for a libration damper
- d. The effect of initial conditions and parameter variations on capture and dynamic behavior.
- e. The flexible nature of the booms

This was the first known development of a flexible-body gravity-gradient dynamics simulation which included thermal bending, solar pressure, occultation and complete three degrees of freedom of motion.

The approach was to develop a system of equations, based on theory and known laboratory results, to describe the motion of the spacecraft and then to program these equations for both analog and digital computer simulation of the dynamics. It was necessary to extrapolate from laboratory data and make several assumptions since "in-orbit" data on boom characteristics are not available. The non-linear nature of the problem does not allow a concise closed form solution; therefore, many approximations are necessary. The assumptions and formulations for the analog and digital simulations were different. For the flexible-body, planar, analog simulation, a series of lumped mass and spring systems was assumed to represent the X antennas. The classical Newtonian type formulation was used. For the flexible-body digital simulation the continuous beam approach was used by expanding the antenna deflections in terms of a set of ortho-normal cantilever beam mode shapes. The formulation used the Lagrangian approach.

Since this was a pioneer effort, it was essential to develop means for evaluating the validity of the assumptions and approximations involved so as to have a high degree of confidence in the resulting computer simulation. This capability of self evaluation was achieved by using the following four techniques:

1. Three separate computer simulations were developed which are capable of checking each other at some specific limit. These simulations are:

- a. Aplanar, flexible-body simulation on the analog computer.
 - b. A three-dimensional, rigid-body simulation on the digital computer.
 - c. A three-dimensional, flexible-body simulation on the digital computer.
2. The computer simulations were developed modularly to allow systematic check-out of each separate function of the program. Thus, it was often possible to check separate functions of a program against known classical results to provide a measure of confidence in the complete simulation.
 3. The complete simulations were checked, where possible, against any known results from independent sources. There are a few specific limiting cases where this check is possible.
 4. The flexible-body digital simulation was further checked for conservation of energy. The system energy was computed at some initial time; the simulation was then allowed to run for several orbits, after which the system energy was again computed and compared to the initial value.

The significant contribution of this study effort is the incorporation of flexible-body effects into the dynamic motions of a gravity-gradient stabilization system. The rigid body dynamics of gravity-gradient have been studied rather extensively; however, little or no analysis was available on flexible-body gravity-gradient dynamics at the time this study was conducted. It is apparent that the flexible nature of the system becomes important when one is considering antenna lengths of 1500 feet with equilibrium tip deflections of about 150 feet. When the effects of solar pressure, thermal bending, orbit eccentricity, and occultation are included in the

formulation, the development of a flexible-body dynamic model is a very complicated and tedious procedure. Consequently, some of the assumptions and approaches made in this first try at the problem are not as accurate as one would like. Present effort is directed toward refining the assumptions to make them less restrictive than those described in this report.

David L. Blanchard
Technical Director
of Contract

CONTENTS

1. Introduction	1
1.1 Objectives of the Study	1
1.2 Method of Approach	1
1.3 Summary of Results	2
1.4 Format of the Report	3
2. Description of the Problem	4
2.1 Mission Objectives	4
2.2 Operational Sequence of Mission	4
2.3 Nominal Satellite Properties	4
2.4 Nominal Antenna Properties	5
2.5 Nominal Orbital Parameters	5
2.6 Initial Conditions Prior to Deployment	5
2.7 Disturbing Influences in the Orbital Environment	5
3. Analog Simulation	7
3.1 Purpose of the Simulation Program	7
3.2 Model Formulation	7
3.3 Analog Simulation	24
4. Rigid-Body Simulation	39
4.1 Introduction	39
4.2 Coordinate Transformation Methods	40
4.3 Error Propagation	43
4.4 Vehicle Ephemeris Generation Techniques	48
4.5 Rigid-Body Moments	49
5. Flexible Body Simulation	51
5.1 Introduction	51
5.2 Derivation of Equations of Motion	52
5.3 Summary of Equations of Motion	86
5.4 Delemination of Constants	92
5.5 List of Symbols	93
6. Control Systems	97
6.1 General Requirements	97
6.2 Candidate Systems	97
6.3 General Properties of Candidate Systems	99
6.4 Mathematical Models	100
6.5 Parameter Selection	106

CONTENTS (Concl'd)

7. Preliminary Results	108
7.1 Preliminary Evaluation of Digital Results	108
7.2 Preliminary Results from Analog Simulation	116
8. Conclusions and Recommendation	124
8.1 Summary of Results	124
8.2 Recommendations for Future Work	125

Appendixes

A. Mathematical Model for Structural Damping	A-1
B. Relative Contributions of Beam Bending Modes to Static Tip Deflection	B-1
C. Rigid Body Digital Computer Program	C-1
D. Tip Deflections of Spiraled Antenna	D-1
E. Linear Equations of Motion for Elementized Cantilever Beam..	E-1
F. Dead Beat Control for the Deployment/Acquisition Phase	F-1

ILLUSTRATIONS

Figure	1	Analog Dynamics Study Coordinate Systems	9
	2	Continuous and Lumped-Mass Boom Models	10
	3	Boom Coordinate Axes	16
	4	Boom Deployment Model	22
	5	Moments Acting on Central Body during Deployment	22
	6	Simulation Block Diagram	25
	7	Boom Bending Simulation	26
	8	Central Body Dynamics (Extended Boom)	28
	9	Mass Element Location Simulation	30
	10	Normal Gravity Gradient Force Simulation	31
	11	Boom Section Switching for Deployment Simulation	32
	12	Acceleration Generator Circuit for Undeployed Boom Section	33
	13	Circuit for Simulating Central Body Dynamics during Deployment	34
	14	Central Body Torque Generator.....	34
	15	Switching Logic for Applying Central Body Moments during Deployment	35
	16	Deployment Excited Oscillation ($\dot{r} = 1$ ft/sec)	38
	17	Error Angle versus Number of Integration Steps	45
	18	Error Angle versus Number of Revolutions	46
	19	Error Angle versus Number of Revolutions	47
	20	Reference Coordinate System	53
	21	Geometry of Deployment Mechanism	66

ILLUSTRATIONS (Cont'd)

Figure 22	Geometry of Antennas	67
23	Antenna Deflections	69
24	Candidate Damper Boom Configuration for Three - Axis Control.....	101
25	Schematic of Magnetic Hysteresis Damper	103
26	Schematic of Planar Two-Body Model	104
27	Hysteresis Damper Characteristics (Magnetic Torques Only)	107
28	Comparison of Analytical and Digital Results for Planar Libration Period (Normalized)	111
29	Period of Planar Libration versus Oscillation Amplitude...	112
30	Plot of Pitch Oscillation versus Time	113
31	Angle between Satellite Pitch Axis and the Normal to the Orbital Plane (Deg).....	114
32	Angle between Satellite Pitch Axis and the Normal to the Orbital Plane (Deg).....	115
33	Planar Pitch Oscillation Forced by Orbital Eccentricity ...	117
34	Planar Pitch Oscillation Forced by Orbital Eccentricity ...	118
C-1	Flow Chart of 1048 Program.....	C-2
C-2	Flow Diagram of ETD.....	C-6
C-3	Flow Diagram of Convin	C-9
C-4	Flow Chart of Exec	C-12
C-5	Flow Chart of Subs	C-14
D-1	Beam Cross Section	D-1

ILLUSTRATIONS (Concl'd)

Figure	D-2	Effect of Spiraling on Out-of-Plane Tip Deflections	D-5
	E-1	Natural Mode Shapes for Eight-Section, Lumped-Mass Cantilever Beam Simulation	E-7
	E-2	Comparison of Actual and Simulated Mode Shapes for First and Second Modes	E-8
	E-3	Comparison of Actual and Simulated Mode Shapes for Third and Fifth Modes	E-9
	F-1	Analog Simulation of Rigid Body Antenna Deployment ..	F-4
	F-2	Analog Simulation of Dead-Beat Antenna Deployment...	F-5

1. INTRODUCTION

- 1.1 OBJECTIVES OF THE STUDY. -- The primary objective of Phase A of the RAE dynamics study is the development of a suitable system of equations and both analog and digital computer programs for the dynamics analysis of a RAE satellite of the general double-V antenna configuration. Capability will be provided for (a) the inclusion of all significant disturbing influences in the orbital environment, (b) parametric studies of satellite design characteristics and orbital parameters, (c) the investigation of long-term satellite stability, and (d) the evaluation of damping and control system requirements and performance.

Secondary objectives of Phase A are the use of these equations and computer programs to perform preliminary evaluations of satellite and control system dynamics over a limited range of conditions during the deployment/acquisition and mission phases of satellite operation.

- 1.2 METHOD OF APPROACH -- The general approach of the study has been to provide (through three separate computer programs) a capability for analyzing and determining the significance of individual aspects of the dynamics problem, as well as a means for comparing results and evaluating the validity of pertinent assumptions and approximations involved in the respective simulations. The three programs, described briefly here and extensively in later sections of this report, are a flexible-body analog program, a rigid-body digital program, and a flexible-body digital program.

- 1.2.1 Analog Computer Program. -- The basic objectives of the analog simulation of the flexible satellite are to investigate planar dynamics in the gravity-gradient field, and to evaluate the effectiveness of various deployment techniques and the performance of proposed control system models. The analog simulation is specifically adaptable to monitoring of a continuous output to provide a visual display of the satellite in operation. System performance and the effects of parameter changes are readily observed and quickly evaluated.

- 1.2.2 Rigid-Body Digital Computer Program. -- The purpose of the rigid-body digital simulation is basically to provide checks for the flexible-body analog and digital programs, and a means for evaluating, through comparison of results, the effects of flexibility on deployment techniques, control system performance, and long-term stability. In addition, the rigid-body program provides the capability for determining the effects of three-dimensional inertial coupling and non-Keplerian orbital perturbations, independent of the dynamics associated with flexibility. Quite apart from the dynamics analysis itself, the rigid-body program is employed in the evaluation of numerical techniques

applicable to both digital programs, in particular, the comparison of various integration routines for three-degree-of-freedom rotational dynamics on the basis of computational speed and accuracy.

1.2.3 Flexible-Body Digital Computer Program. -- The flexible-body digital computer program furnishes a complete and accurate simulation of three-dimensional, flexible-body dynamics in the orbital environment. It provides the capability for analyzing, either combined or separately, the effects on deployment, acquisition, and long-term stability of the following: antenna flexibility, three-dimensional inertial coupling, all significant disturbances of the orbital environment, inherent damping within the satellite, the performance of control systems and additional damping devices, initial conditions and errors in orbital injection and in vehicle attitude and attitude-rate, and parametric changes in vehicle design variables and orbital elements. The program also allows evaluation of the relative importance of higher bending modes for the flexible antennas, and of bending moments at the antenna roots.

1.3 SUMMARY OF RESULTS. -- Results of Phase A of the RAE dynamics study are described here briefly; more extensive descriptions are contained in later sections dealing with details of the computer programs and derivations of the dynamical equations.

1.3.1 Analog Program. -- The analog simulation of the flexible body has been programmed for planar motion of the satellite in a circular orbit. Two beams, each representing a symmetric pair of diametrically opposite antennas, are simulated by eight-element, lumped-parameter models. Deployment is simulated by a switching technique that switches in successive mass elements as they are extended from the central hub of the satellite. A simple control system is represented by torquing at the central hub. A visual display has been developed to permit continuous observation of the entire satellite, as well as to locate its position in orbit. Check cases have been run to measure static tip deflections due to gravity gradient, and fundamental oscillatory modes and frequencies of the satellite as a whole. Thermal bending and solar pressure are not included in the simulation.

1.3.2 Rigid-Body Digital Program. -- The digital simulation of the rigid body has been programmed for full three-dimensional motion of the satellite with either an analytic (Keplerian) orbital ephemeris or a more exact N-body ephemeris including the effect of Earth oblateness. The program calculates the direction of the sun-line and the visible fraction of the solar disc during occultation. Either direction cosines or quaternions may be used in the integration routine for rotational dynamics, though quaternions have been demonstrated somewhat superior on the basis of computational speed and accuracy. Check

cases have been run for the frequencies and amplitudes of planar libration, and for the inertial coupling of non-planar dynamics.

1.3.3 Flexible-Body Digital Program. -- The digital simulation of the flexible body has been programmed for full three-dimensional motion of the satellite relative to its center of mass in a Keplerian orbit. Deflections of each antenna in two perpendicular planes relative to its undeformed axis are described by series expansions in terms of the small-deflection mode shapes. Gravity-gradient forces and the effects of thermal bending, solar pressure, and axial tension are evaluated for the deformed configuration to first order in the modal coefficients of the series expansions. The location of the sun-line relative to the orbital plane is calculated using an analytic expression for regression of the line of nodes; the visible fraction of the solar disc is determined during occultation. Check cases for the program are being run during the debugging process. Additional terms describing the dynamics of deployment have been derived but are not included in the program for Phase A.

1.3.4 Damper System Studies. -- A review of currently available and proposed damping techniques applicable to gravity-gradient stabilized satellites has indicated a passive magnetic hysteresis damper to be desirable for investigation in conjunction with the RAE design. This damper, basically a TRW Systems concept, involves the addition of an auxiliary pair of opposed booms skewed to the satellite antenna plane and fixed within the central body so as to allow one relative rotary degree of freedom. Relative motion is constrained by a torsion wire and damped by magnetic hysteresis. The skewed two-body system provides damping about all three satellite axes through inertial cross-coupling. Advantages of the system are mechanical simplicity, reliability, and relatively high damping capability and low steady-state attitude errors compared to other damper concepts. This system has been incorporated in the rigid-body digital computer program.

1.4 FORMAT OF THE REPORT. -- A brief description of the satellite, the antennas, the mission, and other pertinent data is contained in section 2. The next three sections provide a detailed description of the three computer simulations; the analog computer simulation, rigid-body digital computer program, and flexible-body digital computer program are described respectively in sections 3, 4, and 5. Section 6 gives a discussion of control system concepts and describes the control system which has been programmed for the computer. Section 7 contains results of checkout runs and typical cases from the computer programs. Section 8 presents conclusions and recommendations for future work. The appendixes contain detailed analyses to support various aspects of the work and to justify the methods of approach. The complete description of the rigid body digital computer program is also given as appendix C.

2. DESCRIPTION OF THE PROBLEM

- 2.1 MISSION OBJECTIVES. -- The basic mission objective of the RAE satellite is to measure both the power spectral density and the location on the celestial sphere of extraterrestrial radio signals over the range of frequencies from 0.3 to 7 mc. To permit quantization and separation of outer space signals from Earth-generated signals, the satellite employs a double-V antenna configuration with suitable radiometers and switching circuitry, providing simultaneous and separate signal reception from celestial and terrestrial sources. In addition, the double-V configuration is ideally suited to gravity-gradient attitude stabilization. The variation of antenna gain pattern with antenna deflection, and of effective antenna boresight with both antenna deflection and vehicle attitude, constitutes a critical and direct dependence of the radiometric mission upon satellite dynamics.
- 2.2 OPERATIONAL SEQUENCE OF MISSION. -- The RAE satellite after boost and injection into orbit is separated from the final rocket stage and despun by "yo-yo" despin devices. The satellite is then oriented with respect to the local vertical by active control prior to deployment of the primary antennas. Deployment is effected in such a fashion as to permit capture of the satellite by the gravity-gradient field; this operation is denoted the deployment/acquisition phase and is discussed in more detail later in this report. Finally, the so-called mission phase involves damping of satellite motion to a steady-state orientation aligned in the orbital plane along the local vertical; measurements of power spectral density and direction of radio signals are performed from this orientation. Precession of the orbital line of nodes in inertial space, a function of orbital altitude, inclination, and direction, permits coverage of a calculable percentage of the celestial sphere during the useful operational lifetime of the satellite.
- 2.3 NOMINAL SATELLITE PROPERTIES. -- The relatively long wavelengths of interest -- 40 to 1000 meters -- require correspondingly long antenna lengths; the nominal length of each antenna rod is 750 feet. The vertex angle of each antenna V is a design variable influenced by desirable antenna directivity, satellite attitude stability, and permissible static deflections of the antenna tips due to gravity gradient; the nominal angle is 60 degrees. Two dipole antennas of nominal length 75 feet are located perpendicular to the plane of the four primary antennas. (These cross-orbit dipoles are not included in the Phase A dynamics simulation of the RAE.) The total weight of the satellite is 326-1/4 pounds, the central hub being 36 inches in diameter. The moments of inertia of the satellite with undeployed antennas are 14.50 slug-ft.² about the yaw axis, 13.37 slug-ft.² about the pitch axis, and 11.03 slug-ft.² about the roll axis; after deployment of the four primary antennas, these inertias increase, respectively, to 67,750 slug-ft.², 271,000 slug-ft.², and 203,250 slug-ft.² for the undeformed configuration. The nominal antenna deployment rate is 0.5 ft/sec.

- 2.4 NOMINAL ANTENNA PROPERTIES. -- Both the four primary and two cross-orbit antennas are overlapped deHavilland tubes of alloy 125 gold flash on beryllium-copper. The tubes have a tape width of 2.0 inches and a thickness of 0.002 inches of BeCu coated with 0.0002 inch of silver. The tube overlap at the seam is 81 degrees, resulting in a tube diameter of 0.52 inch. The mass per unit length of the tube is 0.482×10^{-3} slug/ft. (0.0155 lb/ft.), and the average cross-sectional inertia, based on a spiraled antenna, is 105×10^{-6} in.⁴ Young's modulus for BeCu is 19×10^6 lb/in.² Structural damping is nominally 0.00366 of critical, corresponding to a log decrement of 0.023 per cycle. Tube thermal properties are as follows: specific heat 0.10 Btu/lb-°F; coefficient of thermal expansion $9.4 \times 10^{-6}/°F$; thermal conductivity 65 Btu/hr-ft-°F for alloy 125, and 230 Btu/hr-ft-°F for silver. Absorptivity of the external silver is 0.10, and emissivity is 0.035 for the silver and 0.87 for the internal black paint.
- 2.5 NOMINAL ORBITAL PARAMETERS. -- The nominal orbit for the RAE is a circular orbit of 6000 km. altitude and 50-degree inclination. The 1σ value for orbital eccentricity due to injection errors is 0.02. Direction of travel in the orbit is prograde, and regression of the line of nodes in inertial space is 0.6344 deg/day about the Earth's polar axis. The orbital period is 228.4 minutes. The maximum time between periods of solar occultation by the Earth is 77 days. The nominal launch date to provide this maximum time outside the Earth's shadow is 54 days after the vernal or autumnal equinox, e.g., May 15, 1967; the corresponding longitude of the ascending node at launch is 207.46 degrees, measured in the equatorial plane of the Earth from the first point of Aries, γ .
- 2.6 INITIAL CONDITIONS PRIOR TO DEPLOYMENT. -- The nominal satellite attitude relative to the local vertical just prior to deployment of the primary antennas is as follows: pitch 0 ± 2 degrees (1σ), roll 15 ± 2 degrees (1σ), and yaw unspecified. The initial angular rates relative to the local vertical are 0 ± 0.1 rpm (1σ), about each axis.
- 2.7 DISTURBING INFLUENCES IN THE ORBITAL ENVIRONMENT. -- The primary agent acting to cause static deflections of the satellite antennas is the gravity-gradient force. In addition, the gravity gradient produces a torque causing three-dimensional oscillations when the satellite is displaced arbitrarily from its stable attitude aligned with the local vertical in the orbital plane. Further disturbances causing dynamic bending of the antennas and overall satellite oscillation about the local vertical are orbital eccentricity, thermal temperature gradient across the antenna cross-sections, and solar pressure, each of which represents a forcing function of fundamental period equal to the orbital period. Coupling of the dynamics associated with these forcing functions occurs because of their dependence upon satellite attitude and geometric shape as well as upon orbital position. Higher frequency excitation is also caused by non-spherical nature of the Earth's gravitational field. Occultation of the sun during passage through

the Earth's shadow presents a serious problem designated as "solar shock. " The sudden switching off and subsequent switching on of thermal bending and solar pressure excites transient bending modes of the antennas which may add constructively during successive occultations; structural damping is not expected to provide significant transient decay during one orbit.

Disturbances that are not considered to be of primary importance, and are therefore neglected in Phase A of the dynamics study, are those due to interaction of the satellite charge distribution and residual magnetic moment with the Earth's magnetic field.

3. ANALOG SIMULATION

- 3.1 PURPOSE OF THE SIMULATION PROGRAM. -- The purpose of the analog dynamics simulation of the NASA-Goddard Radio Astronomy Explorer satellite is to evaluate deployment schemes and to study the acquisition phase of the mission under the assumption of flexible booms. These problems have been considered in the past for rigid booms, but little effort has been expended on the flexible-boom problem.

The deployment techniques which will be evaluated using the analog dynamics simulation will be primarily dead-beat control schemes in which antenna deployment rate is modulated such that the error in the final attitude and energy state at the time the booms are completely extended is minimized. A study of this technique with the rigid boom assumption has been made and is reported in appendix F.

Oscillations present after deployment will be reduced by internal damping in the booms and by a central body damping system which may be either active or passive. The effect of the internal damping will be evaluated. Models of several central body damping systems will be simulated so that parameters of these systems can be, in some sense, optimized.

3.2 MODEL FORMULATION.

- 3.2.1 Assumptions. -- A suitable model of the satellite must be detailed and accurate enough to perform acceptable studies of the deployment and acquisition phases, yet must be compatible with the capacity and capability of the analog computation facility. Consequently, several assumptions have been made to reduce the size of the required simulation without excessively compromising its usefulness. These assumptions reduce the problem to the planar case in which symmetry exists with respect to the central body such that diametrically opposite booms have the same shape, and only two booms need be simulated. Without these conditions a useful analog simulation would be impossible with the analog facility available. The assumptions made are:

- a. Only the planar case in which the plane of the booms coincides with the orbital plane is considered.
- b. The only significant external force acting on the external booms is the gravity-gradient force. Radiation pressure and thermal bending have been neglected.
- c. The orbit is circular.
- d. Initial conditions on opposing booms are symmetrical with respect to the central body.

Assumptions 2, 3, and 4 are necessary for symmetry to exist in the diametrically opposite booms.

Recent results indicate that a very short time constant is associated with the establishment of a thermal gradient, so that thermal bending will have some effect during the deployment/acquisition phase of the mission.

- 3.2.2 Coordinates. -- Let the x and z axes be the local horizontal and local vertical axes passing through the center of the satellite as shown in figure 1. These axes are contained in the plane of the orbit. Since the orbit is circular, these axes rotate with respect to inertial space at the constant orbital rate Ω . The rotation angle at any time is given by the angle γ .

The orientation of the central body is defined with respect to the local axes by the angle ϕ which is the angle between the z-axis and the center line of the satellite. The angle α defines the undeflected positions of the booms as shown. In general, the booms are given as displacements from these undeflected axes. To allow larger deflections in the model than would be possible with a single baseline, it has been convenient to define a secondary baseline from which the displacements of the outer section of the boom are measured.

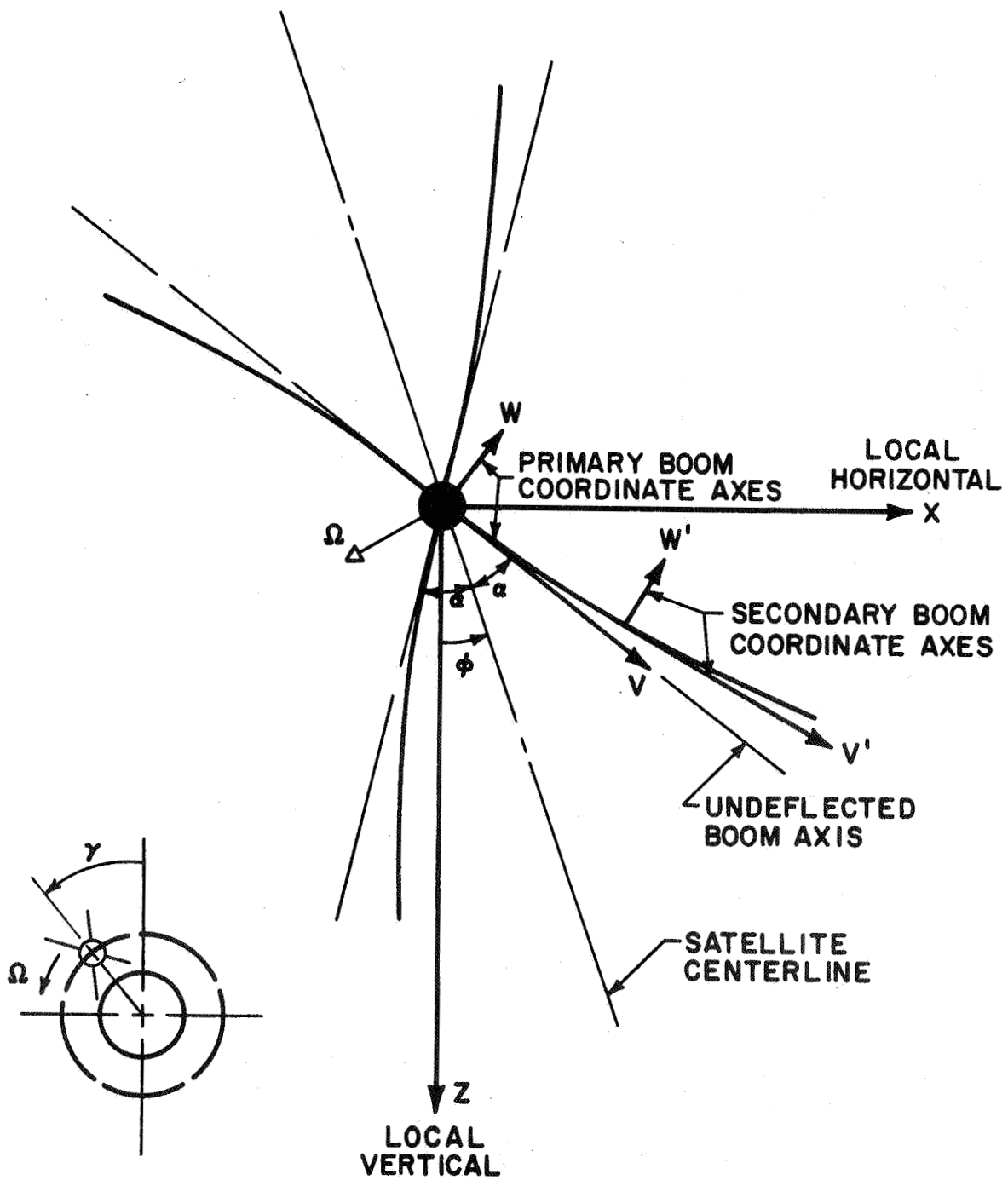
The boom coordinate axes using the two baselines are also shown in figure 1. The V-W axes are fixed to the central body and describe the deflection of the section of the boom nearest the central body. The V-axis is taken in the direction of the undeflected boom. The deflection of the outer section of the boom is defined by the V'-W' axes. The origin of these axes is fixed to the end of the inner boom section and the V' axis is taken tangent to the boom at this origin.

3.2.3 Formulation of the Boom Dynamics Equation

- 3.2.3.1 Approximate Boom Model. -- The usual mathematical model describing the vibrational dynamics of a continuous beam is shown in figure 2. The internal forces acting upon a deformed element of length dl consist of moments, axial forces, and shear forces. The external forces may be considered to be comprised of inertial forces and externally applied forces. These may be expressed in terms of convenient components.

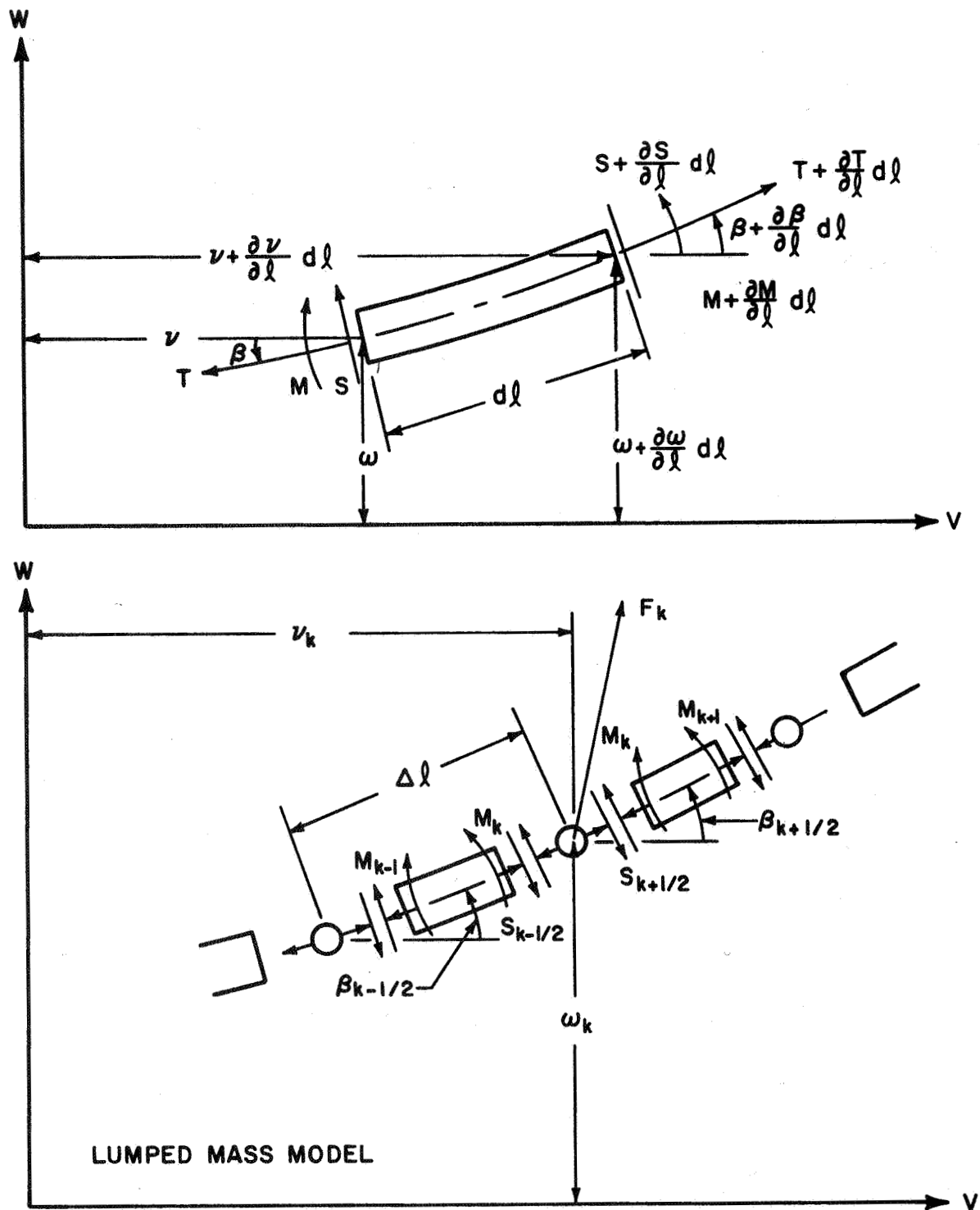
The differential equations of dynamic equilibrium are:

$$\frac{\partial}{\partial l} (T \cos \beta) + \frac{\partial}{\partial l} (S \sin \beta) + F_v(l) - \rho a_v = 0 \quad (3-1)$$



65-12005

Figure 1 ANALOG DYNAMICS STUDY COORDINATE SYSTEMS



65-12002

Figure 2 CONTINUOUS AND LUMPED-MASS BOOM MODELS

$$\frac{\partial}{\partial l} (T \sin \beta) - \frac{\partial}{\partial l} (S \cos \beta) + F_w(l) - \rho a_w = 0 \quad (3-2)$$

where ρ is the mass per unit length of the beam, $F_v(l)$ and $F_w(l)$ are the components of the external forces per unit length acting on the element, and a_v and a_w are the components of the inertial acceleration experienced by the element.

The equation for moment equilibrium neglecting rotary inertia is:

$$\frac{\partial M}{\partial l} - S = 0. \quad (3-3)$$

These equations can be expressed in finite difference form by dividing the continuous beam into segments of length Δl . The following expressions result (see reference 1):

$$\begin{aligned} \frac{1}{\Delta l} [T_{k+1/2} \cos \beta_{k+1/2} - T_{k-1/2} \cos \beta_{k-1/2}] + \frac{1}{\Delta l} [S_{k+1/2} \sin \beta_{k+1/2} - S_{k-1/2} \sin \beta_{k-1/2}] \\ + F_v(l_k) - \rho a_{v_k} = 0 \end{aligned} \quad (3-4)$$

$$\begin{aligned} \frac{1}{\Delta l} [T_{k+1/2} \sin \beta_{k+1/2} - T_{k-1/2} \sin \beta_{k-1/2}] - \frac{1}{\Delta l} [S_{k+1/2} \cos \beta_{k+1/2} - S_{k-1/2} \cos \beta_{k-1/2}] \\ + F_w(l_k) - \rho a_{w_k} = 0 \end{aligned} \quad (3-5)$$

$$\frac{M_{k+1} - M_k}{\Delta l} - S_{k+1/2} = 0 \quad (3-6)$$

The following substitutions can be made after the above equations are multiplied by :

$$m_k = \Delta l \rho \quad (3-7)$$

$$F_{w_k} = \Delta l F_w(l_k) \quad F_{v_k} = \Delta l F_v(l_k) \quad (3-8)$$

¹Witmer, E. A., H. A. Balmer, J. W. Leech, and T. H. Pian, Large Dynamic Deformations of Beams, Rings, Plates, and Shells, AIAA Journal, p. 1848 (1963).

where m_k is an equivalent point mass at the k^{th} station, and F_{v_k} and F_{w_k} are the components of the equivalent external force acting on the k^{th} mass.

The finite difference equations effectively describe the lumped mass model of the beam as shown in figure 2. The beam is assumed to consist of point masses at each station connected by massless bending sections between each station. The external forces act only on the point masses, and all bending occurs at these masses.

Equations (3-4) and (3-5) are now written in terms of components along and normal to the boom at each station. Define the average slope, β_k , and the change in slope, $\Delta\beta_k$, at the k^{th} station as follows:

$$\beta_k \triangleq \frac{1}{2} (\beta_{k+1/2} + \beta_{k-1/2}) \quad (3-9)$$

$$\Delta\beta_k \triangleq \beta_{k+1/2} - \beta_{k-1/2} \quad (3-10)$$

Then the slope of the $k + 1/2$ and $k - 1/2$ sections can be written as follows:

$$\begin{aligned} \beta_{k+1/2} &= \beta_k + \frac{1}{2} \Delta\beta_k \\ \beta_{k-1/2} &= \beta_k - \frac{1}{2} \Delta\beta_k \end{aligned} \quad (3-11)$$

Since $\frac{1}{2} \Delta\beta_k$ is small, we may assume $\cos \frac{1}{2} \Delta\beta_k = 1$ and $\sin \frac{1}{2} \Delta\beta_k = \frac{1}{2} \Delta\beta_k$. The trigonometric functions appearing in equations (3-4) and (3-5) to a good approximation are:

$$\begin{aligned} \cos \beta_{k \pm 1/2} &= \cos \beta_k \mp \frac{1}{2} \Delta\beta_k \sin \beta_k \\ \sin \beta_{k \pm 1/2} &= \sin \beta_k \pm \frac{1}{2} \Delta\beta_k \cos \beta_k \end{aligned} \quad (3-12)$$

Using these approximations, the following expressions can be written from equation (3-4) and (3-5) by multiplying by the appropriate trigonometric functions of β_k and adding the resulting equations:

$$\begin{aligned}
& T_{k+1/2} - T_{k-1/2} + \frac{1}{2} \Delta \beta_k (S_{k+1/2} + S_{k-1/2}) \\
& + F_{v_k} \cos \beta_k + F_{w_k} \sin \beta_k \\
& - m_k (a_{v_k} \cos \beta_k + a_{w_k} \sin \beta_k) = 0
\end{aligned} \tag{3-13}$$

$$\begin{aligned}
& \frac{1}{2} \Delta \beta_k (T_{k+1/2} + T_{k-1/2}) - (S_{k+1/2} - S_{k-1/2}) \\
& + F_{w_k} \cos \beta_k - F_{v_k} \sin \beta_k \\
& - m_k (a_{w_k} \cos \beta_k - a_{v_k} \sin \beta_k) = 0
\end{aligned} \tag{3-14}$$

The two external force terms in each equation (3-13) and (3-14) are the tangential and normal components, respectively, of the external force applied to the k th station:

$$\begin{aligned}
& F_{v_k} \cos \beta_k + F_{w_k} \sin \beta_k \triangleq F_{T_k} \\
& - F_{v_k} \sin \beta_k + F_{w_k} \cos \beta_k \triangleq F_{N_k}
\end{aligned} \tag{3-15}$$

Similarly the acceleration terms are the tangential and normal components of the inertial acceleration of each mass:

$$\begin{aligned}
& a_{v_k} \cos \beta_k + a_{w_k} \sin \beta_k \triangleq a_{T_k} \\
& - a_{v_k} \sin \beta_k + a_{w_k} \cos \beta_k \triangleq a_{N_k}
\end{aligned} \tag{3-16}$$

so that equations (3-13) and (3-14) become:

$$T_{k+1/2} - T_{k-1/2} + \frac{1}{2} \Delta \beta_k (S_{k+1/2} + S_{k-1/2}) + F_{T_k} - m_k a_{T_k} = 0 \tag{3-17}$$

$$\frac{1}{2} \Delta \beta_k (T_{k+1/2} + T_{k-1/2}) - (S_{k+1/2} - S_{k-1/2}) + F_{N_k} - m_k a_{N_k} = 0 \tag{3-18}$$

From equation (3-6) we can write:

$$S_{k+1/2} - S_{k-1/2} = \frac{1}{\Delta l} (M_{k+1} - 2M_k + M_{k-1}). \quad (3-19)$$

The moment at the k^{th} section is proportional to the change in slope, $\Delta\beta_k$:

$$M_k = \frac{EI}{\Delta l} \Delta\beta_k \quad (3-20)$$

Substituting equations (3-19) and (3-20) into (3-18) gives:

$$\begin{aligned} \frac{1}{2} \Delta\beta_k (T_{k+1/2} + T_{k-1/2}) - \frac{EI}{\Delta l^2} (\Delta\beta_{k+1} - 2\Delta\beta_k + \Delta\beta_{k-1}) \\ + F_{N_k} - m_k a_{N_k} = 0 \end{aligned} \quad (3-21)$$

The term in equation (3-21) involving the tension can be neglected if:

$$T_k \ll 2 \frac{EI}{\Delta l^2} \quad (3-22)$$

where T_k is the average tension force at the k^{th} element:

$$T_k = \frac{1}{2} (T_{k+1/2} + T_{k-1/2}). \quad (3-23)$$

The tension force can be evaluated using equation (3-17). However, for simplicity we will compute the maximum tensile force which exists in a straight vertical beam in the gravity gradient field.

The differential tensile force over an element of length dz which is a distance z from the central body is:

$$dT = 3\Omega^2 z \rho dz \quad (3-24)$$

where Ω is the orbital rate. The maximum tensile force then exists at the root and is:

$$T = \int_0^L 3\Omega^2 \rho z dz = \frac{3}{2} \Omega^2 \rho L^2 \quad (3-25)$$

where L is the total length of the boom.

Substituting in the following values:

$$\Omega = 4.58 \times 10^{-4} \text{ sec}^{-1}$$

$$\rho = 4.82 \times 10^{-4} \text{ slug/ft}$$

$$L = 750 \text{ ft}$$

$$EI = 13.85 \text{ lb-ft}^2$$

$$\Delta l = 93.7 \text{ ft}$$

gives

$$T = 8.56 \times 10^{-5} \text{ lb and}$$

$$\frac{2EI}{\Delta l^2} = 3.15 \times 10^{-3} \text{ lb.}$$

Hence by the condition given in equation (3-22), the tensile forces can be neglected in equation (3-21), and it becomes:

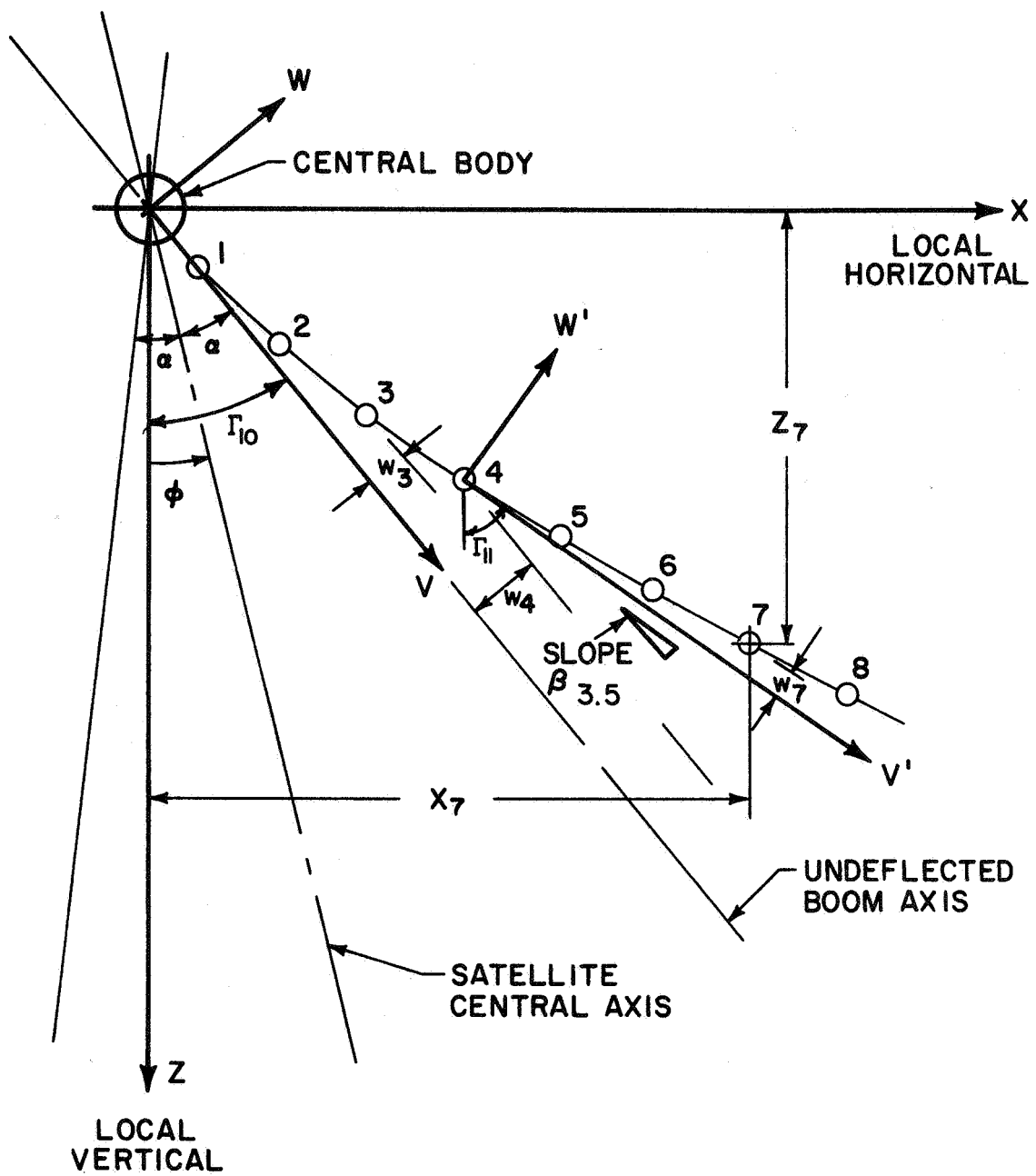
$$F_{N_k} - \frac{EI}{\Delta l^2} (\Delta\beta_{k+1} - 2\Delta\beta_k + \Delta\beta_{k-1}) = m_k a_{N_k} \quad (3-26)$$

The coordinate systems which have been used to define the location of each mass are shown in detail in figure 3. Eight mass elements are used for each boom. The first four are defined with the V-W axes and the outer four with the V'-W' axes. The origin of the V'-W' axes is fixed to the mass element at the fourth station from the central body, and the V' axis has the same slope as the section between stations 3 and 4 as shown.

To simplify the problem so that it can be handled by the analog facility, the normal force component (F_{N_k}) and the shear forces acting on the k^{th} mass are in the direction of the Waxis for elements 1 through 4, and in the direction of the W' axis for elements 5 through 8. The coordinate of each mass element location in the direction of the V or V' axes, as appropriate, is constant for the extended boom so that motion of any mass element is always perpendicular to the corresponding baseline.

The following applies to each baseline. The slope of the $k + \frac{1}{2}$ section is:

$$\beta_{k+\frac{1}{2}} = \frac{1}{\Delta l} (w_{k+1} - w_k) \quad (3-27)$$



65-12003

Figure 3 BOOM COORDINATE AXES

The change in slope at the k^{th} station is:

$$\Delta \beta_k \triangleq \beta_{k+1/2} - \beta_{k-1/2} = \frac{1}{\Delta l} (w_{k+1} - 2w_k + w_{k-1}) . \quad (3-28)$$

Differentiating this twice gives:

$$\Delta l \Delta \ddot{\beta}_k = \ddot{w}_{k+1} - 2\ddot{w}_k + \ddot{w}_{k-1} . \quad (3-29)$$

It remains now only to relate the acceleration with respect to inertial space to the \ddot{w} 's. This is done in the next section.

3.2.3.2 Derivation of Linear Acceleration in Boom Coordinates. --

The analysis of two coordinate systems in simultaneous translation and rotation relative to each other has been treated in reference 2. Consider an inertial coordinate system with its center fixed to the center of the Earth. The center of mass of the satellite is defined by the vector \bar{h} which originates from the center of the Earth. Let \bar{r} be a vector from the satellite center of mass to a mass element on one boom.

The element can also be defined by a location vector \bar{R} from the center of the Earth so that:

$$\bar{R} = \bar{h} + \bar{r} . \quad (3-30)$$

The inertial acceleration of the mass element, $\frac{d^2 \bar{R}}{dt^2}$, can be expressed as follows (reference 2):

$$\frac{d^2 \bar{R}}{dt^2} = \frac{d^2 \bar{r}}{dt^2} + \bar{\omega} \times (\bar{\omega} \times \bar{r}) + 2\bar{\omega} \times \frac{d\bar{r}}{dt} + \frac{d\bar{\omega}}{dt} \times \bar{r} + \frac{d^2 \bar{h}}{dt^2} \quad (3-31)$$

where $\frac{d^*}{dt}$ and $\frac{d^{*2}}{dt^2}$ denote the first and second derivatives with respect to the satellite coordinate system with origin at the center of mass, and $\bar{\omega}$ is the angular velocity of the satellite coordinate system with respect to the Earth-centered inertial frame.

It is convenient to define, in addition, a local, non-rotating coordinate system which has its origin fixed to the center of mass of the satellite and whose axes remain parallel to the Earth-centered inertial axes. In this manner we can consider external forces on each mass element which are due only to the gravity gradient.

²Symon, K. R., Mechanics, Second Edition (Addison-Wesley Publishing Co., Inc., Reading, Massachusetts, 1960) p. 277.

Since we are considering a circular orbit, the vector \bar{h} has a constant magnitude and rotates in the orbital plane at the constant rate $\bar{\Omega}$; hence:

$$\frac{d^2 \bar{h}}{dt^2} = \bar{\Omega} \times (\bar{\Omega} \times \bar{h}) = -|\bar{\Omega}|^2 \bar{h} \quad (3-32)$$

This term is the centripetal acceleration of the mass center, which equals the gravitational acceleration at the mass center in the equation of motion. The term does not appear in the acceleration as expressed in the satellite coordinate frame described above.

Let \bar{a}_k be the "inertial" acceleration of the k th mass element in the local non-rotating frame. Then, from equation (3-31),

$$\bar{a}_k = \frac{d^{*2}}{dt^2} \bar{r}_k - |\bar{\omega}|^2 \bar{r}_k + 2\bar{\omega} \times \frac{d^*}{dt} \bar{r}_k + \frac{d\bar{\omega}}{dt} \times \bar{r}_k \quad (3-33)$$

Referring to figure 3, these equations may be expressed for each baseline. Note that for baseline 0, the component of the acceleration in the direction of W is used; for baseline 1, the component in the direction of W' is used. For convenience, the differential centripetal acceleration due to orbital rate, e.g., $\bar{\Omega} \times (\bar{\Omega} \times \bar{r}_k) = -|\bar{\Omega}|^2 \bar{r}_k$, will be subtracted out from the right hand sides of these equations and reinserted later in the left hand sides as a differential centrifugal force (see section 3.3.2.4). The normal components of the acceleration, now minus the differential centripetal term, are denoted by a_{N_k} .

a. For baseline 0 (V-W axes):

$$|\bar{\omega}| = \dot{\phi} + \Omega \quad (3-34)$$

$$a_{N_k} = \ddot{w}_k - (\dot{\phi}^2 + 2\dot{\phi}\Omega) w_k + 2(\dot{\phi} + \Omega) \dot{v}_k + \ddot{\phi} v_k \quad (k = 1, 2, 3, 4)$$

b. For baseline 1 (V'-W' axes):

Let

$$\bar{r}_k = \bar{r}_4 + \bar{r}_k' \quad (3-35)$$

Then using an operation similar to that defined in equation (3-31):

$$\begin{aligned} \frac{d^{*2} \bar{r}_k}{dt^2} &= \frac{d^{**2}}{dt^2} \bar{r}_k' + \bar{\omega}' \times (\bar{\omega}' \times \bar{r}_k') + 2\bar{\omega}' \times \frac{d^{**}}{dt} \bar{r}_k' \\ &+ \frac{d^* \bar{\omega}'}{dt} \times \bar{r}_k' + \frac{d^{*2}}{dt^2} \bar{r}_4 \end{aligned} \quad (3-36)$$

where the double asterisk denotes differentiation with respect to the V'-W' axes. $\bar{\omega}'$ is the angular rate of the V'-W' coordinate axes with respect to the V-W axes.

Also from reference 2:

$$\frac{d^* \bar{r}_k}{dt} = \frac{d^{**} \bar{r}'}{dt} + \bar{\omega}' \times \bar{r}' + \frac{d^* \bar{r}_4}{dt} \quad (3-37)$$

Substituting (3-36) into (3-37) into (3-33) and noting that $\bar{\omega}' = \dot{\beta}_{3.5}$ gives:

$$\begin{aligned} a_{N_k} = & \ddot{w}_k' + \ddot{w}_4 - [(\dot{\phi} + \Omega + \beta_{3.5})^2 - \Omega^2] w_k' \\ & - (\dot{\phi}^2 + 2\dot{\phi}\Omega)(w_4 - v_4 \sin \beta_{3.5}) \\ & + 2(\dot{\phi} + \Omega + \dot{\beta}_{3.5}) \dot{v}_k' \\ & + 2(\dot{\phi} + \Omega)(\dot{v}_4 - \dot{w}_4 \sin \beta_{3.5}) \\ & + (\ddot{\phi} + \ddot{\beta}_{3.5}) v_k' + \ddot{\phi}(v_4 + w_4 \sin \beta_{3.5}) \\ & (k = 5, 6, 7, 8) \end{aligned} \quad (3-38)$$

where the approximation $\cos \beta_{3.5} = 1$ has been made, and v_k' are the coordinates of the k^{th} mass element with respect to the V'-W' axes.

From equation (3-29):

$$\begin{aligned} \Delta l \Delta \ddot{\beta}_k = & \ddot{w}_{k+1} - 2\ddot{w}_k + \ddot{w}_{k-1} \\ = & [a_{k+1} + (\dot{\phi}^2 + 2\dot{\phi}\Omega) w_{k+1} - 2(\dot{\phi} + \Omega) \dot{v}_{k+1} - \ddot{\phi} v_{k+1}] \\ & - 2[a_k + (\dot{\phi}^2 + 2\dot{\phi}\Omega) w_k - 2(\dot{\phi} + \Omega) \dot{v}_k - \ddot{\phi} v_k] \\ & + [a_{k-1} + (\dot{\phi}^2 + 2\dot{\phi}\Omega) w_{k-1} - 2(\dot{\phi} + \Omega) \dot{v}_{k-1} - \ddot{\phi} v_{k-1}] \\ = & a_{k+1} - 2a_k + a_{k-1} - \ddot{\phi}(v_{k+1} - 2v_k + v_{k-1}) \\ & + (\dot{\phi}^2 + 2\dot{\phi}\Omega)(w_{k+1} - 2w_k + w_{k-1}) \end{aligned}$$

Since we have $v_{k+1} = v_k + \Delta l$, and $v_{k-1} = v_k - \Delta l$, then:

$$v_{k+1} - 2v_k + v_{k-1} = 0$$

and

$$\begin{aligned} \ddot{w}_{k+1} - 2\ddot{w}_k + \ddot{w}_{k-1} &= a_{k+1} - 2a_k + a_{k-1} \\ &+ (\dot{\phi}^2 + 2\dot{\phi}\Omega)(w_{k+1} - 2w_k + w_{k-1}) \end{aligned} \quad (3-39)$$

Similarly for the other baseline, this procedure results in:

$$\begin{aligned} \ddot{w}'_{k+1} - 2\ddot{w}'_k + \ddot{w}'_{k-1} &= a_{k+1} - 2a_k + a_{k-1} \\ &+ [(\dot{\phi} + \Omega + \dot{\beta}_{3.5})^2 - \Omega^2](w'_{k+1} - 2w'_k + w'_{k-1}) \end{aligned} \quad (3-40)$$

In both equations (3-39) and (3-40), the centripetal acceleration terms arising from boom curvature cannot be simulated with the present analog capability and are neglected. Referring back to equations (3-34) and (3-38), one can see that these terms must be small relative to a_{N_k} for the simplification to be valid. a_{N_k} includes the differential gravity and centrifugal accelerations described in section 3.3.2.4, and is usually large compared to the neglected terms. The exceptional cases are those which involve large boom deflections occurring simultaneously with large librations approaching tumbling. For these cases, the analog output parameters may be inspected to determine the relative magnitudes of the neglected terms and the associated degree of inaccuracy. Eliminating the terms in question reduces both equation (3-39) and (3-40) to

$$\ddot{w}_{k+1} - 2\ddot{w}_k + \ddot{w}_{k-1} = a_{k+1} - 2a_k + a_{k-1} \quad (3-41)$$

This equation holds for both baselines.

Equation (3-41) implies that we can obtain the deflection, w_k , from the moving boom coordinate axes using the "inertial" acceleration, a_k , by neglecting the fact that the coordinate system is moving with respect to inertial space at all. In fact, except for the requirement to switch in sections sequentially, the model holds even during deployment of the booms with no modification. However, care must be taken to obtain the correct boom end conditions.

3.2.4 Boom Deployment Model

3.2.4.1 Description of Boom Deployment Scheme. -- For the simulation of deployment, the boom is assumed initially to be extended backward; however, the undeployed portion of the boom is assumed to have no mass and no deflection. The position of all of the elements during deployment is shown in figure 4. Although the undeployed section of the boom has no mass, the acceleration for each position still exists:

$$a'_k = 2(\dot{\phi} + \Omega) \dot{r}_k + \ddot{\phi} r_k \quad (\ddot{w} = 0) \quad (3-42)$$

When this acceleration is integrated, the instantaneous velocity (u_k) with respect to inertial space is obtained for each station along the undeployed boom. During deployment each r_k varies continuously from an initial negative value to its final positive value for the fully extended boom condition.

The following steps are made to introduce each boom section, as it is deployed, into the simulation:

- a. All torques and forces are applied to the section, but deflection is not allowed during the period in which $0 \leq r_k < 3\Delta l/2$
- b. While $0 \leq r_k < 3\Delta l/2$, the mass of the section is added to the central body as an effective increase in moment of inertia.
- c. When a mass reaches $r_k = 3\Delta l/2$, it is allowed to deflect by closing the acceleration loop ($F_{w_k} = m_k a_k$). This allows bending to occur at any mass element that has reached or passed the station $\Delta l/2$.
- d. Simultaneously, the moments acting on the central body from the deploying boom are switched from the section that has reached $r_n = 3\Delta l/2$ to the next one (which has no deflection) at $r_{n-1} = 1/2 \Delta l$.

In following subsections the length of each boom segment will be denoted by l rather than Δl for convenience.

3.2.4.2 Moments Acting on Central Body during Deployment of One Section ($1/2 l < r_n < 3l/2$). -- As shown in figure 5, the equation of motion for the central body if there were only one antenna is:

$$(I_v + m r_n^2) \ddot{\phi} + 2m r_n \dot{r}_n (\dot{\phi} + \Omega) = -M_n + S_{n+1/2} + N_n r_n \quad (3-43)$$

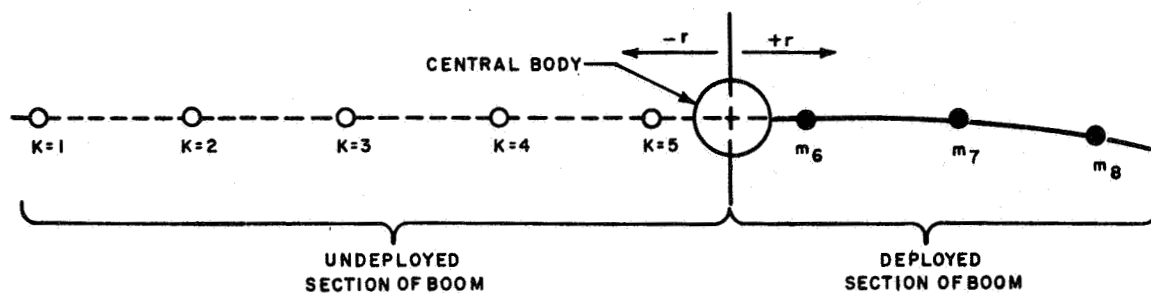
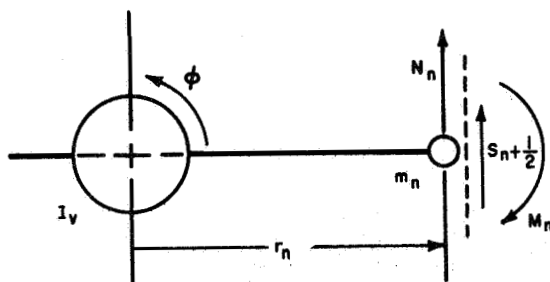


Figure 4 BOOM DEPLOYMENT MODEL



85-0125

Figure 5 MOMENTS ACTING ON CENTRAL BODY DURING DEPLOYMENT

$$\text{but: } S_{n+1/2} = -\frac{1}{l} (M_n - M_{n+1}) \quad (3-44)$$

$$\therefore (I_v + m r_n^2) \ddot{\phi} + 2 m r_n \dot{r} (\dot{\phi} + \Omega) = - \left(1 + \frac{r_n}{l} \right) M_n + \frac{r_n}{l} M_{n+1} + r_n N_n \quad (3-45)$$

For the simulation where two boom pairs are simulated, the equation of motion for the central body is:

$$\begin{aligned} (I_v + 4 m r_n^2) \ddot{\phi} + 8 m r_n \dot{r} (\dot{\phi} + \Omega) = & - 2 (M_{1n} + M_{2n}) \\ & - \frac{2 r_n}{l} (M_{1n} + M_{2n}) \\ & + \frac{2 r_n}{l} (M_{1n+1} + M_{2n+1}) \\ & - 2 r_n (N_{1n} + N_{2n}) \end{aligned} \quad (3-46)$$

3.2.4.3 Boom End Conditions. -- The torques acting on the central body define the deployed boom end conditions at the central body. There still remain end conditions at the free end of the deployed boom and the "free" end of the undeployed boom section. First, the free end of the deployed boom section is defined by the following expression:

$$M_8 = 0 \quad (M_8 = 0) \quad (3-47)$$

For the free end of the undeployed section ($k = 1$) several parameters have to be evaluated. The general boom bending equation states:

$$\ddot{M}_k = \frac{EI}{l^2} (u_{k-1} - 2u_k + u_{k+1}) \quad (3-48)$$

The known values at the end ($k = 1$) are u_1 and u_2 , while u_{k-1} can be expressed as follows:

$$u_{k-1} = \dot{\phi} r_{k-1} + (\dot{\phi} + \Omega t) \dot{r} \quad (3-49)$$

$$\dot{\phi} r_{k-1} = \dot{\phi} (r_k - l) \quad (3-50)$$

Thus:

$$u_{k-1} = u_k - l \dot{\phi}. \quad (3-51)$$

Therefore the end condition for the undeployed boom is defined by:

$$\dot{M}_1 = \frac{EI}{l^2} (u_2 - u_1 - l \dot{\phi}). \quad (3-52)$$

3.3 ANALOG SIMULATION

3.3.1 Simulation Block Diagram. -- A simulation block diagram including the deployment simulation and central body control torque addition is shown in figure 6. The most critical block in the program is the Boom Bending Simulation. This block simulates two booms, each consisting of eight discrete mass elements equally spaced along the length of the boom. The deflections of the masses in each boom are defined with respect to two baselines, one attached to the central body and the other passing through two adjacent masses near the center of the boom. The linear velocity of each mass with respect to the local rotating frame and the boom root torque at the central body junction are computed in this block.

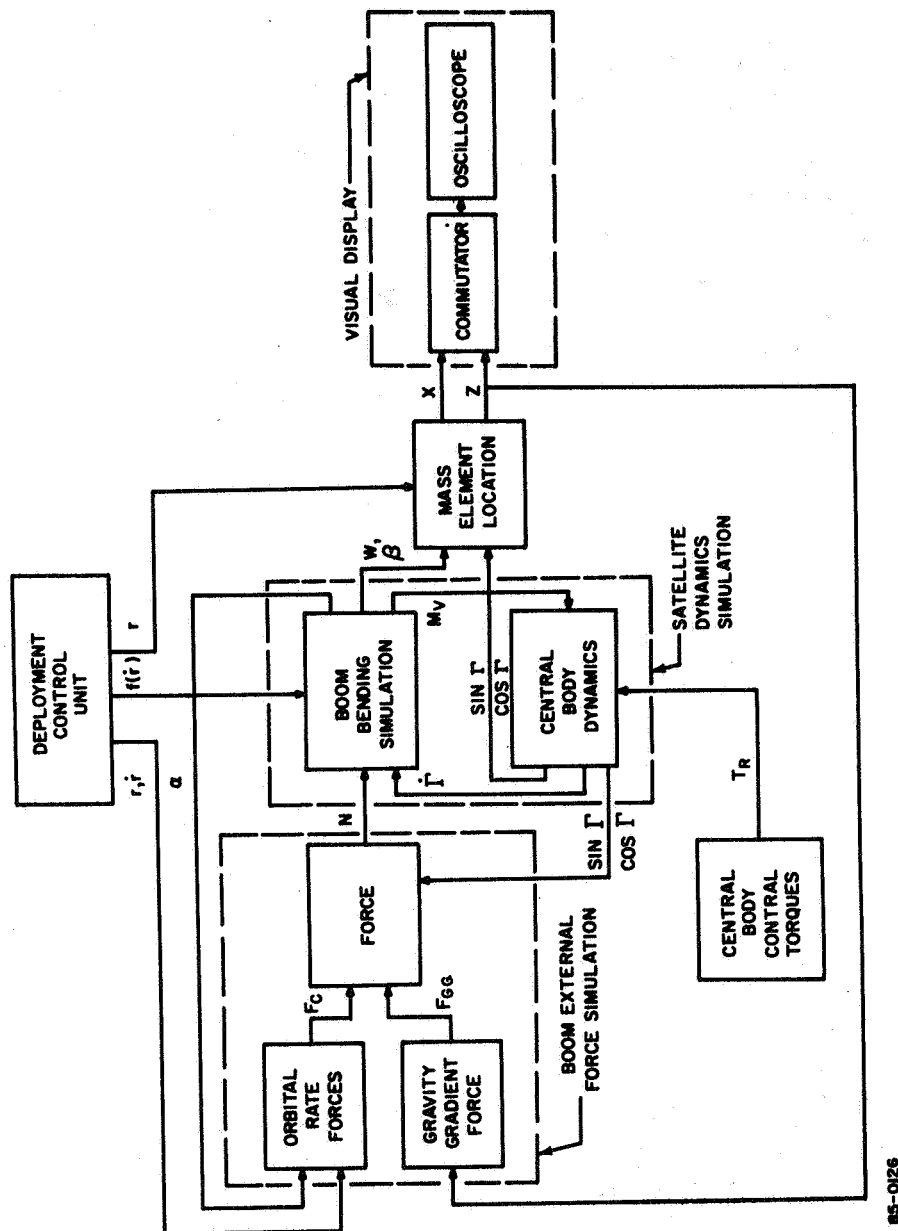
The components of the external forces acting on each mass in the boom normal to the respective baselines are computed in the External Force Simulation block. The attitude of the central body with respect to the local vertical axis is computed in the Central Body Dynamics block. The Mass Element Location block involves a large number of trigonometric computations to locate each mass element in the local rotating (x-z) coordinate system. The gravity gradient force on any mass is proportional to the distance of that mass from the local horizontal axis. Lastly, a Visual Display technique has been developed. Points corresponding to each mass are displayed on an oscilloscope so that a motion picture output of the boom motion can be obtained for both the deployment and the extended boom cases.

3.3.2 Typical Analog Circuits. -- The following pages show typical analog simulation circuits.

3.3.2.1 Boom Bending Simulation. -- An analog circuit for three sections of a boom is shown in figure 7. The equations simulated in figure 7 are:

$$\dot{M}_{18} = 0 \quad (3-53)$$

$$\frac{1}{l} \dot{M}_{17} = \frac{EI}{l^3} (u_{18} - 2u_{17} + u_{16}) \quad (3-54)$$



85-0126

Figure 6 SIMULATION BLOCK DIAGRAM

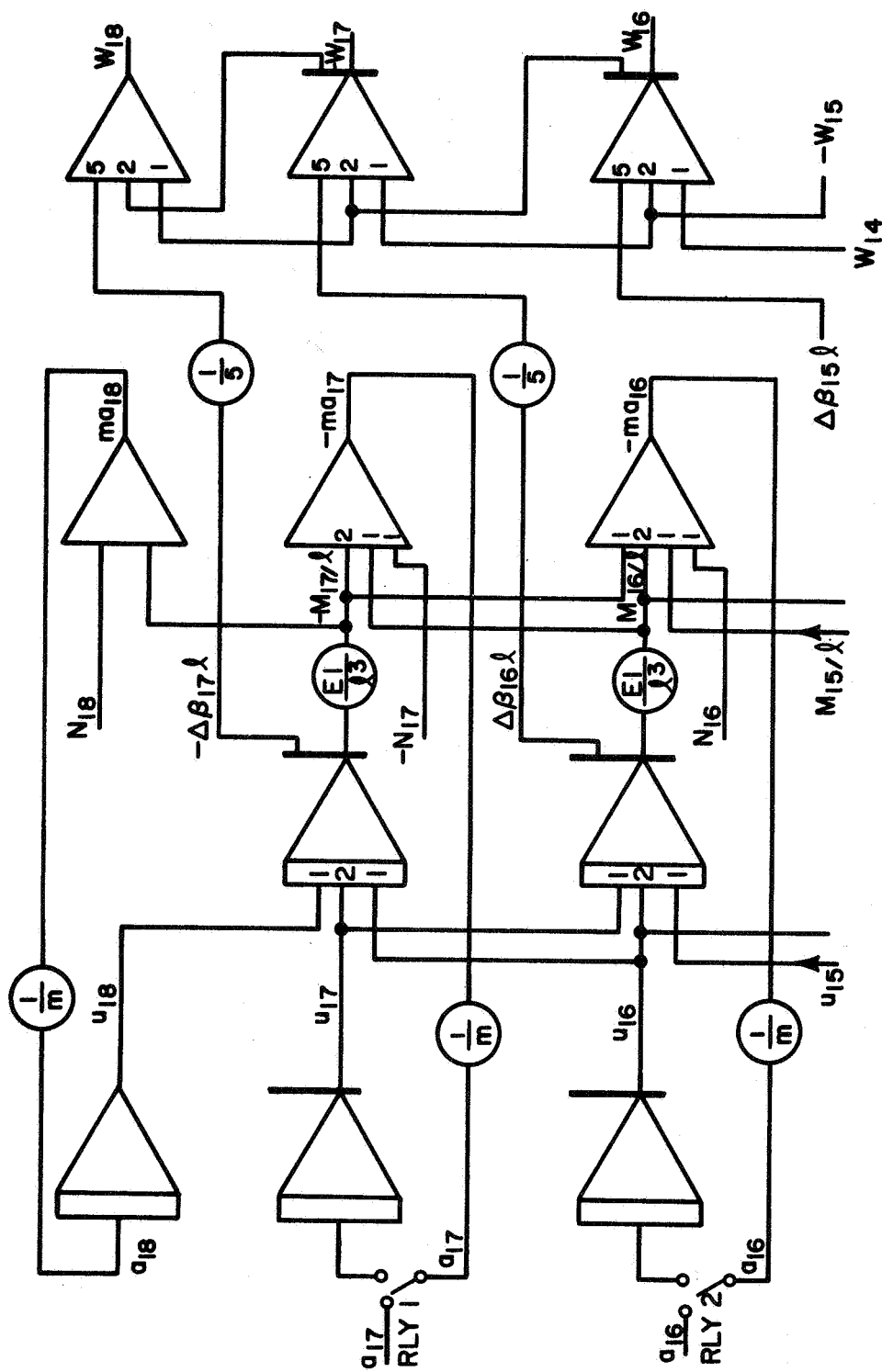


Figure 7 BOOM BENDING SIMULATION

65-12004

$$\frac{1}{l} \dot{M}_{16} = \frac{EI}{l^3} (u_{17} - 2u_{16} + u_{15}) \quad (3-55)$$

$$ma_{18} = \frac{1}{l} M_{17} + N_{18} \quad (3-56)$$

$$ma_{17} = \frac{1}{l} (M_{16} - 2M_{17}) + N_{17} \quad (3-57)$$

$$ma_{16} = \frac{1}{l} (M_{15} - 2M_{16} + M_{17}) + N_{16} \quad (3-58)$$

$$w_{18} = l\Delta\beta_{17} + 2w_{17} - w_{16} \quad (3-59)$$

$$w_{17} = l\Delta\beta_{16} + 2w_{16} - w_{15} \quad (3-60)$$

$$w_{16} = l\Delta\beta_{15} + 2w_{15} - w_{14} \quad (3-61)$$

3.3.2.2 Central Body Dynamics. -- The simulation equations for the extended boom central body dynamics are:

$$M_v = \frac{3}{2} (M_{11} + M_{21}) - \frac{l}{2} (M_{12} + M_{22}) + \frac{l}{2} (N_{11} + N_{21}) \quad (3-62)$$

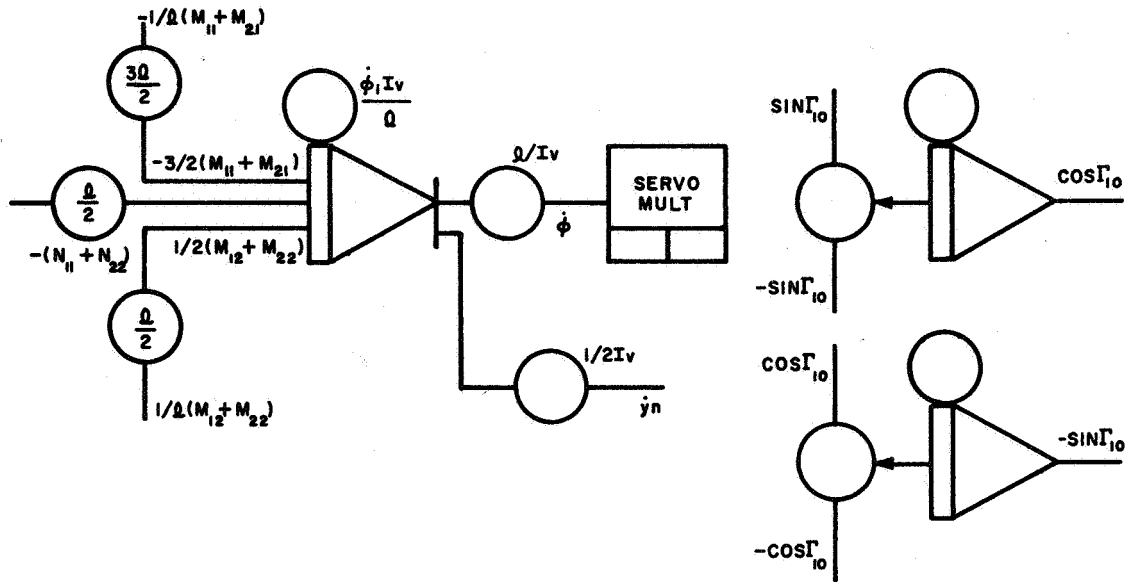
$$\ddot{\phi} I_v = M_v \quad (3-63)$$

$$\sin \Gamma_{10} = \int \dot{\phi} \cos \Gamma_{10} dt \quad (3-64)$$

$$\cos \Gamma_{10} = - \int \dot{\phi} \sin \Gamma_{10} dt \quad (3-65)$$

The corresponding circuit is shown in figure 8.

3.3.2.3 Mass Element Location. -- The location (x_{ik}, z_{ik}) of the i^{th} mass element of the i^{th} boom ($i = 1, 2$), can be written in terms of w , Γ and r . Deflections w_{ik} of the inner four elements ($1 \leq k \leq 4$) are defined relative to a baseline 0 along the undeformed boom axis; deflections w'_{ik} of the outer four elements ($5 \leq k \leq 8$) are defined relative to a baseline 1 tangent to the deformed boom at station $k = 3.5$.



85-0127

Figure 8 CENTRAL BODY DYNAMICS (EXTENDED BOOM)

Baseline 0 ($1 \leq k \leq 4$):

$$x_{ik} = r_k \sin \Gamma_{io} + w_{ik} \cos \Gamma_{io} \quad (3-66)$$

$$z_{ik} = r_k \cos \Gamma_{io} - w_{ik} \sin \Gamma_{io} \quad (3-67)$$

Baseline 1 ($5 \leq k \leq 8$):

$$\begin{aligned} x'_{ik} = & r_k \sin \Gamma_{i1} - r_4 \beta_{13.5} \cos \Gamma_{io} \\ & + w'_{ik} \cos \Gamma_{i1} + w_{i4} \cos \Gamma_{io} \end{aligned} \quad (3-68)$$

$$\begin{aligned} z'_{ik} = & r_k \cos \Gamma_{i1} + r_4 \beta_{13.5} \sin \Gamma_{io} \\ & - w'_{ik} \sin \Gamma_{i1} - w_{i4} \sin \Gamma_{io} \end{aligned} \quad (3-69)$$

where the angle Γ_{i1} is determined from the relations

$$\sin \Gamma_{i1} = \sin \Gamma_{io} + \beta_{i3.5} \cos \Gamma_{io} \quad (3-70)$$

$$\cos \Gamma_{i1} = \cos \Gamma_{io} - \beta_{i3.5} \sin \Gamma_{io} \quad (3-71)$$

and $\beta_{i3.5}$ is the slope of the i^{th} boom just inside (towards the central hub) the $k = 4$ mass element:

$$\beta_{i3.5} = \frac{1}{l} (w_{i4} - w_{i3}) \quad (3-72)$$

A typical circuit is shown in figure 9.

3.3.2.4 Normal Gravity Gradient Force. -- The sum of the differential gravity force and the differential centrifugal force (due to the orbital rates, as discussed in section 3.2.3.2) on the k^{th} mass element can be written as:

$$f_{GG_k} = 3\Omega^2 m_k z_k \quad (3-73)$$

where Ω is the constant angular rate of the circular orbit, and f_{GG_k} is directed parallel to the local vertical. The component of f_{GG_k} normal to the baseline from which deflections of m_k are measured is:

$$N_{GG_k} = - f_{GG_k} \sin \Gamma \quad (3-74)$$

For baseline 0 elements ($1 \leq k \leq 4$):

$$N_{GG_{ik}} = - 3\Omega^2 m_k z_{ik} \sin \Gamma_{io} \quad (3-75)$$

For baseline 1 elements ($5 \leq k \leq 8$):

$$N'_{GG_{ik}} = 3\Omega^2 m'_k z'_{ik} \sin \Gamma_{i1} \quad (3-76)$$

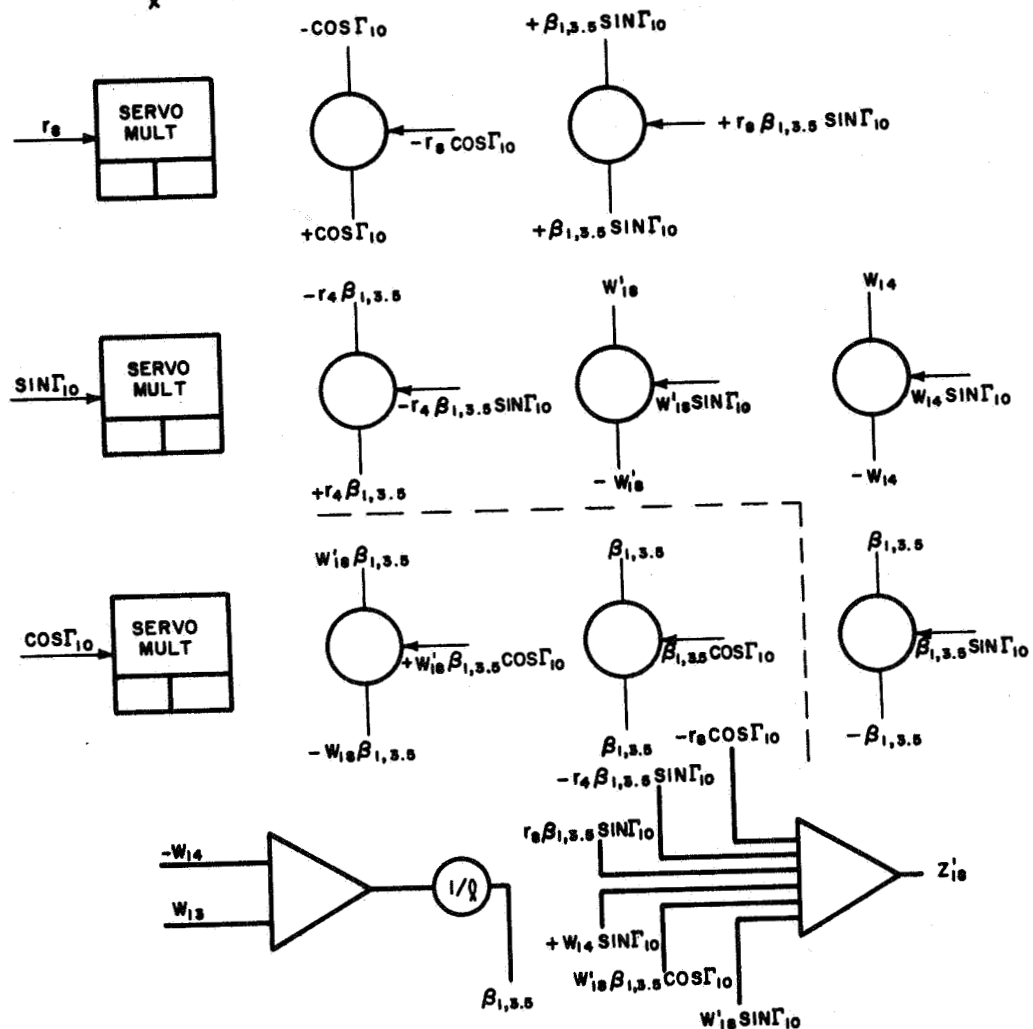
where, again, i is the boom index, 1 or 2.

A typical circuit is shown in figure 10.

SIMULATION EQUATIONS:

$$Z'_{18} = r_8 (\cos \Gamma_{10} - \beta_{1,3,5} \sin \Gamma_{10}) + r_4 \beta_{1,3,5} \sin \Gamma_{10} - w'_{18} (\sin \Gamma_{10} + \beta_{1,3,5} \cos \Gamma_{10}) - w_{14} \sin \Gamma_{10}$$

$$\beta_{1,3,5} = \frac{w_{14} - w_{13}}{q}$$



85-0128

Figure 9 MASS ELEMENT LOCATION SIMULATION

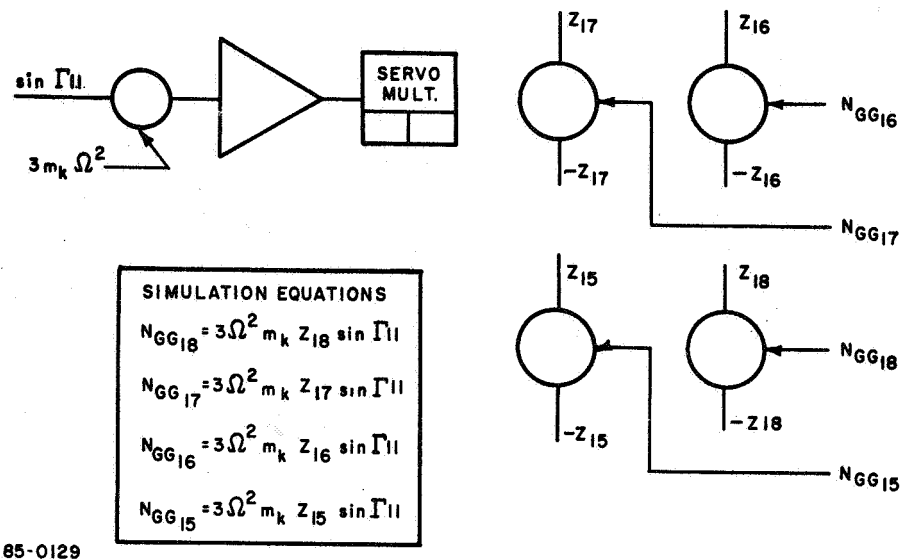
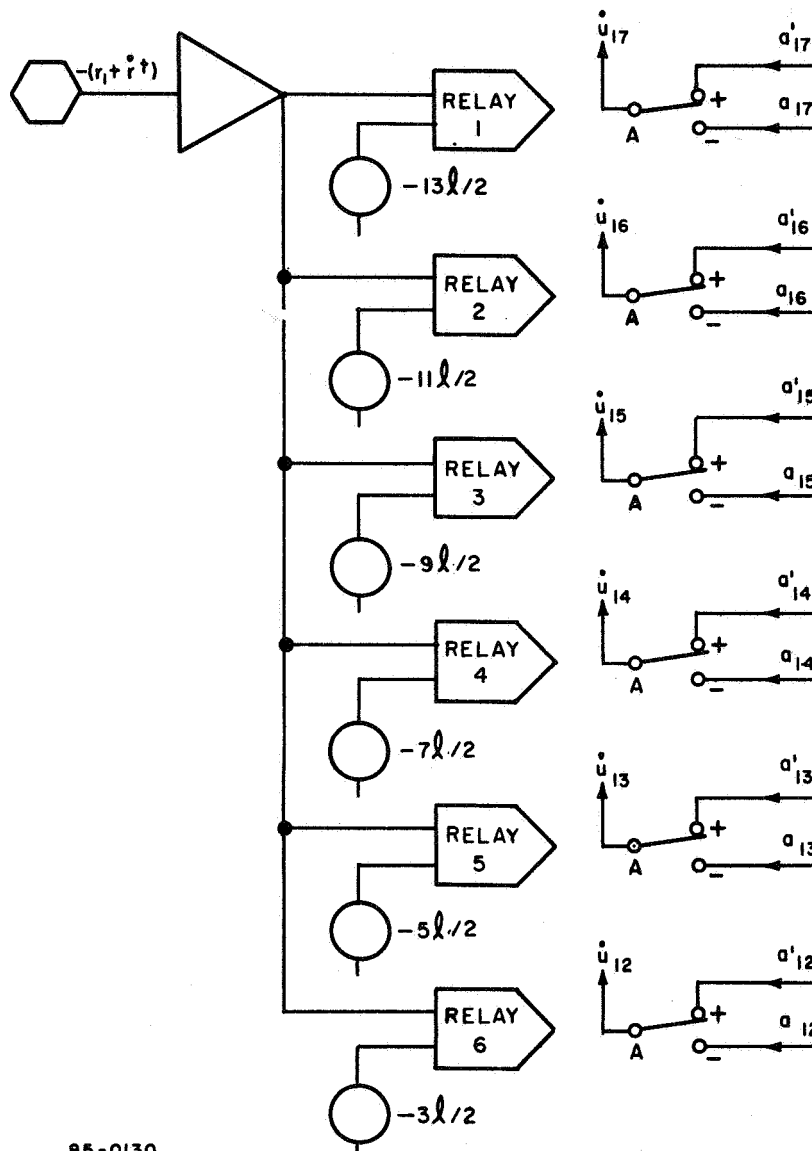


Figure 10 NORMAL GRAVITY GRADIENT FORCE SIMULATION

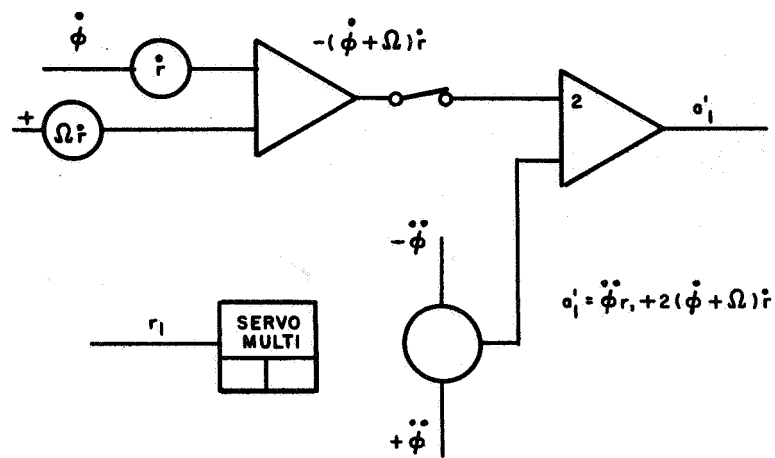
3.3.3 Deployment Simulation. -- The following modifications of the boom simulation are required to accomplish deployment:

- a. The section switching of the boom simulation is accomplished by opening the section loops and adding the acceleration (a') needed before deployment. The pertinent analog circuit is shown in figure 11.
- b. The time-varying r_k term is generated with an integrator which simulates mass element 1 location. At $t = 0$ the integrator locates mass element 1 at $r_1 = -15 l/2$. During deployment the r_1 value changes with i from $-15 l/2$ to $+ l/2$. Other mass element locations are generated from the constant mass element spacing ($r_{k+1} = r_k + l$). The time-varying r_k is used to switch the boom sections with biased operational relays (see figure 15).
- c. Acceleration terms required for sections before deployment must be generated. A typical circuit is shown in figure 12.
- d. The central body dynamics are modified to include a time-varying r_k and to switch the takeoff point for the end moments of the boom from section to section. These end moments are derived and summed for each section and switched into central body dynamics at the appropriate time during which $l/2 \leq r_n < 3l/2$. Typical analog circuits are shown in figures 13, 14 and 15.



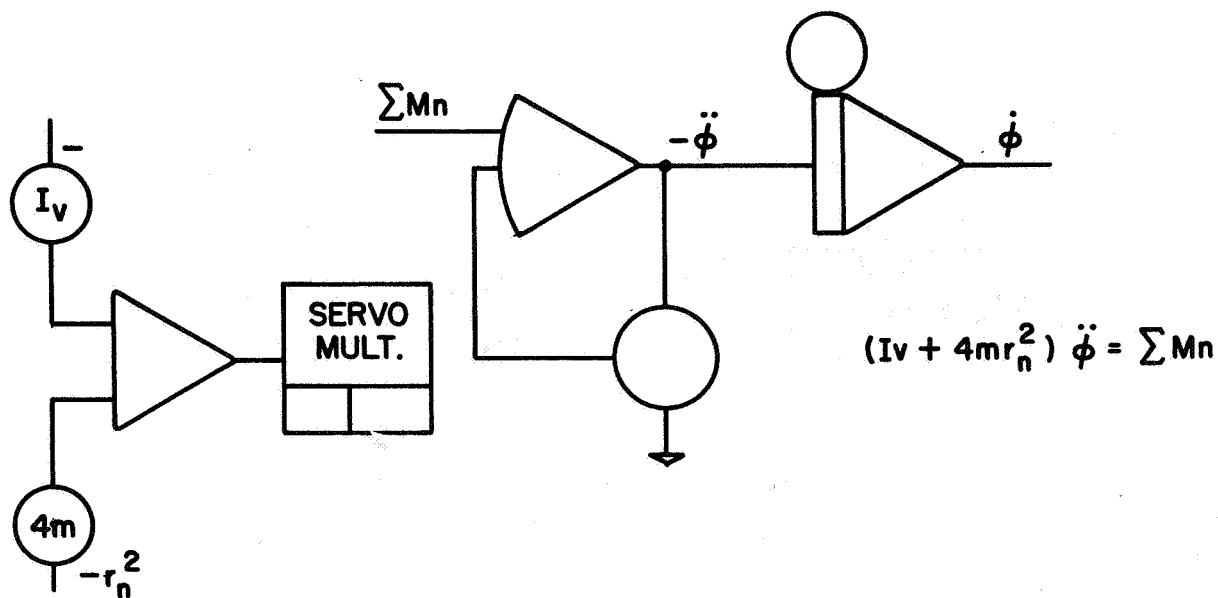
85-0130

Figure 11 BOOM SECTION SWITCHING FOR DEPLOYMENT SIMULATION



85-0131

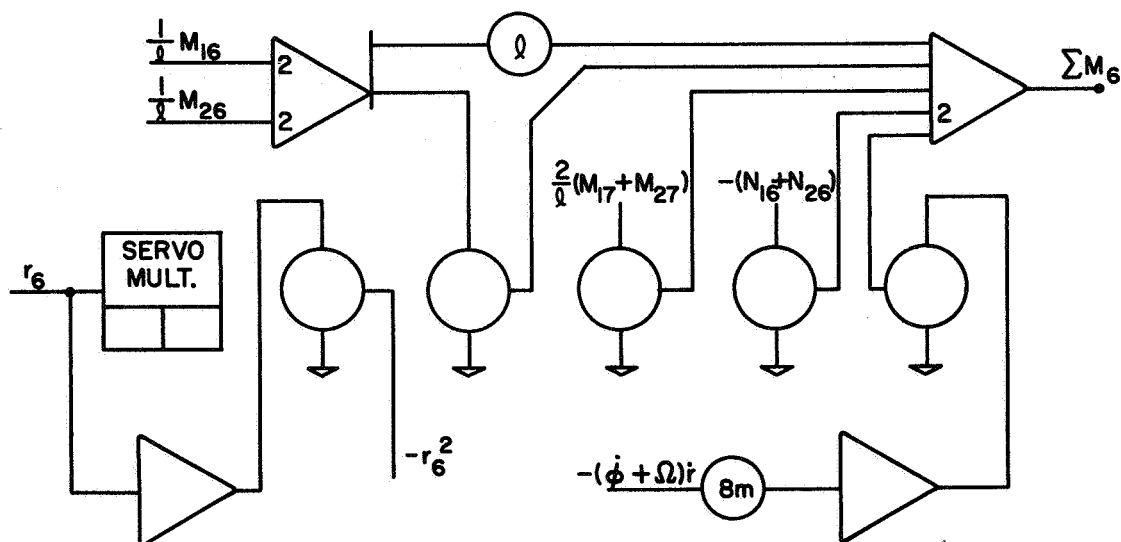
Figure 12 ACCELERATION GENERATOR CIRCUIT FOR UNDEPLOYED BOOM SECTION



85-0132

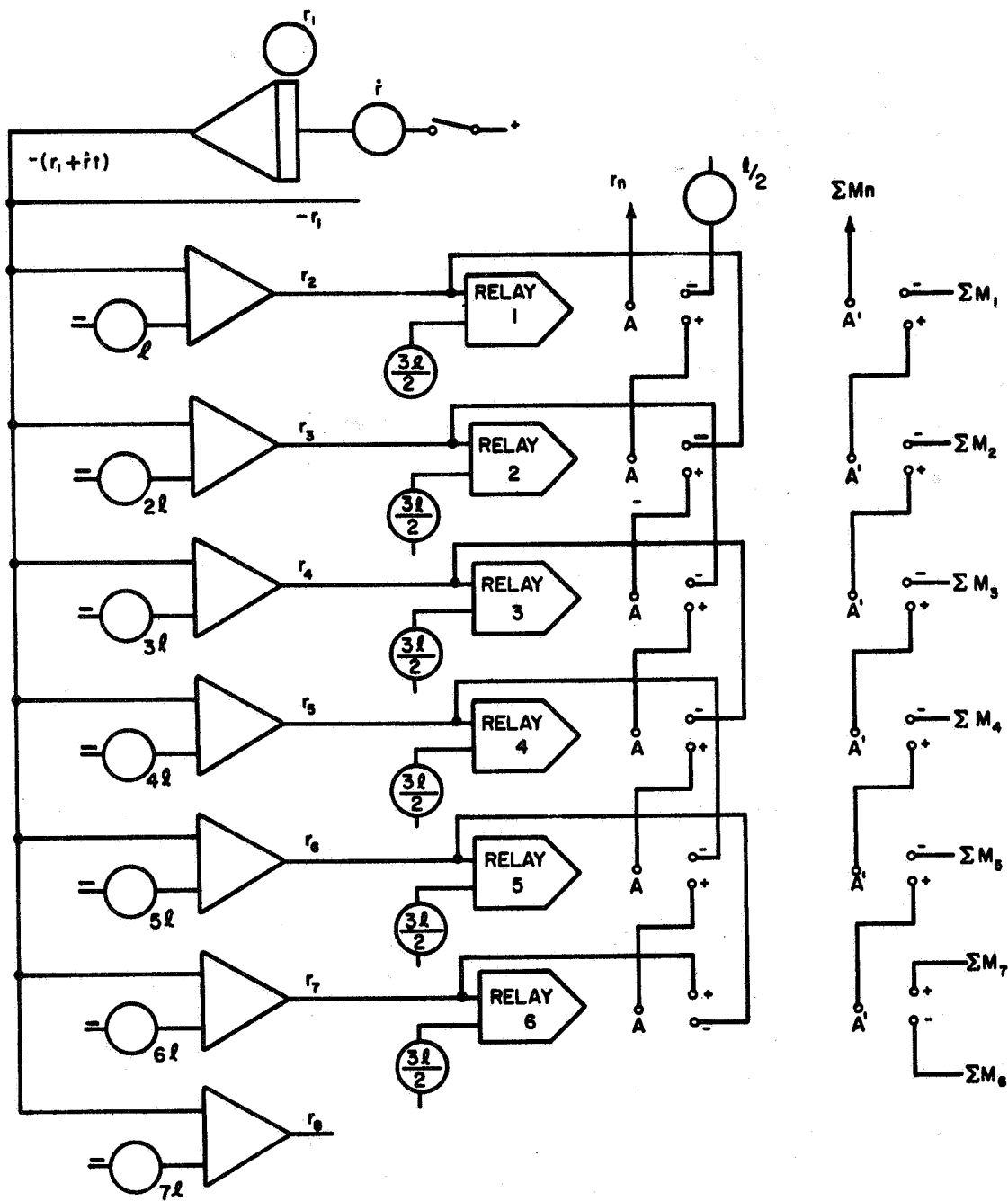
Figure 13 CIRCUIT FOR SIMULATING CENTRAL BODY DYNAMICS DURING DEPLOYMENT

$$\sum M_n = -8mr_n \dot{r}(\dot{\phi} + \Omega) - 2(M_{1n} + M_{2n}) - \frac{2r_n}{e}(M_{1n} + M_{2n}) + \frac{2r_n}{e}(M_{1n+1} + M_{2n+1}) - 2r_n(N_{1n} + N_{2n})$$



85-0133

Figure 14 CENTRAL BODY TORQUE GENERATOR



85-0134

Figure 15 SWITCHING LOGIC FOR APPLYING CENTRAL BODY MOMENTS DURING DEPLOYMENT

- 3.3.4 Internal Boom Damping Simulation. -- Linear internal boom damping can be simulated if care is exercised in applying the damping term so that only boom oscillations are reduced but not central body libration. For the extended boom simulation, let

$$\dot{u}_k = a_k - \lambda \dot{w}_k \quad (3-77)$$

where $\dot{w}_k = u_k - \dot{\phi} r_k$ and λ is the internal boom damping factor. (3-78)

Since the simulation of the booms does not produce \dot{w}_k explicitly, equation (3-65) must be used for each boom section damping simulation. Non-linear boom damping can be added similarly if the non-linear component parameters are known.

- 3.3.5 Central Body Control System Simulation. -- A central body control system can easily be added to the present simulation. The control system applies central body torques which are a function of the central body angle and its derivatives.

A very simple control system was added to the extended boom simulation. The control torque acting on the central body consisted of proportional rate damping.

$$T_c = -K \dot{\phi}. \quad (3-79)$$

This addition demonstrated that central body damping is feasible. More elaborate control systems will be added to the simulation in a similar fashion later in the dynamics study.

- 3.3.6 Visual Display. -- A visual display technique has been developed in which a commutator is used to sample the two components of each mass location in a sequential manner and apply the pulses obtained simultaneously to the vertical and horizontal deflection inputs of an oscilloscope. A visual, motion-picture type display is produced. Additional displays, useful in interpreting and reducing the data, can also be introduced with the commutator. In particular, an orbit location indicator showing the satellite position in orbit has been added to the display.

To locate the central body in the center of the visual display, an offset voltage is needed to displace the origin of the x, z axes:

$$x = k_x \left(v_x - \frac{v_{max}}{2} \right) \quad (3-80)$$

$$z = k_z \left(v_z - \frac{v_{max}}{2} \right). \quad (3-81)$$

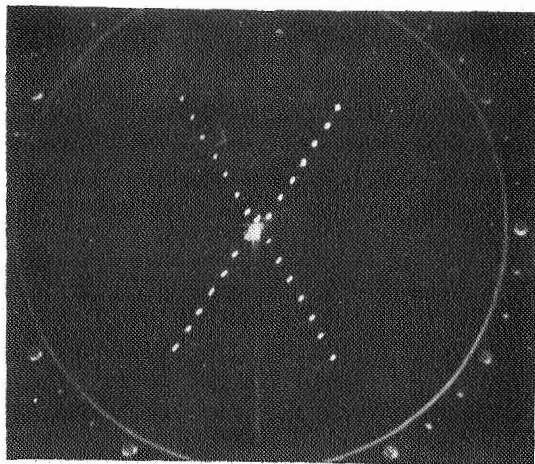
v_{\max} is the maximum commutator voltage (4 volts). Also, the orbital location indicator is effected with an oscillator:

$$X = k_0 \sin (\Omega t + \gamma_0) \quad (3-82)$$

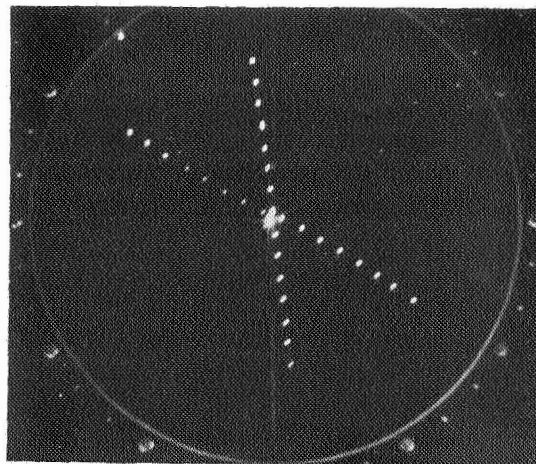
$$Z = -k_0 \cos (\Omega t + \gamma_0) \quad (3-83)$$

where X and Z are satellite positional coordinates in its orbit, and γ_0 defines the starting point.

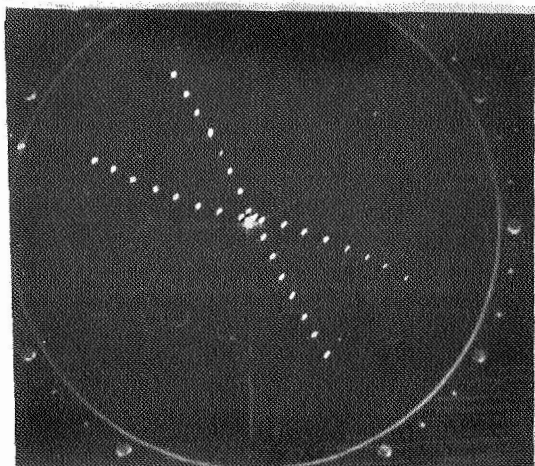
A sequence of six photographs of the oscilloscope display is given in figure 16 for a deployment-excited oscillation resulting from deployment at the rate of 1 ft/sec.



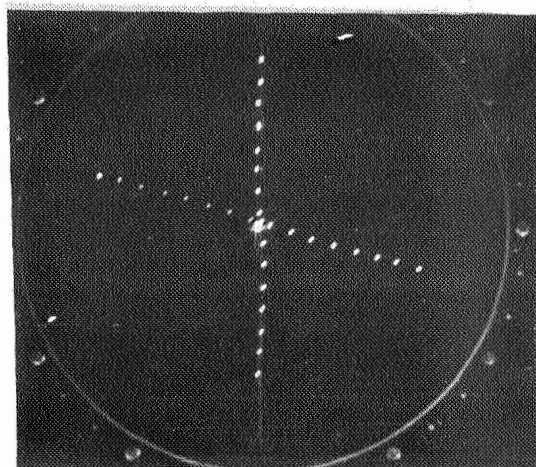
(1) DURING DEPLOYMENT



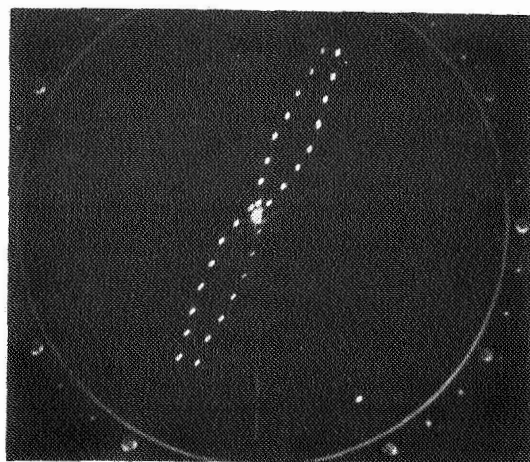
(2) $T = 3000 \text{ SEC.}$



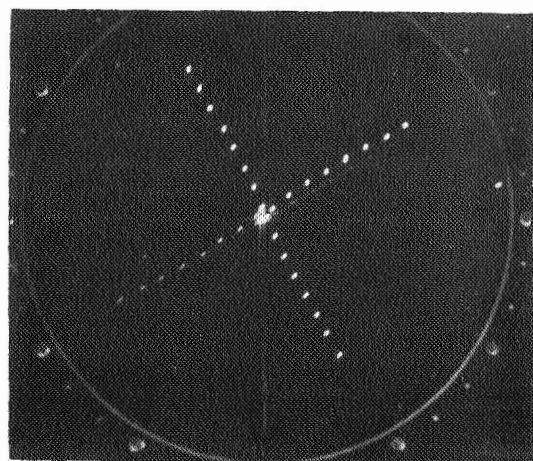
(3) $T = 4000 \text{ SEC.}$



(4) $T = 4500 \text{ SEC.}$



(5) $T = 7500 \text{ SEC.}$



(6) $T = 10,500 \text{ SEC.}$

Figure 16 DEPLOYMENT EXCITED OSCILLATION ($\dot{r} = 1 \text{ ft/sec}$)

4. RIGID-BODY SIMULATION

4.1 INTRODUCTION. -- The complexity of the flexible body dynamics problem makes it desirable to attempt to categorize the various observed effects as to whether they are principally due to rigid body motion or beam dynamics. This task can be accomplished by comparing the results obtained using a rigid body with those obtained using a flexible body. Although it will be possible to run the flexible body program as a rigid body, it was felt that it would be desirable also to develop a separate rigid-body program for the following reasons:

- a. The approach used to develop the appropriate equations for the rigid-body program is completely independent of that used for the flexible-body program, thus providing an independent check for those cases for which an analytical solution cannot be developed.
- b. The rigid-body program could be developed more quickly than the flexible-body program since a considerable portion of the program had been previously developed on other projects. This allowed experimentation with various techniques which would later be incorporated into the flexible body program on an earlier time schedule.
- c. The rigid-body program can provide check cases for both the analog and digital flexible-body programs more economically than the flexible-body program used to generate rigid-body motion.

In the analysis of rigid-body motion, it is necessary to express the motion relative to some frame of reference. The specific problem for the RAE dynamics study consists of expressing the rotary motion of a satellite body-fixed frame with respect to an inertial frame. The rotational form of Newton's second law ($p_1 \vec{H}_c = \vec{M}_c^*$) together with the required initial conditions will then allow us to express the motion as a set of time-dependent differential equations.

The angular momentum \vec{H}_c of the body about its center of mass can be expressed in terms of the inertia tensor I and the angular rate \vec{W}_{ib} of the body with respect to inertial space ($\vec{H}_c = I \vec{W}_{ib}$). Since the inertia tensor I is a real, symmetric matrix, a transformation of axes that will diagonalize the matrix always exists. The body-fixed frame which produces a diagonal matrix is generally called the principal axes set and is used in this study since the body geometry can be conveniently expressed in this frame, and the elimination of the product-of-inertia terms results in some useful simplification.

* Where p_1 represents the time derivative d/dt taken with respect to inertial space, \vec{H}_c is the angular momentum about the center of mass, and \vec{M}_c^* is the sum of the moments about the center of mass.

The two principal frames therefore will be the inertial frame and the body-fixed, principal-axes frame. Let us now define a transformation matrix C such that $(\vec{V})_i = C(\vec{V})_b$ where $(\vec{V})_i$ is an arbitrary vector coordinatized in the inertial frame and $(\vec{V})_b$ is the same vector coordinatized in the body frame. The time dependence of the transformation matrix C can be expressed as $p_i C = C \bar{W}_{ib}$. The solution to the rigid body problem can now be described as the solution of the two matrix differential equations $p_i (I \bar{W}_{ib}) = M_c$ and $p_i C = C \bar{W}_{ib}$ coordinatized in a suitable frame (either body or inertial). To solve these equations, three general areas must be examined: (1) the choice of coordinate transformation method, and (2) the technique used to generate the body's translational motion information (vehicle ephemeris data) needed for (3) the generation of the external moments.

- 4.2 COORDINATE TRANSFORMATION METHODS. -- There are four main methods for transforming between two right-handed orthogonal coordinate systems. Euler angles are probably the most commonly used technique. There are two distinct types of Euler angle rotations: the normal Euler angles are characterized by a rotation about an original axis, followed by a rotation about some new axes, followed by a rotation about the carried direction of the original axis (example 3-1' -3'); modified Euler angles are defined by sequential rotations about three different axes (example 1-2' -3'). The entire set of 12 possible rotations can be generated by merely relabeling these two types. The transformation matrices relating coordinates and their angular velocity are now given.

Normal Euler Angles

Let

$$\Phi = \begin{pmatrix} \cos \phi & \sin \phi & 0 \\ -\sin \phi & \cos \phi & 0 \\ 0 & 0 & 1 \end{pmatrix}$$

$$\theta = \begin{pmatrix} 1 & 0 & 0 \\ 0 & \cos \theta & \sin \theta \\ 0 & -\sin \theta & \cos \theta \end{pmatrix}$$

$$\Psi = \begin{pmatrix} \cos \psi & \sin \psi & 0 \\ -\sin \psi & \cos \psi & 0 \\ 0 & 0 & 1 \end{pmatrix}$$

Then

$$\begin{pmatrix} x' \\ y' \\ z' \end{pmatrix} = \Psi \theta \Phi \begin{pmatrix} x \\ y \\ z \end{pmatrix}$$

$$\begin{pmatrix} \omega_{x'} \\ \omega_{y'} \\ \omega_{z'} \end{pmatrix} = \Psi \theta \begin{pmatrix} 0 \\ 0 \\ \dot{\phi} \end{pmatrix} + \Psi \begin{pmatrix} \dot{\theta} \\ 0 \\ 0 \end{pmatrix} + \begin{pmatrix} 0 \\ 0 \\ \dot{\psi} \end{pmatrix}$$

Modified Euler Angles

Let

$$\Gamma = \begin{pmatrix} \cos \gamma & 0 & -\sin \gamma \\ 0 & 1 & 0 \\ \sin \gamma & 0 & \cos \gamma \end{pmatrix}$$

then

$$\begin{pmatrix} x' \\ y' \\ z' \end{pmatrix} = \Psi \Gamma \theta \begin{pmatrix} x \\ y \\ z \end{pmatrix}$$

$$\begin{pmatrix} \omega_{x'} \\ \omega_{y'} \\ \omega_{z'} \end{pmatrix} = \Psi \Gamma \begin{pmatrix} \dot{\theta} \\ 0 \\ 0 \end{pmatrix} + \Psi \begin{pmatrix} 0 \\ \dot{\gamma} \\ 0 \end{pmatrix} + \begin{pmatrix} 0 \\ 0 \\ \dot{\psi} \end{pmatrix}$$

Cayley-Klein parameters use complex numbers to generate the transformation matrices. Four parameters are used, arrayed in a matrix $Q = \begin{pmatrix} \alpha & \gamma \\ \beta & \delta \end{pmatrix}$ where Q is required to be unitary and the determinant of Q equal to +1. Now if we let $P = \begin{pmatrix} z & x-iy \\ x+iy & -z \end{pmatrix}$ and $P' = QPQ^T$, then, since P is hermitian ($P = \bar{P}^T$), P' is also hermitian and $|P'| = |P|$ and the transformation is orthogonal.

Cayley-Klein Parameters

$$\begin{pmatrix} x' \\ y' \\ z' \end{pmatrix} = \begin{pmatrix} \frac{1}{2}(a^2 - \gamma^2 + \delta^2 - \beta^2) & \frac{1}{2}i(\gamma^2 - a^2 + \delta^2 - \beta^2) & \gamma\delta - a\beta \\ \frac{1}{2}i(a^2 + \gamma^2 - \beta^2 - \delta^2) & \frac{1}{2}(a^2 + \gamma^2 + \beta^2 + \delta^2) & -i(a\beta + \gamma\delta) \\ \beta\delta - a\gamma & i(a\gamma - \beta\delta) & a\delta + \beta\gamma \end{pmatrix} \begin{pmatrix} x \\ y \\ z \end{pmatrix}$$

$$\begin{pmatrix} \omega_{x'} \\ \omega_{y'} \\ \omega_{z'} \end{pmatrix} = i \begin{pmatrix} \beta \dot{a} - a \dot{\beta} + \gamma \dot{\delta} - \delta \dot{\gamma} \\ \delta \dot{\beta} - \beta \dot{\delta} + \gamma \dot{a} - a \dot{\gamma} \\ \beta \dot{\gamma} - \gamma \dot{\beta} + a \dot{\delta} - \delta \dot{a} \end{pmatrix}$$

The general rotation of a body can be considered to be a rotation through an angle A about a vector \vec{W} . A quaternion is a set of four real numbers. The first component q_0 can be geometrically interpreted in terms of the rotation angle A [$q_0 = \cos A/2$]. The other three components, -- q_1 , q_2 , and q_3 -- can be interpreted as the components of the rotation vector \vec{W} [$\vec{W} = i q_1 + j q_2 + k q_3$]. Euler parameters and the Gibbs vector differ from quaternions essentially only in terminology. The Gibbs vector is the \vec{W} vector but with magnitude equal to the angle of rotation A , while Euler parameters are just twice the quaternion components.

Quaternions

$$\begin{pmatrix} x' \\ y' \\ z' \end{pmatrix} = 2 \begin{pmatrix} (q_0^2 + q_1^2) - \frac{1}{2} & q_1 q_2 + q_0 q_3 & q_1 q_3 - q_0 q_2 \\ q_1 q_2 - q_0 q_3 & (q_0^2 + q_2^2) - \frac{1}{2} & q_2 q_3 + q_0 q_1 \\ q_1 q_3 + q_0 q_2 & q_2 q_3 - q_0 q_1 & (q_0^2 + q_3^2) - \frac{1}{2} \end{pmatrix} \begin{pmatrix} x \\ y \\ z \end{pmatrix}$$

$$\begin{pmatrix} \omega_{x'} \\ \omega_{y'} \\ \omega_{z'} \end{pmatrix} = 2 \begin{pmatrix} -q_1 \dot{q}_0 + q_0 \dot{q}_1 + q_3 \dot{q}_2 - q_2 \dot{q}_3 \\ -q_2 \dot{q}_0 - q_3 \dot{q}_1 + q_0 \dot{q}_2 + q_1 \dot{q}_3 \\ -q_3 \dot{q}_0 + q_2 \dot{q}_1 - q_1 \dot{q}_2 + q_0 \dot{q}_3 \end{pmatrix}$$

Direction cosines form the most direct method of transformation. Each of the prime coordinates has three components when coordinatized in the original frame. These nine components are the direction cosines and completely specify the transformation.

Direction Cosines

$$\begin{pmatrix} x' \\ y' \\ z' \end{pmatrix} = \begin{pmatrix} \vec{i}' \cdot \vec{i} & \vec{i}' \cdot \vec{j} & \vec{i}' \cdot \vec{k} \\ \vec{j}' \cdot \vec{i} & \vec{j}' \cdot \vec{j} & \vec{j}' \cdot \vec{k} \\ \vec{k}' \cdot \vec{i} & \vec{k}' \cdot \vec{j} & \vec{k}' \cdot \vec{k} \end{pmatrix} \begin{pmatrix} x \\ y \\ z \end{pmatrix}$$

$$\begin{pmatrix} \omega_{x'} \\ \omega_{y'} \\ \omega_{z'} \end{pmatrix} = \begin{pmatrix} \dot{d}_{21} \dot{d}_{31} + \dot{d}_{22} \dot{d}_{32} + \dot{d}_{23} \dot{d}_{33} \\ \dot{d}_{31} \dot{d}_{11} + \dot{d}_{32} \dot{d}_{12} + \dot{d}_{33} \dot{d}_{13} \\ \dot{d}_{11} \dot{d}_{21} + \dot{d}_{12} \dot{d}_{22} + \dot{d}_{13} \dot{d}_{23} \end{pmatrix}$$

Euler angles and the Gibbs vector are subject to singularities since the rotation is specified by only three quantities. In addition, Euler angles introduce the computation of trigonometric functions in the determination of derivatives. The singularities impose difficulties when it is necessary to allow complete freedom about all three axes, while the necessary algorithms for the trigonometric functions can introduce considerable additional error in the derivative computations. Cayley-Klein parameters require the additional complication of complex number arithmetic. For these reasons, Euler angles, the Gibbs vector, and Cayley-Klein parameters are not further considered.

The choice between direction cosines and quaternions (where Euler parameters are considered as a form of the quaternions) cannot be made so readily. Both methods enjoy an absence of singularities and a meaningful physical interpretation.

- 4.3 ERROR PROPAGATION. -- Since more than three equations are being integrated, the additional information can be used in conjunction with constraint equations to reduce the error under certain conditions. Actually five different schemes using direction cosines or quaternions have been programmed and briefly examined. These schemes are integration of: (a) direction cosines with no correction, (b) nine direction cosines normalized by row after each integration step, (c) six direction cosines using three constraint equations to generate the additional three elements, (d) four quaternion components with no correction, and (e) four normalized quaternion components. A preliminary investigation was conducted to determine the relative advantages of these five schemes. The test case selected to evaluate the schemes consists of a constant rate skewed with respect to the principal body axes so that each axis sees the same rate. The body was assumed to have equal principal moments of inertia.

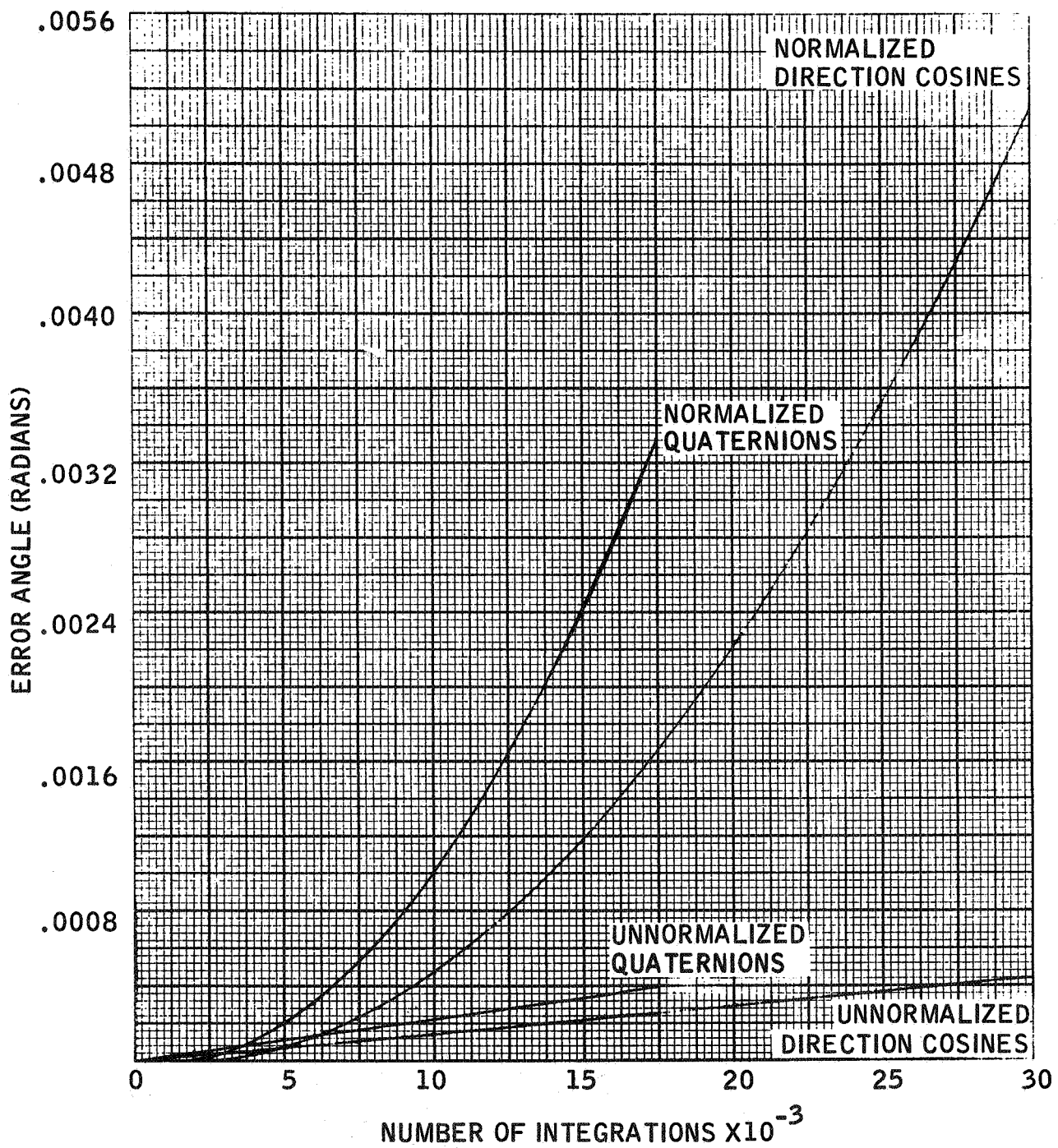
No external moments were applied to the body. Thus the rate should remain constant and a simple analytic solution could be used to verify the accuracy of the integration.

A measure of the accuracy, suggested by Dr. Wallace Vander Velde, is generated by the following technique. Let the subscripts I and B denote the inertial and body axes, respectively, while the subscripts M and T denote measured and true values. The transformation matrix can be defined by the equation $\vec{V}_I = C_{BI} \vec{V}_B$ where \vec{V} is an arbitrary vector and C is the matrix of direction cosines. Now $\vec{V}_{IT} = C_{BIT} \vec{V}_{BT}$ and $\vec{V}_{IM} = C_{BIM} \vec{V}_{BT}$. There exists a transformation between \vec{V}_{IT} and \vec{V}_{IM} such that $\vec{V}_{IT} = C_{ERR} \vec{V}_{IM}$; it can be shown that this transformation is $C_{ERR} = C_{BIM} C_{BIT}^{-1}$. If the error matrix C_{ERR} represents a small angle transformation, it is approximately of the form:

$$C_{ERR} = \begin{bmatrix} 1 & A_3 & -A_2 \\ -A_3 & 1 & A_1 \\ A_2 & -A_1 & 1 \end{bmatrix}$$

where A_i is the i^{th} component of the vector rotation carrying the frame into the I frame. (The order of rotation makes no difference since the rotations are considered to be small.) The rotation angle A where $A = (A_i \delta_{ij} A_j)^{1/2}$ is used as an approximate measure of the error. Two classes of errors appear to be present. The IBM 7094 truncates the results of multiplication operations to maintain a specified number of significant figures. The truncation takes place on the absolute value of the product. The effect is to cause the rotation angle error to grow as a function of the number of integrations (as opposed to the function growing as the square root of the number of integrations for the case of machine round-off). The error should also grow as a function of the number of multiplications involved in the evaluation of the derivative and computation of the integrand. Thus the error angle A should have the form, $A = f(m) E n$, where n is the number of integrations, E is the average value of the truncation error per multiplication, and $f(m)$ is a function of the number of multiplications. The average truncation error should be about 3.7×10^{-9} ($1/2 \times 2^{-27}$ binary) when considered for either direction cosines or quaternions (maximum value of 1). Referring to figure 17, it will be noted that the error angles associated with the unnormalized direction cosines and the unnormalized quaternions are linear functions of the number of integration steps. Using the values plotted in the figure, $f(m)$ calculated for the quaternions is ~ 6 while the direction cosines produce a value of $f(m) \cong 4$. This appears to be consistent since there are two additional multiplications in the computation of the quaternion derivatives.

The second class of error can be categorized as scheme error. Two types of scheme error are present: the error associated with the integration scheme and the error associated with the normalization scheme. Referring again to figure 17, it will be observed that the normalization apparently introduces a systematic error which eventually dominates the significant figure truncation error. Thus it would appear that normalization with its additional computational requirements is generally not a desirable feature. Figures 18 and 19 show the error angle plotted as a function of the number of revolutions of the body with respect to inertial space. Low amplitude oscillations of approximately the orbital frequency will be observed, particularly with the quaternions. This error can probably be associated with the integration scheme. The problem here is a matter of attempting to fit a basically sinusoidal function (the quaternion derivatives) with a cubic (the interpolator and extrapolator of the ADMS4 routine).



65-11998

Figure 17 ERROR ANGLE VERSUS NUMBER OF INTEGRATION STEPS

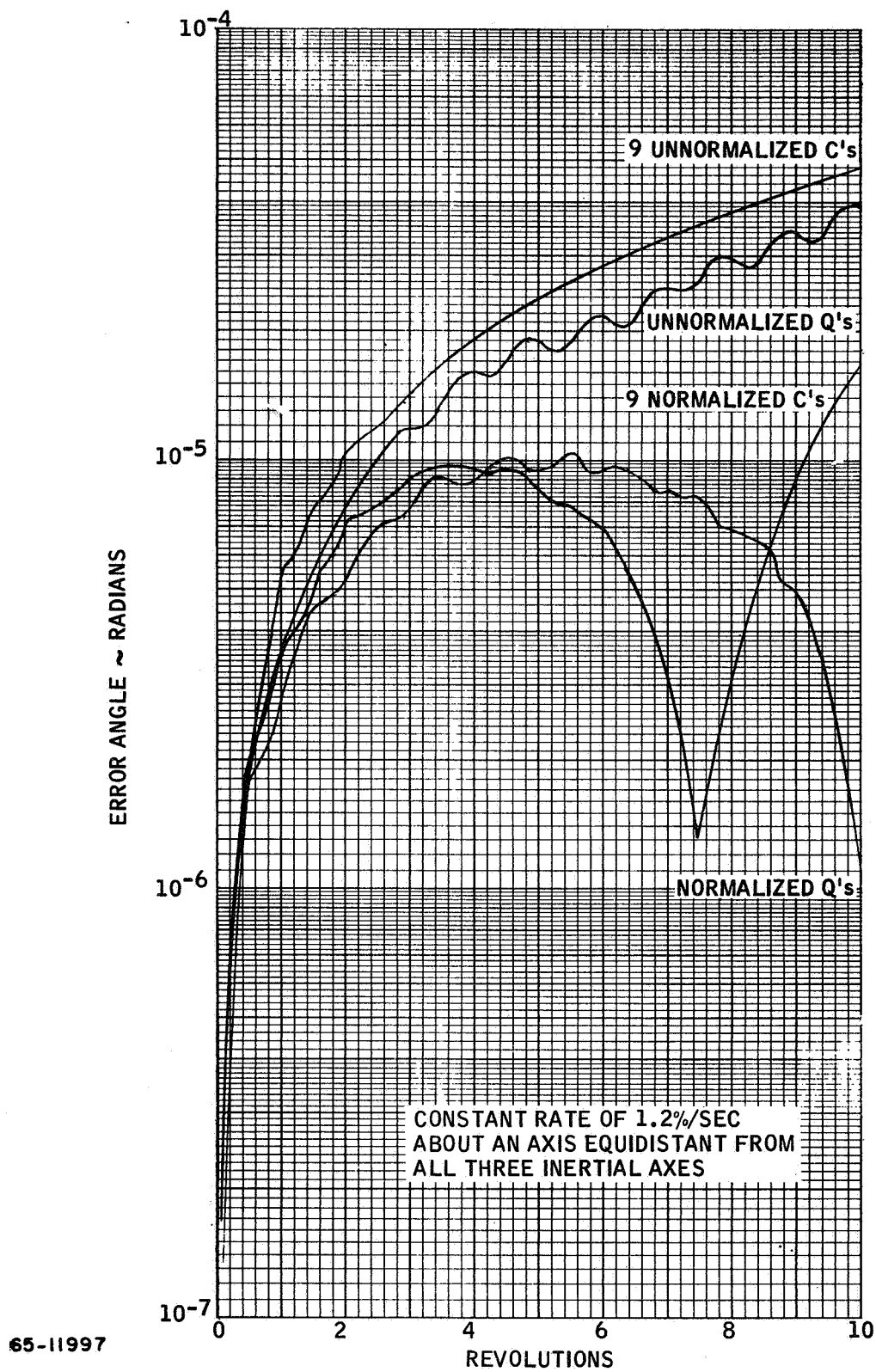


Figure 18 ERROR ANGLE VERSUS NUMBER OF REVOLUTIONS

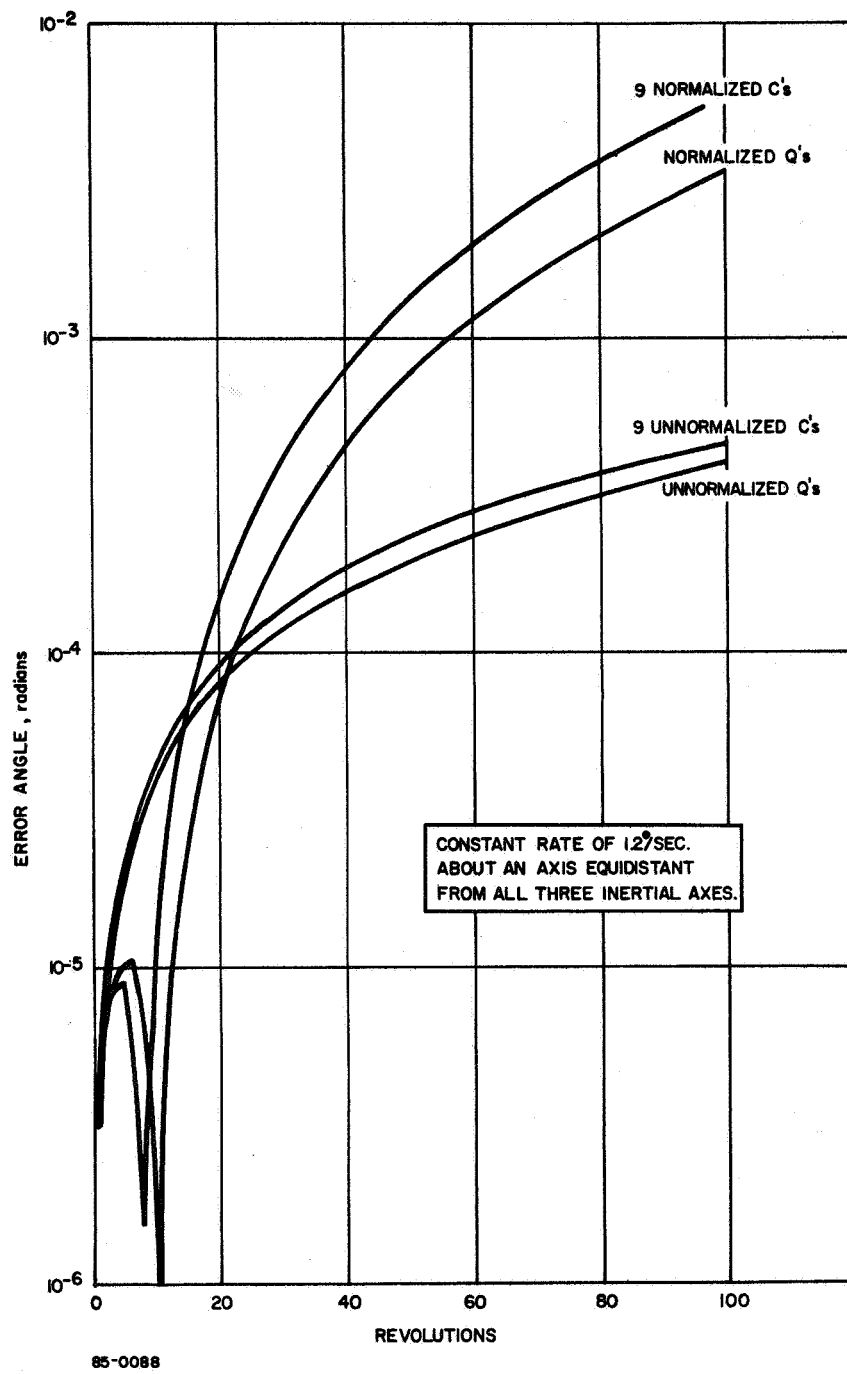


Figure 19 ERROR ANGLE VERSUS NUMBER OF REVOLUTIONS

From these preliminary results, it would appear that unnormalized quaternions are the most advantageous method of generating the transformation matrix since they produce the least error with the fewest integration steps. It would also appear that relaxing the integration bounds and thus increasing the integration scheme error would be beneficial since the significant-figure truncation error would be reduced by the reduction in the number of integration steps; at the same time, the running time would be decreased. Further investigation of these areas will be undertaken in Phase B. Additionally, the possible merits of Runge-Kutta will be investigated.

- 4.4 VEHICLE EPHEMERIS GENERATION TECHNIQUES. -- A completely general rigid-body simulation would of necessity include coupled differential equations for both the translational and rotary degrees of freedom. Thus the vehicle's position, velocity, and acceleration would influence the rotational behavior of the vehicle (example: the vehicle position influences the computation of the gravity-gradient moment), while the vehicle's orientational state introduces similar perturbations to the translational state (example: the acceleration of the center of mass caused by solar radiation pressure is a function of the vehicle's orientation with respect to the Sun). In the interest of somewhat simplifying a rather complex problem (considerably more complex when the additional degrees of freedom associated with the flexible beams are introduced), it was assumed that the coupling was not complete; specifically, that the only coupling involved the effect of the translational state on the rotary state and that the rotary state did not significantly affect the translational state. This simplification implies that translational effects that normally include both orientation-dependent terms and other terms which are not dependent upon orientation can now be simulated only as functions of the orientation-independent terms. Thus the average acceleration due to solar pressure can be accounted for, but the immediate change in acceleration due to the changing cross-sectional area and aspect angle cannot.

This simplification now allows the generation of the vehicle's translational motion (vehicle ephemeris) entirely independent of (and completely separate from, if it proves desirable) the vehicle's rotary motion. Two methods for generating the necessary data have been developed. The first method, called the analytical ephemeris, uses a simple conical representation of the orbit. The vehicle's initial position and velocity are used in conjunction with Kepler's equation to provide instantaneous position and velocity. The orbit is assumed to be fixed in inertial space and therefore acceleration terms attributable to the actual rotation of the orbital frame with respect to inertial space have been neglected. The computation

for the direction of the Sun includes a term accounting for the rotation of the orbital frame with respect to inertial space caused by the oblateness perturbation in addition to the diurnal motion. Thus the correct geometry is maintained. A solar illumination factor (fraction of the solar disc visible) is also computed as a function of the vehicle's instantaneous position relative to the Earth and Sun.

A more complete (but also more costly in terms of machine time) option is also provided in the program. The computed ephemeris allows the computation of position and velocity to be performed by a completely independent program and then to be transferred to the rotary dynamics program using a binary magnetic tape. Presently an N-body variation of parameters program (1546) is being used to generate the necessary information, but any orbital program can be used for this purpose provided that it is suitably modified to write the required tape. The presently used program allows a variety of perturbations including gravitational perturbations caused by other (up to 11) planetary bodies (using JPL ephemeris data), solar radiation pressure, atmospheric drag, and oblateness (including triaxiality) perturbations.

- 4.5 RIGID BODY MOMENTS. -- The gravity-gradient moment is of course the principal forcing function with which we are concerned, and at the present time it is the only type of external moment programmed and available for use with the rigid-body program. The gravitational force at any point i on the rigid body is given by \vec{F}_i , where

$$\vec{F}_i = \frac{m_i \mu_E \vec{R}_i}{R_i^3}$$

and

m_i = the mass of the i^{th} point on the body

μ_E = the gravitational parameter of the Earth

\vec{R}_i = the vector from the center of the Earth to the i^{th} body point,

$R_i = |\vec{R}_i|$.

The torque contribution \vec{T}_i of the i^{th} mass point about the center of mass of the RAE configuration due to this gravitational force \vec{F}_i is given by $\vec{T}_i = \vec{Z}_i \times \vec{F}_i$ where \vec{Z}_i is the vector from the center of mass of the satellite to the i^{th} point. Summing the individual torques over all the i^{th} mass points, we obtain the total torque \vec{T} for one pair of diametrically opposed antennas:

$$\vec{T} = \vec{k} \mu_E \rho R_o \sin \theta \int_{-L}^L \frac{Z_i dZ_i}{R_i^3}$$

where

ρ = the linear mass density of the antenna

R_o = the distance from the center of the Earth to the center of mass of the satellite

θ = the angle between the local vertical and the antenna axis

\vec{Z}_i = $Z_i \vec{i}_z$ where \vec{i}_z is the unit vector in the direction of the antenna

$\vec{k} = \frac{\vec{R}_o \times \vec{i}_z}{|\vec{R}_o \times \vec{i}_z|}$ where k is the unit vector normal to the antenna-local vertical plane

L = the antenna length measured from the center of the satellite.

Evaluation of this integral gives:

$$\vec{T} = \frac{\mu_E \rho L^3}{R^3} \vec{k} \sin 2\theta.$$

Only one term of a binomial expansion of the gravity expression was utilized in the evaluation of the torque integral since it was found that the symmetry of the RAE configuration resulted in only even terms in the expansion. The torque contributed by two pair of diametrically

opposed antennas is of course given by $\vec{T}_{1+2} = \frac{\mu_E \rho L^3}{R^3} \vec{k} (\sin 2\theta_1 + \sin 2\theta_2).$

The problem of introducing libration damping by means of an additional rigid body coupled to the first by means of a torsion spring and magnetic hysteresis damper has also been investigated and programmed. It has not been completely debugged at this point, however. The technique employed in incorporating this additional body consists of adding a series of subroutines that are essentially duplicates of those used for the satellite vehicle itself. The moment summation block is modified to include the reactive torque of one body on the other caused by the spring and damper.

A detailed description of the various subroutines including the equations which have been programmed is included in appendix C.

5. FLEXIBLE BODY SIMULATION

5.1 INTRODUCTION. -- The equations of motion describing the dynamic behavior of the RAE satellite during both the deployment and operational phases of the mission are developed in the following paragraphs. The basic approach used in the derivation is to apply LaGrange's equation to suitably constructed dynamic system functions. The application of LaGrange's equation requires the description of the position of a point on the satellite in terms of a set of coordinates, q_p , depending on time only. The coordinates used to describe the position of a point on the satellite are

- a. Three Cartesian coordinates to locate the C. M. of the central core of the satellite relative to the center of the Earth
- b. Three angles to orient the undeformed geometry of the satellite with respect to the non-rotating Earth Cartesian coordinate system
- c. The amplitudes of a set of shape functions used to describe the position of a point on the antenna relative to its undeformed rigid body position.

The kinetic energy of the system is obtained by writing the kinetic energy of an element of mass at a general point on the satellite and then integrating over all points of the satellite. The velocity components of a general point on the satellite are obtained by differentiation of the position components in the fixed reference frame with respect to time. The generalized forces for LaGrange's equation are obtained by evaluating the work done by all forces in a virtual displacement of each coordinate q_p . The external forces considered are the Earth's gravitation and the radiation pressure of the sun. The internal forces considered are the effects of strain energy due to deformation of the antenna and temperature gradients in the antennas due to solar radiation.

Several assumptions are made in the development of the equations of motion. These assumptions are listed below.

- a. The central core of the satellite is rigid.
- b. The behavior of an antenna can be represented by a series expansion in terms of the small-displacement mode shapes with time-varying amplitudes.
- c. Strains on the axis of an antenna are negligible in all respects.
- d. The contribution of twisting motions of the antenna to the kinetic energy are negligible.

e. There are several assumptions of detail associated with the number of terms to be retained in various expansions which must be considered with respect to the particular detail at issue.

5.2 DERIVATION OF EQUATIONS OF MOTION. -- The equations of motion for the RAE satellite are written by means of LaGrange's equation

$$\frac{d}{dt} \left[\frac{\partial(T - V)}{\partial \dot{q}_n} \right] - \frac{\partial(T - V)}{\partial q_n} = Q_n \quad (5-1)$$

In this equation T is the kinetic energy of the system, V is the potential energy of the system, and Q_n is the generalized force associated with the generalized coordinate q_n . The superscript dot is used to indicate differentiation with respect to time.

In the application of LaGrange's equation to formulating the equations of motion of a flexible body, the basic requirement is to express the position of a point on the deformed body in terms of a set of product functions which separate time-dependence from space-dependence. In essence, this means that the deformation of the body is assumed to be represented by a set of shape functions with time-dependent amplitudes. The set of time-dependent amplitudes, along with the set of six quantities needed to specify the position and orientation of a body-fixed reference frame, comprises the set of generalized coordinates q_n for LaGrange's equation.

In the following paragraphs a set of equations describing the dynamic behavior of the RAE satellite is derived. The first section develops the general framework for describing the dynamic behavior of a flexible body. The inertial terms (left hand side of equation (5-1)) are then specialized for the particular configuration of the RAE satellite. The relative displacements of the antennas, in two perpendicular directions normal to the undeformed antenna position, are expressed in terms of series expansions using the linear cantilever mode shapes. The axial displacement is specified in terms of these two series by requiring that the length of the antenna always be its unstrained length. The effect of axial strain and torsional rotation on the kinetic energy is neglected. The validity of the use of small-displacement mode shapes in this manner should be examined by comparison of this procedure with the solution of appropriately derived large-deformation beam equations of motion for a simplified dynamic case.

The final two sections are concerned with developing the generalized forces (right hand sides of equation (5-1)) for the conditions of the RAE satellite. The external effects of gravity and solar pressure are formulated in the first section. The internal forces due to strain caused by deformation and by temperature gradients are treated in the last section.

5.2.1 General. -- The position of a point on the vehicle is written in terms of its location relative to the center of the Earth. A set of Cartesian coordinates X_{i0} is constructed, with origin at the center of the Earth, and being fixed with respect to time and space. A local Cartesian coordinate system, X_{iL} , moving with the vehicle, but fixed in orientation parallel to the Earth-centered system, is taken at the center of mass of the satellite central hub. Finally, a Cartesian coordinate system, X_{iB} , fixed to the vehicle and moving with it, is constructed with origin at the center of mass of the satellite central hub and axes parallel to the principal axes of inertia of the undeformed vehicle. The orientation with respect to the local frame, X_{iL} , is specified by a matrix of direction cosines. The various coordinate frames are illustrated in figure 20.

The position of a point P on the vehicle with respect to the center of the Earth is given by the following equation. The subscript i indicates the three Cartesian components.

$$\{X_{i0}\} = \{X_{i0L}\} + [a_{ij}]\{X_{jB}\} \quad (5-2)$$

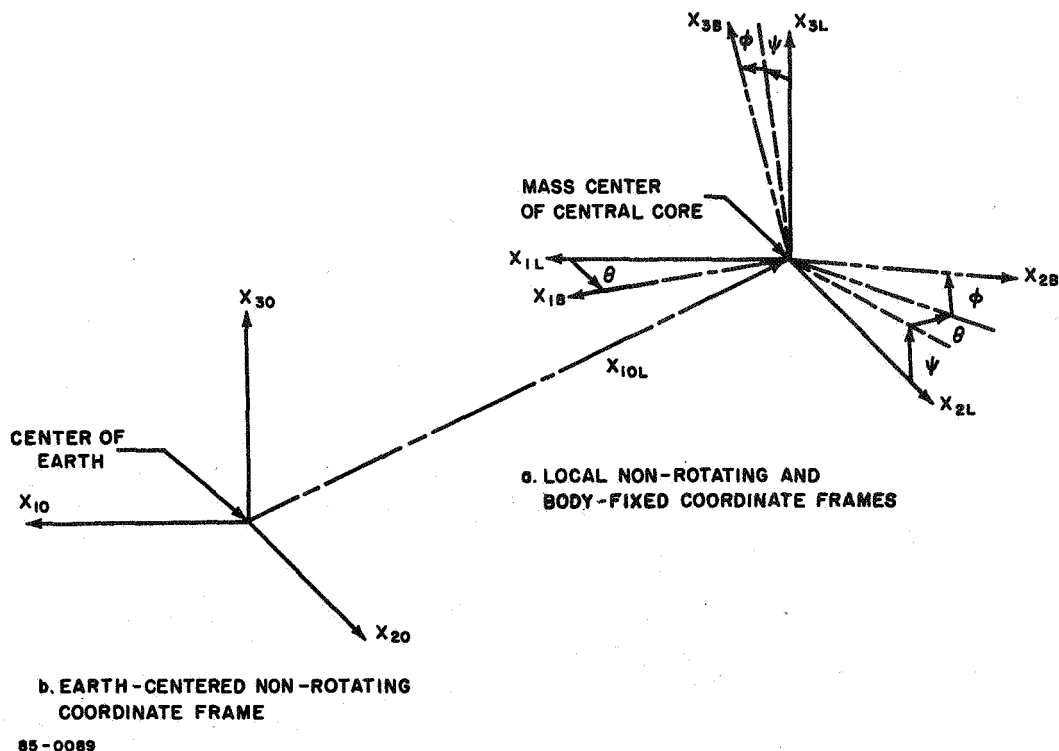


Figure 20 REFERENCE COORDINATE SYSTEM

The direction cosine matrix $[a_{ij}]$ transforms vector components from body-fixed coordinates to local non-rotating coordinates:

$$\{X_{iL}\} = [a_{ij}] \{X_{jB}\}$$

In terms of the Euler angles ψ , θ , and ϕ , the matrix is

$$[a_{ij}] = \begin{bmatrix} C\theta & -S\theta C\phi & S\theta S\phi \\ C\psi S\theta & -S\psi S\phi + C\psi C\theta C\phi & -S\psi C\phi - C\psi C\theta S\phi \\ S\psi S\theta & C\psi S\phi + S\psi C\theta C\phi & C\psi C\phi - S\psi C\theta S\phi \end{bmatrix} \quad (5-3)$$

The velocity of a point is obtained by differentiation of the components of position:

$$\{\dot{X}_{io}\} = \{\dot{X}_{ioL}\} + [\dot{a}_{ij}] \{X_{jB}\} + [a_{ij}] \{\dot{X}_{jB}\} \quad (5-4)$$

Now the derivative of the transformation can be written as follows. The instantaneous angular velocities about the three body axes are introduced:

$$[\dot{a}_{ij}] \{X_{jB}\} = [a_{ij}] \{\omega_{kB} X_{lB} - \omega_{lB} X_{kB}\} \quad (5-5)$$

With this the velocity components can be written:

$$\{X_{io}\} = \{\dot{X}_{ioL}\} + [a_{ij}] \{\dot{X}_{jB}\} + \omega_{kB} X_{lB} - \omega_{lB} X_{kB} \quad (5-6)$$

Introducing for convenience the parameter

$$\dot{\delta}_{iB} = \dot{X}_{iB} + \omega_{jB} X_{kB} - \omega_{kB} X_{jB} \quad (5-7)$$

the velocity components become

$$\{\dot{X}_{io}\} = \{\dot{X}_{ioL}\} + [a_{ij}] \{\dot{\delta}_{jB}\} \quad (5-8)$$

The kinetic energy is obtained by the standard relation. Considering an element of mass, the differential kinetic energy is given by

$$dT = \frac{1}{2} dm \{\dot{X}_{io}\}^T \{\dot{X}_{io}\} \quad (5-9)$$

where K is the kinetic energy. The velocity-squared term is expanded as follows:

$$\begin{aligned}
\{\dot{\mathbf{x}}_{io}\}^T \{\dot{\mathbf{x}}_{io}\} &= \{\dot{\mathbf{x}}_{ioL}\}^T \{\dot{\mathbf{x}}_{ioL}\} \\
&+ 2 \{\dot{\mathbf{x}}_{ioL}\}^T [\mathbf{a}_{ij}] \{\dot{\delta}_{jB}\} \\
&+ \{\dot{\delta}_{iB}\}^T \{\dot{\delta}_{iB}\}
\end{aligned} \tag{5-10}$$

Note that:

$$[\mathbf{a}_{ij}]^T [\mathbf{a}_{ij}] = \mathbf{I} \text{ (unit matrix)}$$

since $[\mathbf{a}_{ij}]$ is an array of direction cosines between two Cartesian frames. Further expansion of the terms in equation (5-10) yields

$$\{\dot{\mathbf{x}}_{ioL}\}^T \{\dot{\mathbf{x}}_{ioL}\} = \dot{x}_{1oL}^2 + \dot{x}_{2oL}^2 + \dot{x}_{3oL}^2 \tag{5-11}$$

$$\begin{aligned}
2 \{\dot{\mathbf{x}}_{ioL}\}^T [\mathbf{a}_{ij}] \{\dot{\delta}_{jB}\} &= 2 \dot{x}_{1oL} [a_{11} \dot{\delta}_{1B} + a_{12} \dot{\delta}_{2B} + a_{13} \dot{\delta}_{3B}] \\
&+ 2 \dot{x}_{2oL} [a_{21} \dot{\delta}_{1B} + a_{22} \dot{\delta}_{2B} + a_{23} \dot{\delta}_{3B}] \\
&+ 2 \dot{x}_{3oL} [a_{31} \dot{\delta}_{1B} + a_{32} \dot{\delta}_{2B} + a_{33} \dot{\delta}_{3B}]
\end{aligned} \tag{5-12}$$

$$\{\dot{\delta}_{iB}\}^T \{\dot{\delta}_{iB}\} = \dot{\delta}_{1B}^2 + \dot{\delta}_{2B}^2 + \dot{\delta}_{3B}^2 \tag{5-13}$$

To obtain the kinetic energy these expressions are integrated over the entire body. The integration variables involved are the independent spatial variables in the body frame. These appear only in the body system coordinate terms \mathbf{x}_{iB} and $\dot{\mathbf{x}}_{iB}$. Note that

$$\dot{\delta}_{1B} = \dot{x}_{1B} + \frac{\omega_{2B} x_{3B}}{} - \frac{\omega_{3B} x_{2B}}{}$$

$$\dot{\delta}_{2B} = \dot{x}_{2B} + \frac{\omega_{3B} x_{1B}}{} - \frac{\omega_{1B} x_{3B}}{}$$

$$\dot{\delta}_{3B} = \dot{x}_{3B} + \frac{\omega_{1B} x_{2B}}{} - \frac{\omega_{2B} x_{1B}}{}$$

$$\begin{aligned}
\dot{\delta}_{1B}^2 + \dot{\delta}_{2B}^2 + \dot{\delta}_{3B}^2 &= \dot{x}_{1B}^2 + \dot{x}_{2B}^2 + \dot{x}_{3B}^2 \\
&+ 2 \omega_{1B} [x_{2B} \dot{x}_{3B} - \dot{x}_{2B} x_{3B}] \\
&+ 2 \omega_{2B} [x_{3B} \dot{x}_{1B} - \dot{x}_{3B} x_{1B}] \\
&+ 2 \omega_{3B} [x_{1B} \dot{x}_{2B} - \dot{x}_{1B} x_{2B}] \\
&+ \omega_{1B}^2 [x_{2B}^2 + x_{3B}^2] + \omega_{2B}^2 [x_{1B}^2 + x_{3B}^2] + \omega_{3B}^2 [x_{1B}^2 + x_{2B}^2] \\
&- 2 \omega_{1B} \omega_{2B} [x_{1B} x_{2B}] - 2 \omega_{1B} \omega_{3B} [x_{1B} x_{3B}] \\
&\quad - 2 \omega_{2B} \omega_{3B} [x_{2B} x_{3B}]
\end{aligned}$$

The quantities x_{iB} and \dot{x}_{iB} are the only terms which contain variables involved in the integration over the body.

The meaning of the various terms can be understood in some respect by considering the case of a rigid body. In the present case the position coordinates in the body frame vary with time because deformation of the body is being included. In the rigid case the body system coordinates of a point, x_{iB} , are independent of time. The underlined terms are then the only terms which would appear in the rigid case. Moreover, the integrals of the terms involving x_{iB} would vanish in the rigid case if the body axis origin were placed at the C. M. of the body. The integrals of terms containing x_{iB}^2 and $x_{iB} x_{jB}$ would not vanish, but would give rise to the body moments and products of inertia, respectively.

The kinetic energy of the system is obtained by integration over the body in the body coordinate system:

$$T = \frac{1}{2} \int_B [\dot{x}_{10}^2 + \dot{x}_{20}^2 + \dot{x}_{30}^2] dm \quad (5-14)$$

Introducing the appropriate expressions for the components x_{i0} yields:

$$T = \frac{1}{2} \{\dot{X}_{ioL}\}^T \{\dot{X}_{ioL}\} \int_B dm$$

$$+ \{\dot{X}_{ioL}\}^T [a_{ij}] \left\{ \begin{array}{l} \int_B \dot{X}_{1B} dm + \omega_{2B} \int_B X_{3B} dm - \omega_{3B} \int_B X_{2B} dm \\ \int_B \dot{X}_{2B} dm + \omega_{2B} \int_B X_{1B} dm - \omega_{1B} \int_B X_{3B} dm \\ \int_B \dot{X}_{3B} dm + \omega_{1B} \int_B X_{2B} dm - \omega_{2B} \int_B X_{1B} dm \end{array} \right\}$$

$$+ \frac{1}{2} \int_B [\dot{X}_{1B}^2 + \dot{X}_{2B}^2 + \dot{X}_{3B}^2] dm$$

$$+ \omega_{1B} \int_B [X_{2B} \dot{X}_{3B} - \dot{X}_{2B} X_{3B}] dm$$

$$+ \omega_{2B} \int_B [X_{3B} \dot{X}_{1B} - \dot{X}_{3B} X_{1B}] dm$$

$$+ \omega_{3B} \int_B [X_{1B} \dot{X}_{2B} - \dot{X}_{1B} X_{2B}] dm$$

$$\begin{aligned}
& + \frac{1}{2} \omega_{1B}^2 \int_B [X_{2B}^2 + X_{3B}^2] dm \\
& + \frac{1}{2} \omega_{2B}^2 \int_B [X_{1B}^2 + X_{3B}^2] dm \\
& + \frac{1}{2} \omega_{3B}^2 \int_B [X_{1B}^2 + X_{2B}^2] dm \\
& - \omega_{1B} \omega_{2B} \int_B [X_{1B} X_{2B}] dm \\
& - \omega_{1B} \omega_{3B} \int_B [X_{1B} X_{3B}] dm \\
& - \omega_{2B} \omega_{3B} \int_B [X_{2B} X_{3B}] dm
\end{aligned} \tag{5-15}$$

Substituting expression (5-15) for the kinetic energy into LaGrange's equation gives the required equations of motion.

For \ddot{X}_{ioL} :

$$M_s \{ \ddot{X}_{ioL} \} + \frac{d}{dt} [a_{ij}] \left\{ \begin{array}{l} \int_B \dot{X}_{1B} dm + \omega_{2B} \int_B X_{3B} dm - \omega_{3B} \int_B X_{2B} dm \\ \int_B \dot{X}_{2B} dm + \omega_{3B} \int_B X_{1B} dm - \omega_{1B} \int_B X_{3B} dm \\ \int_B \dot{X}_{3B} dm + \omega_{1B} \int_B X_{2B} dm - \omega_{2B} \int_B X_{1B} dm \end{array} \right\} = \{ F_{io} \} \quad (5-16)$$

M_s is the total mass of the satellite. Operating on the direction cosines only and introducing the notation

$$\bar{\delta}_{iB} = \int_B \dot{X}_{iB} dm + \omega_{jB} \int_B X_{kB} dm - \omega_{kB} \int_B X_{jB} dm \quad (5-17)$$

reduces the above expression to

$$M_s \{ \ddot{X}_{ioL} \} + [a_{ij}] \left\{ \begin{array}{l} \frac{d}{dt} \bar{\delta}_{1B} + \omega_{2B} \bar{\delta}_{3B} - \omega_{3B} \bar{\delta}_{2B} \\ \frac{d}{dt} \bar{\delta}_{2B} + \omega_{3B} \bar{\delta}_{1B} - \omega_{1B} \bar{\delta}_{3B} \\ \frac{d}{dt} \bar{\delta}_{3B} + \omega_{1B} \bar{\delta}_{2B} - \omega_{2B} \bar{\delta}_{1B} \end{array} \right\} = \{ F_{io} \} \quad (5-18)$$

The equation of motion for the origin of the body frame can be simplified somewhat. The coordinates of the origin of the body frame can be written as follows:

$$X_{ioL} = X_{ioC} + \bar{X}_{iCL} \quad (5-19)$$

In this expression, X_{ioC} is the coordinate of the center of mass of the body and \bar{X}_{iCL} is the distance from the center of mass to the origin of the local body frame. It should be noted that X_{ioC} is the new generalized coordinate and that \bar{X}_{iCL} cannot be varied independently. Then

$$M_s \{ \ddot{X}_{ioC} \} = \{ F_{io} \} \quad (5-20)$$

$$M_s \{ \ddot{\bar{X}}_{iCL} \} + [a_{ij}] \left\{ \frac{d}{dt} \bar{\delta}_{jB} + \omega_{kB} \bar{\delta}_{lB} - \omega_{lB} \bar{\delta}_{kB} \right\} = 0 \quad (5-21)$$

The first of these equations is the standard equation for the motion of the center of mass. The second equation states that the net or summed motion of all mass points relative to the center of mass must be zero. It is clear from this equation that \bar{X}_{iCL} cannot be varied independently. The separation of these equations is advantageous in separating the orbit from the local dynamics of the body.

Using the three Euler angles as generalized coordinates (see figure 20), a set of three equations of motion for the rotation of the body-fixed reference frame is obtained. This set can be reduced to the following three equations written in terms of the instantaneous angular velocities about the body axes:

$$\begin{aligned} & \frac{d}{dt} \left[\int_B (\dot{\delta}_{3B} X_{2B} - \dot{\delta}_{2B} X_{3B}) dm \right] + \omega_{3B} \left[\int_B (\dot{\delta}_{2B} X_{1B} - \dot{\delta}_{1B} X_{2B}) dm \right] \\ & - \omega_{3B} \left[\int_B (\dot{\delta}_{1B} X_{3B} - \dot{\delta}_{3B} X_{1B}) dm \right] \\ & + \{ \ddot{X}_{ioL} \}^T \left\{ \begin{array}{c} 0 \\ - \int_B X_{3B} dm \\ \int_B X_{2B} dm \end{array} \right\} = M_{1B} \end{aligned} \quad (5-22)$$

$$\frac{d}{dt} \left[\int_B (\dot{\delta}_{1B} X_{3B} - \dot{\delta}_{3B} X_{1B}) dm \right] + \omega_{3B} \left[\int_B (\dot{\delta}_{3B} X_{2B} - \dot{\delta}_{2B} X_{3B}) dm \right] - \omega_{1B} \left[\int_B (\dot{\delta}_{2B} X_{1B} - \dot{\delta}_{1B} X_{2B}) dm \right]$$

$$+ \{ \ddot{X}_{ioL} \}^T \left\{ \begin{array}{c} \int_B X_{3B} dm \\ 0 \\ - \int_B X_{1B} dm \end{array} \right\} = M_{2B} \quad (5-23)$$

$$\frac{d}{dt} \left[\int_B (\dot{\delta}_{2B} X_{1B} - \dot{\delta}_{1B} X_{2B}) dm \right] + \omega_{1B} \left[\int_B (\dot{\delta}_{1B} X_{3B} - \dot{\delta}_{3B} X_{1B}) dm \right] - \omega_{2B} \left[\int_B (\dot{\delta}_{3B} X_{2B} - \dot{\delta}_{2B} X_{3B}) dm \right]$$

$$+ \{ \ddot{X}_{ioL} \}^T \left\{ \begin{array}{c} - \int_B X_{2B} dm \\ \int_B X_{1B} dm \\ 0 \end{array} \right\} = M_{3B} \quad (5-24)$$

where, as before,

$$\dot{\delta}_{iB} = \dot{X}_{iB} + \omega_{jB} X_{kB} - \omega_{kB} X_{jB}$$

Substituting equations (5-20) and (5-21) into (5-22) through (5-24) gives the following:

$$\begin{aligned}
& \frac{d}{dt} \left[\int_B (\dot{\delta}_{3B} X_{2B} - \dot{\delta}_{2B} X_{3B}) dm \right] + \omega_{2B} \left[\int_B (\dot{\delta}_{2B} X_{1B} - \dot{\delta}_{1B} X_{2B}) dm \right] - \omega_{3B} \left[\int_B (\dot{\delta}_{1B} X_{3B} - \dot{\delta}_{3B} X_{1B}) dm \right] \\
& + \left[\frac{d}{dt} \bar{\delta}_{2B} + \omega_{3B} \bar{\delta}_{1B} - \omega_{1B} \bar{\delta}_{3B} \right] \left[\frac{1}{M_s} \int_B X_{3B} dm \right] - \left[\frac{d}{dt} \bar{\delta}_{3B} + \omega_{1B} \bar{\delta}_{2B} - \omega_{2B} \bar{\delta}_{1B} \right] \left[\frac{1}{M_s} \int_B X_{2B} dm \right]
\end{aligned}$$

$$= M_{1B} - \{F_{io}\}^T [a_{ij}] \begin{pmatrix} 0 \\ -\frac{1}{M_s} \int_B X_{3B} dm \\ \frac{1}{M_s} \int_B X_{2B} dm \end{pmatrix} \quad (5-25)$$

$$\begin{aligned}
& \frac{d}{dt} \left[\int_B (\dot{\delta}_{1B} X_{3B} - \dot{\delta}_{3B} X_{1B}) dm \right] + \omega_{3B} \left[\int_B (\dot{\delta}_{3B} X_{2B} - \dot{\delta}_{2B} X_{3B}) dm \right] - \omega_{1B} \left[\int_B (\dot{\delta}_{2B} X_{1B} - \dot{\delta}_{1B} X_{2B}) dm \right] \\
& - \left[\frac{d}{dt} \bar{\delta}_{1B} + \omega_{2B} \bar{\delta}_{3B} - \omega_{3B} \bar{\delta}_{2B} \right] \left[\frac{1}{M_s} \int_B X_{3B} dm \right] + \left[\frac{d}{dt} \bar{\delta}_{3B} + \omega_{1B} \bar{\delta}_{2B} - \omega_{2B} \bar{\delta}_{1B} \right] \left[\frac{1}{M_s} \int_B X_{1B} dm \right]
\end{aligned}$$

$$= M_{2B} - \{F_{io}\}^T [a_{ij}] \begin{pmatrix} \frac{1}{M_s} \int_B X_{3B} dm \\ 0 \\ -\frac{1}{M_s} \int_B X_{1B} dm \end{pmatrix} \quad (5-26)$$

$$\begin{aligned}
& \frac{d}{dt} \left[\int_B (\dot{\delta}_{2B} X_{1B} - \dot{\delta}_{1B} X_{2B}) dm \right] + \omega_{1B} \left[\int_B (\dot{\delta}_{1B} X_{3B} - \dot{\delta}_{3B} X_{1B}) dm \right] - \omega_{2B} \left[\int_B (\dot{\delta}_{3B} X_{2B} - \dot{\delta}_{2B} X_{3B}) dm \right] \\
& + \left[\frac{d}{dt} \bar{\delta}_{1B} + \omega_{2B} \bar{\delta}_{3B} - \omega_{3B} \bar{\delta}_{2B} \right] \left[\frac{1}{M_s} \int_B X_{2B} dm \right] - \left[\frac{d}{dt} \bar{\delta}_{2B} + \omega_{3B} \bar{\delta}_{1B} - \omega_{1B} \bar{\delta}_{3B} \right] \left[\frac{1}{M_s} \int_B X_{1B} dm \right] \\
& = M_{3B} - \{z_{io}\}^T [a_{ij}] \begin{pmatrix} -\frac{1}{M_s} \int_B X_{2B} dm \\ \frac{1}{M_s} \int_B X_{1B} dm \\ 0 \end{pmatrix} \quad (5-27)
\end{aligned}$$

The above equations deal with the behavior of a reference frame fixed to a point of the body and rotating with the undeformed geometry of the body. The fact that a body is not rigid is treated by expressing the deformed position of a point in the body frame in terms of a set of generalized coordinates and any desired explicit functions of time. The position components X_{iB} are of a form such that motions relative to the undeformed position in the body frame are expressed in terms of products of (functions of a time varying amplitude) with (functions of the undeformed space variables in the body frame). The generalized coordinates are the time-varying amplitudes of these motions. The form of the equation of motion for one of these coordinates q_n is given by equation (5-29), where

$$q_n = A_{mn} \text{ or } B_{mn} \quad (5-28)$$

$$\begin{aligned}
& \frac{d}{dt} \left[\int_{nB} \left(\dot{\delta}_{1B} \frac{\partial \dot{X}_{1B}}{\partial \dot{q}_n} + \dot{\delta}_{2B} \frac{\partial \dot{X}_{2B}}{\partial \dot{q}_n} + \dot{\delta}_{3B} \frac{\partial \dot{X}_{3B}}{\partial \dot{q}_n} \right) dm \right] \\
& - \left[\int_{nB} \left(\dot{\delta}_{1B} \frac{\partial \dot{\delta}_{1B}}{\partial q_n} + \dot{\delta}_{2B} \frac{\partial \dot{\delta}_{2B}}{\partial q_n} + \dot{\delta}_{3B} \frac{\partial \dot{\delta}_{3B}}{\partial q_n} \right) dm \right] \\
& + \{\ddot{X}_{ioL}\} [a_{ij}] \left\{ \int_{nB} \frac{\partial \dot{X}_{jB}}{\partial \dot{q}_n} dm \right\} = F_{qn} \quad (5-29)
\end{aligned}$$

Introducing the relations (5-20) and (5-21) into equation (5-29) gives the following:

$$\begin{aligned}
& \frac{d}{dt} \left[\int_{nB} \left(\dot{\delta}_{1B} \frac{\partial \dot{X}_{1B}}{\partial \dot{q}_n} + \dot{\delta}_{2B} \frac{\partial \dot{X}_{2B}}{\partial \dot{q}_n} + \dot{\delta}_{3B} \frac{\partial \dot{X}_{3B}}{\partial \dot{q}_n} \right) dm \right] \\
& - \left[\int_{nB} \left(\dot{\delta}_{1B} \frac{\partial \dot{\delta}_{1B}}{\partial q_n} + \dot{\delta}_{2B} \frac{\partial \dot{\delta}_{2B}}{\partial q_n} + \dot{\delta}_{3B} \frac{\partial \dot{\delta}_{3B}}{\partial q_n} \right) dm \right] \\
& - \frac{1}{M_s} \left\{ \frac{d}{dt} \bar{\delta}_{iB} + \omega_{jB} \bar{\delta}_{kB} - \omega_{kB} \bar{\delta}_{jB} \right\}^T \left\{ \int_{nB} \frac{\partial \dot{X}_{iB}}{\partial \dot{q}_n} \right\} \\
& = F_{qn} - \frac{1}{M_s} \{F_{io}\}^T [q_{ij}] \left\{ \int_{nB} \frac{\partial \dot{X}_{jB}}{\partial \dot{q}_n} \right\} \quad (5-30)
\end{aligned}$$

5.2.2 RAE Geometry and Deformation Characteristics. -- The equations of motion have been written in terms of the body geometry as represented by X_{iB} . It is now necessary to write these expressions and

their integrals for the particular body under consideration. This body has three basic parts: a central core assumed rigid, a set of mast deployment mechanisms, and the set of mast antennas.

5.2.2.1 Central Core. -- For the central core, the various integrals can be evaluated symbolically:

$$\dot{x}_{1B} = \dot{x}_{2B} = \dot{x}_{3B} = 0$$

$$\frac{\partial \delta_{1B}}{\partial q_n} = \frac{\partial \delta_{2B}}{\partial q_n} = \frac{\partial \delta_{3B}}{\partial q_n} = 0 \quad (q_n = A_{mn} \text{ or } B_{mn})$$

$$\int_c x_{1B} dm = \int_c x_{2B} dm = \int_c x_{3B} dm = 0$$

$$\int_c (x_{2B}^2 + x_{3B}^2) dm = I_{11c} \quad \int_c x_{1B} x_{2B} dm = I_{12c}$$

$$\int_c (x_{1B}^2 + x_{3B}^2) dm = I_{22c} \quad \int_c x_{1B} x_{3B} dm = I_{13c}$$

$$\int_c (x_{1B}^2 + x_{2B}^2) dm = I_{33c} \quad \int_c x_{2B} x_{3B} dm = I_{23c} \quad (5-31)$$

5.2.2.2 Deployment Mechanism. -- A simple mathematical model is introduced for the deployment mechanism to ensure conservation of mass in the system during deployment (see figure 21).

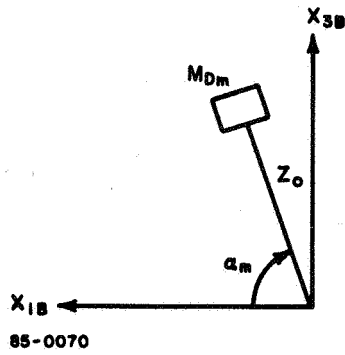


Figure 21 GEOMETRY OF DEPLOYMENT MECHANISM

For the m^{th} deployment mechanism, the position and velocity components and derivative of δ_{jB} in body coordinates are

$$\begin{aligned} X_{1B} &= Z_o \cos \alpha_m & \dot{X}_{1B} &= \dot{X}_{2B} = \dot{X}_{3B} = 0 \\ X_{2B} &= 0 \\ X_{3B} &= Z_o \sin \alpha_m & \frac{\partial \dot{\delta}_{jB}}{\partial q_n} &= 0 \quad (q_n = A_{mn} \text{ or } B_{mn}) \end{aligned}$$

The mass of the deployment mechanism (undeployed antenna) is:

$$M_{Dm} = M_{ma} - \rho l_m$$

The various integrals then have the following form:

$$\int_{mD} X_{1B} dm = Z_o c a_m [M_{ma} - \rho l_m] \quad \int_{mD} X_{2B} dm = 0 \quad \int_{mD} X_{3B} dm = Z_o s a_m [M_{ma} - \rho l_m]$$

$$\int_{mD} (X_{2B}^2 + X_{3B}^2) dm = Z_o^2 s^2 a_m [M_{ma} - \rho l_m] \quad \int_{mD} X_{1B} X_{2B} dm = 0$$

$$\int_{mD} (X_{1B}^2 + X_{3B}^2) dm = Z_o^2 [M_{ma} - \rho l_m] \quad \int_{mD} X_{1B} X_{3B} dm = Z_o^2 s a_m c a_m [M_{ma} - \rho l_m]$$

$$\int_{mD} (X_{1B}^2 + X_{2B}^2) dm = Z_o^2 c^2 a_m [M_{ma} - \rho l_m] \quad \int_{mD} X_{2B} X_{3B} dm = 0 \quad (5-32)$$

5.2.2.3 Antenna Booms. -- The antenna booms are located in the X_{1B} , X_{3B} plane as shown in figure 22. The displacements of a point on the antenna from its undeformed position are given by the three components u, v, w .

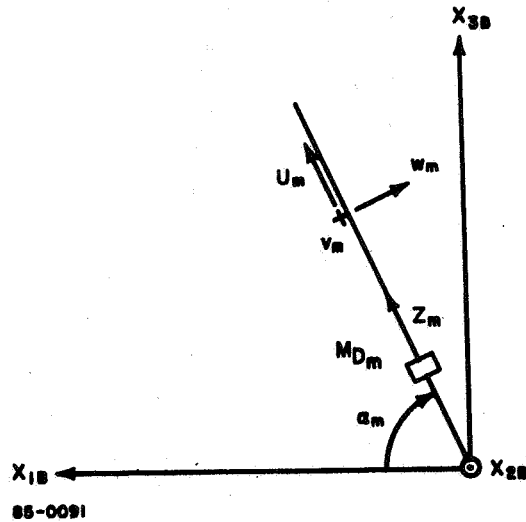


Figure 22 GEOMETRY OF ANTENNAS

The position of a point on the m^{th} antenna in the body reference frame is given as follows:

$$\begin{aligned} X_{1B} &= (Z_{om} + Z_m + u_m) c a_m - w_m s a_m \\ X_{2B} &= v_m \\ X_{3B} &= (Z_{om} + Z_m + u_m) s a_m + w_m c a_m \end{aligned} \quad (5-33)$$

The velocities of a point on the antenna are given by

$$\begin{aligned} \dot{X}_{1B} &= (\dot{Z}_m + \dot{u}_m) c a_m - \dot{w}_m s a_m \\ \dot{X}_{2B} &= \dot{v}_m \\ \dot{X}_{3B} &= (\dot{Z}_m + \dot{u}_m) s a_m + \dot{w}_m c a_m \end{aligned} \quad (5-34)$$

Since the axial strain along the beam is assumed negligible, the velocity \dot{Z}_m is independent of position Z : $\dot{Z}_m = \dot{l}_m$. Equations (5-34) then become

$$\begin{aligned} \dot{X}_{1B} &= (\dot{l}_m + \dot{u}_m) c a_m - \dot{w}_m s a_m \\ \dot{X}_{2B} &= \dot{v}_m \\ \dot{X}_{3B} &= (\dot{l}_m + \dot{u}_m) s a_m + \dot{w}_m c a_m \end{aligned} \quad (5-35)$$

The displacement functions for the antenna, v and w , are taken as cantilever small-displacement mode shapes (see figure 23). The axial displacement is determined by requiring that the axial strain vanish. These various functions are given as follows (reference 3):

$$\begin{aligned} v_m &= \sum_n A_{mn} \chi_n \left(\bar{k}_n \frac{Z_m}{l_m} \right) \\ w_m &= \sum_n B_{mn} \chi_n \left(\bar{k}_n \frac{Z_m}{l_m} \right) \end{aligned} \quad (5-36)$$

3. Timoshenko, S., Vibration Problems in Engineering, Van Nostrand Company, Inc., New York, N. Y. (1953).

1. IN-PLANE DEFLECTION OF m^{th} ANTENNA:

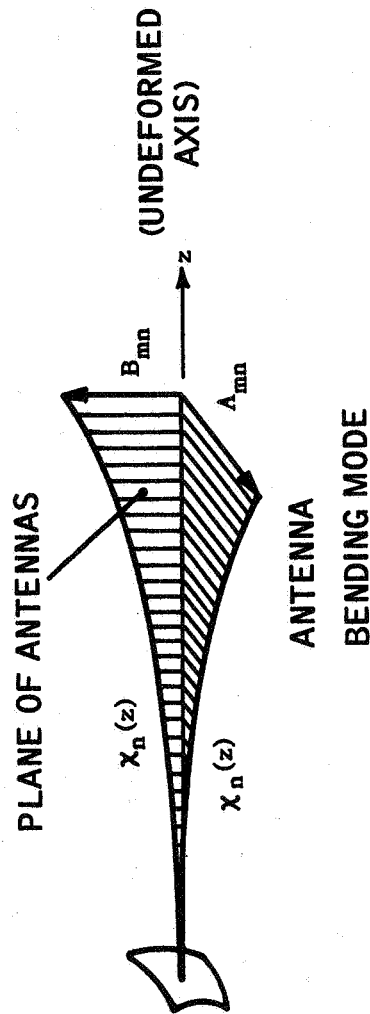
$$w_m(z, t) = \sum_n B_{mn}(t) X_n(z)$$

2. OUT-OF-PLANE DEFLECTION OF m^{th} ANTENNA:

$$v_m(z, t) = \sum_n A_{mn}(t) X_n(z)$$

$X_n(z)$ ARE NORMALIZED CANTILEVER MODE SHAPES

A_{mn}, B_{mn} ARE TIP DEFLECTIONS IN RESPECTIVE PLANES



65-10194-A

Figure 23 ANTENNA DEFLECTIONS

where $\chi_n \left(\bar{k}_n \frac{Z_m}{l_m} \right)$ satisfies the equation:

$$\frac{d^4 \chi_n}{d \left(\frac{Z_m}{l_m} \right)^4} + \bar{k}_n^4 \chi_n = 0 \quad (5-37)$$

At

$$\begin{aligned} \left(\frac{Z_m}{l_m} \right) = 0 & \quad \chi_n = 0, \chi_n' = 0 \\ \left(\frac{Z_m}{l_m} \right) = 1 & \quad \chi_n'' = 0, \chi_n''' = 0. \end{aligned}$$

The boundary conditions for χ_n give the following relation defining the values of the dimensionless parameter \bar{k}_n :

$$\cos \bar{k}_n \cosh \bar{k}_n = -1. \quad (5-38)$$

The numerical evaluation of the various constants used in this development is given in section 5.4.

The axial displacement u is given by requiring that an infinitesimal axial length in the deformed state be identical to the infinitesimal undeformed length. The equation governing u is therefore determined as follows (reference 4):

$$\left(1 + \frac{\partial u}{\partial Z} \right)^2 + \left(\frac{\partial v}{\partial Z} \right)^2 + \left(\frac{\partial w}{\partial Z} \right)^2 = 1 \quad (5-39)$$

$$\frac{\partial u}{\partial Z} = \sqrt{1 - \left[\left(\frac{\partial v}{\partial Z} \right)^2 + \left(\frac{\partial w}{\partial Z} \right)^2 \right]} - 1. \quad (5-40)$$

Expanding this about the point where the bracket is zero and retaining only the first term gives:

$$u_m = - \frac{1}{2l_m} \left[\sum_n A_{mn} \sum_p A_{mp} Z_{np} \left(\frac{Z_m}{l_m} \right) + \sum_n B_{mn} \sum_p B_{mp} Z_{np} \left(\frac{Z_m}{l_m} \right) \right]$$

4. Novozhilov, V. V., Foundations of the Nonlinear Theory of Elasticity, Graylock Press, Rochester, New York (1953).

where

$$Z_{np} = \int \chi'_n \left(\bar{k}_n \frac{Z_m}{l_m} \right) \chi'_p \left(\bar{k}_p \frac{Z_m}{l_m} \right) d \left(\frac{Z_m}{l_m} \right); \quad \chi'_n \left(\bar{k}_n \frac{Z_m}{l_m} \right) = \frac{d\chi_n}{d \left(\frac{Z_m}{l_m} \right)}$$

Z_{np} is an indefinite integral subject to the condition that $Z_{np}(0) = 0$. For simplicity in further development the following notation is introduced:

$$\bar{z} = \left(\frac{Z_m}{l_m} \right) \quad \chi_n \left(\bar{k}_n \frac{Z_m}{l_m} \right) = \chi_n \quad Z_{np} \left(\frac{Z_m}{l_m} \right) = Z_{np}$$

Employing this notation gives:

$$u_m = - \frac{1}{2l_m} \left[\sum_n A_{mn} \sum_p A_{mp} Z_{np} + \sum_n B_{mn} \sum_p B_{mp} Z_{np} \right]$$

$$v_m = \sum_n A_{mn} \chi_n$$

$$w_m = \sum_n B_{mn} \chi_n \quad (5-42)$$

During deployment the antenna length is time-dependent. The velocities are then as follows:

$$\begin{aligned}
\dot{u}_m &= -\frac{1}{l_m} \left[\sum_n \dot{A}_{mn} \sum_p A_{mp} Z_{np} + \sum_n \dot{B}_{mn} \sum_p B_{mp} Z_{np} \right] \\
&+ \frac{i_m}{2l_m^2} \left\{ \sum_n A_{mn} \sum_p A_{mp} \left[Z_{np} - (1 - \bar{z}) Z'_{np} \right] \right. \\
&\left. + \sum_n B_{mn} \sum_p B_{mp} \left[Z_{np} - (1 - \bar{z}) Z'_{np} \right] \right\} \\
\dot{v}_m &= \sum_n \dot{A}_{mn} \chi_n + \frac{i_m}{l_m} \sum_n A_{mn} (1 - \bar{z}) \chi'_n \\
\dot{w}_m &= \sum_n \dot{B}_{mn} \chi_n + \frac{i_m}{l_m} \sum_n B_{mn} (1 - \bar{z}) \chi'_n
\end{aligned} \tag{5-43}$$

The expression used herein for the axial displacement term u requires some further comment. By introducing a single-term expansion for the radical function it must be recognized that it is not proper to consider the square of u ; u^2 will be of the same order as the neglected terms in the expansion for u itself. Therefore in the subsequent formulation u^2 is always deleted. Also, the degree of approximation inherent in the use of a single term expansion for u must be further examined at a later time.

The terms required to express the equations of motion are now constructed to exhibit their dependence on the generalized coordinates:

$$X_{1B} = (Z_{om} + Z_m + u_m) c a_m - w_m s a_m$$

$$X_{2B} = v_m$$

$$X_{3B} = (Z_{om} + Z_m + u_m) s a_m + w_m c a_m$$

$$\dot{X}_{1B} = (\dot{i}_m + \dot{u}_m) c a_m - \dot{w}_m s a_m$$

$$\dot{X}_{2B} = \dot{v}_m$$

$$\dot{X}_{3B} = (\dot{i}_m + \dot{u}_m) s a_m + \dot{w}_m c a_m$$

$$\dot{\delta}_{1B} = \dot{X}_{1B} + \omega_{2B} X_{3B} - \omega_{3B} X_{2B}$$

$$\dot{\delta}_{2B} = \dot{X}_{2B} + \omega_{3B} X_{1B} - \omega_{1B} X_{3B}$$

$$\dot{\delta}_{3B} = \dot{X}_{3B} + \omega_{1B} X_{2B} - \omega_{2B} X_{1B}$$

$$\begin{aligned}\dot{\delta}_{3B} X_{2B} - \dot{\delta}_{2B} \dot{X}_{3B} &= \dot{X}_{3B} X_{2B} - X_{3B} \dot{X}_{2B} \\ &+ \omega_{1B} (X_{2B}^2 + X_{3B}^2) - \omega_{2B} X_{1B} X_{2B} - \omega_{3B} X_{1B} X_{3B}\end{aligned}$$

$$\begin{aligned}\dot{\delta}_{1B} X_{3B} - \dot{\delta}_{3B} X_{1B} &= \dot{X}_{1B} X_{3B} - X_{1B} \dot{X}_{3B} \\ &- \omega_{1B} X_{1B} X_{2B} + \omega_{2B} (X_{1B}^2 + X_{3B}^2) - \omega_{3B} X_{2B} X_{3B}\end{aligned}$$

$$\begin{aligned}\dot{\delta}_{2B} X_{1B} - \dot{\delta}_{1B} X_{2B} &= \dot{X}_{2B} X_{1B} - X_{2B} \dot{X}_{1B} \\ &- \omega_{1B} X_{1B} X_{3B} - \omega_{2B} X_{2B} X_{3B} + \omega_{3B} (X_{1B}^2 + X_{2B}^2)\end{aligned}$$

$$\dot{\delta}_{1B} \frac{\partial \dot{X}_{1B}}{\partial \dot{q}_n} = \frac{\partial \dot{X}_{1B}}{\partial \dot{q}_n} [\dot{X}_{1B} + \omega_{2B} X_{3B} - \omega_{3B} X_{2B}]$$

$$\dot{\delta}_{2B} \frac{\partial \dot{X}_{2B}}{\partial \dot{q}_n} = \frac{\partial \dot{X}_{2B}}{\partial \dot{q}_n} [\dot{X}_{2B} + \omega_{3B} X_{1B} - \omega_{1B} X_{3B}]$$

$$\dot{\delta}_{3B} \frac{\partial \dot{X}_{3B}}{\partial \dot{q}_n} = \frac{\partial \dot{X}_{3B}}{\partial \dot{q}_n} [\dot{X}_{3B} + \omega_{1B} X_{2B} - \omega_{2B} X_{1B}]$$

$$\dot{\delta}_{1B} \frac{\partial \dot{\delta}_{1B}}{\partial \dot{q}_n} = \left[\frac{\partial \dot{X}_{1B}}{\partial \dot{q}_n} + \omega_{2B} \frac{\partial X_{3B}}{\partial \dot{q}_n} - \omega_{3B} \frac{\partial X_{2B}}{\partial \dot{q}_n} \right] [\dot{X}_{1B} + \omega_{2B} X_{3B} - \omega_{3B} X_{2B}]$$

$$\dot{\delta}_{2B} \frac{\partial \dot{\delta}_{2B}}{\partial \dot{q}_n} = \left[\frac{\partial \dot{X}_{2B}}{\partial \dot{q}_n} + \omega_{3B} \frac{\partial X_{1B}}{\partial \dot{q}_n} - \omega_{1B} \frac{\partial X_{3B}}{\partial \dot{q}_n} \right] [\dot{X}_{2B} + \omega_{3B} X_{1B} - \omega_{1B} X_{3B}]$$

$$\dot{\delta}_{3B} \frac{\partial \dot{\delta}_{3B}}{\partial \dot{q}_n} = \left[\frac{\partial \dot{X}_{3B}}{\partial \dot{q}_n} + \omega_{1B} \frac{\partial X_{2B}}{\partial \dot{q}_n} - \omega_{2B} \frac{\partial X_{1B}}{\partial \dot{q}_n} \right] [\dot{X}_{3B} + \omega_{1B} X_{2B} - \omega_{2B} X_{1B}]$$

Expanding these terms and introducing the definitions of X_{iB} in terms of displacements gives the following set of integrals:

$$\int_{ma} X_{iB} dm$$

$$\int_{ma} \dot{X}_{iB} dm$$

$$\int_{ma} \dot{X}_{iB} \dot{X}_{jB} dm$$

$$\int_{ma} \dot{X}_{iB} \dot{X}_{jB} dm \quad i \neq j$$

$$\int_{ma} \frac{\partial \dot{X}_{iB}}{\partial \dot{q}_n} \dot{X}_{iB} dm$$

$$\int_{ma} \frac{\partial \dot{X}_{iB}}{\partial \dot{q}_n} \dot{X}_{jB} dm \quad i \neq j$$

$$\int_{ma} \frac{\partial \dot{X}_{iB}}{\partial q_n} \dot{X}_{iB} dm$$

$$\int_{ma} \frac{\partial \dot{X}_{iB}}{\partial q_n} \dot{X}_{jB} dm \quad i \neq j$$

$$\int_{ma} \frac{\partial X_{iB}}{\partial q_n} \dot{X}_{jB} dm \quad i \neq j$$

$$\int_{ma} \frac{\partial X_{iB}}{\partial q_n} X_{jB} dm$$

$$\begin{aligned}
\int_{ma} X_{1B} dm &= \left\{ c a_m \frac{\rho l_m^2}{2} \left(1 + 2 \frac{Z_o}{l_m} \right) - s a_m \rho l_m \left[\sum_n B_{mn} \bar{X}_{an} + c a_m \frac{\rho}{2} \sum_n \Lambda_{mp} \sum_p \Lambda_{mp} \bar{Z}_{anp} \right. \right. \\
&\quad \left. \left. + \sum_n B_{mn} \sum_p B_{mp} \bar{Z}_{anp} \right] \right\} \\
\int_{ma} X_{2B} dm &= \left\{ \rho l_m \sum_n \Lambda_{mn} \bar{X}_{an} \right\} \\
\int_{ma} X_{3B} dm &= \left\{ s a_m \frac{\rho l_m^2}{2} \left(1 + 2 \frac{Z_{om}}{l_m} \right) + c a_m \rho l_m \sum_n B_{mn} \bar{X}_{an} + s a_m \frac{\rho}{2} \left[\sum_n \Lambda_{mn} \sum_p \Lambda_{mp} \bar{Z}_{anp} \right. \right. \\
&\quad \left. \left. + \sum_n B_{mn} \sum_p B_{mp} \bar{Z}_{anp} \right] \right\}
\end{aligned}$$

5.2.3 Generalized Forces (External). -- The generalized forces associated with the gravity field and solar pressure are derived in the following sections.

5.2.3.1 Gravity. -- The vector components of the gravitational acceleration in the region occupied by the body are expanded in a first-order Taylor series about the satellite center of mass. In non-rotating coordinates,

$$\{q_{iL}\} = \{q_{ciL}\} + [G_{ij}] \{X_{jo} - X_{joc}\} \quad (5-44)$$

where the following notation has been used:

$$g_{iL} = g_{iL}(X_{jo})$$

$$g_{ciL} = g_{iL}(X_{joc})$$

$$G_{ij} = \frac{\partial g_{iL}}{\partial X_{jo}}(X_{joc})$$

$$X_{joc} = \frac{1}{M_s} \int_B X_{jo} dm$$

Observe next that

$$\begin{aligned}\{X_{jo} - X_{joc}\} &= \left\{ X_{jL} - \frac{1}{M_s} \int_B X_{jL} dm \right\} \\ &= [a_{jk}] \left\{ X_{kB} - \frac{1}{M_s} \int_B X_{kB} dm \right\}\end{aligned}$$

The components of gravitational force acting on an element of mass dm are then:

$$\{dF_{giL}\} = \{g_{ciL}\} + [G_{ij}] [a_{jk}] \left\{ X_{kB} - \frac{1}{M_s} \int_B X_{kB} dm \right\}. \quad (5-45)$$

Integrating this expression over the body yields the gravity forces associated with the coordinates X_{ioc} :

$$\{F_{giL}\} = \int_B \{dF_{giL}\} = \{g_{ciL}\} M_s. \quad (5-46)$$

To determine the gravity forces associated with the other generalized coordinates, the incremental forces must be transformed into body coordinates:

$$\{dF_{giB}\} = [a_{ij}]^T \{dF_{gjL}\} \quad (5-47)$$

$$\{dF_{giB}\} = [a_{ij}]^T \{g_{cjL}\} dm + [a_{ij}]^T [G_{jk}] [a_{kl}] \left\{ X_{lB} dm - \frac{dm}{M_s} \int_B X_{lB} dm \right\}$$

The gravity-gradient moments associated with the three body axes are given by

$$\{M_{giB}\} = \int_B \{X_{jB} dF_{gkB} - X_{kB} dF_{gjB}\} \quad (5-48)$$

where the subscripts i, j, k are cyclic. Making the appropriate substitutions results in the following moment equations:

$$M_{g1B} = -\{a_{i2}\}^T [G_{ij}] [a_{jk}] \left\{ \int_B X_{3B} X_{kB} dm - \frac{1}{M_s} \int_B X_{3B} dm \int_B X_{kB} dm \right\} \\ + \{a_{i3}\}^T [G_{ij}] [a_{jk}] \left\{ \int_B X_{2B} X_{kB} dm - \frac{1}{M_s} \int_B X_{2B} dm \int_B X_{kB} dm \right\} \quad (5-49)$$

$$M_{g2B} = \{a_{i1}\}^T [G_{ij}] [a_{jk}] \left\{ \int_B X_{3B} X_{kB} dm - \frac{1}{M_s} \int_B X_{3B} dm \int_B X_{kB} dm \right\} \\ - \{a_{i3}\}^T [G_{ij}] [a_{jk}] \left\{ \int_B X_{1B} X_{kB} dm - \frac{1}{M_s} \int_B X_{1B} dm \int_B X_{kB} dm \right\} \quad (5-50)$$

$$M_{g3B} = -\{a_{i1}\}^T [G_{ij}] [a_{jk}] \left\{ \int_B X_{2B} X_{kB} dm - \frac{1}{M_s} \int_B X_{2B} dm \int_B X_{kB} dm \right\} \\ + \{a_{i2}\}^T [G_{ij}] [a_{jk}] \left\{ \int_B X_{1B} X_{kB} dm - \frac{1}{M_s} \int_B X_{1B} dm \int_B X_{kB} dm \right\} \quad (5-51)$$

The generalized gravity-gradient forces associated with the coordinates A_{mn} and B_{mn} are obtained as follows:

$$q_n = A_{mn} \text{ or } B_{mn}$$

$$F_{g q_n} = \int_{ma} \left\{ \frac{\partial X_{iB}}{\partial q_n} \right\}^T \{ dF_{giB} \} \quad (5-52)$$

$$\begin{aligned} F_{g q_n} = & \{a_{i1}\}^T [G_{ij}] [a_{jk}] \left\{ \int_{ma} X_{kB} \frac{\partial X_{1B}}{\partial q_n} dm - \frac{1}{M_s} \int_B X_{kB} dm \int_{ma} \frac{\partial X_{1B}}{\partial q_n} dm \right\} \\ & + \{a_{i2}\}^T [G_{ij}] [a_{jk}] \left\{ \int_{ma} X_{kB} \frac{\partial X_{2B}}{\partial q_n} dm - \frac{1}{M_s} \int_B X_{kB} dm \int_{ma} \frac{\partial X_{2B}}{\partial q_n} dm \right\} \\ & + \{a_{i3}\}^T [G_{ij}] [a_{jk}] \left\{ \int_{ma} X_{kB} \frac{\partial X_{3B}}{\partial q_n} dm - \frac{1}{M_s} \int_B X_{kB} dm \int_{ma} \frac{\partial X_{3B}}{\partial q_n} dm \right\} \quad (5-53) \end{aligned}$$

In both the moment expressions and the generalized beam force expressions, the terms resulting from the gravitational acceleration at the satellite center of mass have been omitted. These terms drop out when the center of mass motion is separated from the local dynamics and removed from the equations. Note that the gravity-gradient matrix $[G_{ij}]$ nevertheless remains a function of C. M. position relative to the Earth.

5.2.3.2 Solar Pressure. -- A unit vector \vec{i}_s in the direction from the sun to the body is assumed given. This vector is defined in the local non-rotating frame and is computed separately in the digital computer program.

$$\vec{i}_s = d_{1L} \vec{i}_{1L} + d_{2L} \vec{i}_{2L} + d_{3L} \vec{i}_{3L} \quad (5-54)$$

The components of a unit vector \vec{i}_B along the local tangent of the antenna are given in the rotating body frame:

$$\vec{i}_B = e_{1B} \vec{i}_{1B} + e_{2B} \vec{i}_{2B} + e_{3B} \vec{i}_{3B} \quad (5-55)$$

Also, the components of a vector in the rotating body frame and the components of a vector in the non-rotating local frame are related:

$$\{e_{iL}\} = [a_{ij}]\{e_{jB}\} \quad \{d_{iB}\} = [a_{ij}]^T \{d_{jL}\}$$

The two vectors \vec{i}_s and \vec{i}_B form a plane. The component of \vec{i}_s lying in this plane, perpendicular to \vec{i}_B , is required. This vector is designated by \vec{i}_n :

$$\begin{aligned} \vec{i}_n &= \vec{i}_B \times (\vec{i}_s \times \vec{i}_B) \\ \vec{i}_n &= \vec{i}_s - (\vec{i}_s \cdot \vec{i}_B) \vec{i}_B \end{aligned} \quad (5-56)$$

In terms of the vector \vec{i}_n , the solar pressure force acting on an effective element of area ds can be written as follows:

$$d\vec{F}_{pB} = \vec{i}_{nB} |\vec{i}_{nB}| p_0 ds \quad (5-57)$$

where p_0 is the solar pressure at normal incidence on a perfect reflector, and the effective area increment for the cylindrical antenna of diameter $2h$ is

$$ds = \frac{2}{3} (2h) dz$$

$$\vec{i}_s \cdot \vec{i}_B = \{d_i\}^T [a_{ij}] \{e_{jB}\}$$

$$\{dF_{piB}\}^T = |\vec{i}_{nB}| p_0 ds \{d_j\}^T [a_{jk}] [\delta_{ik} - e_{iB} e_{kB}] \quad (5-58)$$

$$|\vec{i}_{nB}| = \left[1 - (\{d_i\}^T [a_{ij}] \{e_{jB}\})^2 \right]^{1/2} \quad (5-59)$$

The moments due to solar pressure including the correction for center of mass motion are given by

$$\begin{aligned}
M_{p1B} = & p_o \{d_i\}^T \{a_{i1}\} \left[\left[\int_B |\vec{i}_{nB}| e_{1B} e_{2B} X_{3B} ds \left(\frac{1}{M_s} \int_B X_{3B} dm \right) \int_B |\vec{i}_{nB}| e_{1B} e_{2B} ds \right] \right. \\
& - \left. \left[\int_B |\vec{i}_{nB}| e_{1B} e_{3B} X_{2B} ds - \left(\frac{1}{M_s} \int_B X_{2B} dm \right) \int_B |\vec{i}_{nB}| e_{1B} e_{3B} ds \right] \right] \\
& + p_o \{d_i\}^T \{a_{i2}\} \left[- \left[\int_B |\vec{i}_{nB}| (1 - e_{2B}^2) X_{3B} ds - \left(\frac{1}{M_s} \int_B X_{3B} dm \right) \int_B |\vec{i}_{nB}| (1 - e_{2B}^2) ds \right] \right. \\
& - \left. \left[\int_B |\vec{i}_{nB}| e_{2B} e_{3B} X_{2B} ds - \left(\frac{1}{M_s} \int_B X_{2B} dm \right) \int_B |\vec{i}_{nB}| e_{2B} e_{3B} ds \right] \right] \\
& + p_o \{d_i\}^T \{a_{i3}\} \left[\left[\int_B |\vec{i}_{nB}| e_{2B} e_{3B} X_{3B} ds - \left(\frac{1}{M_s} \int_B X_{2B} dm \right) \int_B |\vec{i}_{nB}| e_{2B} e_{3B} ds \right] \right. \\
& + \left. \left[\int_B |\vec{i}_{nB}| (1 - e_{3B}^2) X_{2B} ds - \left(\frac{1}{M_s} \int_B X_{2B} dm \right) \int_B |\vec{i}_{nB}| (1 - e_{3B}^2) ds \right] \right]
\end{aligned}
\tag{5-60}$$

$$\begin{aligned}
M_{p2B} = P_o \{d_i\}^T \{a_{i1}\} & \left[\int_B |\vec{i}_{nB}| (1 - e_{1B}^2) X_{3B} ds - \left(\frac{1}{M_s} \int_B X_{3B} dm \right) \int_B |\vec{i}_{nB}| (1 - e_{1B}^2) ds \right] \\
& + \left[\int_B |\vec{i}_{nB}| e_{1B} e_{3B} X_{1B} ds - \left(\frac{1}{M_s} \int_B X_{1B} dm \right) \int_B |\vec{i}_{nB}| e_{1B} e_{3B} ds \right] \\
& + P_o \{d_i\}^T \{a_{i2}\} \left[- \left[\int_B |\vec{i}_{nB}| e_{1B} e_{2B} X_{3B} ds - \left(\frac{1}{M_s} \int_B X_{3B} dm \right) \int_B |\vec{i}_{nB}| e_{1B} e_{2B} ds \right] \right. \\
& \quad \left. + \left[\int_B |\vec{i}_{nB}| e_{2B} e_{3B} X_{1B} ds - \left(\frac{1}{M_s} \int_B X_{1B} dm \right) \int_B |\vec{i}_{nB}| e_{2B} e_{3B} ds \right] \right] \\
& + P_o \{d_i\}^T \{a_{i3}\} \left[- \left[\int_B |\vec{i}_{nB}| e_{1B} e_{3B} X_{3B} ds - \left(\frac{1}{M_s} \int_B X_{3B} dm \right) \int_B |\vec{i}_{nB}| e_{1B} e_{3B} ds \right] \right. \\
& \quad \left. - \left[\int_B |\vec{i}_{nB}| (1 - e_{3B}^2) X_{1B} ds - \left(\frac{1}{M_s} \int_B X_{1B} dm \right) \int_B |\vec{i}_{nB}| (1 - e_{3B}^2) ds \right] \right]
\end{aligned}$$

(5-61)

$$\begin{aligned}
M_{p3B} = & p_o \{d_i\}^T \{a_{i1}\} \left[- \left[\int_B |\vec{i}_{nB}| (1 - e_{1B}^2) X_{2B} ds - \left(\frac{1}{M_s} \int_B X_{2B} dm \right) \int_B |\vec{i}_{nB}| (1 - e_{1B}^2) ds \right] \right. \\
& \left. - \left[\int_B |\vec{i}_{nB}| e_{1B} e_{2B} X_{1B} ds - \left(\frac{1}{M_s} \int_B X_{1B} dm \right) \int_B |\vec{i}_{nB}| e_{1B} e_{2B} ds \right] \right] \\
& + p_o \{d_i\}^T \{a_{i2}\} \left[\left[\int_B |\vec{i}_{nB}| e_{1B} e_{2B} X_{2B} ds - \left(\frac{1}{M_s} \int_B X_{2B} dm \right) \int_B |\vec{i}_{nB}| e_{1B} e_{2B} ds \right] \right. \\
& \left. + \left[\int_B |\vec{i}_{nB}| (1 - e_{2B}^2) X_{1B} ds - \left(\frac{1}{M_s} \int_B X_{1B} dm \right) \int_B |\vec{i}_{nB}| (1 - e_{2B}^2) ds \right] \right] \\
& + p_o \{d_i\}^T \{a_{i3}\} \left[\left[\int_B |\vec{i}_{nB}| e_{1B} e_{3B} X_{2B} ds - \left(\frac{1}{M_s} \int_B X_{2B} dm \right) \int_B |\vec{i}_{nB}| e_{1B} e_{3B} ds \right] \right. \\
& \left. - \left[\int_B |\vec{i}_{nB}| e_{2B} e_{3B} X_{1B} ds - \left(\frac{1}{M_s} \int_B X_{1B} dm \right) \int_B |\vec{i}_{nB}| e_{2B} e_{3B} ds \right] \right]_{(5-62)}
\end{aligned}$$

The generalized solar pressure forces associated with the generalized antenna coordinates (q_n, A_{mn} or B_{mn}) are given by

$$\begin{aligned}
 F_{pq_n} = & p_o \{d_i\}^T \{a_{i1}\} \left[\left[\int_{ma} |\vec{i}_{nB}| (1 - e_{1B}^2) \frac{\partial X_{1B}}{\partial q_n} ds - \left(\frac{1}{M_s} \int_{ma} \frac{\partial X_{1B}}{\partial q_n} dm \right) \int_B |\vec{i}_{nB}| (1 - e_{1B}^2) ds \right] \right. \\
 & - \left[\int_{ma} |\vec{i}_{nB}| e_{1B} e_{2B} \frac{\partial X_{2B}}{\partial q_n} ds - \left(\frac{1}{M_s} \int_{ma} \frac{\partial X_{2B}}{\partial q_n} dm \right) \int_B |\vec{i}_{nB}| e_{1B} e_{2B} ds \right] \\
 & - \left. \left[\int_{ma} |\vec{i}_{nB}| e_{1B} e_{3B} \frac{\partial X_{3B}}{\partial q_n} ds - \left(\frac{1}{M_s} \int_{ma} \frac{\partial X_{3B}}{\partial q_n} dm \right) \int_B |\vec{i}_{nB}| e_{1B} e_{3B} ds \right] \right] \\
 & + p_o \{d_i\}^T \{a_{i2}\} \left[- \left[\int_{ma} |\vec{i}_{nB}| e_{1B} e_{2B} \frac{\partial X_{1B}}{\partial q_n} ds - \left(\frac{1}{M_s} \int_{ma} \frac{\partial X_{1B}}{\partial q_n} dm \right) \int_B |\vec{i}_{nB}| e_{1B} e_{3B} ds \right] \right. \\
 & + \left[\int_{ma} |\vec{i}_{nB}| (1 - e_{2B}^2) \frac{\partial X_{2B}}{\partial q_n} ds - \left(\frac{1}{M_s} \int_{ma} \frac{\partial X_{2B}}{\partial q_n} dm \right) \int_B |\vec{i}_{nB}| (1 - e_{2B}^2) ds \right] \\
 & - \left. \left[\int_{ma} |\vec{i}_{nB}| e_{2B} e_{3B} \frac{\partial X_{3B}}{\partial q_n} ds - \left(\frac{1}{M_s} \int_{ma} \frac{\partial X_{3B}}{\partial q_n} dm \right) \int_B |\vec{i}_{nB}| e_{2B} e_{3B} ds \right] \right] \\
 & + p_o \{d_i\}^T \{a_{i3}\} \left[- \left[\int_{ma} |\vec{i}_{nB}| e_{1B} e_{3B} \frac{\partial X_{1B}}{\partial q_n} ds - \left(\frac{1}{M_s} \int_{ma} \frac{\partial X_{1B}}{\partial q_n} dm \right) \int_B |\vec{i}_{nB}| e_{1B} e_{3B} ds \right] \right. \\
 & - \left[\int_{ma} |\vec{i}_{nB}| e_{2B} e_{3B} \frac{\partial X_{2B}}{\partial q_n} ds - \left(\frac{1}{M_s} \int_{ma} \frac{\partial X_{2B}}{\partial q_n} dm \right) \int_B |\vec{i}_{nB}| e_{2B} e_{3B} ds \right] \\
 & + \left. \left[\int_{ma} |\vec{i}_{nB}| (1 - e_{3B}^2) \frac{\partial X_{3B}}{\partial q_n} ds - \left(\frac{1}{M_s} \int_{ma} \frac{\partial X_{3B}}{\partial q_n} dm \right) \int_B |\vec{i}_{nB}| (1 - e_{3B}^2) ds \right] \right]
 \end{aligned}$$

(5-63)

The various terms and integrals used in the solar pressure loadings are given in the following pages.

$$e_{1B} = \left(1 + \frac{\partial u_m}{\partial z}\right) c a_m - \frac{\partial w}{\partial z} s a_m$$

$$e_{2B} = \frac{\partial v}{\partial z}$$

$$e_{3B} = \left(1 + \frac{\partial u_m}{\partial z}\right) s a_m + \frac{\partial w_m}{\partial z} c a_m \quad (5-64)$$

$$\int_{ma} |\vec{i}_{nB}| e_{iB} e_{jB} ds \quad i \neq j$$

$$\int_{ma} |\vec{i}_{nB}| (1 - e_{iB}^2) ds$$

$$\int_{ma} |\vec{i}_{nB}| e_{iB} e_{jB} X_{kB} ds \quad i \neq j$$

$$\int_{ma} |\vec{i}_{nB}| (1 - e_{iB}^2) X_{jB} ds \quad i \neq j$$

$$\int_{ma} |\vec{i}_{nB}| e_{iB} e_{jB} \frac{\partial X_{jB}}{\partial q_n} ds \quad i \neq j$$

$$\int_{ma} |\vec{i}_{nB}| (1 - e_{iB}^2) \frac{\partial X_{iB}}{\partial q_n} ds$$

5.2.4 Generalized Forces (Internal). -- The initial determination of the generalized forces associated with deformation and temperature gradients is limited to the consideration of small displacements. The large displacement treatment of these generalized forces will be included in the final report for Phase B.

5.2.4.1 Forces Due to Deformation. -- The strain energy due to bending for a cantilever beam is given by the following relation:

$$V = \frac{EI}{2l_m^3} \sum_n \bar{k}_n^4 q_n^2 \int_{ma0}^1 \chi_n^2(\bar{z}) d\bar{z} \quad (5-65)$$

The generalized force associated with a potential is given by

$$F_{sq_n} = - \frac{\partial V}{\partial q_n}$$

$$F_{sq_n} = - \frac{\bar{k}_n^4 EI}{l_m^3} q_n \int_0^1 \chi_n^2(\bar{z}) d\bar{z} \quad (5-66)$$

5.2.4.2 Forces Due to Temperature Gradients. -- The effect of a temperature gradient is obtained by using the standard relation for temperature stress:

$$\sigma_z = -E\alpha T$$

Evaluating the work done in an incremental displacement δq_n gives the generalized force associated with the temperature differential across the beam section, ΔT_{q_n} .

$$F_{Tq_n} = \frac{\bar{k}_n EI \alpha}{2hl_m} \int_0^1 \Delta T_{q_n} \bar{k}_n \chi_n''(\bar{z}) d\bar{z} \quad (5-67)$$

It is assumed that the temperature varies linearly across the beam diameter. The magnitude of the temperature differential in the direction of the displacement q_n is obtained by taking the appropriate component as illustrated in the derivation of the solar pressure loadings. This gives the following relation for the generalized forces associated with the temperature gradient, assuming also a constant gradient along the length of the member computed on the basis of the undeformed geometry:

$$F_{T_{A_{mn}}} = k_{T_n} \Delta T_o \{d_i\}^T \{a_{i2}\} \quad (5-68)$$

$$F_{T_{B_{mn}}} = k_{T_n} \Delta T_o [-s a_m \{d_i\}^T \{a_{i1}\} + c a_m \{d_i\}^T \{a_{i3}\}] \quad (5-69)$$

$$k_{T_n} = \frac{\bar{k}_n E I a}{2 h l_m} \chi'_n(1) \quad (5-70)$$

ΔT_o is the temperature differential experienced under the condition of normal incidence.

5.2.4.3 Forces Due to Damping. -- The effect of internal losses in the motion of the antenna is taken into account by a force of the standard damping form in the equation for any beam mode.

$$F_{Dq_n} = -D_n \dot{q}_n \quad (5-71)$$

where

$$D_n = 2 \zeta_n \bar{k}_n^2 \rho l \bar{\chi}_{cn} \sqrt{\frac{EI}{\rho l^4}} \quad (5-72)$$

A detailed discussion of damping is given in appendix A.

5.3 SUMMARY OF EQUATIONS OF MOTION

5.3.1 Position of Center of Mass of Central Core. --

$$\begin{aligned} & M_s \ddot{x}_{iCL} \\ & + \dot{\omega}_{1B} \left[a_{i3} \int_B X_{2B} dm - a_{i2} \int_B X_{3B} dm \right] \\ & + \dot{\omega}_{2B} \left[a_{i1} \int_B X_{3B} dm - a_{i3} \int_B X_{1B} dm \right] \\ & + \dot{\omega}_{3B} \left[a_{i2} \int_B X_{1B} dm - a_{i1} \int_B X_{2B} dm \right] \end{aligned}$$

$$\begin{aligned}
& + a_{i1} \left[\frac{d}{dt} \int_B \dot{X}_{1B} dm \right] \\
& + a_{i2} \left[\frac{d}{dt} \int_B \dot{X}_{2B} dm \right] \\
& + a_{i3} \left[\frac{d}{dt} \int_B \dot{X}_{3B} dm \right] \\
& + a_{i1} \left\{ \omega_{2B} \left[\frac{d}{dt} \int_B X_{3B} dm + \int_B \dot{X}_{3B} dm \right] - \omega_{3B} \left[\frac{d}{dt} \int_B X_{2B} dm + \int_B \dot{X}_{2B} dm \right] \right\} \\
& + a_{i2} \left\{ \omega_{3B} \left[\frac{d}{dt} \int_B X_{1B} dm + \int_B \dot{X}_{1B} dm \right] - \omega_{1B} \left[\frac{d}{dt} \int_B X_{3B} dm + \int_B \dot{X}_{3B} dm \right] \right\} \\
& + a_{i3} \left\{ \omega_{1B} \left[\frac{d}{dt} \int_B X_{2B} dm + \int_B \dot{X}_{2B} dm \right] - \omega_{2B} \left[\frac{d}{dt} \int_B X_{1B} dm + \int_B \dot{X}_{1B} dm \right] \right\} \\
& + a_{i1} \left\{ -(\omega_{2B}^2 + \omega_{3B}^2) \int_B X_{1B} dm + \omega_{1B} \omega_{2B} \int_B X_{2B} dm + \omega_{1B} \omega_{3B} \int_B X_{3B} dm \right\} \\
& + a_{i2} \left\{ \omega_{1B} \omega_{2B} \int_B X_{1B} dm - (\omega_{1B}^2 + \omega_{3B}^2) \int_B X_{2B} dm + \omega_{2B} \omega_{3B} \int_B X_{3B} dm \right\} \\
& + a_{i3} \left\{ \omega_{1B} \omega_{3B} \int_B X_{1B} dm + \omega_{2B} \omega_{3B} \int_B X_{2B} dm - (\omega_{1B}^2 + \omega_{2B}^2) \int_B X_{3B} dm \right\} = 0
\end{aligned}$$

(5-73)

5.3.2 Angular Orientation of Body Frame. --

$$\begin{aligned}
& \ddot{\bar{X}}_{1cL} \left[a_{13} \int_B X_{2B} dm - a_{12} \int_B X_{3B} dm \right] \\
& + \ddot{\bar{X}}_{2CL} \left[a_{23} \int_B X_{2B} dm - a_{22} \int_B X_{3B} dm \right] \\
& + \ddot{\bar{X}}_{3CL} \left[a_{33} \int_B X_{2B} dm - a_{32} \int_B X_{3B} dm \right] \\
& + \dot{\omega}_{1B} \left[\int_B (X_{2B}^2 + X_{3B}^2) dm \right] \\
& - \dot{\omega}_{2B} \left[\int_B X_{1B} X_{2B} dm \right] \\
& - \dot{\omega}_{3B} \left[\int_B X_{1B} X_{3B} dm \right] \\
& + \frac{d}{dt} \left[\int_B (\dot{X}_{3B} X_{2B} - X_{3B} \dot{X}_{2B}) dm \right] \\
& + \omega_{1B} \frac{d}{dt} \left[\int_B (X_{2B}^2 + X_{3B}^2) dm \right] \\
& - \omega_{2B} \left[\frac{d}{dt} \int_B X_{1B} X_{2B} dm - \int_B (\dot{X}_{2B} X_{1B} - X_{2B} \dot{X}_{1B}) dm \right] \\
& - \omega_{3B} \left[\frac{d}{dt} \int_B X_{1B} X_{3B} dm + \int_B (\dot{X}_{1B} X_{3B} - X_{1B} \dot{X}_{3B}) dm \right] \\
& - \omega_{1B} \omega_{2B} \left[\int_B X_{1B} X_{3B} dm \right] \\
& + \omega_{1B} \omega_{3B} \left[\int_B X_{1B} X_{2B} dm \right] \\
& + \omega_{2B} \omega_{3B} \left[\int_B (X_{1B}^2 + X_{2B}^2) dm - \int_B (X_{1B}^2 + X_{3B}^2) dm \right] \\
& + (\omega_{3B}^2 - \omega_{2B}^2) \int_B X_{2B} X_{3B} dm = M_{g1B} + M_{p1B} \quad (5-74)
\end{aligned}$$

$$\begin{aligned}
& \ddot{\bar{X}}_{1cL} \left[a_{11} \int_B \bar{X}_{3B} dm - a_{13} \int_B \bar{X}_{1B} dm \right] \\
& + \ddot{\bar{X}}_{2cL} \left[a_{21} \int_B \bar{X}_{3B} dm - a_{23} \int_B \bar{X}_{1B} dm \right] \\
& + \ddot{\bar{X}}_{3cL} \left[a_{31} \int_B \bar{X}_{3B} dm - a_{33} \int_B \bar{X}_{1B} dm \right] \\
& - \dot{\omega}_{1B} \left[\int_B \bar{X}_{1B} \bar{X}_{2B} dm \right] \\
& + \dot{\omega}_{2B} \left[\int_B (\bar{X}_{1B}^2 + \bar{X}_{3B}^2) dm \right] \\
& - \dot{\omega}_{3B} \left[\int_B \bar{X}_{2B} \bar{X}_{3B} dm \right] \\
& + \frac{d}{dt} \left[\int_B (\dot{\bar{X}}_{1B} \bar{X}_{3B} - \bar{X}_{1B} \dot{\bar{X}}_{3B}) dm \right] \\
& - \omega_{1B} \left[\frac{d}{dt} \int_B \bar{X}_{1B} \bar{X}_{2B} dm + \int_B (\dot{\bar{X}}_{2B} \bar{X}_{1B} - \bar{X}_{2B} \dot{\bar{X}}_{1B}) dm \right] \\
& + \omega_{2B} \left[\frac{d}{dt} \int_B (\bar{X}_{1B}^2 + \bar{X}_{3B}^2) dm \right] \\
& - \omega_{3B} \left[\frac{d}{dt} \int_B \bar{X}_{2B} \bar{X}_{3B} dm - \int_B (\dot{\bar{X}}_{3B} \bar{X}_{2B} - \bar{X}_{3B} \dot{\bar{X}}_{2B}) dm \right] \\
& + \omega_{1B} \omega_{2B} \left[\int_B \bar{X}_{2B} \bar{X}_{3B} dm \right] \\
& + \omega_{1B} \omega_{3B} \left[\int_B (\bar{X}_{2B}^2 + \bar{X}_{3B}^2) dm - \int_B (\bar{X}_{1B}^2 + \bar{X}_{2B}^2) dm \right] \\
& - \omega_{2B} \omega_{3B} \left[\int_B \bar{X}_{1B} \bar{X}_{2B} dm \right] \\
& + (\omega_{1B}^2 - \omega_{3B}^2) \left[\int_B \bar{X}_{1B} \bar{X}_{3B} dm \right] = M_{g2B} + M_{p2B} \tag{5-75}
\end{aligned}$$

$$\begin{aligned}
& \ddot{\bar{X}}_{1cL} \left[a_{12} \int_B X_{1B} dm - a_{11} \int_B X_{2B} dm \right] \\
& + \ddot{\bar{X}}_{2cL} \left[a_{22} \int_B X_{1B} dm - a_{21} \int_B X_{2B} dm \right] \\
& + \ddot{\bar{X}}_{3cL} \left[a_{32} \int_B X_{1B} dm - a_{31} \int_B X_{2B} dm \right] \\
& - \dot{\omega}_{1B} \left[\int_B X_{1B} X_{3B} dm \right] \\
& - \dot{\omega}_{2B} \left[\int_B X_{2B} X_{2B} dm \right] \\
& + \dot{\omega}_{3B} \left[\int_B (X_{1B}^2 + X_{2B}^2) dm \right] \\
& + \frac{d}{dt} \left[\int_B (\dot{X}_{2B} X_{1B} - X_{2B} \dot{X}_{1B}) dm \right] \\
& - \omega_{1B} \left[\frac{d}{dt} \int_B X_{1B} X_{3B} dm - \int_B (\dot{X}_{1B} X_{3B} - X_{1B} \dot{X}_{3B}) dm \right] \\
& - \omega_{2B} \left[\frac{d}{dt} \int_B X_{2B} X_{3B} dm + \int_B (\dot{X}_{3B} X_{2B} - X_{3B} \dot{X}_{2B}) dm \right] \\
& + \omega_{3B} \left[\frac{d}{dt} \int_B (X_{1B}^2 + X_{2B}^2) dm \right] \\
& + \omega_{1B} \omega_{2B} \left[\int_B (X_{1B}^2 + X_{3B}^2) dm - \int_B (X_{2B}^2 + X_{3B}^2) dm \right] \\
& - \omega_{1B} \omega_{3B} \left[\int_B X_{2B} X_{3B} dm \right] \\
& + \omega_{2B} \omega_{3B} \left[\int_B X_{1B} X_{3B} dm \right] \\
& + (\omega_{2B}^2 - \omega_{1B}^2) \left[\int_B X_{1B} X_{2B} dm \right] = M_{g3B} + M_{p3B} \tag{5-76}
\end{aligned}$$

5.3.3 Relative Deformation of Antenna Booms. --

$$\begin{aligned}
& \{\ddot{\mathbf{X}}_{icL}\}^T [\mathbf{a}_{ij}] \left\{ \int_{ma} \frac{\partial \dot{\mathbf{X}}_{jB}}{\partial \dot{q}_n} dm \right\} \\
& + \dot{\omega}_{1B} \left[\int_{ma} \left(\mathbf{X}_{2B} \frac{\partial \dot{\mathbf{X}}_{3B}}{\partial \dot{q}_n} - \mathbf{X}_{3B} \frac{\partial \dot{\mathbf{X}}_{2B}}{\partial \dot{q}_n} \right) dm \right] \\
& + \dot{\omega}_{2B} \left[\int_{ma} \left(\mathbf{X}_{3B} \frac{\partial \dot{\mathbf{X}}_{1B}}{\partial \dot{q}_n} - \mathbf{X}_{1B} \frac{\partial \dot{\mathbf{X}}_{3B}}{\partial \dot{q}_n} \right) dm \right] \\
& + \dot{\omega}_{3B} \left[\int_{ma} \left(\mathbf{X}_{1B} \frac{\partial \dot{\mathbf{X}}_{2B}}{\partial \dot{q}_n} - \mathbf{X}_{2B} \frac{\partial \dot{\mathbf{X}}_{1B}}{\partial \dot{q}_n} \right) dm \right] \\
& + \frac{d}{dt} \left[\int_{ma} \left(\dot{\mathbf{X}}_{1B} \frac{\partial \dot{\mathbf{X}}_{1B}}{\partial \dot{q}_n} + \dot{\mathbf{X}}_{2B} \frac{\partial \dot{\mathbf{X}}_{2B}}{\partial \dot{q}_n} + \dot{\mathbf{X}}_{3B} \frac{\partial \dot{\mathbf{X}}_{3B}}{\partial \dot{q}_n} \right) dm \right] \\
& - \left[\int_{ma} \left(\dot{\mathbf{X}}_{1B} \frac{\partial \dot{\mathbf{X}}_{1B}}{\partial \dot{q}_n} + \mathbf{X}_{2B} \frac{\partial \dot{\mathbf{X}}_{2B}}{\partial \dot{q}_n} + \dot{\mathbf{X}}_{3B} \frac{\partial \dot{\mathbf{X}}_{3B}}{\partial \dot{q}_n} \right) dm \right] \\
& + \omega_{1B} \left[\frac{d}{dt} \int_{ma} \left(\mathbf{X}_{2B} \frac{\partial \dot{\mathbf{X}}_{3B}}{\partial \dot{q}_n} - \mathbf{X}_{3B} \frac{\partial \dot{\mathbf{X}}_{2B}}{\partial \dot{q}_n} \right) dm + \int_{ma} \left(\dot{\mathbf{X}}_{2B} \frac{\partial \dot{\mathbf{X}}_{3B}}{\partial \dot{q}_n} - \dot{\mathbf{X}}_{3B} \frac{\partial \dot{\mathbf{X}}_{2B}}{\partial \dot{q}_n} \right) dm \right] \\
& + \omega_{2B} \left[\frac{d}{dt} \int_{ma} \left(\mathbf{X}_{3B} \frac{\partial \dot{\mathbf{X}}_{1B}}{\partial \dot{q}_n} - \mathbf{X}_{1B} \frac{\partial \dot{\mathbf{X}}_{3B}}{\partial \dot{q}_n} \right) dm + \int_{ma} \left(\dot{\mathbf{X}}_{3B} \frac{\partial \dot{\mathbf{X}}_{1B}}{\partial \dot{q}_n} - \dot{\mathbf{X}}_{1B} \frac{\partial \dot{\mathbf{X}}_{3B}}{\partial \dot{q}_n} \right) dm \right] \\
& + \omega_{3B} \left[\frac{d}{dt} \int_{ma} \left(\mathbf{X}_{1B} \frac{\partial \dot{\mathbf{X}}_{2B}}{\partial \dot{q}_n} - \mathbf{X}_{2B} \frac{\partial \dot{\mathbf{X}}_{1B}}{\partial \dot{q}_n} \right) dm + \int_{ma} \left(\dot{\mathbf{X}}_{1B} \frac{\partial \dot{\mathbf{X}}_{2B}}{\partial \dot{q}_n} - \dot{\mathbf{X}}_{2B} \frac{\partial \dot{\mathbf{X}}_{1B}}{\partial \dot{q}_n} \right) dm \right] \\
& - (\omega_{2B}^2 + \omega_{3B}^2) \left[\int_{ma} \mathbf{X}_{1B} \frac{\partial \dot{\mathbf{X}}_{1B}}{\partial \dot{q}_n} dm \right] - (\omega_{1B}^2 + \omega_{3B}^2) \left[\int_{ma} \mathbf{X}_{2B} \frac{\partial \dot{\mathbf{X}}_{2B}}{\partial \dot{q}_n} dm \right] - (\omega_{1B}^2 + \omega_{2B}^2) \left[\int_{ma} \mathbf{X}_{3B} \frac{\partial \dot{\mathbf{X}}_{3B}}{\partial \dot{q}_n} dm \right] \\
& + \omega_{1B} \omega_{2B} \left[\int_{ma} \left(\mathbf{X}_{2B} \frac{\partial \dot{\mathbf{X}}_{1B}}{\partial \dot{q}_n} + \mathbf{X}_{1B} \frac{\partial \dot{\mathbf{X}}_{2B}}{\partial \dot{q}_n} \right) dm \right]
\end{aligned}$$

(Eq. 5.77 cont'd on next page)

$$\begin{aligned}
& + \omega_{1B} \omega_{3B} \left[\int_{ma} \left(X_{3B} \frac{\partial X_{1B}}{\partial q_n} + X_{1B} \frac{\partial X_{3B}}{\partial q_n} \right) dm \right] \\
& + \omega_{2B} \omega_{3B} \left[\int_{ma} \left(X_{3B} \frac{\partial X_{2B}}{\partial q_n} + X_{2B} \frac{\partial X_{3B}}{\partial q_n} \right) dm \right] = F_{g_{q_n}} + F_{p_{q_n}} + F_{s_{q_n}} + F_{T_{q_n}} + F_{D_{q_n}} \quad (5-77)
\end{aligned}$$

The various integral terms in equations (5-73) through (5-77) can be expanded in terms of the beam coordinates A_{mn} and B_{mn} by substitution of relations (5-34) through (5-36) where appropriate. These expansions have been carried out, and first order terms in A_{mn} and B_{mn} included in the present flexible-body digital computer program. The details of the expanded equations will be summarized in the final report for Phase B of the dynamics study.

5.4 DETERMINATION OF CONSTANTS. -- The various definite integrals developed in the derivation of the equations of motion are evaluated in this section. The mode shape function used is the linear-theory cantilever mode shape given by

$$X_n(\bar{k}_n \bar{Z}) = C_{1n} [\sin(\bar{k}_n \bar{Z}) - \sinh(\bar{k}_n \bar{Z})] + C_{2n} [\cos(\bar{k}_n \bar{Z}) - \cosh(\bar{k}_n \bar{Z})] \quad (5-78)$$

where

$$\begin{aligned}
C_{1n} &= \frac{\cos \bar{k}_n + \cosh \bar{k}_n}{2 \sin \bar{k}_n \cosh \bar{k}_n - 2 \cos \bar{k}_n \sinh \bar{k}_n} \\
C_{2n} &= - \frac{\sin \bar{k}_n + \sinh \bar{k}_n}{2 \sin \bar{k}_n \cosh \bar{k}_n - 2 \cos \bar{k}_n \sinh \bar{k}_n}
\end{aligned}$$

The expressions for the various constants are as follows:

$$\begin{aligned}
a. \quad \bar{X}_{an} &= \int_0^1 X_n d\bar{Z} \\
\bar{X}_{an} &= \frac{1}{\bar{k}_n} \left[\frac{\cos \bar{k}_n + \cosh \bar{k}_n}{\sin \bar{k}_n \cosh \bar{k}_n - \cos \bar{k}_n \sinh \bar{k}_n} \right] = \frac{2 C_{1n}}{\bar{k}_n} \quad (5-79)
\end{aligned}$$

$$\begin{aligned}
\text{b. } \bar{X}_{bn} &= \int_0^1 \bar{Z} \chi_n d\bar{Z} \\
\bar{X}_{bn} &= \frac{1}{\bar{k}_n^2} \left[\frac{\sin \bar{k}_n + \sinh \bar{k}_n}{\sin \bar{k}_n \cosh \bar{k}_n - \cos \bar{k}_n \sinh \bar{k}_n} \right] = -\frac{2 C_{2n}}{\bar{k}_n^2} \quad (5-80)
\end{aligned}$$

$$\begin{aligned}
\text{c. } \bar{X}_{cn} &= \int_0^1 \chi_n^2 d\bar{Z} \\
\bar{X}_{cn} &= \frac{1}{4} \text{ for all } n \quad (5-81)
\end{aligned}$$

The function associated with the axial displacement term is given by

$$Z_{np}(Z) = \int \chi_n' \chi_p' dZ \quad (5-82)$$

and $Z_{mp}(0) = 0$

5.5 LIST OF SYMBOLS

- A_{mn} Amplitude of the nth mode of the mth antenna in X_{2B} direction
- $[a_{ij}]$ Matrix of direction cosines transforming vector components from body-fixed coordinates to local non-rotating coordinates:
- $$\{X_L\} = [a_{ij}] \{X_{jB}\}$$
- B_{mn} Amplitude of the nth mode of the mth antenna in the $X_{1B} X_{3B}$ plane perpendicular to the undeformed axis
- D_n Generalized damping coefficient for nth mode of antenna
- d_i Components of unit sun-vehicle vector
- E Young's modulus for antenna material
- e_i Components of unit vector tangent to satellite surface

F_{iL}	Components of total external force in the local non-rotating reference frame
F_{q_n}	Generalized forces associated with a coordinate q_n
$[G_{ij}]$	Gravity gradient matrix in non-rotating reference frame
g_i	Components of gravitational acceleration vector
$2h$	Diameter of antenna
I	Area moment of inertia of antenna cross-section
I_{ijc}	Mass moments and products of inertia for central core
l_m	Length of mth antenna
M_s	Total mass of the satellite
M_{iB}	Components of the moment vector due to applied forces in the rotating body frame
M_{ma}	Total mass of mth antenna
p_o	Solar radiation pressure at normal incidence on a perfect reflector.
Q_n	Generalized force associated with generalized coordinate q_n
q_n	Any generalized coordinate
T	Kinetic energy of the system
ΔT_o	Temperature differential across antenna diameter at normal solar incidence
V	Strain energy of deformation
u, v, w	Components of displacement of antenna relative to its undeformed position
X_{io}	Cartesian components of position relative to center of Earth
X_{ioL}	Cartesian components of origin of local reference frame relative to center of Earth
X_{iB}	Cartesian components of a point in the rotating body-fixed reference frame relative to the CM of the central core

x_{iL}	Cartesian components of a point in the non-rotating local reference frame relative to the CM of the central core
x_{ioc}	Components of position of satellite center of mass relative to center of Earth in non-rotating frame
x_{icL}	Components of vector from center of mass to the origin of the local coordinate system in non-rotating reference frame
α_m	Angular orientation of mth antenna in $x_{1B}x_{3B}$ plane, measured from x_{1B} axis
$\dot{\delta}_{iB}$	Components of velocity relative to the local origin in the rotating frame
ρ	Mass per unit length of antenna
x_n	nth mode shape of cantilever beam
dm	A differential element of mass
ds	A differential element of effective surface area
\int_B	Integration over the entire body
\int_C	Integral over satellite central core
\int_{mD}	Integral over mth deployment mechanism
\int_{ma}	Integral over mth antenna

Subscripts

m	Indicating the mth antenna
n	Indicating the nth mode shape
B	Refers to body-fixed rotating frame
C	Refers to center of mass of entire satellite
L	Refers to local non-rotating frame

- o** Refers to Earth-centered non-rotating frame
- D** Indicates internal damping force; or, refers to a deployment mechanism
- g** Indicates gravity or gravity-gradient force or moment
- p** Indicates solar pressure force or moment
- s** Indicates force due to internal strain energy; or, refers to total satellite
- T** Indicates force due to temperature gradient

6. CONTROL SYSTEMS

6.1 GENERAL REQUIREMENTS. -- The control system discussed in this section is operative only after separation from the booster and initial orientation to the desired attitude have already occurred. (It is presumed that the initial orientation prior to antenna rod deployment is provided by another control system, which is not covered here.) The control system discussed below will be operative during the deployment/acquisition phase and during the mission phase. The control system requirements for a gravity-gradient-stabilized Earth satellite may be broadly classified into performance requirements and design requirements. The performance requirements are as follows:

- a. During the deployment/acquisition phase, the control system is required to supply the necessary damping and/or stabilization for a smooth transition to the mission phase.
- b. During the mission phase, the control system is required to supply the necessary damping to achieve:
 - (1) Adequate damping of both small-angle and large-angle motion about all axes.
 - (2) Adequate control torques to minimize the static errors which result from quasi steady-state disturbance torques, such as solar pressure or residual magnetic moment torques.
 - (3) Minimization of the libration amplitudes due to periodic disturbances such as magnetic moments, or orbital eccentricity.

The design requirements and constraints are as follows:

- a. High reliability over the required mission life
- b. Ability to withstand the boost accelerations and the prolonged exposure to a space environment, including the thermal shocks associated with entering and leaving the Earth shadow
- c. Ability to meet the weight, size, and electrical power constraints imposed by the vehicle
- d. In addition, the control system should be easily maintained and checked out before launch, and should require a minimum of special instrumentation or other input data for its operation.

6.2 CANDIDATE SYSTEMS. -- All control systems considered for the RAE vehicle can be classified into either the active or passive category. An example of

an active control system is a design which uses a body-mounted, three-axis magnetometer, torquer coils mounted along the three vehicle axes, and stabilization and control electronics. Prior to the deployment/acquisition phase, one coil aligns the axis of minimum moment of inertia with the direction of the local Earth magnetic field, while the coils about the other two axes are used to obtain damping by means of appropriate phase shifts in the stabilization electronics, using the magnetometer data as the input signals to the electronics.

When the local magnetic field is aligned to the local vertical within a suitable tolerance (up to 15 degrees), the deployment/acquisition phase may begin. During the deployment/acquisition phase the coils could be operated as before, i. e., one coil for stabilization and the other two coils for damping. During the mission phase, however, all three coils would be operated in the damping mode (by a logic change in the electronics) since stabilization is achieved by means of gravity gradient.

The passive control systems considered for this vehicle can be classified into three broad categories, according to the methods and means used to damp oscillations about the equilibrium orientation:

- a. TRAAC-type configurations
- b. Magnetic anchor configurations
- c. Hinged multibody configurations.

The TRAAC-type configurations employ a "tip-mass" attached to one end of a lossy helical spring. The other end of this spring is connected to either a fixed or extendable boom which is a part of the main body. (TRAAC is an acronym for the Transit Research and Attitude Control satellite which was launched from Cape Kennedy on 15 November 1961.) In operation, the pitch and roll librations of the main body about the local vertical will cause the spring to stretch and compress along its axis. Mechanical hysteresis within the spring (due to a cadmium coating) will dissipate energy to provide some measure of damping.

The Rice-Wilberforce damper is a modification of the TRAAC damper in that it employs a winding mode as well as a linear spring mode. Tuning of the individual modes to the pitch and roll libration frequencies, respectively, increases overall effectiveness.

The magnetic anchor configurations use two concentric spheres separated by a viscous fluid. The internal sphere contains a bar magnet which causes the inner sphere to align itself to the Earth's local magnetic field. The outer sphere is attached to the end of an extendible rod which is deployed from the main body. Relative motion of the inner and outer spheres is opposed by the viscous fluid, causing energy to be dissipated.

The hinged multibody configurations use one or more auxiliary damper bodies which are hinged to the main body through elastic and dissipative couplings. The selection of hinge points, the mass distribution of all bodies, and the hinge parameters are so chosen that vehicle libration causes relative motion between the parts of the vehicle, and hence energy is dissipated.

6.3 GENERAL PROPERTIES OF CANDIDATE SYSTEMS. -- As a general comment, the passive systems require no special instrumentation, no controller, and no switching logic. They will always tend to convert kinetic energy to heat, and thereby reduce the vehicle librations. On the other hand, the active systems will, in general, require some instrumentation (such as magnetometers) and controller or switching logic. The applied torques will reduce vehicle librations in a properly designed active system. However, if the torques should be applied at the wrong times (due to flexible body effects or some controller malfunction), the applied torques could actually increase librations and worsen the situation. In general, the passive systems are likely to be simpler and more suitable. The following observations can be made about the three passive configurations:

- a. TRAAC-Type Configurations. -- These configurations are characterized by low damping rates. As an example, the TRAAC satellite pitch libration amplitude was reduced from 25 to 5 degrees over a 15-day period for an average decrease of 1.33 degrees per day.⁵ While the damping rates are higher for the Rice-Wilberforce damper,⁶ settling time constants of about six orbits are typical, with the highest damping in pitch and the lowest damping in yaw.
- b. Magnetic Anchor Configurations. -- The viscous coupling of the Earth's magnetic and gravity-gradient fields creates cyclical disturbance torques for most orbits. A reduction of the fluid viscosity (and hence the coupling) will reduce steady-state error at the expense of degraded transient response. Based upon past practice, a value of viscous coupling should be selected to produce an exponential decay time constant of about 20 orbits.⁷ With typical initial conditions, the vehicle would attain a steady-state attitude in about 40 to 50 orbits. Transient response is therefore only lightly damped with this approach.

5. Fischell, R. E., The TRAAC Satellite, APL Technical Digest, 1, No. 3 (January - February 1962).

6. Buxton, A. C., D. E. Campbell, and K. Losch, Rice/Wilberforce Gravity - Gradient Damping System, presented at the Symposium on Passive Gravity - Gradient Stabilization, NASA Ames Research Center, Moffett Field, California (May 1965).

7. Katucki, R. J., and R. G. Moyer, System Analysis and Design of a Class of Gravity - Gradient Satellites Utilizing Viscous Coupling between the Earth's Magnetic Field and Gravity - Gradient Fields, presented at the Symposium on Passive Gravity - Gradient Stabilization, NASA Ames Research Center, Moffett Field, California (May 1965).

- c. Hinged Multibody Configurations. -- The transient damping achievable is good for both small-angle and large-angle motions. As shown in reference⁸, settling times of about three orbits about all three axes can be attained. In addition, the flexibility available in the geometric arrangement of the damper bodies and the hinges permits a wide range of performance characteristics to be obtained.⁹

6.4 MATHEMATICAL MODELS. -- From the preceding discussion the hinged multibody configuration presently appears to be the most feasible approach for application to the RAE. However, other approaches should not be abandoned at this time. The elastic and dissipative couplings between the main body and the auxiliary body (or bodies) can best be obtained by use of a magnetic hysteresis damper. This device has three advantages when compared to a viscous fluid (linear) damper, namely:

- a. Design is simple and reliable in the space environment, since there are no fluids or fluid seals. Design parameters are unaffected by the space environment.
- b. Damping depends upon angular travel, not angular rate. This is desirable since angular rates of the libration modes are very low.
- c. Design parameters, i. e., the spring constant and maximum damping torque, can be independently varied over wide ranges with relatively minor changes to damper size, weight, or volume.¹⁰

Two candidate configurations for the damper boom geometry are shown in figure 24. Figure 24a shows a four-boom (or three-body) configuration, where one pair of damper booms is in the orbital plane to damp pitch librations, and the second pair of booms lies normal to the orbital plane to damp yaw and roll oscillations. While the main body is nominally oriented along the local vertical, all damper booms are nominally oriented normal to the local vertical.

The second configuration (figure 24b) is a two-boom (or two-body) arrangement, where the damper is nominally normal to the local vertical, and is also skewed by a large angle (about 60 degrees) to the plane which contains the vee antennas. This, in turn, skews the principal axes of the main body with respect to the orbital plane, making the single damper boom effective about all three axes by means of inertial cross coupling.¹¹

⁸Zimmerman, B.C., Study of ATS Gravity-Gradient Experiment, presented at the Symposium on Passive Gravity-Gradient Stabilization, NASA, Ames Research Center, Moffett Field, California (May 1965).

⁹Hartbaum, H., Hooker, W. Leliakov, I., Margulies, G., "Configuration Selection for Passive Gravity-Gradient Satellite", presented at the Symposium on (same as above).

¹⁰Reiter, G.S., O'Neil, J.P., Alper, J.R., "Magnetic Hysteresis Damping for Gravity-Gradient Stabilization", presented at the Symposium on Passive Gravity-Gradient Stabilization, NASA, Moffett Field, California (May 1965).

¹¹Tinling, B.E., and V.K. Merrick, Exploitation of Inertial Coupling in Passive Gravity-Gradient Stabilized Satellites, 1, No. 4 Journal of Spacecraft (July-August 1964).

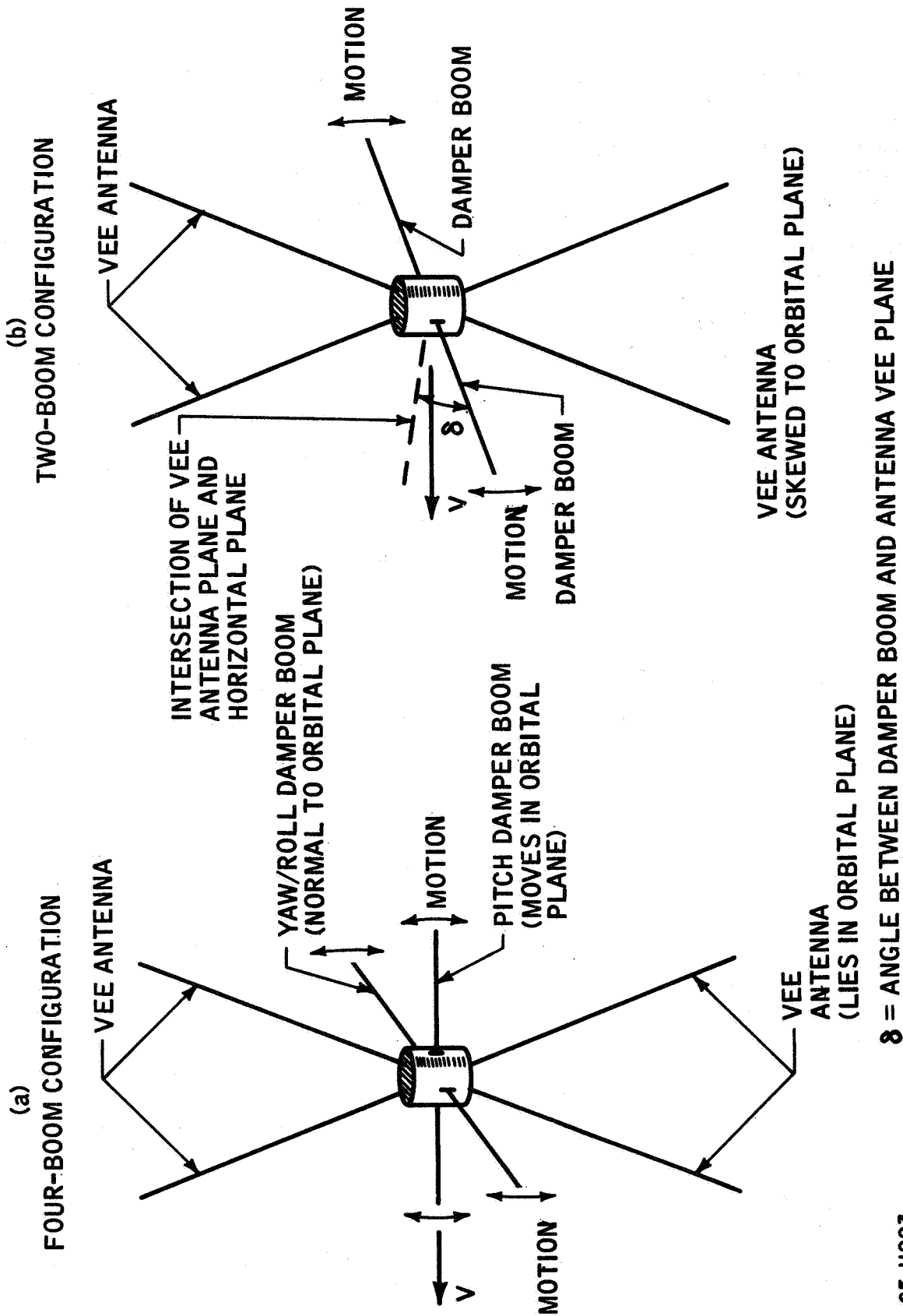


Figure 24 CANDIDATE DAMPER BOOM CONFIGURATION FOR THREE-AXIS CONTROL

65-11993

The configuration of figure 24b appears to be more attractive for this program since a sizable auxiliary body moment of inertia is required (due to the extremely large main body moment of inertia). For a limited total damper boom weight, a single pair of damper booms can provide the greatest moment of inertia since it can locate more boom mass farther from the mass center.

For the first simulation, a planar case will be examined. Therefore, it will resemble a planar version of figure 24a, where only pitch librations are allowed; all motion lies in the orbital plane and there is only one pair of booms.

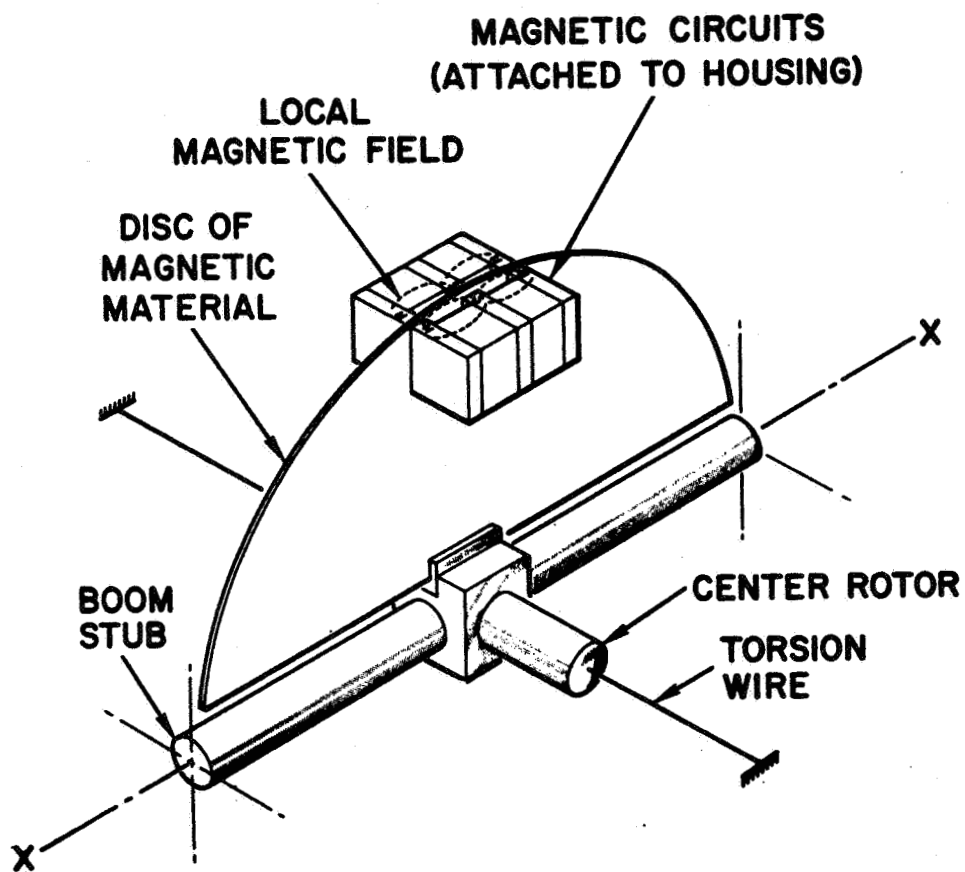
The magnetic hysteresis damper unit which connects the ends of the damper booms to the main body is shown schematically in figure 25 (from reference 6). The damper booms are rigidly attached to a circular vane of magnetically hard material (large area enclosed in magnetic hysteresis loop). A torsional spring is attached at its midpoint to the center of this vane. Both ends of the spring are attached to the main body to provide the elastic coupling between the damper booms and the main body. A set, or sets, of permanent magnets is mounted on the main body close to and around the periphery of the vane. As the boom rotates relative to the main body, the magnetic pole pieces will alter the magnetization pattern within the vane. Dissipative torques will thereby be generated and kinetic energy will be converted to heat. A typical unit weighs approximately 1 pound.⁶ A pair of booms suitable for this satellite and attached to the damper would weigh approximately 12 pounds. The differential equations describing the motion of the auxiliary body (two damper booms) and the main body in body-centered rotating axes (aligned with the local vertical and the normal to the orbital plane) are given here. It is assumed that:

- a. A circular orbit is achieved over a spherical Earth.
- b. Gravity gradient and inertia forces produce the dominant torques.
- c. The main body (with its double-vee antennas) behaves as a rigid body.
- d. The damper boom pair behaves as one rigid body.
- e. The damper mass center coincides with the vehicle mass center.

Referring to figure 26 and using a coordinate frame fixed to the local vertical, we have:

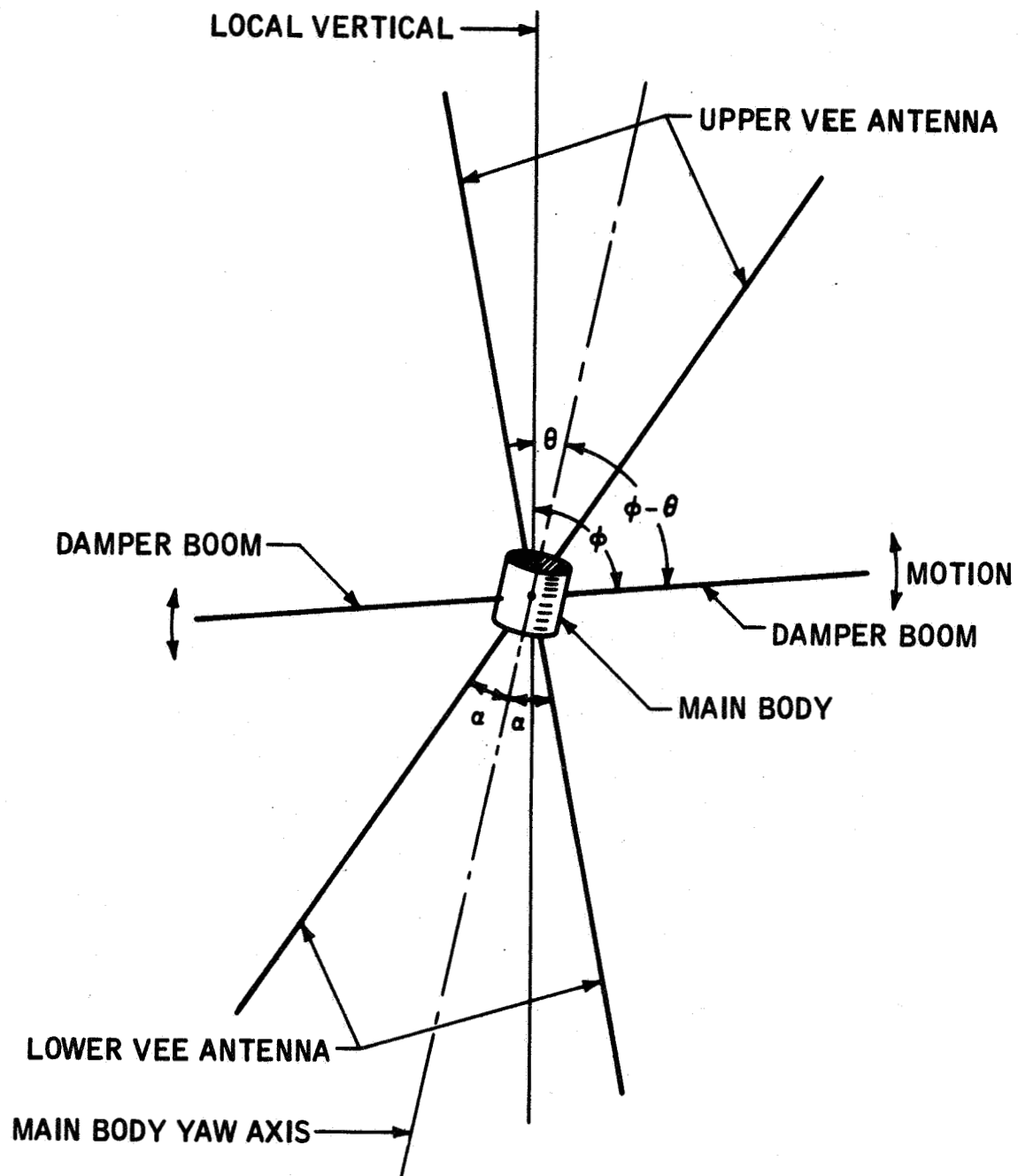
Auxiliary Body:

$$I_B \ddot{\phi} + \frac{3}{2} \Omega^2 I_B \sin 2\phi + K[\phi - \theta - \pi/2] + T_H = 0$$



65-10191

Figure 25 SCHEMATIC OF MAGNETIC HYSTERESIS DAMPER



65-11995

Figure 26 SCHEMATIC OF PLANAR TWO-BODY MODEL

Main Body:

$$I_P \ddot{\theta} + \frac{3}{2} \Omega^2 (I_R - I_Y) \sin 2\theta - K [\phi - \theta - \pi/2] - T_H = 0$$

where

- ϕ = angle between damper booms and the local vertical
- θ = angle between main body yaw axis and the local vertical
- K = torsional spring constant for hysteresis damper (ft-lb/rad)
- T_H = magnetic hysteresis torque (ft-lb)
- Ω = vehicle orbital rate (rad/sec)
- I_B = auxiliary body (composed of two booms) moment of inertia about its mass center
- I_P = main body moment of inertia about pitch axis
- I_Y = main body moment of inertia about yaw axis ($= I_P \sin^2 \alpha$)
- I_R = main body moment of inertia about roll axis ($= I_P \cos^2 \alpha$)
- L_A = length of a single antenna rod (=750 feet)
- L_B = length of a single damper boom (=350 to 450 feet)
- α = antenna vee half-angle.

Since the damper boom pair is nominally at an unstable null with regard to the gravity gradient, the spring constant must be greater than the equivalent gravity gradient "spring constant," that is:

$$K \geq 3\Omega^2 I_B$$

for the damper body to remain extended perpendicular to the main body.

The hysteresis torque, T_H , can be described by the relationship (see reference 12):

¹² Sabroff, A.E., A Two-Damper Passive Gravity Gradient Stabilization System, presented at the Symposium on Passive Gravity-Gradient Stabilization, NASA, Moffett Field, Calif. (May 1965).

$$T_H = \begin{cases} T_m & \text{for } T_H > T_m \\ T_o + [\text{sgn}(\dot{\phi} - \dot{\theta})][h_1 \Delta(\phi - \theta) + h_2 \Delta(\phi - \theta)^2 + h_3 \Delta(\phi - \theta)^3] & \text{for } |T_H| < T_m \\ -T_m & \text{for } T_H < -T_m \end{cases}$$

where T_M is the saturation torque of the hysteresis damper (see figure 27). $(\phi - \theta)$ is the angle between the damper boom and main body yaw axis, and $\Delta(\phi - \theta)$ is the change in this angle since the previous sign change in $(\dot{\phi} - \dot{\theta})$. T_o is the value of magnetic hysteresis torque that existed at the instant $(\dot{\phi} - \dot{\theta})$ changed sign. The coefficients h_1, h_2 , and h_3 are determined from a polynomial fit to test data for a given hysteresis damper. This formulation for the hysteresis torque allows the capability of generating minor loops at any location in the torque-angle space.

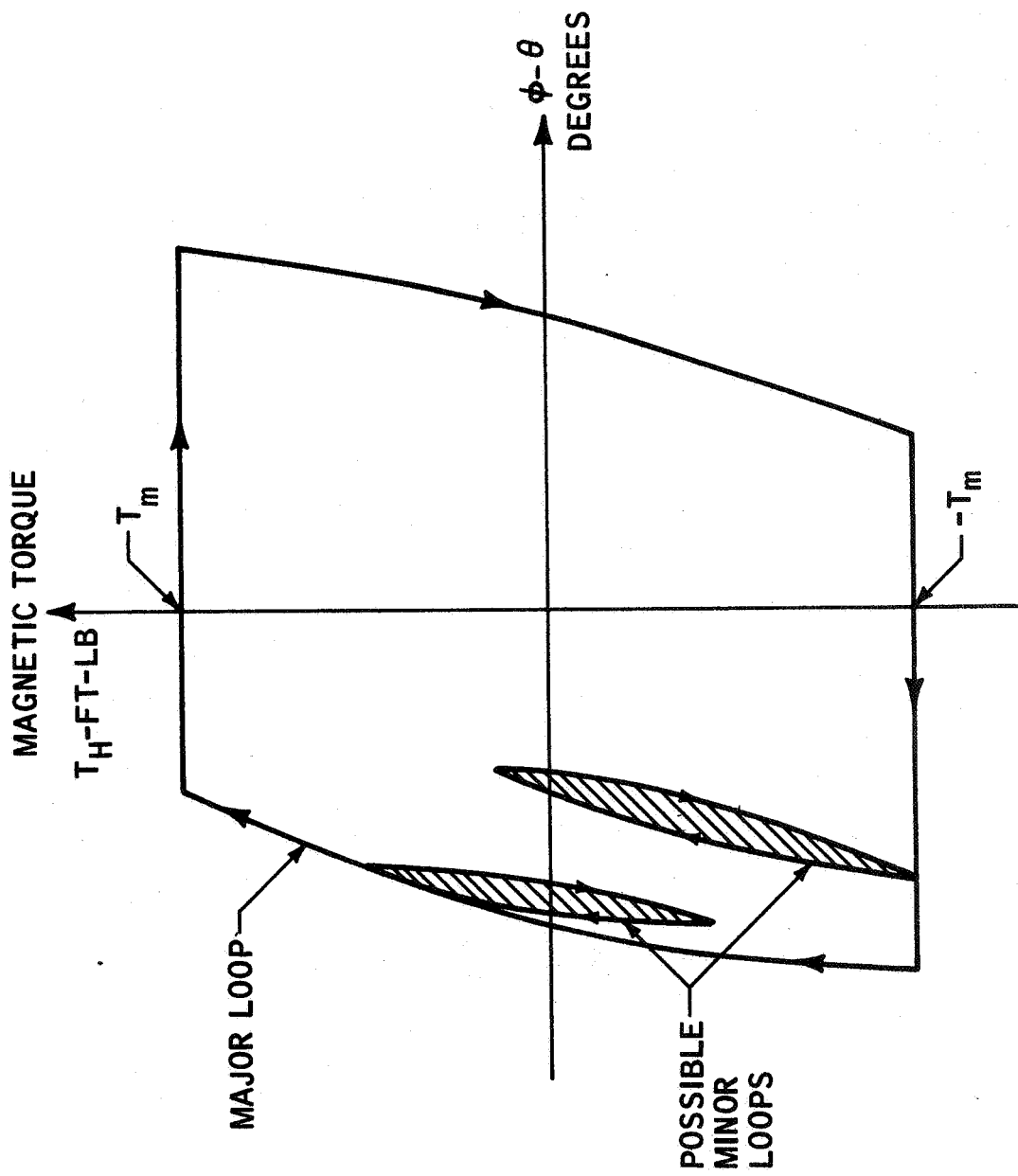
- 6.5 PARAMETER SELECTION. -- The final selection of parameters will be determined by means of analog and digital simulation. A compromise between transient and steady-state performance and practical design constraints shall be considered. From reference 7, a preliminary set of parameters have been estimated for a starting point in the design and are presented in table I below:

TABLE I

HYSTERESIS DAMPER DESIGN PARAMETERS-FIRST CUT

Boom length = 396 feet	
Number of booms = 2 (in-line)	
Total moment of inertia (I_B) = 20,000 slug-ft ²	
Orientation of boom axis: skewed to vee plane by 60 degrees and nominally perpendicular to the main body yaw axis.	
Magnetic hysteresis damper unit	
1) spring constant, $K = 1.9 \times 10^{-2}$ ft-lb/rad	
2) maximum hysteresis torque, $T_M = 1.2 \times 10^{-3}$ ft-lb.	
Est. weight of booms (2)	12.3 lb.
Est. weight of hysteresis damper unit	<u>2 lb*</u>
Total	14.3 lb

* The construction of a hysteresis damper to develop a maximum damping torque of 1.2×10^{-3} ft-lb for a unit weight of less than 2 pounds is considered to be well within the current state of the art.



$\phi - \theta$ = RELATIVE MOTION OF DAMPER BOOMS
AND MAIN BODY

Figure 27 HYSTERESIS DAMPER CHARACTERISTICS (MAGNETIC TORQUES ONLY)

65-11994

7. PRELIMINARY RESULTS

7.1 PRELIMINARY EVALUATION OF DIGITAL RESULTS. -- The comparison of the digital results from the rigid-body program with analytical results has been primarily restricted to planar cases due to the various difficulties inherent in obtaining analytic solutions to the thoroughly coupled three dimensional problem. Even the planar problems such as determining the planar libration period can introduce considerable complexity into the analytical solution.

7.1.1 Planar Libration Period and Amplitude. -- The equation for planar libration of a rigid body in circular orbit is:

$$\ddot{\theta} + \frac{3}{2} \Omega^2 \frac{I_1 - I_3}{I_2} \sin 2\theta = 0 \quad (7-1)$$

where I_1, I_2, I_3 are the principal moments of inertia about the roll, pitch, and yaw axes, respectively, Ω is the orbital rate, and θ is the pitch angle relative to the local vertical. The pitch axis is assumed to be normal to the orbital plane. For the RAE double-vee configuration,

$$\frac{I_1 - I_3}{I_2} = \cos 2\alpha \quad (7-2)$$

where α is the half-angle of the antenna vee. Note that

$$\ddot{\theta} = \frac{d\dot{\theta}}{dt} = \frac{d\theta}{dt} \frac{d\dot{\theta}}{d\theta} = \dot{\theta} \frac{d\dot{\theta}}{d\theta} \quad (7-3)$$

and that $\sin 2\theta = 2 \sin \theta \cos \theta$. Then equation (7-1) becomes:

$$\dot{\theta} \frac{d\dot{\theta}}{d\theta} = - 3 \Omega^2 \cos 2\alpha \sin \theta \cos \theta \quad (7-4)$$

which is easily reduced to

$$\dot{\theta} d\dot{\theta} = - 3 \Omega^2 \cos 2\alpha \sin \theta d(\sin \theta). \quad (7-5)$$

Integrating equation (7-5) yields

$$\dot{\theta}^2 = - 3 \Omega^2 \cos 2\alpha \sin^2 \theta + C. \quad (7-6)$$

The constant C is easily evaluated by observing that $\dot{\theta} = 0$ when $\theta = \theta_{\max}$; hence:

$$\frac{d\theta}{dt} = \pm \sqrt{3 \Omega^2 \cos 2\alpha (\sin^2 \theta_{\max} - \sin^2 \theta)} \quad (7-7)$$

The time to oscillate from $\theta = 0$ to $\theta = \theta_{\max}$, during which $\dot{\theta} \geq 0$, is one-fourth the total libration period. Hence, as a function of θ_{\max} :

$$P_{\text{lib}}(\theta_{\max}) = \frac{4}{\Omega \sqrt{3 \cos 2\alpha}} \int_0^{\theta_{\max}} \frac{d\theta}{\sqrt{\sin^2 \theta_{\max} - \sin^2 \theta}} \quad (7-8)$$

Recall that the small-angle libration period P_0 is:

$$P_0 = P_{\text{lib}}(0) = \frac{2\pi}{\Omega \sqrt{3 \cos 2\alpha}} \quad (7-9)$$

as can be derived easily from equations (7-1) and (7-2). Substituting relation (7-9) into (7-8) then yields:

$$P_{\text{lib}}(\theta_{\max}) = \frac{2}{\pi} P_0 \int_0^{\theta_{\max}} \frac{d\theta}{\sqrt{\sin^2 \theta_{\max} - \sin^2 \theta}} \quad (7-10)$$

The integral in equation (7-10) is simply the complete elliptic integral of the first kind, $F(k, \pi/2)$:

$$\int_0^{\theta_{\max}} \frac{d\theta}{\sqrt{\sin^2 \theta_{\max} - \sin^2 \theta}} = \int_0^1 \frac{d\xi}{\sqrt{1-\xi^2} \sqrt{1-k^2 \xi^2}} \quad (7-11)$$

$$= F\left(k, \frac{\pi}{2}\right) \quad (7-12)$$

where

$$k = \sin \theta_{\max} \quad (7-13)$$

$$\xi = \frac{\sin \theta}{\sin \theta_{\max}} \quad (7-14)$$

Thus, finally, the libration period is:

$$P_{\text{lib}}(\theta_{\text{max}}) = \frac{2}{\pi} P_0 \cdot F\left(\sin \theta_{\text{max}}, \frac{\pi}{2}\right). \quad (7-15)$$

The complete elliptic integral can be expanded as:

$$F\left(k, \frac{\pi}{2}\right) = \frac{\pi}{2} \left[1 + \left(\frac{1}{2}\right)^2 k^2 + \left(\frac{3}{2.4}\right)^2 k^4 + \left(\frac{3 \cdot 5}{2 \cdot 4 \cdot 6}\right)^2 k^6 + \dots \right] \quad (7-16)$$

from which the period can be expressed as:

$$P_{\text{lib}}(\theta_{\text{max}}) = P_0 \left[1 + \left(\frac{1}{2}\right)^2 \sin^2 \theta_{\text{max}} + \left(\frac{3}{2 \cdot 4}\right)^2 \sin^4 \theta_{\text{max}} + \left(\frac{3 \cdot 5}{2 \cdot 4 \cdot 6}\right)^2 \sin^6 \theta_{\text{max}} + \dots \right].$$

It is evident that as θ_{max} approaches zero, P_{lib} approaches P_0 . Figures 28 and 29 show the excellent agreement between the analytical and digital results.

Another planar check case was run with a 30-degree initial pitch angle and zero inertial rate. For this case,

$$\theta_{\text{max}} = \frac{1}{2} \cos^{-1} \left(\cos 2\theta_i - \frac{2}{3 \cos 2\alpha} \right) = 73.2 \text{ degrees} \quad (7-18)$$

Figure 30 shows the excellent agreement.

7.1.2 Non-Planar Oscillations. -- Two non-planar cases were also run.

The effect of a 1-degree yaw offset is shown in figure 31. It would be expected that the pitch axis would be initially unperturbed but that the effect of cross-coupling would eventually cause coupled motion exhibiting a period equal to the orbital period. An initial roll offset of 1 degree would be expected to result in an immediately noticeable motion of the pitch axis, with subsequent oscillations of both orbital and half-orbital period. These effects are shown in figure 32.

7.1.3 Effect of Orbital Eccentricity. -- To check the analytic ephemeris simulation of non-circular orbits, several cases were run to demonstrate the forcing effect of orbital eccentricity on planar libration. It can be shown that for small values of eccentricity, the forced steady-state librational response is:

$$\theta = \frac{2e}{3 \cos 2\alpha - 1} \sin \Omega_o t \quad (7-19)$$

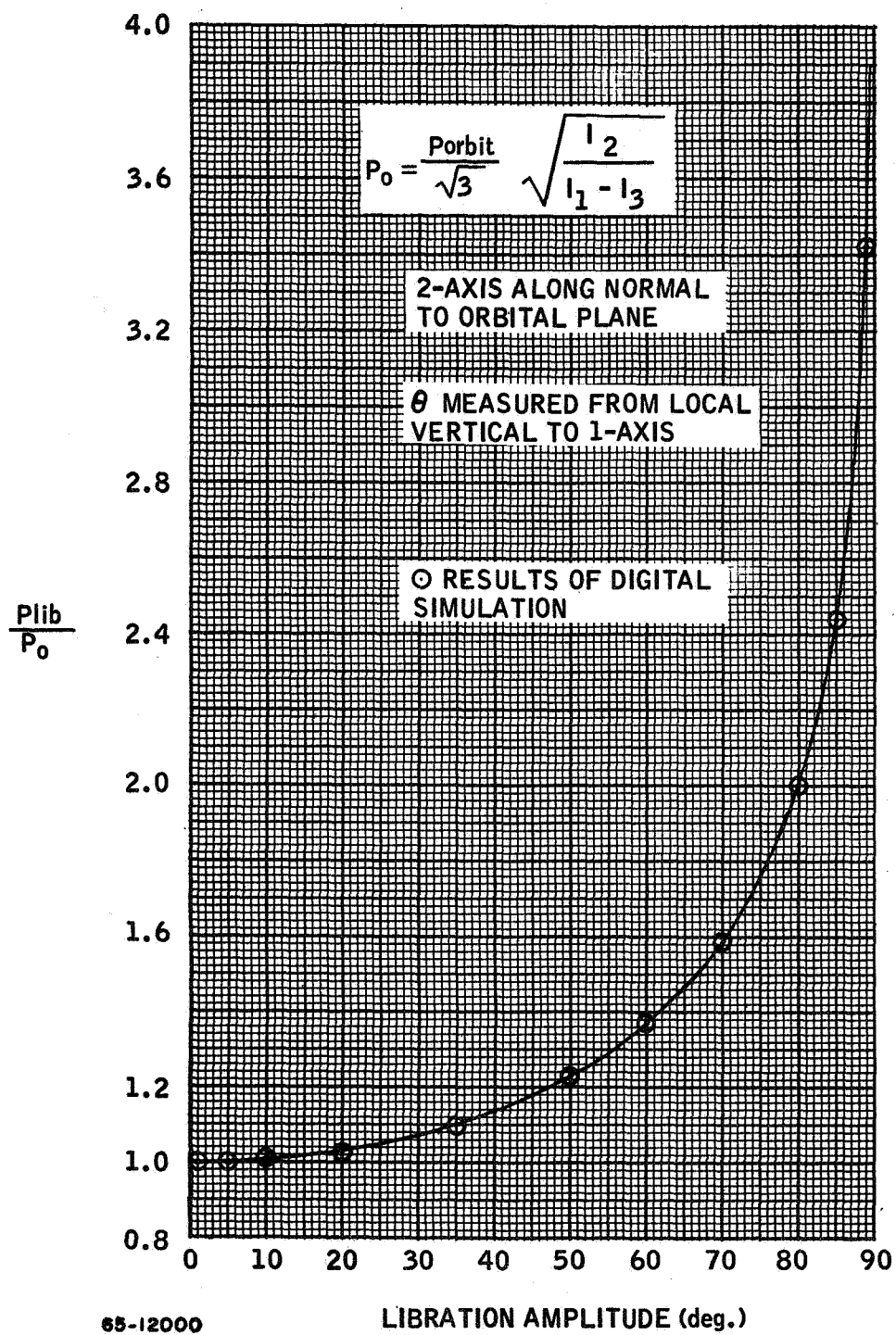
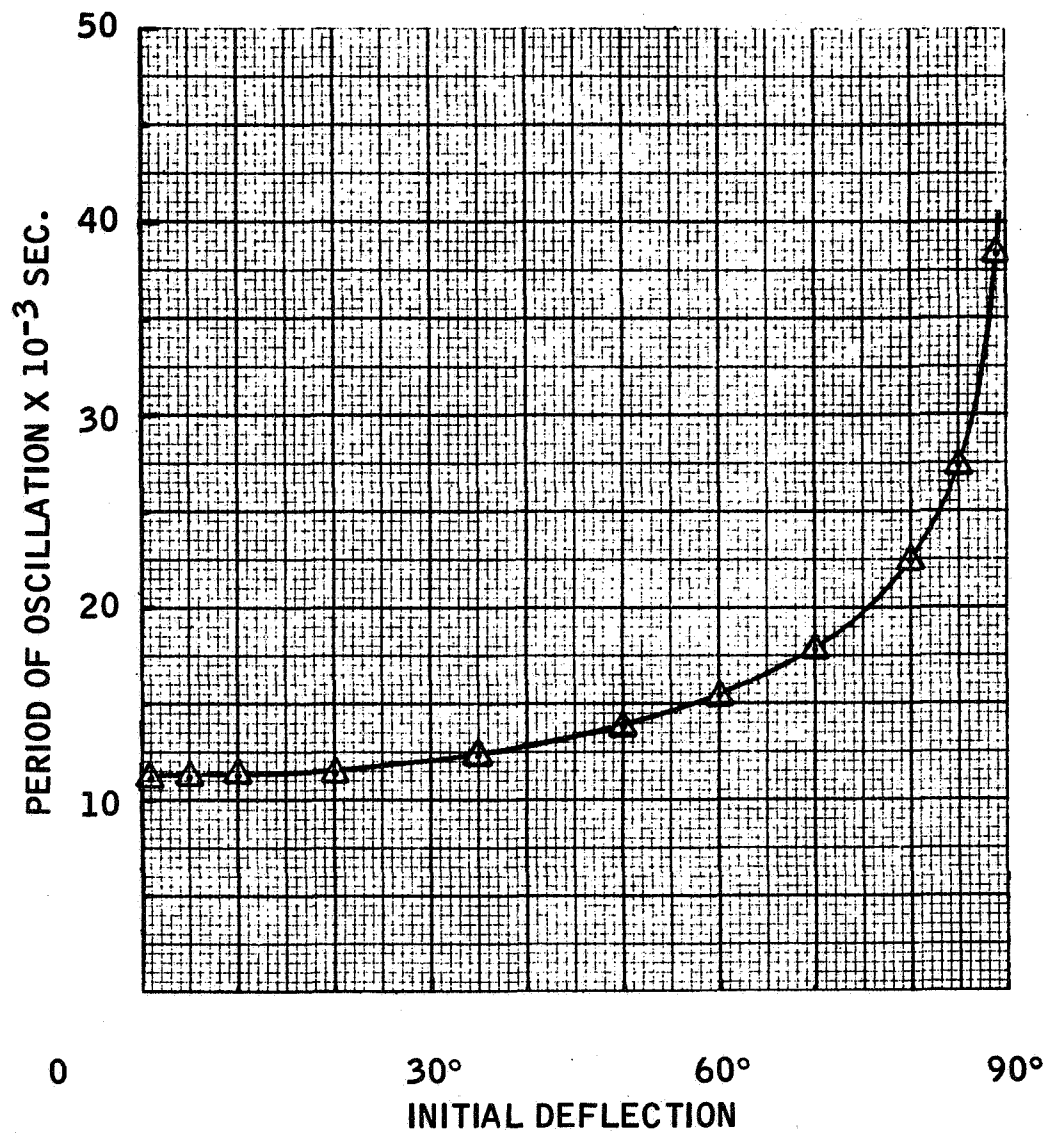
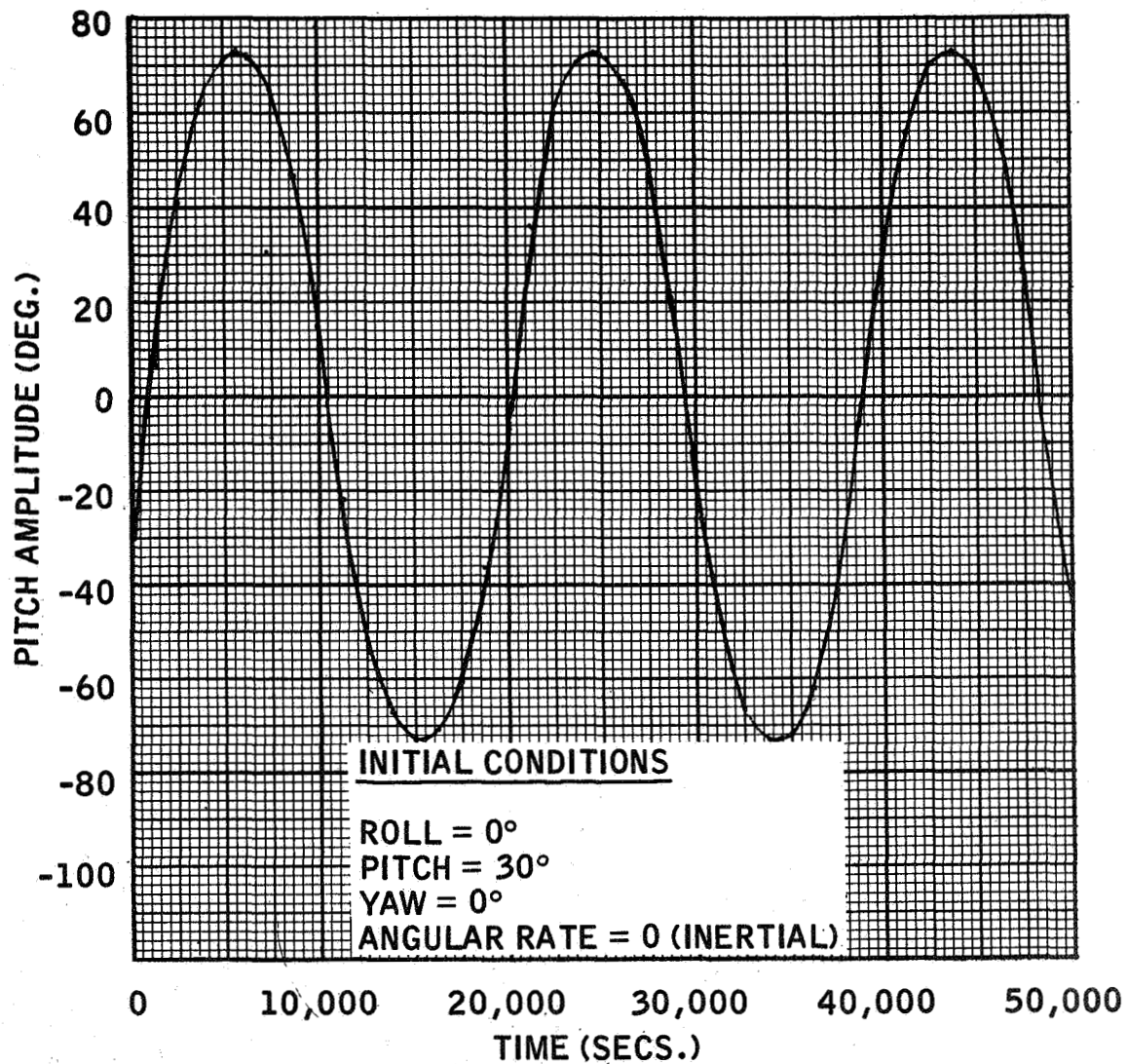


Figure 28 COMPARISON OF ANALYTICAL AND DIGITAL RESULTS FOR PLANAR LIBRATION PERIOD (NORMALIZED)



65-11996

Figure 29 PERIOD OF PLANAR LIBRATION VERSUS OSCILLATION AMPLITUDE



65-11990

Figure 30 PLOT OF PITCH OSCILLATION VERSUS TIME

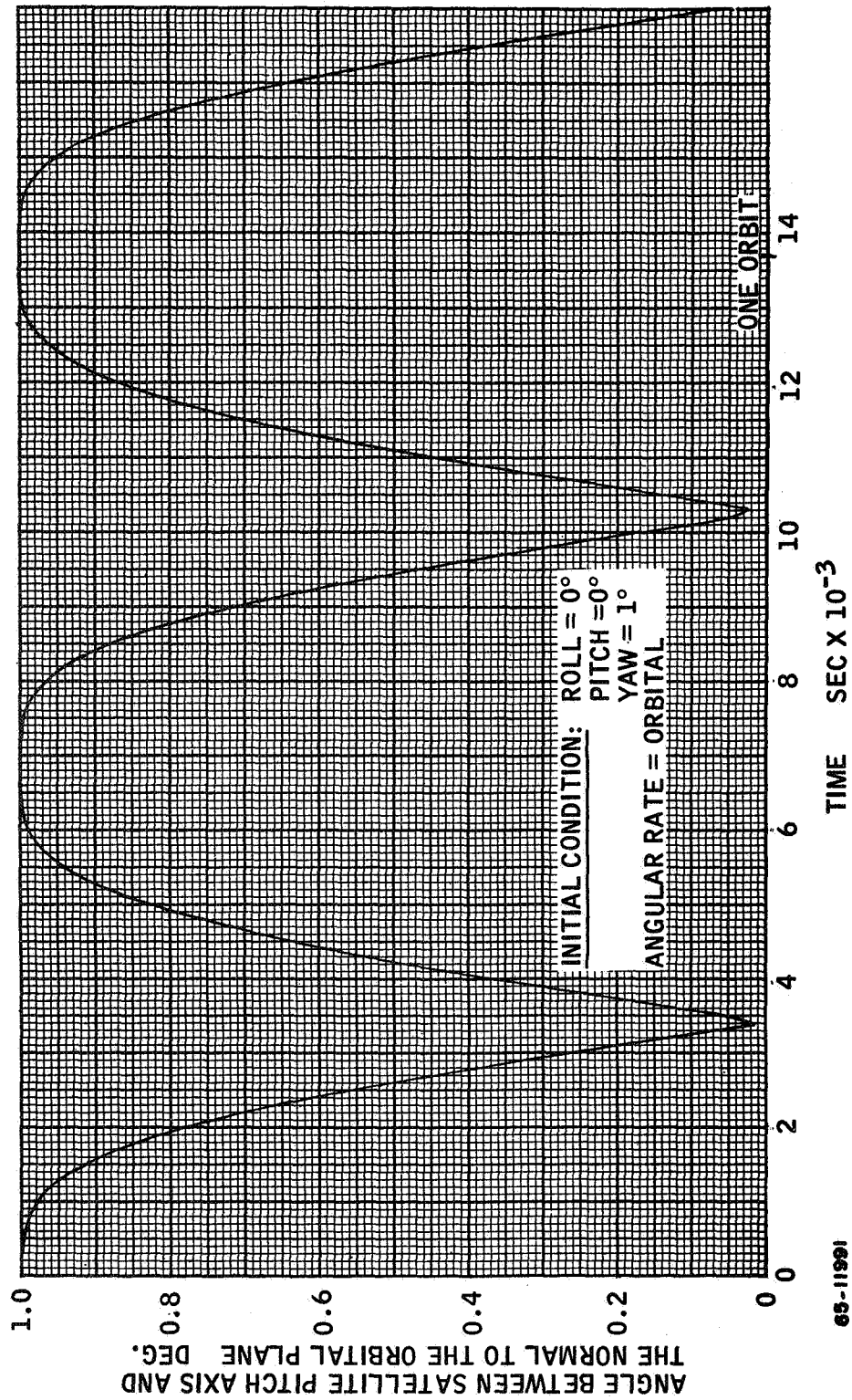


Figure 31 ANGLE BETWEEN SATELLITE PITCH AXIS AND THE NORMAL TO THE ORBITAL PLANE (DEG)

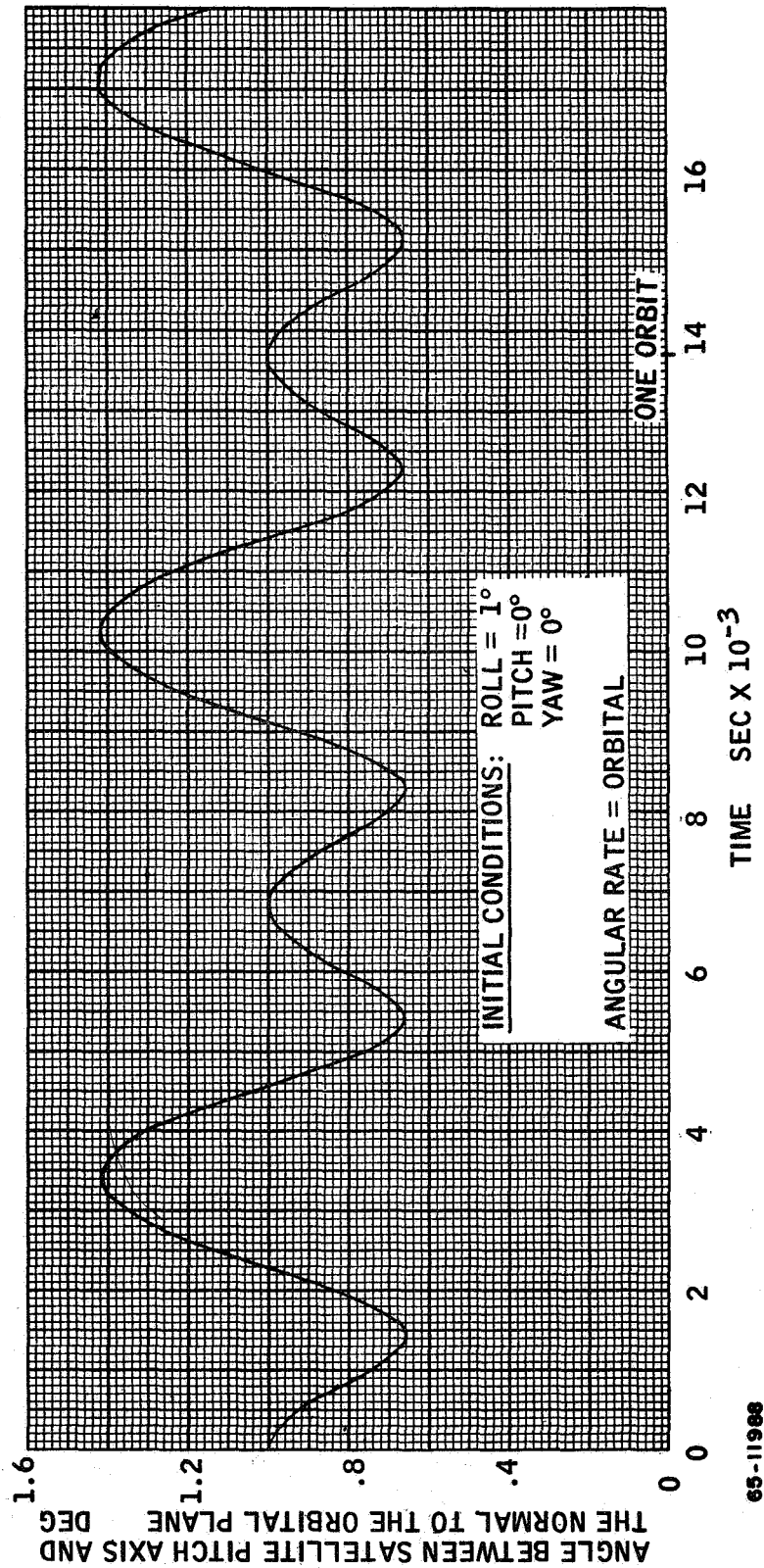


Figure 32 ANGLE BETWEEN SATELLITE PITCH AXIS AND THE NORMAL TO THE ORBITAL PLANE (DEG)

where Ω_0 is the mean orbital rate defined by the relation:

$$\Omega_0 = \sqrt{\frac{\mu}{a^3}} \quad (7-20)$$

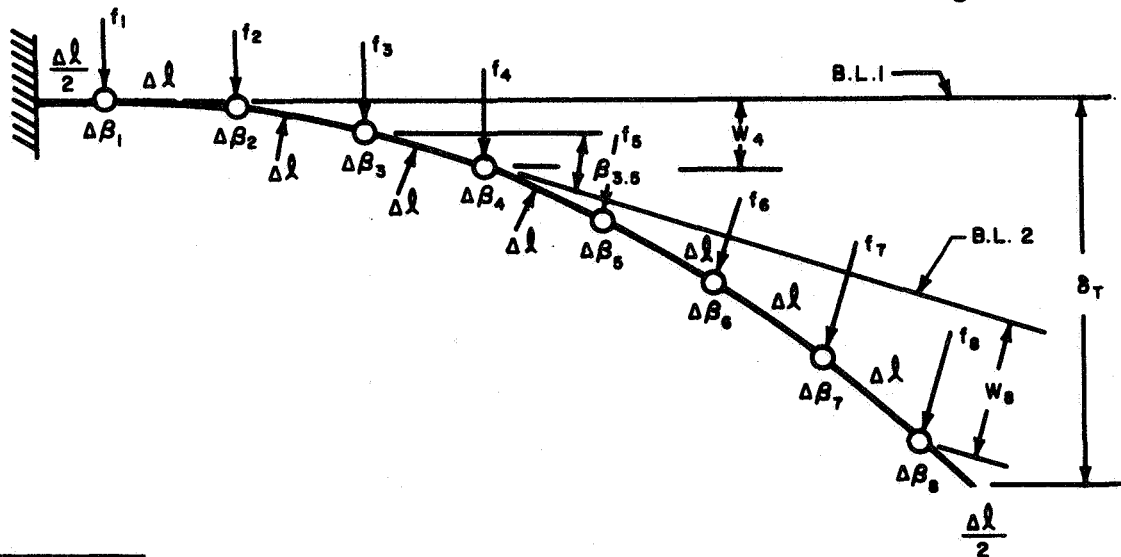
a is the orbital semi-major axis; e the orbital eccentricity, and t is time measured from the moment of perigee passage. At $t = 0$, the vehicle rate with respect to inertial space is:

$$\Omega + \dot{\theta} \approx \Omega_0 \left(1 + 2e + \frac{2e}{3 \cos 2\alpha - 1} \right) \quad (7-21)$$

to first order in e . A vehicle initially aligned with the local vertical at perigee and rotating inertially with the above rate would then be expected to exhibit a sinusoidal pitch motion of orbital period and, for $\alpha = 30$ degrees, amplitude equal to $4e$ in radians. Figure 33 shows excellent agreement with anticipated results for low values of eccentricity. At higher values of eccentricity, the oscillation becomes slightly less symmetric due to terms in higher powers of e . For a value of e equal to 0.1, the motion is unstable, as shown in figure 34. This instability is in agreement with results obtained by DeBra¹³ which indicate an eccentricity of approximately 0.05 to be marginally stable for a body of the nominal RAE inertia ratios.

7.2 PRELIMINARY RESULTS FROM ANALOG SIMULATION

7.2.1 Geometry of Cantilever Simulation. -- Consider the geometry of the deflected cantilever beam simulation shown in the following sketch:



¹³ DeBra, D.B., The Large Attitude Motions and Stability, Due to Gravity, of a Satellite with Passive Damping in an Orbit of Arbitrary Eccentricity about an Oblate Body, Ph.D. Thesis, Division of Engineering Mechanics, Stanford University (June 1962).

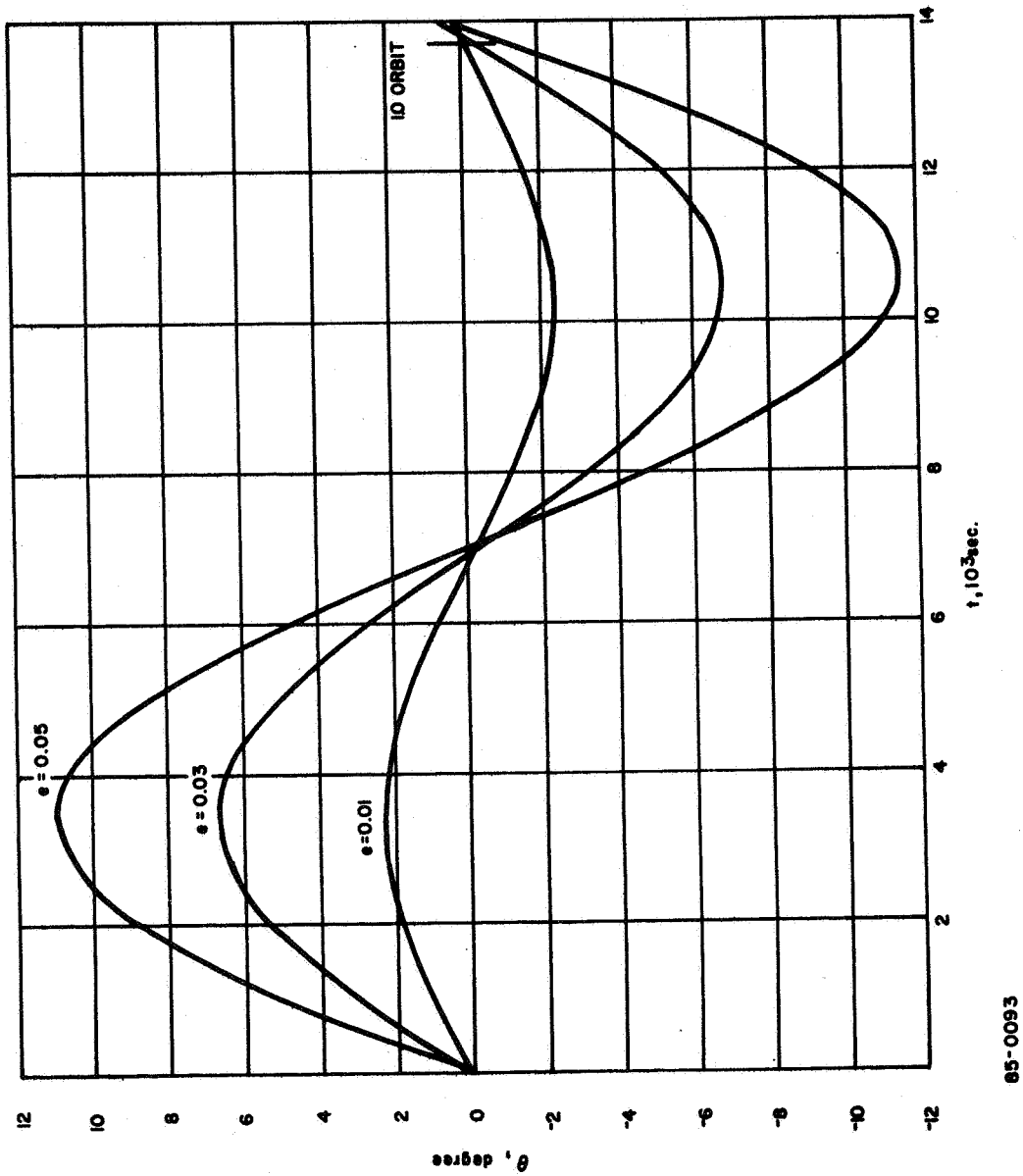
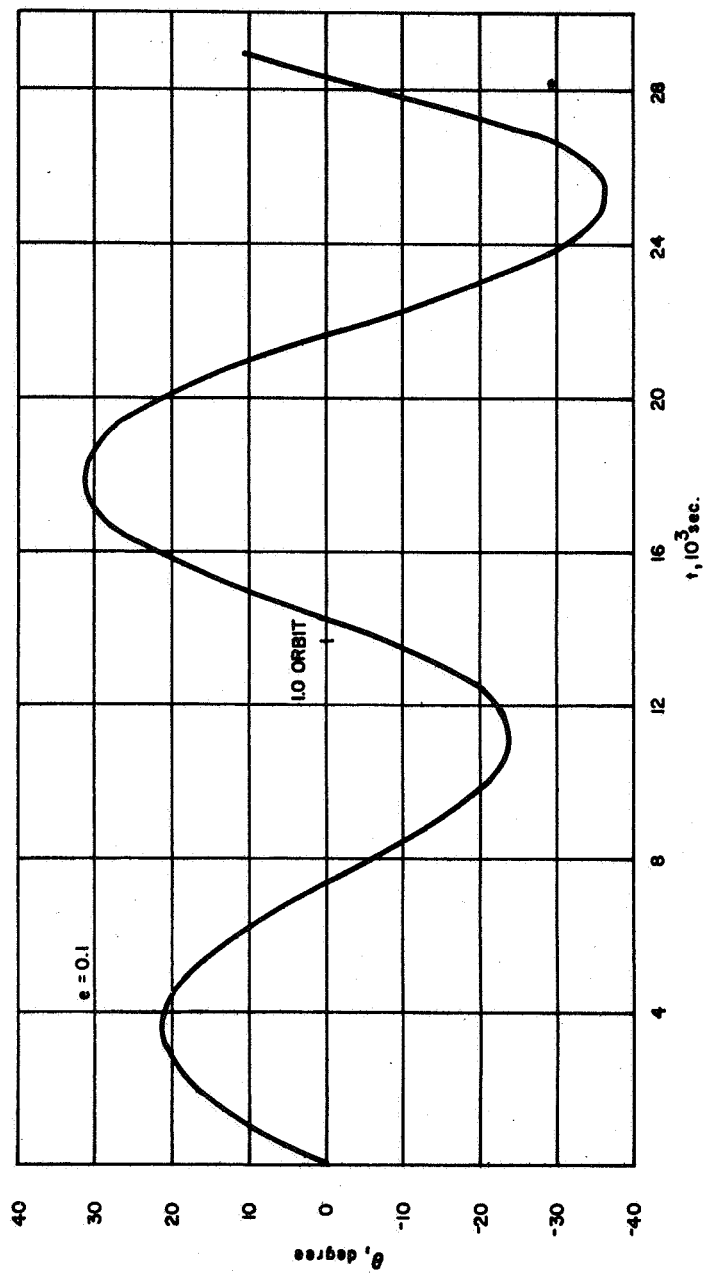


Figure 33 PLANAR PITCH OSCILLATION FORCED BY ORBITAL ECCENTRICITY



85-0094

Figure 34 PLANAR PITCH OSCILLATION FORCED BY ORBITAL ECCENTRICITY

The external forces f_k are applied perpendicular to the respective base lines as illustrated. The effective spring constant of each bending section is:

$$K = \frac{EI}{\Delta l} \quad (7-22)$$

where Δl is the distance between mass elements. It can then be shown that the following relations describe the slope $\beta_{3.5}$ of the second baseline, the deflection w_4 of the fourth mass element measured from the first baseline, and the deflection w_8 of the last mass element measured from the second baseline:

$$\beta_{3.5} = \frac{\Delta l^2}{EI} \left[18 f_8 + 15 f_7 + 12 f_6 + 9 f_5 + 6 f_4 + 3 f_3 + f_2 \right] \quad (7-23)$$

$$w_4 = \frac{\Delta l^3}{EI} \left[38 f_8 + 32 f_7 + 26 f_6 + 20 f_5 + 14 f_4 + 8 f_3 + 3 f_2 \right] \quad (7-24)$$

$$w_8 = \frac{\Delta l^3}{EI} \left[30 f_8 + 20 f_7 + 11 f_6 + 4 f_5 \right] \quad (7-25)$$

The assumption is made in the derivation of these equations that each mass element deflects perpendicular to the appropriate baseline; this assumption, in essence, requires the slope of each beam section to be small relative to that baseline. From the geometry of the deflected antenna, it is clear that the deflections of the first mass element and the antenna tip measured from the first baseline are, respectively:

$$\delta_8 = w_4 + 4 \Delta l \sin \beta_{3.5} + w_8 \cos \beta_{3.5} \quad (7-26)$$

$$\delta_T = w_4 + 4.5 \Delta l \sin \beta_{3.5} + \left(\frac{3}{2} w_8 - \frac{1}{2} w_7 \right) \cos \beta_{3.5} \quad (7-27)$$

7.2.2 Static Deflections. -- To check the analog simulation of the cantilever beam model, values of $\beta_{3.5}$, w_4 , w_8 , and δ_8 were calculated from equations (7-23) through (7-26) for the following cases and compared with output from the analog computer:

Case 1: Constant Applied Force

$$f_k = f = 0.8 \times 10^{-5} \text{ lb.} \quad k = 1 \text{ to } 8$$

$$EI = 13.85 \text{ lb-ft}^2$$

$$\Delta l = 93.75 \text{ ft}$$

	<u>Calculated</u>	<u>Measured</u>
$\beta_{3.5}$	0.325 rad.	0.313 rad.
w_4	67.1 ft.	65.3 ft.
w_8	31.0 ft.	31.3 ft.
δ_8	216.3 ft.	210.5 ft.

Case 2: Linearly Increasing Applied Force

$$f_k = [2(k - 1) + 1] f \quad k = 1 \text{ to } 8$$

$$f = 0.2 \times 10^{-6} \text{ lb.}$$

$$EI = 13.85 \text{ lb} - \text{ft.}^2$$

$$\Delta = 93.75 \text{ ft.}$$

	<u>Calculated</u>	<u>Measured</u>
$\beta_{3.5}$	0.0938 rad.	0.0901 rad.
w_4	19.0 ft.	18.3 ft.
w_8	10.3 ft.	10.0 ft.
δ_8	64.5 ft.	62.7 ft.

The results indicate the analog output to be within a few percent of the calculated values, though generally a little on the low side.

7.2.3 Static Gravity Gradient Deflections. -- To check the analog simulation of the gravity gradient field, the static tip deflection was calculated using equation (7-27) and the analog output of $\beta_{3.5}$, w_4 , w_7 , and w_8 for the following antenna properties and half-angles:

Case 3: $EI = 10.0 \text{ lb} - \text{ft.}^2$

$$\rho = 0.529 \times 10^{-3} \text{ slug/ft. (0.017 lb/ft.)}$$

$$\alpha = 22.5^\circ$$

$$\Delta l = 93.75 \text{ ft.}$$

Measured Results

$$\beta_{3.5} = 0.1851 \text{ rad.}$$

$$w_4 = 36.0 \text{ ft.}$$

$$w_7 = 14.3 \text{ ft.}$$

$$w_8 = 20.8 \text{ ft.}$$

$$\delta_T = 138 \text{ ft.}$$

Case 4: $EI = 13.85 \text{ lb-ft}^2$

$$\rho = 0.482 \times 10^{-3} \text{ slug/ft. (0.0155 lb/ft.)}$$

$$\alpha = 30^\circ$$

$$\Delta l = 93.75 \text{ ft.}$$

Measured Results

$$\beta_{3.5} = 0.2020 \text{ rad.}$$

$$w_4 = 41.2 \text{ ft.}$$

$$w_7 = 17.5 \text{ ft.}$$

$$w_8 = 25.2 \text{ ft.}$$

$$\delta_T = 154.2 \text{ ft.}$$

The tip deflection of 138 feet for case 3 compares with a value of approximately 140 feet obtained by Flatley in reference 14 for the same case. The close agreement indicates that calculating the gravity gradient forces at the deflected positions of the mass elements and taking the force components normal to the deflected baseline for the outer elements are sufficient to account for the non-linear nature of the problem. The inadequacy of evaluating gravity gradient forces at the undeformed beam position, as in a strictly linear analysis (yielding a 260-foot tip deflection), is thus confirmed. In addition, the effect of axial forces and tension within the beam seems to be taken sufficiently into account by evaluating force components normal to the secondary baseline for the outer mass elements.

¹⁴ Flatley, T.W., Equilibrium Shape of an Array of Long, Elastic Structural Members in Circular Orbit, Master's Thesis, School of Engineering and Architecture, Catholic University of America, Washington, D.C. (April 1965).

Case 4 represents the static tip deflection for the nominal antenna parameters and vee angle used in this study.

7.1.4 Oscillation Frequencies in the Gravity Gradient Field. -- To check the dynamics of the analog simulation, a number of cases have been run to measure the frequencies of the fundamental modes of oscillation. For a number of cases the exact frequency cannot be hand-calculated, but is known qualitatively relative to the value for a simpler case. All cases are run for the nominal design parameters:

$$\alpha = 30 \text{ degrees}$$

$$EI = 13.85 \text{ slug-ft.}^2$$

$$\rho = 0.482 \times 10^{-3} \text{ slug/ft.}$$

$$l = 750 \text{ feet}$$

Case 5: Fundamental Cantilever Period. -- Setting the gravity gradient forces to zero and allowing the antennas to oscillate symmetrically so as not to excite central body motion results in an oscillation period of 5900 seconds. The exact fundamental cantilever period is 5930 seconds for the continuous beam, and 5870 seconds for the eight-element lumped-mass approximation (see appendix E). The cantilever dynamics are thus simulated accurately by the analog model.

Case 6: Symmetric Bending Period. -- Rerunning case 5 with the inclusion of gravity-gradient forces results in a symmetric bending period of 4950 seconds. It is known that the gravity gradient acts effectively to stiffen the antennas about their equilibrium position and thus to increase the symmetric frequency; a simple linearized analysis to include the effective increase in stiffness due to gravity gradient yields a reduced bending period of 4990 seconds. The measured value agrees with the calculated value within the expected accuracy of the latter.

Case 7: Small-Angle Libration Period. -- The small-angle libration period of the satellite with the antennas deflected initially in their static equilibrium positions is measured to be 9500 seconds. The exact period for the rigid satellite having $\alpha = 30$ degrees is 11,200 seconds. It is to be expected that the period will decrease for the flexible body since gravity gradient tip deflections reduce the effective half-angle of the antenna vee. The 9500-second period corresponds to an effective half angle of 23.2 degrees, which seems reasonable for the 154-foot tip deflections.

Case 8: Antisymmetric Bending Period. -- The antisymmetric or "jitter" mode of satellite oscillation is that in which the antennas all bend in the same direction, similar to the vanes of a pin-wheel, while the central body rotates in the opposite direction. The measured period is 1330 seconds. The expected period should be close to that of a hinged-free beam without gravity gradient, since the central body at the beam roots has relatively little moment of inertia, and the beam does not, on the average, move significantly in the gravity-gradient field. The period of a hinged-free beam having the nominal antenna properties is 0.2286 times the fundamental cantilever period, or 1355 seconds.

In summary, the analog computer program seems to simulate the static and dynamic behavior of the satellite and flexible antennas to a very reasonable degree of accuracy.

8. CONCLUSIONS AND RECOMMENDATIONS

8.1 SUMMARY OF RESULTS. -- The development of system equations and analog and digital computer programs for the dynamics analysis of the RAE satellite has been described in detail in sections 3, 4, and 5. Section 6 deals with the development of a suitable damper/control system model, and section 7 presents a complete discussion of check cases and preliminary results obtained from the computer programs. A brief summary of the capabilities and results of these programs and studies follows.

8.1.1 Analog Computer Program. -- The analog program simulates the planar dynamics of the RAE in a circular orbit under the influence of the Earth's gravitational gradient field. The two pairs of diametrically opposed antennas are simulated by two lumped-parameter boom models; deployment is simulated by a switching technique that switches in successive mass elements as they extend from the central hub; a simple control system is represented by torquing at the central hub. A visual display technique has been developed to permit continuous observation of satellite motions. Check cases have been run successfully for static tip deflections of the antennas and for frequencies of libration, symmetric antenna bending, and asymmetric antenna bending.

8.1.2 Rigid-Body Digital Computer Program. -- The rigid-body digital program simulates large-angle, three-dimensional motion of the rigid satellite under the influence of the Earth's gravity-gradient field. The capability for using either a Keplerian orbital ephemeris or a tape-generated N-body ephemeris is provided; the direction of the Earth-Sun line relative to the orbit is calculated in both ephemeris routines. In addition, both direction cosine and quaternion integration routines for rotational dynamics are furnished with comparative results for speed and accuracy. Check cases have been run successfully for planar libration periods and amplitudes, for small-angle, three-dimensional oscillations, and for the forced planar libration amplitude due to orbital eccentricity.

8.1.3 Flexible-Body Digital Computer Program. -- The flexible-body digital program simulates large-angle, three-dimensional motion of the flexible satellite in a Keplerian orbit under the influence of the gravitational gradient, solar radiation pressure, thermal bending, and orbital eccentricity. Deflections of the antennas in two perpendicular directions normal to their undeformed axes are represented by series expansions in the small-deflection cantilever mode shapes. The direction of the Sun-line and the visible fraction of the solar disc during occultation are calculated analytically. Structural damping is included as a velocity-dependent term in the generalized beam-bending equations. At the writing of this report, test cases were being run for program debugging and checkout; no results are currently available.

8.1.4 Damper System Studies. -- On the basis of a review of current damping concepts applicable to gravity-gradient stabilized satellites, a passive magnetic hysteresis damper of the TRW Systems type has been chosen for investigation in conjunction with the RAE dynamics study. This damper, consisting of an auxiliary pair of opposed booms, has 1 rotary degree of freedom relative to the satellite central hub. Skewing the booms out of the satellite antenna plane provides damping about all three satellite axes; relative motion of the two bodies is damped by magnetic hysteresis.

8.2 RECOMMENDATIONS FOR FUTURE WORK. -- It is recommended that future investigation of RAE dynamics be carried out in three general areas: (a) improvement of the accuracy and capability of the computer simulations; (b) determination of the significance of additional higher-order terms; and (c) evaluation of the satellite/control system dynamics, damping requirements, and overall satellite design.

8.2.1 Program Modifications. -- The flexible-body digital simulation should first be modified to include the dynamics of the cross-orbit dipole antennas, and the additional terms describing antenna deployment. Higher order terms in the generalized beam coordinates should then also be added. These terms arise from two sources, non-linear strain energy and axial motion of a point on an antenna; both are related to large deformations. Further, terms describing torsion of the antenna rods as well as higher order terms generated in the evaluation of solar pressure and thermal bending at the deformed antenna positions should be included. Finally, any necessary program modifications to simulate an appropriate damper model should be made.

8.2.2 Significance of Higher Order Terms. -- For the purpose of reducing running time and cost of the flexible-body digital program to the lowest value consistent with desired accuracy of the dynamics simulation, it is essential that a study be conducted to evaluate the relative significance of higher order terms. This study in essence involves determining the importance of non-linear strain energy and axial motion of the antennas, higher bending modes of the antennas, more accurate calculation of generalized forces associated with solar pressure and thermal bending, and higher harmonics in the expansion of the Earth's gravitational field. The last item is applicable to the rigid-body digital simulation as well.

8.2.3 Evaluations and Parametric Studies. -- In keeping with the primary purpose of the RAE dynamics study, it is recommended that the developed computer programs be used for the following investigations: evaluation of deployment techniques, determination of satellite damping and control requirements, evaluation of the performance of candidate

damper and control systems, and performance of studies to assess the effects of various parameter changes. These parameters should include (a) satellite configuration design parameters, (b) antenna structural and thermal parameters, (c) orbital parameters, and (d) initial conditions prior to deployment. Items (a) through (c) are essential for a thorough study of the solar shock problem and long-term stability, and (c) and (d) for a study of the effects of errors in orbital injection and pre-deployment attitude control.

APPENDIX A

MATHEMATICAL MODEL FOR STRUCTURAL DAMPING

The mathematical model for structural hysteresis damping that has been incorporated in the flexible beam equations is discussed at some length in reference 1. The model is developed as follows.

The familiar Bernoulli-Euler equation for small-deflection dynamics of a uniform beam is

$$EI \frac{\partial^4 u}{\partial z^4} + \rho \frac{\partial^2 u}{\partial t^2} = f(z, t) \quad (A-1)$$

where E is Young's modulus, I the beam cross-sectional inertia, ρ the mass per unit length, u the deflection normal to the undeformed baseline, f the external force per unit length normal to the baseline, z the distance along the baseline, and t time. In 1927, Sezawa proposed a modification to the Bernoulli-Euler equation based on the assumption that material in the beam follows Stokes' law of viscosity, namely, that stress is a linear function of strain and strain-rate:

$$\sigma = E \epsilon + C \dot{\epsilon} \quad (A-2)$$

where σ is stress, ϵ is axial strain, and C a coefficient of viscosity. Equation (A-1) is modified in accordance with Stokes' law by replacing E by $E + C \frac{\partial}{\partial t}$, the result being Sezawa's equation:

$$EI \frac{\partial^4 u}{\partial z^4} + CI \frac{\partial^5 u}{\partial z^4 \partial t} + \rho \frac{\partial^2 u}{\partial t^2} = f(z, t). \quad (A-3)$$

The deflection u is expanded in terms of the orthogonal natural modes $\chi_n(z)$ of the freely vibrating beam:

$$u(z, t) = \sum_n A_n(t) \chi_n(z). \quad (A-4)$$

Substituting expression (A-4) into equation (A-3), multiplying through by $\chi_n(z)$, integrating from $z = 0$ to $z = l$, and applying orthogonality of the modes yields, finally,

¹ Mindlin, R. D., F. W. Stubner and H. L. Cooper, Response of Damped Elastic Systems to Transient Disturbances, Proceedings of the Society for Experimental Stress Analysis, V, No. II, pp. 69-87 (1948).

$$\rho l \bar{\chi}_{cn} \left[\ddot{A}_n + \dot{A}_n \frac{C}{E} \omega_n^2 + A_n \omega_n^2 \right] = \int_0^l \chi_n(z) f(z,t) dz. \quad (A-5)$$

Equation (A-5) is the second-order generalized beam equation for the coefficient of the n^{th} natural mode shape. The modal constant $\rho l \bar{\chi}_{cn}$ is simply the generalized mass,

$$\rho l \bar{\chi}_{cn} = \int_0^l \chi_n^2(z) \rho dz \quad (A-6)$$

and ω_n is the natural frequency of the n^{th} mode. It follows from equation (A-5) that the damping ratio ζ_n (fraction of critical damping) for the n^{th} mode is proportional to the natural frequency of the mode when C is constant:

$$\zeta_n = \frac{C \omega_n}{2E}. \quad (A-7)$$

Nevertheless, experimental evidence cited in references 1 through 3 indicates that the fraction of critical damping is nearly independent of frequency. Most structural materials do not follow Stokes' law based on a constant value of C ; instead, the viscosity coefficient is to a first approximation inversely proportional to frequency. Much closer agreement with experiment is obtained by assuming -- after going through the mathematics leading up to equation (A-5) -- that

$$\frac{C \omega_n}{E} = \frac{C \omega}{E} = \frac{1}{Q} = \text{constant}. \quad (A-8)$$

This assumption, designated the "constant Q hypothesis" in reference 3, clearly implies that

$$\zeta_n = \zeta = \text{constant} \quad (A-9)$$

for all modes and frequencies of oscillation.

²Wegel, R. L., and H. Walther, Internal Dissipation in Solids for Small Cyclic Strains, *Physics*, **6**, p. 141 (1935).

³Kimball, A. L., Vibration Problems, Part V -- Friction and Internal Damping, A.S.M.E., *Journal of Applied Mechanics* Reprint Series, Book 2, Design Data on Mechanics, p. A-22 (May, 1944).

Damping is incorporated in the flexible beam equations for the generalized coordinates A_{mn} and B_{mn} in the terms $D_n A_{mn}$ and $D_n B_{mn}$. These equations are essentially the same as equation (A-5) of this section, with the addition of inertial terms corresponding to translation and rotation of the baseline in inertial space, and axial terms related to tension in the beam. The damping coefficient D_n is seen from equations (A-5) and (A-7) to be

$$D_n = 2 \zeta_n \omega_n \rho l \bar{\chi}_{cn} . \quad (A-10)$$

Structural damping does not enter directly into the translation and rotational equations of motion for the satellite as a whole. Employing alternately the dimensionless parameter

$$\bar{k}_n = \left(\frac{\rho l^4 \omega_n^2}{EI} \right)^{1/4} \quad (A-11)$$

from which ω_n is determined, the damping coefficient is

$$D_n = 2 \zeta_n \rho l \bar{\chi}_{cn} \bar{k}_n^2 \sqrt{\frac{EI}{\rho l^4}} . \quad (A-12)$$

The actual value of ζ_n used in the digital simulation of the satellite may be varied for different modes if desired. However, until further test data on the deHavilland tubes should indicate otherwise, ζ_n will be assumed constant at the value $\zeta = 0.00366$, corresponding to a log decrement of $\delta = 0.023$ per cycle.

It should be added in passing that the assumption of a constant structural damping ratio for the lower-frequency bending modes is commonly employed in the analysis of flexible boosters for automatic control system design, as in reference 4. Damping will generally be higher for high-frequency modes, however, because of coulomb friction between moving parts. Coulomb friction is, of course, probable within the overlapped seam of the deHavilland tubes used for the RAE antennas.

⁴Lukens, D. R., A. F. Schmitt, and A. J. Broucek, Approximate Transfer Functions for Flexible-Booster-and-Autopilot Analysis, Convair (Astronautics) Report No. AE61-0198, WADD TR-61-93 (April 1961).

APPENDIX B

RELATIVE CONTRIBUTIONS OF BEAM BENDING MODES TO STATIC TIP DEFLECTION

The small-deflection beam equation for planar motion of a uniform beam is

$$EI \frac{\partial^4}{\partial z^4} u(z,t) + \rho \frac{\partial^2}{\partial t^2} u(z,t) = f(z,t) \quad (B-1)$$

where E is Young's modulus, I the cross-sectional inertia, ρ the mass per unit length, u the deflection normal to an undeformed baseline, f the external force per unit length, z distance along the baseline, and t time. The deflection u is written as a series expansion in the natural mode shapes $\chi_n(z)$:

$$u(z,t) = \sum_n A_n(t) \chi_n(z) \quad (B-2)$$

Due to orthogonality of the natural modes, equation (B-1) can be reduced to a set of uncoupled, ordinary, second-order differential equations in A_n :

$$\rho l \bar{\chi}_{cn} (\ddot{A}_n + \omega_n^2 A_n) = Q_n(t) \quad (B-3)$$

where ω_n is the natural frequency of the n^{th} mode, and $\rho l \bar{\chi}_{cn}$ and $Q_n(t)$ are, respectively, the generalized mass and force associated with the n^{th} mode:

$$\rho l \bar{\chi}_{cn} = \int_0^l \chi_n^2(z) \rho dz \quad (B-4)$$

$$Q_n(t) = \int_0^l \chi_n(z) f(z,t) dz \quad (B-5)$$

The natural frequency ω_n is obtained from the relation

$$\omega_n^2 = (k_n l)^4 \frac{EI}{\rho l^4} \quad (B-6)$$

where l is the length of the beam. The static value of the modal coefficient A_n for a steady applied force is clearly

$$A_n = \frac{Q_n}{\omega_n^2 \rho l \bar{\chi}_{cn}} \quad (B-7)$$

If $\chi_n(z)$ is normalized such that $\chi_n(l) = 1.0$, then A_n is simply the tip deflection contributed by the n^{th} mode. The relative tip deflection with respect to that of the first mode is then

$$\frac{A_n}{A_1} = \frac{\omega_1^2}{\omega_n^2} \frac{\bar{\chi}_{c1}}{\bar{\chi}_{cn}} \frac{Q_n}{Q_1} \quad (B-8)$$

For a cantilever beam clamped at $Z = 0$, the natural mode shapes are

$$\chi_n(z) = C_{1n} (\sin k_n z - \sinh k_n z) + C_{2n} (\cos k_n z - \cosh k_n z) \quad (B-9)$$

where k_n is a solution to the equation

$$\cos k_n l \cosh k_n l = -1 \quad (B-10)$$

and the coefficients C_{1n} and C_{2n} are

$$C_{1n} = \frac{\cosh k_n l + \cos k_n l}{2 (\sin k_n l \cosh k_n l - \cos k_n l \sinh k_n l)} \quad (B-11)$$

$$C_{2n} = -\frac{\sinh k_n l + \sin k_n l}{2 (\sin k_n l \cosh k_n l - \cos k_n l \sinh k_n l)} \quad (B-12)$$

The values (B-11) and (B-12) have been chosen such that $\chi_n(l) = 1.0$. It can next be shown that, using these relations, the generalized mass for each mode is the same:

$$\rho l \bar{\chi}_{cn} = \frac{1}{4} \rho l \quad (B-13)$$

Using relations (B-6) and (B-13), equation (B-8) reduces to

$$\frac{A_n}{A_1} = \frac{(k_1 l)^4}{(k_n l)^4} \frac{Q_n}{Q_1} \quad (B-14)$$

It is of interest to evaluate Q_n for a constant external force per unit length, and for a linearly increasing force per unit length. The first corresponds, for example, to solar pressure acting on the undeformed antenna, and the second to a gravity gradient force distribution acting on the same.

1. Constant External Force Per Unit Length

Let $f(z) = K_1$. Then the n^{th} generalized force is

$$\begin{aligned} Q_n &= \int_0^l K_1 \chi_n(z) dz \\ &= K_1' \frac{1}{k_n l} C_{1n} \end{aligned} \quad (\text{B-15})$$

where K_1' is a constant independent of the mode. Hence the relative tip deflection is

$$\frac{A_n}{A_1} = \frac{(k_1 l)^5}{(k_n l)^5} \frac{C_{1n}}{C_{11}}. \quad (\text{B-16})$$

2. Linearly Increasing External Force Per Unit Length

Let $f(z) = K_2 z$. Then the n^{th} generalized force is

$$\begin{aligned} Q_n &= \int_0^l K_2 z \chi_n(z) dz \\ &= -K_2' \frac{1}{(k_n l)^2} C_{2n} \end{aligned} \quad (\text{B-17})$$

where, again, K_2' is a constant independent of the mode. The relative tip deflection is then

$$\frac{A_n}{A_1} = \frac{(k_1 l)^6}{(k_n l)^6} \frac{C_{2n}}{C_{21}}. \quad (\text{B-18})$$

The values of $k_n l$, C_{1n} , C_{2n} , and A_n/A_1 for the first six natural modes are summarized in the following table:

				$\left \frac{A_n}{A_1} \right $: Relative Tip Deflection	
n	$k_n l$	C_{1n}	C_{2n}	$f = K_1$	$f = K_2 z$
1	1.875	0.36703	-0.50001	1.000	1.000
2	4.694	-0.50920	0.49996	0.01411	0.004061
3	7.855	0.49961	-0.50000	0.001054	0.0001850
4	10.996	-0.50002	0.50000	0.0001963	0.00002458
5	14.137	0.50000	-0.50000	0.00005588	0.000005443
6	17.279	-0.50000	0.50000	0.00002049	0.000001632

It is evident that for the two external force distributions considered, only the first natural mode is significant; higher modal contributions converge rapidly toward zero.

APPENDIX C

RIGID BODY DIGITAL COMPUTER PROGRAM (PROGRAM 1048)

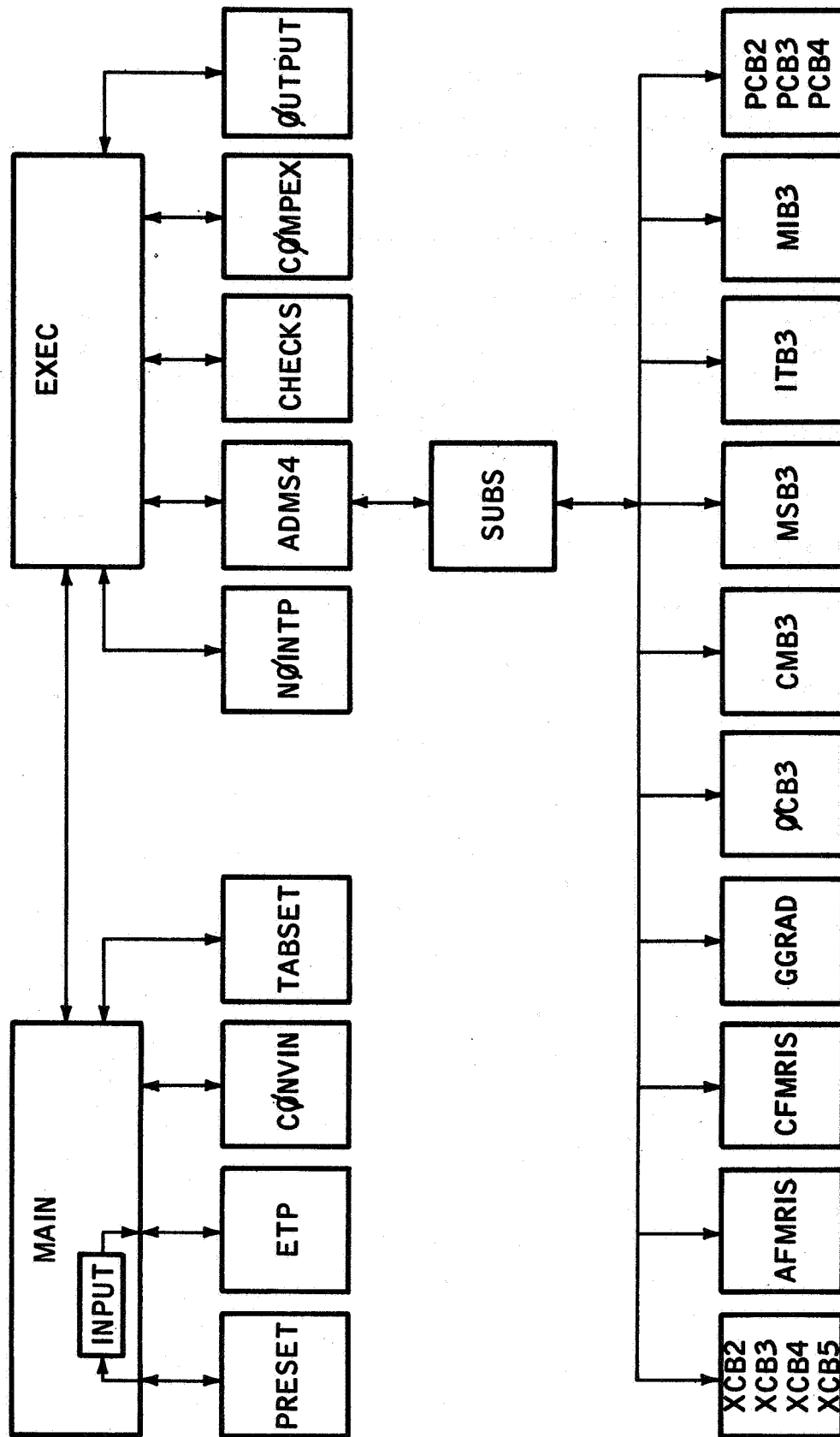
I. PROGRAM STRUCTURE AND DESCRIPTION

Presented herein is a brief description of the general logic flow in program 1048. Figure C-1 illustrates the general flow between the various subroutines of the program. Auxiliary subprograms, such as those requested from the system tape, plus others which perform routine tasks, have been deleted from the diagram. Program 1048 contains several significant features which include flexibility in the input-output routines, selection of running mode at time of execution, and a generalized check-stop routine. Other features include the pre-setting of commonly used quantities in order to reduce the amount of input, a generalized integration routine using a 4-point predictor-corrector scheme, and a selection of methods for computing body orientation.

The input subroutine HØLNAM allows data to be read in a very simple and flexible manner, while also permitting such refinements as the computation of simple arithmetic operations at input time. The output routine also provides considerable flexibility in that any variable in CØMMØN may be printed out with input controllable format. The check-stop routine, called CHECKS, allows any two quantities in CØMMØN storage to be compared, and if the comparison is favorable for a stop, a control word is reset and the program control returns to MAIN to request new data. The integration routine, ADMS4, utilizes updating criteria and bounded error intervals for the integrand on any given time step in addition to the 4-point predictor-corrector scheme mentioned above. This ensures an accurate numerical evaluation of the equations of motion. Additional features contained in 1048 are discussed in the program description following, and the reader is referred to this section of the manuscript for details.

Entry to the program is made through MAIN which directs the flow as indicated. MAIN calls PRESET, INPUT, ETP, CØNVIN, and TABSET, which perform calculations necessary to prepare the program for execution. PRESET pre-sets a series of control words and tables, hence avoiding the necessity of reading these in as part of the input. ETP makes provision for the running of sequential cases and also the stacking of sequential cases. CØNVIN allows the reading in of input in three different forms. TABSET prepares a set of tables which are used later in the program.

After passing through MAIN, control is transferred to EXEC. EXEC calls NØINTP, ADMS4, CHECKS, CØMPEX, and OUTPUT. This combination of subroutines controls the program from this point on, until a stop is determined. NØINTP is a table look-up with no interpolation. ADMS4 performs the integration of the differential equations in addition to calling the remainder of the



65-11989

Figure C-1 FLOW CHART OF 1048 PROGRAM

subroutines. CHECKS is a subroutine which may stop the program when conditions so specify. COMPEX calculates specific quantities which may be printed as part of the output. OUTPUT is the variable format printing routine.

ADMS4 calls SUBS which then calls the remainder of the subroutines. These subroutines under SUBS in figure C-1 set up the form of, and supply numerical values to, the derivative equations for the motion of the rotating body.

II. SUBROUTINE DESCRIPTIONS

1. Introduction

The RAE digital computer program 1048 is presented as a complex of subroutines under the control of two separate calling subroutines, specifically the two program control blocks called (MAIN) and (EXEC). The primary purpose of (MAIN) is to prepare the remainder of the program for running. Control is then transferred to (EXEC) where the actual numerical quantities of interest are generated. Control remains within the (EXEC) combination of subprograms until a stop is determined and at this point return is made back to (MAIN). A decision between exiting or reading new data is made at this time in (MAIN). The outline presented below lists the primary subroutines used in the (MAIN) and (EXEC) blocks. Subsequent discussion of the various subprograms will occur in the order shown.

A. (MAIN)

1. PRESET
2. INPUT - HØLNAM
3. ETP
4. CØNVIN
5. TABSET

B. (EXEC)

1. NØINTP
2. ADMS4

a. SUBS

1. XCB2 - XCB3 - XCB4 - XCB5
2. AFMRIS
3. CFMRIS
4. GGRAD
5. ØCB3
6. CMB3
7. MSB3
8. ITB3

- 9. MIB3
- 10. PCB2 - PCB3 - PCB4

- b. CHECKS
- c. COMPEX
- d. OUTPUT

2. (MAIN)

The purpose of (MAIN) is to prepare completely the remainder of the program for proper execution. Initial entry to (MAIN) erases all of the COMMON storage, hence avoiding any problems due to information being retained from previous jobs. The remainder of (MAIN) consists of a series of "calling" statements which transfer control to the following subroutines:

- a. PRESET
- b. INPUT
- c. ETP
- d. CONVIN
- e. TABSET

A description of these subprograms follows.

3. PRESET

This subroutine performs the following operations upon entry to the program:

- 1. Gives numerical values to control words
- 2. Presents commonly used variables, hence reducing the amount of input
- 3. Utilizes Boolean statements to suppress the printing of unnecessary zeros during output
- 4. Sets the prescribed upper and lower bounds used in the integrating routine
- 5. Establishes the suggested numerical values for updating
- 6. Prepares a table of common locations used for the storage of input for sequential cases.

PRESET is an auxiliary block which may be deleted; however the amount of input data would increase by several orders of magnitude if this were done. This fact alone justifies the existence of such a subprogram.

4. INPUT

This subroutine initiates the reading of data into the program. Subroutine INPUT is used in conjunction with HØLNAM where HØLNAM sets up the variable input text. An example of a typical input sequence is illustrated below.

```
CALL HØLNAM (2HY Y, XX)
```

```
CALL INPUT (I).
```

Upon processing the "CALL INPUT" statement, the value associated with "YY" in the DATA deck is stored in the location set aside for "XX" in the (MAIN) program. For convenience, all of the variable names in HØLNAM statements have been placed in COMMON storage by means of EQUIVALENCE statements. Calling INPUT initiates the reading of sequential data until a transfer card is processed. (A transfer card has a one in column one.) At the end of any given case, return to MAIN generally means processing the next "CALL INPUT" statement. In this manner, sequential cases may be run until an "END-ØF-JØB" card occurs in the data deck, hence terminating the job.

5. ETP

Subroutine ETP performs four basic tasks. The first is to reset the control variables necessary to begin a new case. The second is to store the initial input variables so that sequential cases may be run without repeating all of the data in the "DATA DECK." The third is to provide an option to stop the program at some point, read additional data, and then continue with the running of the program using this point as the start of the next case. This mode of operation will henceforth be referred to as "stacking." The fourth allows the branching of sequential cases from any given stopping point.

Figure C-2 illustrates the basic logic flow in subroutine ETP. The first entry into ETP finds III = 1 and ST2 = 0, as these are the values assigned to III and ST2 in the PRESET subprogram. Following the flow in figure C-1 we see that the initial conditions are stored and the two control words, III and ST2, are recalculated. In this case III is given the value of 2 and ST2 is equated to STACK. Referring to (MAIN) we see that ETP is called again after returning from (EXEC). This indicates that a stop has occurred which generally is the end of a given case. Since III is now 2, a check on

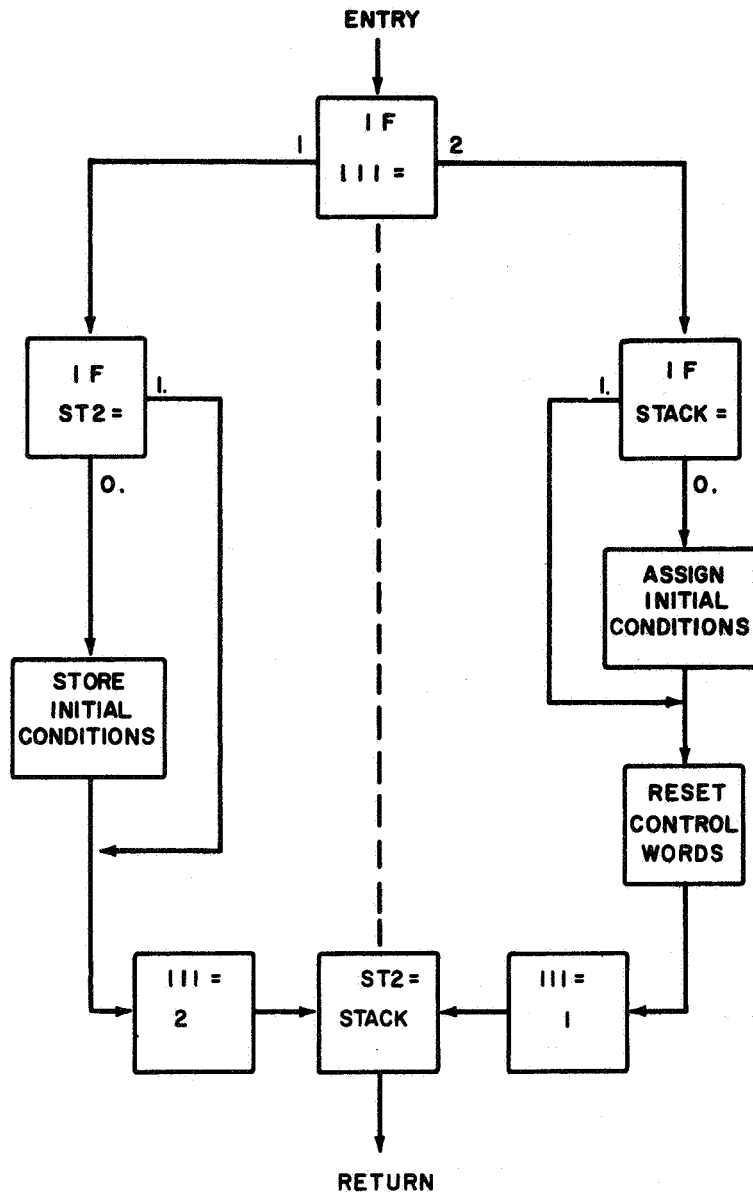


Figure C-2 FLOW DIAGRAM OF ETD

STACK occurs. If stack is zero, the initial conditions from the present data set are reassigned to the running variables. However, if STACK is one (1), this assign condition is bypassed and the end conditions of the present case remain in the COMMON locations of the running variables. In effect, the latter procedure simply allows the next case to be started where the last case stopped. Before exiting from ETP, III is set equal to 1, and ST2 is equated to STACK, along with resetting several control words. Referring again to (MAIN), we see that INPUT is called before entering ETP again. Reading input at this point allows the initial conditions to be changed by writing over the values set up in ETP. The flow logic in ETP, before control transfers to (EXEC), is now controlled by ST2, as III was equated to 1 before the previous exit. Since ST2 has the value of STACK, we see that the storage of initial conditions is bypassed if STACK was one (1.) on the previous case, hence indicating the storage of the final conditions. If STACK were zero (0.) in the previous case, the initial conditions are stored. This sort of flow in and out of ETP continues until a program stop is determined.

6. CØNVIN

Subroutine CØNVIN allows the input to 1048 to be read into the program in various forms. At present, the three rotational degrees of freedom are defined by the direction cosine matrix locating the inertial axes with respect to the body reference frame. In order to utilize a more convenient set of input quantities, subroutine CØNVIN has been generated. The initial values for the rotational degrees of freedom may be read in under three modes. The first method is given by:

PB = the initial rotation rate about the body x axis

QB = the initial rotation rate about the body y axis

RB = the initial rotation rate about the body z axis

C = a matrix containing the nine elements of the transformation between the body and inertial axes. This matrix is read in row-wise as a one-dimensional array.

The above quantities are the running variables for the rotational motion in 1048.

The second method of producing the initial conditions for the rotational motion is by an Euler angle transformation. The initial body rates (PB, QB and RB) must still be used, except now the array EULER and the word INERT2 generate the "C" matrix in CØNVIN. The correct format is:

EULER I. B. J. D. K. F.

INERT 2 2

where I, J and K are fixed point integers defining the axes of rotation, and

1 is rotation about the x axis

2 is rotation about the y axis

3 is rotation about the z axis

The values B, D, and F are the angular rotations about the I, J, and K axes, respectively. Note that the sequence of the rotations must allow the inertial axes to be rotated into the body axes; moreover, each rotation is performed about the most recent direction of the axis in question. INERT2 = 2 permits the generation of this transformation.

A third input option is available as input for the rotational motion. This consists of a local orthogonal coordinate system defined by the satellite position vector, a vector perpendicular to the position vector in the orbital plane containing the position and velocity vectors, and a third vector defined by the vector product of the first two. Reading in the control word INERT2 = 3 automatically defines the above system. The location of the body axes with respect to this local system is then read in according to the following words:

ALFAE, BETAE and GAMAE.

These three angles (in degrees) define a 3-2-1 Euler rotation of the local coordinate system into the body axes. CONVIN then uses the two systems described above to determine the C matrix for program execution. Again, the body angular rates must be supplied in the form previously described. A block diagram is presented in figure C-3 showing the logic flow in CONVIN.

7. TABSET

The purpose of TABSET is primarily to prepare a set of tables which are used in conjunction with the integrating routine (ADMS4) and the derivative calculating subroutines. For the three-degree-of-freedom simulation, various combinations of derivatives are used in the analysis. That is, one may integrate the derivatives of the quaternions or the direction cosines. In addition, it is possible to integrate either six or nine direction cosine derivatives. One of these three systems must be chosen at the time of input to the program. In order to allow the flexibility of using the various

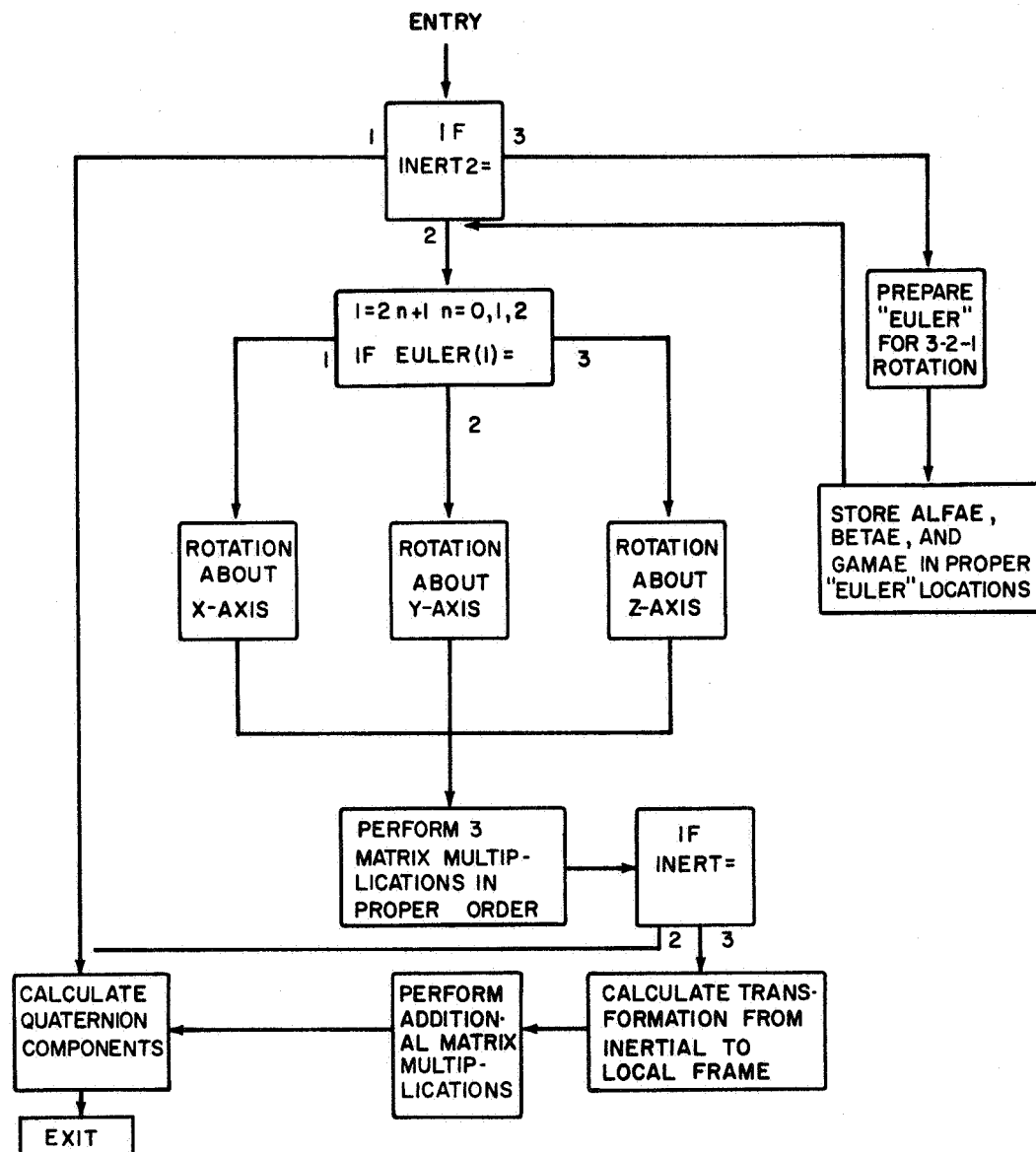


Figure C-3 FLOW DIAGRAM OF CONVIN

methods, the subprogram TABSET has been generated. Control within TABSET is accomplished by the word KD. Depending upon the value of KD, which may range from 1 to 4, the following derivatives will be used.

If KD = 1, set up the integral and derivative tables for the body rate vector only. If KD = 2, prepare the integral and derivative tables for the six direction cosines plus the body rate vector. If KD = 3, set up the integral and derivative tables for the four quaternions plus the body rate vector. Finally, if KD = 4, the derivative and integral tables for the nine direction cosines are prepared along with the body rate vector. The FORTRAN symbols used in TABSET are defined below:

1. KDTBL (I) - a table of numbers defining the common locations containing the values of the derivatives.
2. KITBL (I) - a table of numbers defining the common locations containing the values of the integrals where the Ith location in KITBL is compatible with the Ith location in KDTBL.
3. CØNCK (I) - the numerical value of the updating constant. Again, the Ith value in this table is compatible with the Ith value in KITBL.
4. UPBND (I) and DNBND (I) - the upper and lower bounds utilized in the integrating routine (ADMS4). These tables are set up in conjunction with the above arrays; however, the numerical values in UPBND (I) and DNBND (I) are obtained from either subroutine PRESET or the input.

TABSET also presents the initial values of SAVE, VALUE, and CØNST. By definition, the proper place to preset these tables is in the subprogram PRESET; however, these tables cannot be set up until the values in KITBL are established.

8. (EXEC)

This subroutine controls the complete operation of the program after transfer from (MAIN). (EXEC) performs the function of determining the derivatives for the set of differential equations and then integrating these equations numerically. This task is accomplished in (EXEC) by calling the subprogram ADMS4. The printing frequency is determined in (EXEC) and used in ADMS4. The table look-up routine called NØINTP performs this task of finding the print frequency, which is then used in ADMS4 to calculate the proper time to exit from ADMS4 to print. The printing is done by the subroutine called ØUTPUT. The printing format is completely variable such that any quantity in CØMMØN storage may be typed out. In addition, Hollerith text (up to 6 characters per word) may be printed by ØUTPUT.

(EXEC) also calls a subroutine named CHECKS. The primary function of this routine is to determine the stopping point during the running of the program. This subroutine will check any two numbers in COMMON storage, and when the comparison between the two numbers indicates that a stop should occur, CHECKS resets the control work ISTOP to initiate an exit in (EXEC).

The subprograms NØINTP, ADMS4, CHECKS, and ØUTPUT will be discussed in detail later. A brief flow diagram of (EXEC) is shown in figure C-4. Control in (EXEC) is accomplished by two control words, LADM and ISTOP. When LADM has the value of one, this indicates to the program that it is the first pass through ADMS4. Once integration begins, LADM obtains values of 2 through 6, which are assigned according to the flow in ADMS4. However, if LADM = 6, this indicates that the interval of integration has been made too small and an abnormal exit through (EXEC) occurs. When a normal stop has been found by CHECKS or ADMS4, ISTOP is set equal to one. This indicates to (EXEC) that a normal exit to (MAIN) is in order.

9. NØINTP

This subroutine is used in conjunction with (EXEC) as a no-interpolation table search. The calling sequence for NØINTP as it appears in (EXEC) is as follows:

CALL NØINTP (CD(IFRQ), VFQTBL, FREQ, FRQTBL).

In most cases the print frequency (FREQ) will be determined by time; however, practically any other physical quantity in COMMON storage may be used. The arguments in the calling sequence are defined below:

VFQTBL	= a table of numbers having the same units as CD(IFRQ), where $VFQTBL (MIN) \leq CD(IFRQ) \leq VFQTBL (MAX)$
CD(IFRQ)	= the instantaneous value of CD used in the VFQTBL search. In most cases, CD(IFRQ) will be time; hence IFRQ=595 must be part of the input.
FRQTBL	= a table of numbers representing the various print frequencies being used. For each number in VFQTBL there must be a corresponding number of FRQTBL.
FREQ	= the print frequency interval.

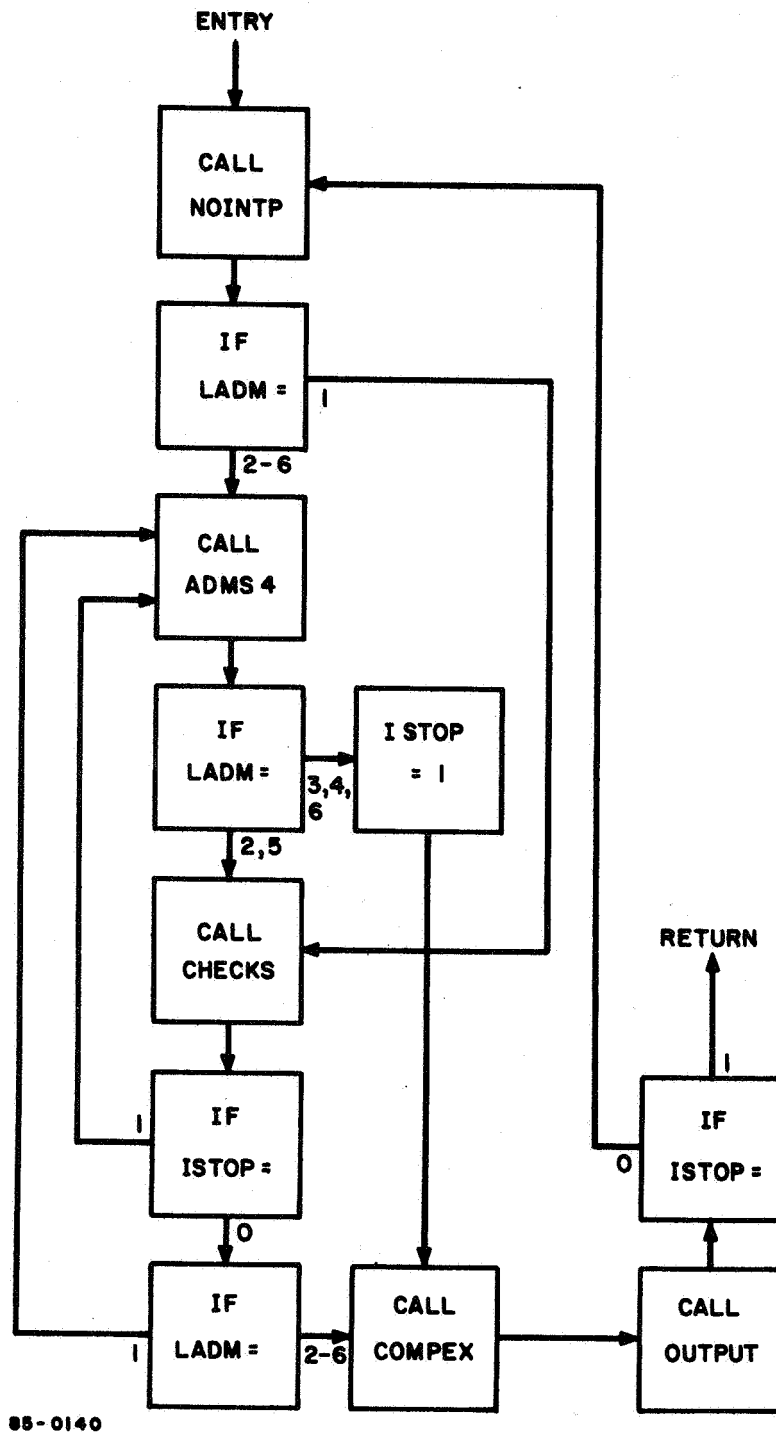


Figure C-4 FLOW CHART OF EXEC

10. ADMS4

A four point Adams integration scheme is used to evaluate the differential equations. The first four points required to start the scheme are calculated by using a Runge Kutta method with a fixed time increment DT0. Once the first four time steps have been evaluated and the integration switches to the Adams method, the time increment is internally controlled by comparing the difference between the extrapolated and the interpolated values of the integrands (a measure of the integration accuracy) with upper and lower bounds (preset or input controlled) and decreasing or increasing the time increment according to whether the error is too large or too small (thus unnecessarily increasing the running time) respectively. If the accuracy restriction cannot be met due to a discontinuity, input error, and so forth, the subroutine will attempt to cut the increment until it becomes less than DELMIT (preset or input controlled) at which time it will stop with the control word LADM = 6. ADMS4 calls the subroutine SUBS in order for SUBS, in turn, to call the necessary derivative evaluations. The COMMON locations of the various derivatives and integrands are controlled by KDTBL (a table specifying where the evaluated derivatives are located) and KITBL (a table specifying where the updated values of the integrals should be stored).

Accuracy is improved (specifically, truncation error is reduced) by means of an automatic updating routine. If the integrand of a particular variable has a large value but is only slowly varying, the amount truncated from the integrand increment when it is added to the previous value of the integrand can seriously affect the accuracy of the result after a number of integration steps. To reduce this error, the major part of the integrand is carried separately as a constant. The slowly time-varying part is allowed to accumulate until it reaches a value specified by CONCK. When this occurs, the time-varying part is added to the constant part, the truncation error is determined, and the time-varying part is started over with the amount which was truncated.

11. SUBS

The purpose of subroutine SUBS is to guide the calling of the proper subprograms in order to obtain the derivative equations which are to be integrated in ADMS4. The logical flow in SUBS is accomplished through the use of the control words KA, KB, KC, and KD. KA and KD are the variables which control the calling sequence for the quaternion or direction cosine derivatives. KD is the same control variable which appeared in TABSET. The control accomplished by using KD ensures that the derivatives which are obtained will be compatible with the logic flow in TABSET. KA operates in conjunction with KD. Referring to figure C-5, we notice that KD controls the calling of the subroutines PCB2, PCB3, and PCB4.

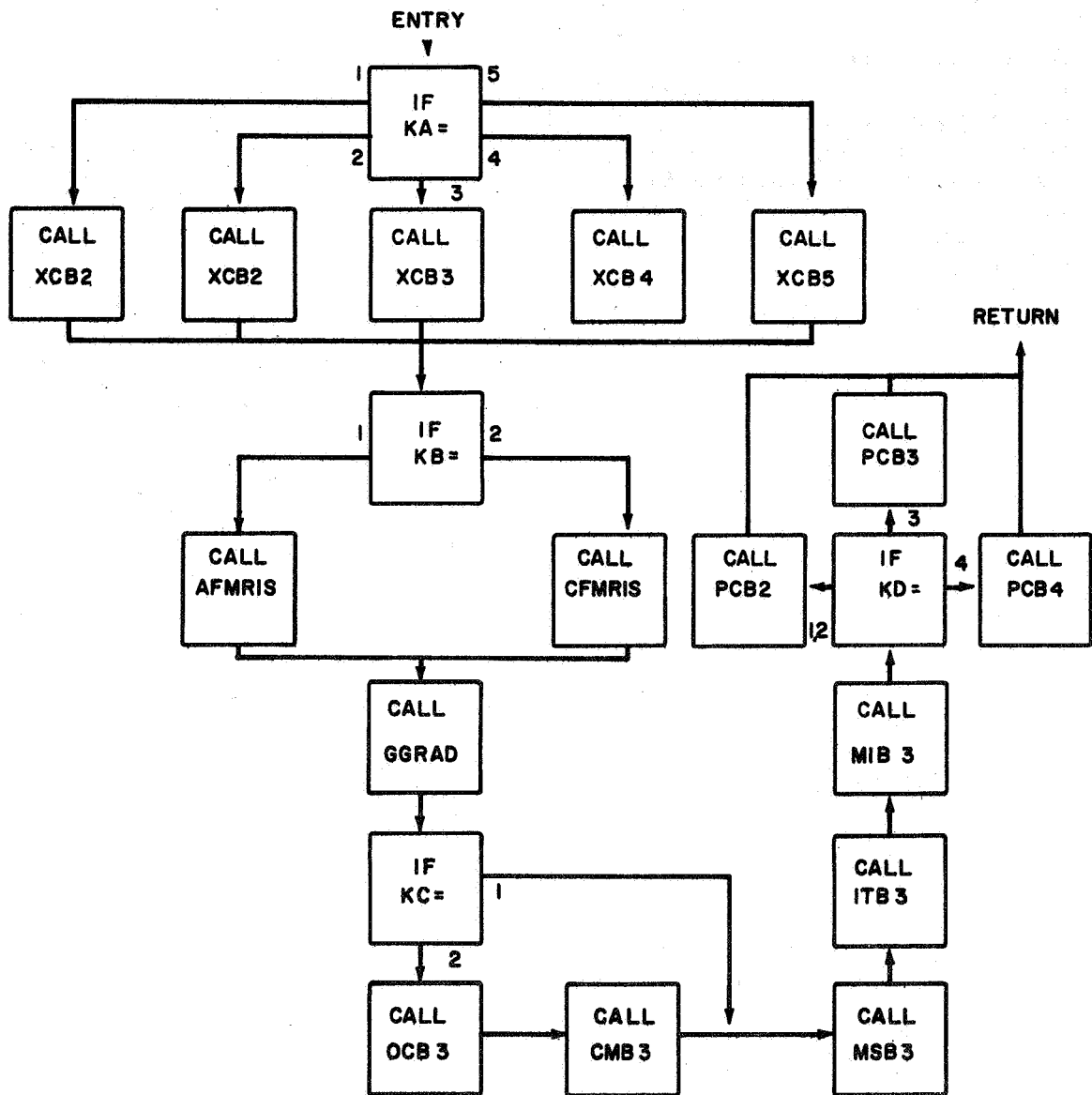


Figure C-5 FLOW CHART OF SUBS

KA controls the calling of XCB2, XCB3 and XCB4. Control must be such that XCB2 is called only with PCB2, XCB3 and XCB5 are called only with PCB3, and XCB4 is called only with PCB4. KB and KC control the calling of the remainder of the subroutines. (Refer to figure C-5 for the flow chart.)

12. XCB2, XCB3, XCB4, and XCB5

These subroutines are auxiliary blocks which are available to make any calculations necessary upon entry into the derivative chain. At the present time their only function is to complete the direction cosine matrix, normalize the quaternions, etc. Each version of XCB performs different tasks as explained below.

a. XCB2

This subprogram simply completes the direction cosine matrix when only 6 direction cosine derivatives are being integrated. Since the first two rows of the matrix are obtained from integration, the remaining 3 elements are found from the orthogonality condition:

$$C_{31} = C_{12} C_{23} - C_{13} C_{22}$$

$$C_{32} = C_{13} C_{21} - C_{11} C_{23}$$

$$C_{33} = C_{11} C_{22} - C_{12} C_{21}$$

Symbol Glossary

Equation Symbol	Comments	Fortran Symbol	COMMON* Location	Input	Output
C ₃₁	The remaining three elements of the (C) matrix to be calculated	C(7)	312		X
C ₃₂		C(8)	313		X
C ₃₃		C(9)	314		X
C ₁₁	The six elements of the direction cosine matrix (C) obtained from integration	C(1)	306	X	
C ₁₂		C(2)	307	X	
C ₁₃		C(3)	308	X	
C ₂₁		C(4)	309	X	
C ₂₂		C(5)	310	X	
C ₂₃		C(6)	311	X	

*Location in CØ array unless otherwise specified.

b. XCB3

This subroutine is used in conjunction with the derivative subprogram for the quaternions, PCB3. Because of the input required by other routines, it is still necessary to obtain the direction cosine matrix. XCB3 performs the following calculations:

- 1) Normalizes the quaternion components from the equation

$$q_i = \frac{q_i}{\sum_{k=0}^3 q_k} \quad i = 0, 1, 2, 3$$

The above calculation was made in an effort to reduce the error in the quaternion components, since

$$\sum_{i=0}^3 q_i = 1.$$

- 2) The components of the direction cosine matrix are calculated from the new quaternion components by the equation:

$$(C) = 2 \begin{pmatrix} (q_0^2 + q_1^2) - 1/2 & q_1 q_2 + q_0 q_3 & q_1 q_3 - q_0 q_2 \\ q_1 q_2 - q_0 q_3 & (q_0^2 + q_2^2) - 1/2 & q_2 q_3 + q_0 q_1 \\ q_1 q_3 + q_0 q_2 & q_2 q_3 - q_0 q_1 & (q_0^2 + q_3^2) - 1/2 \end{pmatrix}^{-1}$$

where (C) is the direction cosine matrix and the q_i 's ($i = 0, 1, 2, 3$) are the quaternion components.

<u>Equation Symbol</u>	<u>Comments</u>	<u>Fortran Symbol</u>	<u>COMMON* Location</u>	<u>Input</u>	<u>Output</u>
(C)	The direction cosine matrix having components C_{ij} .	C(1)..C(9)	306-315		X
q_0	The integrated quaternion components.	Q ₀	26	X	
q_1		Q ₁	27	X	
q_2		Q ₂	28	X	
q_3		Q ₃	29	X	

*Location in CØ array unless otherwise specified.

c. XCB4

This subroutine is used in conjunction with PCB4 which prepared the derivatives for all nine direction cosines. XCB4 normalizes the direction cosine matrix in row-wise fashion in an attempt to improve the accuracy. The equations utilized in XCB4 are:

$$C_{ij} = \frac{C_{ij}}{\sum_{K=1}^3 C_{ik}^2}, \quad i = 1, 2, 3.$$

Symbol Glossary

<u>Equation Symbol</u>	<u>Comments</u>	<u>Fortran Symbol</u>	<u>COMMON** Location</u>	<u>Input*</u>	<u>Output*</u>
C_{ij}	The i, jth component of the direction cosine matrix	C(I)	306	X	X

* Storage of the C matrix back in its original location ensures proper usage later in the calculations.

** Location in CØ array unless otherwise specified.

d. XCB5

This subprogram is identical to XCB 3 except that the normalization of the quaternion components has been deleted.

13. AFMRIS

Subroutine AFMRIS computes the instantaneous position of the satellite, given its initial position and velocity. The instantaneous velocity and the solar illumination factor are also computed to facilitate the subsequent consideration of the effects of solar pressure and the Earth's magnetic field.

In the position and velocity calculation, the angular acceleration of the orbital plane with respect to inertial space is neglected; however, in the calculation of the sun line vector the rotation itself is taken into account. This routine also provides GGRAD with the gravity vector, expressed in the inertial frame.

Equations:*

$$\sqrt{\mu} t = \frac{\vec{r}_0 \cdot \vec{v}_0}{\sqrt{\mu}} x^2 C(a_0 x^2) + (1 - r_0 a_0) x^3 S(a_0 x^2) + r_0 x \quad (C-1)$$

$$x = \frac{E - E_0}{\sqrt{a_0}}$$

$$a_0 = \frac{2}{r_0} - \frac{v_0^2}{\mu}$$

$$S(u) = \begin{cases} (\sqrt{u} - \sin\sqrt{u})/(\sqrt{u})^3, & u > 0 \\ \frac{1}{3!} - \frac{x}{5!} + \frac{x^2}{7!} - \dots, & u \neq 0 \\ (\sinh\sqrt{-u} - \sqrt{-u})/(\sqrt{-u})^3, & u < 0 \end{cases} \quad (C-2a)$$

$$C(u) = \begin{cases} (1 - \cos\sqrt{u})/u, & u > 0 \\ \frac{1}{2!} - \frac{x}{4!} + \frac{x^2}{6!} - \dots, & u \neq 0 \\ (\cosh\sqrt{-u} - 1)/(-u), & u < 0 \end{cases} \quad (C-2b)$$

$$\begin{aligned} \vec{r}(t) &= \left[1 - \frac{x^2}{r_0} C(a_0 x^2) \right] \vec{r}_0 + \left[t - \frac{x^3}{\sqrt{\mu}} S(a_0 x^2) \right] \vec{v}_0 \\ \vec{v}(t) &= \left[a_0 x^3 S(a_0 x^2) - x \right] \frac{\sqrt{\mu}}{r_0} \vec{r}_0 + \left[1 - \frac{x^2}{r} C(a_0 x^2) \right] \vec{v}_0 \end{aligned} \quad (C-3a, b)$$

The subroutine **FINDX** solves the above equations using a Newton-Raphson iteration in double precision arithmetic. AFMRIS provides **FINDX** with the initial values of time, position, and velocity from which **FINDX** computes the orbital elements. Thereafter, once the time is specified, **FINDX** computes the instantaneous position and velocity according to the following scheme: Kepler's equation (equation C-1) is solved iteratively for x ; $C(a_0 x^2)$ and $S(a_0 x^2)$ are computed from equations C-2. Equations C-3 are then used to calculate the position and velocity.

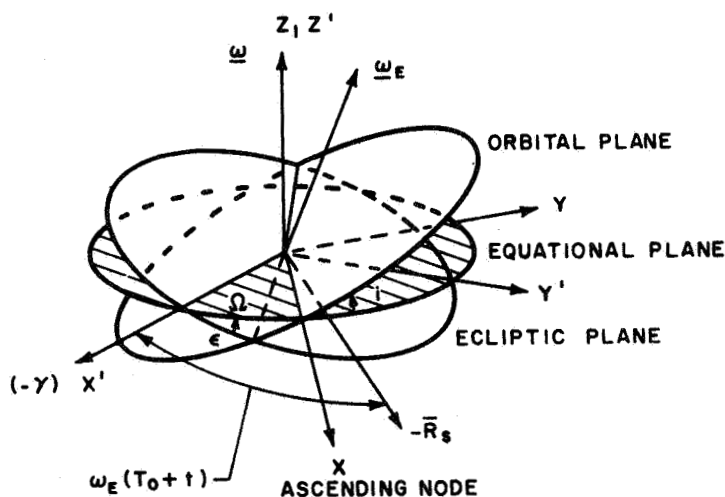
*Battin, R.H., *Astronautical Guidance*, pp. 51-52.

a. Solar Illumination Factor

The vector from the Earth to the Sun is:

$$\vec{R}_S = -A_u \begin{bmatrix} \cos(\Omega_o + \omega t) \cos[\omega_E(T_o + t)] + \sin(\Omega_o + \omega t) \sin[\omega_E(T_o + t)] \cos \epsilon \\ -\sin(\Omega_o + \omega t) \cos[\omega_E(T_o + t)] + \cos(\Omega_o + \omega t) \sin[\omega_E(T_o + t)] \cos \epsilon \\ -\sin \omega_E(T_o + t) \sin \epsilon \end{bmatrix}$$

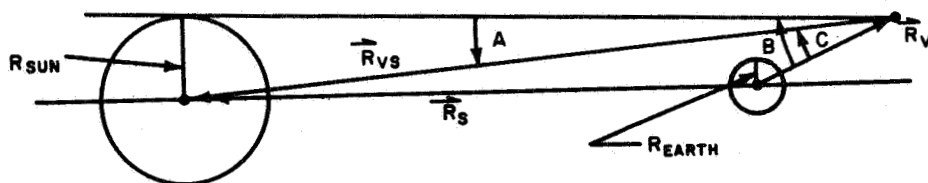
where the components of \vec{R}_S are given in a reference frame fixed in the orbital plane (see sketch below): x is along the ascending node, z is along the Earth's polar axis, and y is in the Earth's equatorial plane, completing the orthonormal triad.



The vector from the vehicle to the Sun is then

$$\vec{R}_{VS} = \vec{R}_S - \vec{R}_V$$

b. Solar Illumination:



If $|\vec{R}_{VS}| \leq |\vec{R}_S|$, $S_I = 1$

If $|\vec{R}_{VS}| > |\vec{R}_S|$

The angles A, B, and C are computed according to the equations,

$$A = \sin^{-1}(R_{\text{sun}}/R_{VS})$$

$$B = \sin^{-1}(R_{\text{earth}}/R_V)$$

$$C = -\vec{R}_V \cdot \vec{R}_{VS} / |\vec{R}_V| |\vec{R}_{VS}|$$

$$A + B \leq C, S_I = 1$$

$$A + B > C \text{ and}$$

$$A + C \leq B, S_I = 0$$

Finally, if $A + B > C$

and $A + C > B$,

$$S_I = 1 - (A^2 \beta + B^2 \alpha + BC \sin \alpha) / 2 \pi A^2$$

where

$$\beta = \cos^{-1} [(C^2 + A^2 - B^2) / 2AC]$$

$$\alpha = A_{\sin} (A \sin \beta / B)$$

c. Gravity Vector

The gravitational acceleration at the vehicle due to a spherical Earth is:

$$\vec{g} = -\mu \frac{\vec{R}_V}{|\vec{R}_V|^3}$$

Symbol Glossary

Equation Symbol	Comments	Program Symbol	COMMON**		Output
			Location	Input	
a	Semi-major axis of satellite orbit	XA			X
A	Planar angle intercepted by the Sun	A			

Symbol Glossary (Cont'd)

<u>Equation Symbol</u>	<u>Comments</u>	<u>Program Symbol</u>	<u>CØMMØN**</u>		<u>Output</u>
			<u>Location</u>	<u>Input</u>	
A_u	Astronomical unit, the mean Earth-Sun distance	AU	76	X	
B	Planar angle intercepted by the Earth	B			
C	Angle between R_{VS} and $-R_V$	C			
E	Eccentric anomaly of the vehicle orbit	E			
e	Eccentricity	EY			
f	True anomaly	F			
$\cos(i)$	Cosine of the angle between the orbital and equatorial planes	CØSI			
p	Semilatus rectum	P			
R_{sun}	Mean radius of the Sun	RSUN	73	X	
R_{earth}	Mean radius of the Earth	RE	500	X	
\vec{R}_S	Position of the Sun with respect to the Earth	RS			
\vec{R}_V	Position of the vehicle w. r. t. the Earth	RV, RVD*	300		X
\vec{R}_{V_0}	Initial position of the vehicle w. r. t. the Sun	RV0, RV0D*	78	X	
$ \vec{R}_V $	Earth-vehicle distance	RVM	91	X	
\vec{R}_{VS}	Position of the vehicle w. r. t. the Sun	RVS			
S_I	Solar illumination factor	SIF	77		X
t	Time	T	CD(595)	X	
T_0	Time of launch reckoned from Vernal Equinox	T0L	72	X	

Symbol Glossary (Concl'd)

<u>Equation Symbol</u>	<u>Comments</u>	<u>Program Symbol</u>	<u>COMMON** Location</u>	<u>Input</u>	<u>Output</u>
$t - T_0$	Time, reckoned from time of launch	DD*			
\vec{V}	Velocity of the vehicle in an Earth-centered "inertial" frame	V, VD*	303		X
$ \vec{V} $	Vehicular speed in the "inertial" frame	VM	92		X
\vec{V}_0	Initial vehicular velocity	V0, V0D*	81	X	
α	$\sin^{-1} (A \sin \beta / B)$	ALFA			
β	$\cos^{-1} (C^2 + A^2 - B^2) / 2AC$	BETA			
ϵ	Obliquity of the ecliptic	EPS	75	X	
μ	Earth's gravitational constant	GMU	501	X	
Ω_0	Initial longitude of the ascending node	OMEG0	74	X	
ω	Mean precessional rate of the line of nodes = $-10.5 (R_E/A) 7/2 \cos i$ deg./day	OMEG			X
ω_E	Earth's mean orbital rate	OMECE	71	X	
.00437	Largest value of $a_0 x^2$ for which series expansions are used for $C(a_0 x^2)$ and $S(a_0 x^2)$	AX2CHK		X	
10	Maximum number of iterations permitted	LCHECK		X	
1×10^{-13}	Maximum allowable fractional error in the time	TCHECK		X	

*Double precision variable

**Location in CØ array unless otherwise specified.

14. CFMRIS

Subroutine CFMRIS is an ephemeris computation routine which uses a six-point Bessel interpolation scheme to obtain the inertial components of position as functions of time. The source data are generated by an independent N-body (or two-body) trajectory program which describes the motion of the satellite's center of mass. The source data are written at specified time intervals on an intermediate tape which is then retained for use in this program.

The six data points used for the interpolation are symmetrically distributed about the time, t , for which values are sought. For this reason, in order to permit the initial time, t_0 , to fall between the 3rd and 4th data points, it is necessary for t_0 to be at least two time intervals greater than the initial time recorded on the ephemeris tape. The Bessel interpolation procedure is described by the following equations:

$$\Delta t = (t - t_3) / (t_4 - t_3)$$

$$C_1 = \Delta t - 1/2$$

$$C_2 = 1/2 \Delta t (\Delta t - 1)$$

$$C_3 = \frac{C_2 C_1}{3}$$

$$C_4 = \frac{C_2 (\Delta t + 1) (\Delta t - 2)}{12}$$

$$C_5 = \frac{C_4 C_1}{5}$$

$$K_1 = \frac{F_3 + F_4}{2}$$

$$K_2 = F_4 - F_3$$

$$K_3 = \frac{F_5 + F_2}{2} - K_1$$

$$K_4 = F_5 - F_2 - 3K_2$$

$$K_5 = \frac{(F_6 + F_1)}{2} - 3K_3 - K_1$$

$$K_6 = F_6 - F_1 + 5(K_2 + K_4)$$

$$F(t) = K_1 + C_1 K_2 + C_2 K_3 + C_3 K_4 + C_4 K_5 + C_5 K_6$$

where

F_n = nth data point

t_n = time corresponding to the nth data point

The interpolation may be performed on a maximum of 20 different quantities. The first 3 are reserved for the position vector, the next 3 for the satellite-Sun vector, the next 3 for the total acceleration vector, and the remaining 11 are at the option of the user. The total number of interpolations is indicated by the input word NINT.

This subroutine also computes the solar illumination factor and the distance from the satellite to the center of the Earth. The appropriate defining equations appear in the section describing subroutine AFMRIS (analytic ephemeris).

Symbol Glossary

<u>Equation Symbol</u>	<u>Comments</u>	<u>Program Symbol</u>	<u>COMMON* Location</u>	<u>Input</u>	<u>Output</u>
t	Time	T	CD(595)	X	
	Number of entries (excluding time) on each ephemeris tape record.	NENT	232	X	
	Number of interpolations to be performed	NINT	255	X	
	Time interval between records on ephemeris tape	FREQEF	234	X	
	Logical unit on which ephemeris tape is mounted	INTAPE	233	X	
	Radius of the Earth	RE	500	X	
	Radius of the Sun	RSUN	73	X	

Symbol Glossary (Concl'd)

<u>Equation Symbol</u>	<u>Comments</u>	<u>Program Symbol</u>	<u>CØMMØN*</u> <u>Location</u>	<u>Input</u>	<u>Output</u>
Δt	Interpolation interval (dimensionless)	PER	256		X
F	Storage array of interpolated quantities	VAL(1-20)	235-254		X
	Position vector	RV(1-3)=VAL(1-3)	300-302		X
	Satellite-Sun vector	RVS(1-3)=VAL(4-6)			X
	Total acceleration vector	G(1-3)=VAL(7-9)			X
	Solar illumination factor	SIF	77		X
	Radial distance from satellite to center of the Earth	RVM	91		X

*Location in CØ array unless otherwise specified.

15. GGRAD

Calculation of the gravity-induced moment exerted on the central body by the two antenna booms and the optional dipole boom is accomplished in GGRAD. The dipole boom is introduced into the calculations when the control quantity DIPØLE is assigned a value of 1. When present, the dipole boom is positioned perpendicular to the plane of the antennas. All booms are considered to be rigid, but have a length which is a function of a quadratic in time.

The torque calculation requires specification of the time, the parameters in the expressions defining boom lengths as a function of time, the gravity vector, the transformation matrix from the body to the inertial frame, the angular position of the antennas, and the lineal mass density of the booms.

In addition to the torque, GGRAD calculates the instantaneous value of the angle between the dipole (body pitch axis) and the normal to the orbital plane. The routine also provides ITB3 with boom lengths and their time derivatives.

Equations:

$$\vec{T}_j = \hat{k}_j (2\mu\rho \hat{L}_A^3 \sin a_j \cos a_j)$$

$$k_j = \begin{bmatrix} -r_{3j} \epsilon_{yB} / B_j \\ (r_{3j} \epsilon_{xB} - r_{1j} \epsilon_{zB}) / L_j \\ r_{1j} \epsilon_{yB} / B_j \end{bmatrix}$$

$$B_j = [(r_{3j} \epsilon_{yB})^2 + (r_{3j} \epsilon_{xB} - r_{1j} \epsilon_{zB})^2 + (r_{1j} \epsilon_{yB})^2]^{1/2}$$

$$a_j = \cos^{-1} [(r_{1j} \epsilon_{xB} + r_{3j} \epsilon_{zB}) / g L_A]$$

$$\underline{g}_B = (C)^{-1} \underline{g}_I$$

If $\cos a_j > 0$,

$$r_{1j} = L_A \sin \beta_j$$

$$r_{2j} = 0$$

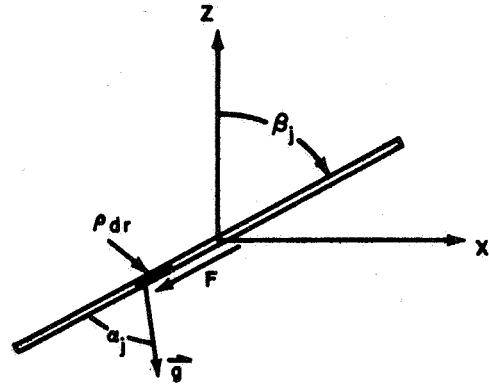
$$r_{3j} = L_A \cos \beta_j$$

If $\cos a_j < 0$,

$$r_{1j} = -L_A \sin \beta_j$$

$$r_{2j} = 0$$

$$r_{3j} = -L_A \cos \beta_j$$



Moment Exerted on the Dipole:

$$\bar{T}_D = \hat{k}_D (2\mu\rho \hat{L}_D^3 \sin a_D \cos a_D)$$

$$\hat{k}_D = \begin{bmatrix} s \epsilon_{zB} / B_D \\ 0 \\ -s \epsilon_{xB} / B_D \end{bmatrix}$$

$$B_D = (\epsilon_{xB}^2 + \epsilon_{zB}^2)^{1/2}$$

$$a_D = \cos^{-1} (\epsilon_{yB} / g)$$

s is assumed +1 so long as $\cos a_D > 0$; for $\cos a_D < 0$, s is set equal to -1.

Boom length as a function of time.

Antenna:

$$L_A(t) = b_0 + b_1 (t - t_0) + b_2 (t - t_0)^2$$

$$\dot{L}_A(t) = b_1 + 2b_2 (t - t_0)$$

Dipole:

$$L_D(t) = d_0 + d_1 (t - t_0) + d_2 (t - t_0)^2$$

$$\dot{L}_D(t) = d_1 + 2d_2 (t - t_0)$$

Discontinuities in deployment, such as occur during deadbeat techniques, can be simulated by using the STACK provision described under the INPUT section of this appendix. Since t_0 is recomputed each time STACK is encountered, it is necessary to re-evaluate the boom deployment constants b and d for these particular times.

Angle between Pitch Axis and the Normal to the Orbital Plane:

The unit normal to the orbital plane is:

$$\vec{P} = \frac{\vec{R} \times \vec{V}}{|\vec{R} \times \vec{V}|}$$

The unit vector in the positive direction of the vehicle pitch axis is \hat{y}_B
The desired angle η is then

$$\eta = \cos^{-1} (\hat{P} \cdot \hat{y}_B)$$

$$= \cos^{-1} (P_1 C_{12} + P_2 C_{22} + P_3 C_{32})$$

Symbol Glossary

<u>Equation</u>	<u>Comments</u>	<u>Program</u>	<u>COMMON Location</u>	<u>Input</u>	<u>Output</u>
B_j B_D	Normalizing factors for \hat{k}_j and \hat{k}_d respectively	B BD			
b_0 b_1 b_2	Parameters in the expression for antenna length	BML0 B61 B62	226 227 228	X X X	
C_{ij}	Element of the transformation matrix (C)	C DBL0	306 229	X X	
d_0 d_1 d_2	Parameters in the expression for dipole length	DG1 DG2	230 231	X X	
	Control quantity indicating presence of the dipole boom by a non-zero value	DIPØLE	219	X	

Symbol Glossary (Cont'd)

<u>Equation</u>	<u>Comments</u>	<u>Program</u>	<u>COMMON</u> <u>Location</u>	<u>Input</u>	<u>Output</u>
g	The magnitude of the gravity vector	G			
g_x	The gravity vector G, expressed in inertial components	GX	36	X	
g_y		GY	37	X	
g_z		GZ	38	X	
		GXB			
g_{x_b}	The gravity vector expressed in body components	GYB			
g_{y_b}		GZB			
k_{1j}	Elements of the unit vector which specified the direction of the torque on the jth antenna	UK1			
k_{2j}		UK2			
k_{3j}		UK3			
k_{iD}	Element of the unit vector \hat{k}_D , which specified the direction of the torque on the dipole	DK			
$\hat{L}_A = L_A/R_o$	dimensionless antenna length	BARL			
$\hat{L}_D = L_D/R_o$	dimensionless dipole length	BARLD			
$\dot{L}_A(t)$	Length of an antenna	BQOML	358		X
$L_A(t)$	Time derivative of antenna length	BLDOT	223		X
$\dot{L}_D(t)$	Length of the dipole	DBL	58		X
$L_D(t)$	Time derivative of dipole length	DLDOT	222		X
N	Number of antenna booms	NBOM	362	X	
p_j	Element of \hat{p} , the unit normal to the orbital plane	P			
R_o	Distance from the center of the earth to the satellite center of mass	RHO	91	X	

Symbol Glossary (Concl'd)

<u>Equation</u>	<u>Comments</u>	<u>Program</u>	<u>COMMON Location</u>	<u>Input</u>	<u>Output</u>
R_1 R_2 R_3	Elements of \bar{R} , the satellite position vector	RIX RIZ	301	X	
r_1 r_3	x, z components of the vector defining the angular orientation of the antennas	RI R3			
s	Sense of the vector defining the orientation of the dipole; i. e., s can be (+) or (-) unity	SGNRD			
t t_0	Instantaneous and initial value of time	T T0	CD(595) CD(594)	X X	
T_{ji}	ith component of the torque on the jth antenna component	GRVT(J, I)			
T_{Di}	ith component of the dipole torque vector	DGRVT			
T_i	ith component of the total torque vector	GRAVT(I)	359-361		
α_j	Angle between the orientation vector for the gravity vector and the jth antenna	ALPH			
α_D	Angle between the orientation vector for the dipole and the gravity vector	ALPHD			
β_j	Angular position of the jth antenna, reckoned with respect to the (+) z-axis	VBETA	351	X	
μ	Earth's gravitational constant	GMU	501	X	
ρ	Boom lineal mass density	TAU	357	X	

16. ØB3

This subroutine is not presently used in the computer program. It consists of a dummy block which causes control to exit immediately after entry to the subroutine. This subroutine will eventually be used for the computation of orientation commands associated with the active control system.

17. CMB3

(Same as ØCB3). This subroutine will calculate the control moments called for by ØCB3.

18. MSB3

The function of this subprogram is to sum the components of the moments from the various external torques acting on the rotating body. At the present time, the only external torque being considered is due to the gravity gradient effect. The result is a simple MSB3 subprogram having only a few statements. Later in the dynamics study, when additional torques are present, the coordination effort between subroutines supplied by MSB3 will become apparent.

Symbol Glossary

Equation Symbol	Comments	Fortran Symbol	COMMON Location	Input	Output
T_1 }	The three components of the gravity gradient torque vector.	GRAVT (1)	359	X	
T_2 }		GRAVT (2)	360	X	
T_3 }		GRAVT (3)	361	X	
ΣM_{j1} }	The three components of the total external torque acting on the body.	SIGMP	270		X
ΣM_{j2} }		SIGMQ	271		X
ΣM_{j3} }		SIGMR	272		X

19. ITB3

This subroutine calculates the inertia tensor (I) and its time derivative (\dot{I}). Only principal body axes are considered; the off-diagonal terms in both tensors are then zero. The elements of (I) and (\dot{I}) are calculated as functions of time as follows:

$$I_{11}(t) = I_{o11} + \frac{4}{3} \rho l^3(t) \sin^2 a$$

$$I_{22}(t) = I_{o22} + \frac{4}{3} \rho l^3(t) \cos^2 a$$

$$I_{33}(t) = I_{o33} + \frac{4}{3} \rho l^3(t)$$

hence

$$\dot{I}_{11}(t) = 4 \rho l^2(t) \dot{l}(t) \sin^2 a$$

$$\dot{I}_{22}(t) = 4 \rho l^2(t) \dot{l}(t) \cos^2 a$$

$$\dot{I}(t) = 4 \rho l^2(t) \dot{l}(t)$$

where $I_{ii}(t)$ and $\dot{I}_{ii}(t)$ are the diagonal elements of (I) and (\dot{I}), respectively, and

ρ = the linear mass density of the antenna

$l(t)$ = the instantaneous length of the antenna

a = the antenna-vee half angle.

and I_{o11} , I_{o22} and I_{o33} are the moments of inertia at $t = 0$.

In addition to calculating the moments of inertia due to the main antenna, ITB3 calculates the inertia components due to the two cross orbit dipole antennas:

$$\Delta I_D(t) = \frac{2}{3} \rho l_D^3(t - t_D)$$

This term must be added to $I_{11}(t)$ and $I_{22}(t)$ when the dipole is considered in the analysis; l_D is the length of the dipole antenna and t_D is the time of initiation of the dipole deployment. From the above equation, the time rate of change of $\Delta I_D(t)$ is obtained:

$$\Delta \dot{I}_D(t) = 2 \rho l_D^2 (t - t_D) \dot{l}_D (t - t_D) .$$

The quantities obtained directly from input are ρ , a , $I_{o_{ii}}$ and t_D , whereas l , \dot{l} , l_D and \dot{l}_D are calculated in the GGRAD subroutine.

Symbol Glossary

<u>Equation Symbol</u>	<u>Comments</u>	<u>Program Symbol</u>	<u>COMMON Location</u>	<u>Input</u>	<u>Output</u>
$I_{11}(t)$	the diagonal elements of the inertia tensor (I) at any time (t).	BIZZ	287		X
$I_{22}(t)$		BIXX	285		X
$I_{33}(t)$		BIYY	286		X
$I_{o_{11}}$	the elements of the inertia tensor at time $t = 0$.	BIZZ0	218	X	
$I_{o_{22}}$		BIXX0	216	X	
$I_{o_{33}}$		BIYY0	217	X	
ρ	Linear mass density of the antennas	DENS	225	X	
$l(t)$	the instantaneous length of the antennas	BØØML	358	X	

Symbol Glossary (Concl'd)

Equation Symbol	Comments	Program Symbol	COMMON* Location	Input	Output
α	the antenna-vee half angle	BALPHA	224	X	
\dot{i}_{11}	the time derivatives of the elements of the inertia tensor	BIZZT	287		X
\dot{i}_{22}		BIXXT	285		X
\dot{i}_{33}		BIYYT	286		
ΔI_D	the moment of inertia	DELI	calculated internally		
$\Delta \dot{I}_D$	due to the dipole antenna, and its time derivative.	DIDOT	calculated internally		

* location in CØ array.

20. MIB2

This subprogram calculates the derivative of the angular rate vector of the body axes. The complete equations of motion are written in the rotating body frame and all significant terms in these equation are included in the program. The equations of motion may be written as

$$\dot{\vec{\omega}} = (I)^{-1} \left(\sum_j \vec{M}_j - (I) \dot{\vec{\omega}} - \vec{\omega} \times (I) \vec{\omega} \right)$$

where

- $\vec{\omega}$ = the angular rate vector of the body
- $\dot{\vec{\omega}}$ = the time derivative of the angular rate vector
- (I) = the inertia tensor of the body
- \vec{M}_j = the jth torque applied external to the body
- $\dot{(I)}$ = the time derivative of (I) .

The "off-diagonal" terms in the inertia tensor vanish when principal body axes are used. To avoid unnecessary calculations when these cases arise, a control word called "IPRØD" is used in the subprogram. The correct usage of IPRØD is described below.

IPRØD

Program Control

- 1 $(\dot{I}) = 0$, and no off-diagonal terms in (I) are calculated or used during execution.
- 2 No off-diagonal terms are present in the calculations, however, the diagonal terms in (\dot{I}) may be non-zero.
- 3 $(\dot{I}) = 0$, but all terms in the inertia tensor are used in the calculations.
- 4 The complete set of derivative equations for $\vec{\omega}$ are used in the calculations.

Since, by definition, the inertia tensor and its derivative are symmetric about the diagonal, six terms are necessary to describe all the elements in (I) and six terms are necessary to describe (\dot{I}) . The terms in (I) and

(\dot{I}) are obtained from ITB3 which was previously discussed. $\sum \vec{M}_i$ is obtained in MSB3 for usage in MIB2.

Symbol Glossary

Equation Symbol	Comments	Program Symbol	CØMMØN* Location	Input	Output
$\dot{\omega}_x$ }	derivative of the angular	PDØT	260		X
$\dot{\omega}_y$ }	rate of the body about its	QDØT	261		X
$\dot{\omega}_z$ }	x, y, and z axes	RDØT	263		X
ω_x }	angular rate of the body	PB	315	X	
ω_y }	about its x, y, and	QB	316	X	
ω_z }	z axes	RB	317	X	

* Locations are in the CØ array

Symbol Glossary (Concl'd)

Equation Symbol	Comments	Program Symbol	COMMON* Location	Input	Output
(I)	the inertia tensor	BIXX	288	X	
		BIYY	289	X	
		BIZZ	290	X	
		BIXY	291	X	
		BIXZ	292	X	
		BIYZ	293	X	
(I)	the time of the inertia tensor	BIXXT	291	X	
		BIYYT	292	X	
		BIZZT	293	X	
		BIXYT	294	X	
		BIXZT	295	X	
		BIYZT	296	X	
$\sum_j \vec{M}_j$	The total torque acting on the body	SIGMP	270	X	
		SIGMQ	271	X	
		SIGMR	272	X	

* Locations are in the CØ array

21. PCB2, PCB3 and PCB4

These two subroutines supply the differential equations which describe the motion of the body axes. PCB2 uses a direction cosine analysis and PCB3 utilizes quaternions to locate the body axes. The two methods are described below.

a. PCB2

The direction cosines, describing the location of one set of rotating axes with respect to another set, may be defined as:

$$(\dot{C}) = (C)(\omega)$$

where:

$$(\omega) = \begin{matrix} \text{the skew-symmetric matrix of the angular} \\ \text{rate about the body axes} \end{matrix} = \begin{bmatrix} 0 & -\omega_z & \omega_y \\ \omega_z & 0 & -\omega_x \\ -\omega_y & \omega_x & 0 \end{bmatrix}$$

(C) = the direction cosine matrix locating one set of axes with respect to another.

(\dot{C}) = the time derivative of (C).

In 1048, the (C) matrix rotates the body axes into the inertial axes. The equation $(\dot{C}) = (C)(\omega)$ comprises nine differential equations with nine unknown quantities; however, due to the orthogonality and normality of the transformation matrix (C), the nine differential equations can be reduced to three differential equations. In reducing the number of differential equations, various singular solutions and ambiguities occur which make it undesirable to integrate only three equations. It has been found that a reasonable compromise is six differential equations containing no singularities or ambiguities. These six are listed below:

$$\dot{C}_{11} = C_{12} \omega_z - C_{13} \omega_y$$

$$\dot{C}_{12} = C_{13} \omega_x - C_{11} \omega_z$$

$$\dot{C}_{13} = C_{11} \omega_y - C_{12} \omega_x$$

$$\dot{C}_{21} = C_{22} \omega_z - C_{23} \omega_y$$

$$\dot{C}_{23} = C_{21} \omega_y - C_{22} \omega_x$$

$$\dot{C}_{22} = C_{23} \omega_x - C_{21} \omega_z$$

The remainder of the (C) matrix is calculated in XCB2.

Symbol Glossary

Equation Symbol	Comments	Program Symbol	COMMON Location	Input	Output
(C _i)	9 element direction	C(1)	306	X	
	cosine matrix: (the	.	.	.	
	2 dimensional array	C(9)	314	X	
	is stored by rows)				
(Ċ)	time derivative of (C)	CDOT(1)	20		X
	containing the first	.	.		.
	two rows	CDOT(6)	25		.
					X
ω _x	angular rate vector of the body in body Coordinates	PB	315	X	
ω _y		QB	316	X	
ω _z		RB	317	X	

b. PCB3

This subroutine calculates the time derivatives of the quaternion components. The four components of a quaternion may be expressed in terms of α_j , the three direction cosines of the axis, and θ , the rotation that carries the body frame into the inertial frame.

Equations:

The time derivatives are easily express in terms of the angular rate and the quaternion components themselves. Using matrix notation,

$$\begin{bmatrix} \dot{q}_0 \\ \dot{q}_1 \\ \dot{q}_2 \\ \dot{q}_3 \end{bmatrix} = -\frac{1}{2} \begin{bmatrix} 0 & P_B & Q_B & R_B \\ -P_B & 0 & -R_B & Q_B \\ -Q_B & R_B & 0 & -P_B \\ -R_B & -Q_B & P_B & 0 \end{bmatrix} \begin{bmatrix} q_0 \\ q_1 \\ q_2 \\ q_3 \end{bmatrix}$$

where, as indicated above,

$$q_0 = \cos \theta/2$$

$$q_j = a_j \sin \theta/2, \quad j = 1, 2, 3$$

Symbol Glossary

<u>Equation Symbol</u>	<u>Comments</u>	<u>Program Symbol</u>	<u>COMMON Location</u>	<u>Input</u>	<u>Output</u>
P_B	Angular rate of the body about its x axis	PB	315	X	
Q_B	Angular rate of the body about its y axis	QB	316	X	
$\left. \begin{matrix} \dot{q}_0 \\ \dot{q}_1 \\ \dot{q}_2 \\ \dot{q}_3 \end{matrix} \right\}$	$\left\{ \begin{matrix} \text{Time derivatives of the} \\ \text{quaternion components} \end{matrix} \right.$	QDOT0	16		X
		QDOT1	17		X
		QDOT2	18		X
		QDOT3	19		X
$\left. \begin{matrix} q_0 \\ q_1 \\ q_2 \\ q_3 \end{matrix} \right\}$	$\left\{ \begin{matrix} \text{Quaternion components} \end{matrix} \right.$	Q0	26	X	
		Q1	27	X	
		Q2	28	X	
		Q3	29	X	
R_B	Angular rate of the body about its z axis	RB	317	X	

c. PCB4

This subroutine is identical to PCB2 with the exception that all nine direction cosines are calculated instead of the first six only.

22. CHECKS

This subprogram allows 1048 to compare any two COMMON locations in various fashions and, if the conditions for a program stop are fulfilled, CHECKS resets a control word to accomplish the stop. When a stop is indicated, the control word ISTOP is set equal to the value one (1), interpolation on time occurs and return is made to the (EXEC) subroutine. In (EXEC), a final integration is made and then a final block of output is printed before exiting to the (MAIN) program.

The checking sequence is accomplished by a pair of fixed point arrays. These arrays contain the common locations of the variable which are to be compared, and are read into the program as part of the input. The FORTRAN names of the arrays used both in CHECKS and the data are ICON and ICHK. A distinction between a CD COMMON location and a CØ location in CD must be made. The reason is that CØ begins at CD location 2001, and hence CØ(N) corresponds to CD(2000 + N). To avoid difficulties, the CD COMMON locations which are less than 2001 for ICHK and ICON are read into the program as negative numbers and the CØ locations are positive. ICHK represents the COMMON locations which do the checking and ICON is the array of COMMON locations which are to be checked. CHECKS utilizes ICON and ICHK in a variety of ways including subtracting, multiplying, dividing and taking the absolute values of the respective COMMON locations. Checking occurs on both fixed and floating point numbers depending upon the location of the check in the ICON and ICHK table.

As an example, let us require that a stop occurs when the floating point number is CD(595) becomes greater than the floating point number in CØ (1000), i. e., the stop occurs when $CØ(1000) - CD(595) \leq 0$. Reference to CHECKS indicates that this operation may be accomplished by using any of the first 10 locations in ICON and ICHK in the following manner. Read in ICHK 1000 and ICON - 595 and the program stop will occur when the above conditions are fulfilled.

23. COMPEX

The primary purpose of COMPEX is to do all the auxiliary computations which are necessary or convenient for printing. At present, the only computations made in COMPEX are the location of the rotating body frame with respect to the local coordinate frame. This transformation is convenient for the purpose of interpreting the motion of the rotating body. The computations performed in this subroutine are described below.

Let us define a local rotating coordinate frame as $\hat{R}, \hat{k}, \hat{\eta}$ and $\hat{\eta}$ where \hat{R} is the unit vector in the direction of the radius vector from the center of the Earth to the center of mass of the satellite.

Then, let $\hat{\eta} = \frac{\vec{R} \times \vec{V}}{|\vec{R} \times \vec{V}|}$ where \hat{V} is the unit velocity vector of the center of mass

of the satellite, and finally, let $\hat{k} = \hat{\eta} \times \hat{R}$, hence defining the third component of the orthonormal triad. The components of these three unit vectors define a transformation from the local to the inertial system.

Transformations between the inertial, local, and body-fixed coordinate frames can be defined as follows. Let:

$$\vec{\zeta}_I = (A) \vec{\zeta}_L$$

$$\vec{\zeta}_B = (E) \vec{\zeta}_L$$

$$\vec{\zeta}_I = (C) \vec{\zeta}_B$$

where $\vec{\zeta}$ is any vector and the subscripts I, L, and B refer respectively to coordinatization in the inertial, local, and body frames. (A), (E), and (C) are the transformation matrices between the various frames as indicated. The direction cosine matrix (C) can be written in terms of the other transformations:

$$(C) = (A) (E)^{-1} = (A) (E)^T$$

The 3-2-1 Euler rotation set is characterized by the consecutive angular notations α, β , and γ , which may be obtained directly from the above equations.

Symbol Glossary

Equation Symbol	Comments	Program Symbol	COMMON * Location	Input	Output
(C)	Direction cosine matrix	C(I, J)	306	X	
(A)	Inertial to local coordinate transformation	A(I, J)	Calculated from R and V		
(E)	Euler transformation	Calculated internal to subroutine			X
α	3	ALFAE			X
β	2 Euler Rotation Angles	BETAE			X
γ	1	GAMAE			X

*Locations in CØarray.

24. OUTPUT

Subroutine `OUTPUT` controls almost all of the printed output generated by 1048. Any quantity in `COMMON` storage may be printed; in addition, the selection of these quantities is made at execution time.

Complete output control is thus determined at time of input, including all of the Hollerith text and the units of the output quantities. In addition to the BCD information discussed above, subprogram `OUTPUT` also has the flexibility to write binary tapes for any of the quantities in `COMMON` storage.

The BCD symbolic tape writing is controlled by four arrays of information, two of which contain Hollerith text. Of the remaining two arrays, one contains the `COMMON` locations specifying the quantities which define the variables to be printed, and the other array contains the multiplicative factors defining the units of the output quantities. These arrays exist for both fixed and floating point numbers. In addition to the Hollerith text which is printed on the top of each page of output, a heading consisting of up to 60 characters is available. Discussion of the individual arrays and their usage is presented below.

a. Hollerith Text

Four arrays, two for fixed point and two for floating point designations, are available. The input names of these four arrays are `CN`, `CM`, `IN`, and `IM`, respectively. The heading which may be printed at the top of each page is controlled by the word `HEAD`. To illustrate, let us suppose it is desired to print the following Hollerith text at the top of each printed page:

GRAVITY GRADIENT CASE, DELTA = 24 DEGREES

TIME	PDOT	QDOT	RDOT
SECS	DPS	DPS	DPS
LADM	ICUNIT		
MUNIT			

This print-out is accomplished by having the following cards in the data deck where no symbols appear in column 1 or columns 73 to 80 on the standard punched computation card:

HEAD "GRAVITY GRADIENT CASE, DELTA = 24 DEGREES"

CN/TIME/PDOT/QDOT/RDOT

CM/SECS/DPS/DPS/DPS

IN/LADM/ICUNIT

IM/NUNIT

b. Numerical Arrays

Numerical information is printed according to the COMMON location of the desired variable. Both CD and CØ locations may be printed; however, locations in CD below 2001 must be designated by a minus sign as was illustrated in subroutine CHECKS. Let us assume some COMMON locations which may be compatible with the printed heading above:

Let TIME be stored in the COMMON location CD(595)
Let PDØT be stored in the COMMON location CØ(260)
Let QDØT be stored in the COMMON location CØ(261)
Let RDØT be stored in the COMMON location CØ(262)
Let LADM be stored in the COMMON location CD(593)
Let ICØUNT be stored in the COMMON location CD(586)

The inclusion of the following cards in the data deck will initiate the printing of the given quantities:

M - 595 260 261 262

M(51) - 593 - 586

The reason for the term M(51) is that the IN fixed point array begins at the 51st location in M. In the above example, the numerical value of TIME is printed in seconds, as this is one of the running units of the program. If one wishes to print the time in hours, the addition of the following card in the data deck will suffice:

CK 2.78E-4.

The units of the other printed quantities may be changed accordingly.

Additional features such as controlling the number of printed lines per page are available; however, these features will not be discussed here.

ØUTPUT also permits the writing of a binary (intermediate) tape with the variable format feature. The control word is INTTAP: if INTTAP = 0, no tape is written; if INTTAP ≠ 0, writing occurs on logical tape channel ITPINT. If time (t) is zero, a 10-word heading is written using TN(1-10). The desired data storage locations are entered into KK, and the desired scale factors are stored in TK.

III. SAMPLE CASE DESCRIPTION

To illustrate the input and output of the digital simulation, we have chosen a gravity-gradient capture case.

Initially the body is moving in a 6000-km circular orbit. Its angular rate, measured with respect to inertial space, is zero.

We shall examine the input line by line, indicate the function of each quantity, and, when appropriate point out the corresponding line of output. A facsimile of the input and a portion of the output may be found in the two computer run pages that follow.

The first 17 lines generate the heading at the top of every page of printed output. Lines 1-7 contain the names of the quantities to be printed, lines 8-11 call out the physical units of these quantities, while lines 12-17 specify the locations in the CØ array where the numerical output is stored.

For example, consider the fourthline of the heading in the computer run (page C-46): This line contains the four quaternion components, q_0 , q_1 , q_2 , q_3 ; the Euler angles of the local coordinate system, α , β , γ ; and the diagonal elements of the inertia tensor, I_{xx} , I_{yy} , I_{zz} . The quaternions are dimensionless, the Euler angles are measured in degrees and the inertias bear the units of slug-ft². Finally, the quaternions are stored in CØ locations 26-29; the Euler angles, in locations 55-57; and the inertias, in locations 285-287.

Different applications may require different physical units. Thus, provision has been made for external specification of scale factors for the output. Lines 18 and 19 make use of this provision in converting angles from machine units of radians to the desired output units of degrees.

Since the present edition of PRESET specifies lines 1-19 automatically, they might have been omitted from the sample case. However, the heading and scaling specification were read in expressly to provide a concrete illustration of how the heading is set up in the event it becomes desirable to alter it.

Lines 20 and 21 contain certain control quantities common to a great many cases, e. g., the CØ locations of T, TSTØP, and print interval, values for the control quantities KA-KD, vehicle mass (no longer needed), and finally, the number of the output tape. This last quantity need not be read in when the deck is used at the NASA facility, since the appropriate input tape (number 3) has already been specified in PRESET.

Data for writing an intermediate tape are given in lines 22-25. INTTAP# 0 indicates that an intermediate tape is to be written while ITPINT = 12 calls out the number of the tape unit upon which the intermediate tape is mounted. Line 23 contains the CØ locations of the quantities to be written on tape, and lines 24 and 25 specify the corresponding scale factors to be used when plots are generated by the tape.

The data peculiar to this particular case begins with the heading card, line 26. Line 27 contains the number and angular position of the symmetrical antenna

booms, a control word commanding CONVIN to generate an identity "C"-matrix, a table of print interval, and the initial value of the time increment to be used in ADMS4, the integrating routine. Values for the terminal running time, boom density, and initial boom length are found in line 28. (The initial and final boom lengths are identical because the coefficients of the linear and quadratic terms in the boom length expression are not specified and are, accordingly, set to zero.) Line 29 gives the initial values for the diagonal elements of the inertia tensor, and for the position and velocity of the body.

Finally, line 30 contains the control word 1 in column one, which specifies to the INPUT routine that the data for this particular case are now complete.

INPUT CARDS READ		/RI	/RIX	/RIY	/RIZ	/VI	/VIX	/VIY	/VIZ	/DT0	/DATA
1	DATA/ CN(1) /TIME										/DATA
2	DATA/ CN(1) /P8 /R8 /THETA /PHI /PSI /MASS /STOMP /STOMG /SIGMR										/DATA
3	DATA/ CN(2) /C1 /C2 /C3 /C4 /C5 /C6 /C7 /C8 /C9 /SIF										/DATA
4	DATA/ CN(3) /Q0 /Q1 /Q2 /Q3 /ALPHA /BETA /GAMA										/DATA
5	DATA/ CN(38) /B1XX /B1YY /B1ZZ										/DATA
6	DATA/ CN(4) /B00ML /ETA										/DATA
7	DATA/ CN(1) /LADM /ICOUNT										/DATA
8	DATA/ CN(1) /SEC /FT /FT /FT /FT /FPS /FPS /FPS /FPS /SEC										/DATA
9	DATA/ CN(1) /DPS /DPS /DPS /DPS /DEG /DEG /DEG /DEG /PFT /PFT /PFT										/DATA
10	DATA/ CN(35) /DEGS /DEGS /DEGS /DEGS /SLOFT2 /SLOFT2 /SLOFT2										/DATA
11	DATA/ CN(4) /FEET /RAD										/DATA
12	DATA/ M(1) 595 91 300 301 302 92 303 304 305 597										/DATA
13	DATA/ M(1) 315 316 317 166 167 168 401 270 271 272										/DATA
14	DATA/ M(2) 306 307 308 309 310 311 312 313 314 77										/DATA
15	DATA/ M(3) 26 27 28 29 55 56 57 285 286 287										/DATA
16	DATA/ M(4) 558 59										/DATA
17	DATA/ M(5) 593 586										/DATA
18	DATA/ CN(1) 57.2957 57.2957 57.2957 57.2957 57.2957 57.2957										/DATA
19	DATA/ CN(35) 57.2957 57.2957 57.2957										/DATA
20	DATA/ ICON 595 ICHK 595 IFRQ 595 IRT1761 1 1 1 2 VMASS 10.										/DATA
21	DATA/ ITOUT 6										/DATA
22	DATA/ INTAP 10 ITPINT 12										/DATA
23	DATA/ N 595 59 55 56 57 315 316 317 270 271 272										/DATA
24	DATA/ TK 1. 57.2957 57.2957 57.2957 57.2957 57.2957 57.2957										/DATA
25	DATA/ 57.2957 1. 1. 1.										/DATA
26	DATA/ HEAD ZERO INERTIAL RATE. DEMONSTRATION OF CAPTURE.										/DATA
27	DATA/ NB00M 2 VBETA 30. 150. INERT2 3 FRQ18L 200. 200. DT0 15.										/DATA
28	DATA/ TSTOP 18000. DENS .000461 BML0 750.										/DATA
29	DATA/ B1XX 15. B1YY 15. B1ZZ 15. RIZ 40587900. VIX 18623.001										/DATA
30	DATA/ 1										/DATA

NON-ZERO INPUT VALUES USED BY THIS CASE

CD	= -595	M	= -595	IK	= 0.00001000000 IN	= 0.3257667E-31	IM	= 6.095238	
CK	= 1.0000000	CN	= -0.2630354E+08	CM	= -173958.09	N	= -595	TK	= 1.0000000
HEAD	= -7.167285	ITPINT	= 0.0001000000	ITPOUT	= 0.0000000000	IPCTR	= 0.0000000000	INTAP	= 0.0001000000
ICON	= -595	ICLK	= -590	ISTOP	= 18000.000	IFRQ	= 0.01123000000	LADM	= 0.00001000000
DT0	= 15.000000	FACTOR	= 0.8000000	FRQ18L	= 200.00000	VMASS	= 10.000000	AREA	= 1.0000000
VIX	= 18623.001	RIZ	= 0.4058790E+08	GMU	= 0.1407654E+17	VBETA	= 30.000000	DENS	= 0.4810000E-03
B0MT8L	= 750.00000	NB00M	= 0.00002000000	KA	= 0.00001000000	K8	= 0.00001000000	KC	= 0.00001000000
KD	= 0.00002000000	B1XX0	= 15.000000	B1YY0	= 15.000000	B1ZZ0	= 15.000000	BML0	= 750.00000
P	= 1.0000000	IPR00	= 0.00001000000	SING	= 1.0000000	R5	= 0.2090290E+08	EULER	= 1.0000000
INERT2	= 0.00003000000								

ZERO INERTIAL RATE. DEMONSTRATION OF CAPTURE.

TIME SEC	R1 FT	R1X FT	R1Y FT	R1Z FT	V1 FPS	V1X FPS	V1Y FPS	V1Z FPS	OTO SEC
PB	QB	RB	THETA DEG	PHI DEG	PSI DEG	MASS SLUGS	SIGMP PFT	SIGMQ PFT	SIGMR PFT
DPS	DPS	DPS							
C1	C2	C3	C4	C5	C6	C7	C8	C9	SIF

Q0	Q1	Q2	Q3	ALFA DEGS	BETA DEGS	GAMA DEGS	B1XX SLGFT2	B1YY SLGFT2	B1ZZ SLGFT2
----	----	----	----	--------------	--------------	--------------	----------------	----------------	----------------

BOOM FEET	ETA RAD
--------------	------------

LAOW	TCOUNT
------	--------

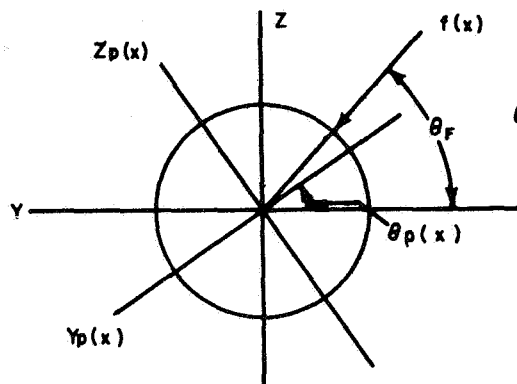
0.	4.0588E+07	0.	0.	4.0588E+07	1.8623E+04	1.8623E+04	0.	0.	1.5000E+01
0.	0.	0.	0.	0.	0.	1.0000E+01	0.	0.	0.
10.0000E-01	0.	0.	0.	10.0000E-01	0.	0.	0.	10.0000E-01	1.0000E+00
10.0000E-01	0.	0.	0.	0.	5.1419E-04	0.	2.0294E+05	2.7058E+05	6.7656E+04
7.5000000E+02	1.7263349E-04	0.	0.	0.	0.	0.	0.	0.	0.
0.	0.	0.	0.	0.	0.	0.	0.	0.	0.
2	1	0	0	0	0	0	0	0	0
2.0000E+02	4.0588E+07	3.7194E+06	0.	4.0417E+07	1.8623E+04	1.8545E+04	0.	-1.7066E+03	8.7480E+01
0.	1.6539E-04	0.	0.	0.	0.	1.0000E+01	0.	7.7804E-03	0.
10.0000E-01	0.	1.9275E-04	0.	10.0000E-01	0.	-1.9275E-04	0.	10.0000E-01	1.0000E+00
10.0000E-01	0.	0.	0.	0.	-5.2465E+00	0.	2.0294E+05	2.7058E+05	6.7656E+04
7.5000000E+02	1.7263349E-04	0.	0.	0.	0.	0.	0.	0.	0.
0.	0.	0.	0.	0.	0.	0.	0.	0.	0.
2	21	0	0	0	0	0	0	0	0
4.0000E+02	4.0588E+07	7.4075E+06	0.	3.9906E+07	1.8623E+04	1.8310E+04	0.	-3.3988E+03	1.0204E+02
0.	5.5402E-04	0.	0.	0.	0.	1.0000E+01	0.	1.5209E-02	0.
10.0000E-01	0.	1.5314E-03	0.	10.0000E-01	0.	-1.5314E-03	0.	10.0000E-01	1.0000E+00
10.0000E-01	0.	0.	0.	0.	-1.0428E+01	0.	2.0294E+05	2.7058E+05	6.7656E+04
7.5000000E+02	1.7263349E-04	0.	0.	0.	0.	0.	0.	0.	0.
0.	0.	0.	0.	0.	0.	0.	0.	0.	0.
2	2	0	0	0	0	0	0	0	0
6.0000E+02	4.0588E+07	1.033E+07	0.	3.9060E+07	1.8623E+04	1.7922E+04	0.	-5.0624E+03	1.1902E+02
0.	1.4433E-03	0.	0.	0.	0.	1.0000E+01	0.	2.1978E-02	0.
9.9999E-01	0.	5.1102E-03	0.	10.0000E-01	0.	-5.1102E-03	0.	9.9999E-01	1.0000E+00
10.0000E-01	0.	0.	0.	0.	-1.5480E+01	0.	2.0294E+05	2.7058E+05	6.7656E+04
7.5000000E+02	1.7263349E-04	0.	0.	0.	0.	0.	0.	0.	0.
0.	0.	0.	0.	0.	0.	0.	0.	0.	0.
2	39	0	0	0	0	0	0	0	0

APPENDIX D

TIP DEFLECTIONS OF SPIRALED ANTENNA

A well known result of beam deflection theory is that a beam having different values of the two principal cross-sectional moments of inertia will bend in a direction skewed from that of an applied force when the applied force is not aligned with a principal axis. In order to reduce the tip deflection normal to the plane defined by the applied force and the undeformed beam axis, the beam may be twisted or spiraled along its length. The result is an effective averaging of the cross-sectional inertias and beam bending properties. The following analysis was suggested and carried out in part by Dr. Wallace Vander Velde of M.I.T.

Consider the beam cross section shown in figure D-1. The Y and Z axes are the beam principal axes at the root. Define a twist rate $T(\text{rad/ft})$. Then the principal axes y_p and z_p twist along the beam according to the relation



$$\theta_p(x) = Tx \quad y_p(x) = y \cos Tx - z \sin Tx \quad (D-1)$$

$$z_p(x) = z \cos Tx + y \sin Tx$$

85-0092

Figure D-1 BEAM CROSS SECTION

where x is distance from the root along the undeformed beam axis. Apply a constant distributed force f (lb/ft) along the length of the beam in a plane skewed at some angle θ_F relative to the Y principal axis at the root. Then at a point x on the beam, the external load on the portion of the beam beyond x is $f(l-x)$, where l is the length of the beam. The external moment at x due to this force has magnitude $1/2 f(l-x)^2$. The components of this moment about the local principal axes are

$$M_{y_p} = -\frac{1}{2} f(l-x)^2 \sin(Tx - \theta_F) \quad (D-2)$$

$$M_{z_p} = \frac{1}{2} f(l-x)^2 \cos(Tx - \theta_F) \quad (D-3)$$

These moment components produce a local beam curvature in each principal direction of

$$\frac{d^2 y_p}{dx^2} = \frac{M_{zp}}{E I_z} \quad (D-4)$$

$$\frac{d^2 z_p}{dx^2} = - \frac{M_{yp}}{E I_y} \quad (D-5)$$

where I_y and I_z are the principal cross-sectional inertias. Reflected to the y and z axes defined at the root, the local curvatures are

$$\frac{d^2 y}{dx^2} = \frac{M_{zp}}{E I_z} \cos Tx - \frac{M_{yp}}{E I_y} \sin Tx \quad (D-6)$$

$$\frac{d^2 z}{dx^2} = - \frac{M_{yp}}{E I_y} \cos Tx - \frac{M_{zp}}{E I_z} \sin Tx \quad (D-7)$$

Substitution of equations (D-2) and (D-3) into (D-6) and (D-7) yields

$$\begin{aligned} \frac{d^2 y}{dx^2} &= \frac{f}{2E I_z} (l-x)^2 \cos Tx \cos (Tx - \theta_F) \\ &+ \frac{f}{2E I_y} (l-x)^2 \sin Tx \sin (Tx - \theta_F) \end{aligned} \quad (D-8)$$

$$\begin{aligned} \frac{d^2 z}{dx^2} &= \frac{f}{2E I_y} (l-x)^2 \cos Tx \sin (Tx - \theta_F) \\ &- \frac{f}{2E I_z} (l-x)^2 \sin Tx \cos (Tx - \theta_F) \end{aligned} \quad (D-9)$$

Equations (D-8) and (D-9) can be integrated over the interval $0 \leq x \leq l$ from the initial conditions $y = z = y' = z' = 0$ at $x = 0$. The result is the tip deflections $y(l)$ and $z(l)$ along the root principal axes:

$$\begin{aligned} y(l) &= \frac{f l^4}{16E I_z} \left\{ \cos \theta_F \left(1 + \frac{I_z}{I_y} \right) + \cos \theta_F \left(1 - \frac{I_z}{I_y} \right) \left[\frac{3}{l^2 T^2} + \frac{3}{2l^4 T^4} \right. \right. \\ &\quad \left. \left. (\cos 2lT - 1) \right] + \sin \theta_F \left(1 - \frac{I_z}{I_y} \right) \left[\frac{2}{lT} - \frac{3}{l^3 T^3} + \frac{3}{2l^4 T^4} \sin 2lT \right] \right\} \end{aligned} \quad (D-10)$$

$$\begin{aligned} z(l) &= \frac{f l^4}{16E I_z} \left\{ - \sin \theta_F \left(1 + \frac{I_z}{I_y} \right) + \sin \theta_F \left(1 - \frac{I_z}{I_y} \right) \left[\frac{3}{l^2 T^2} + \frac{3}{2l^4 T^4} \right. \right. \\ &\quad \left. \left. (\cos 2lT - 1) \right] - \cos \theta_F \left(1 - \frac{I_z}{I_y} \right) \left[\frac{2}{lT} - \frac{3}{l^3 T^3} + \frac{3}{2l^4 T^4} \sin 2lT \right] \right\} \end{aligned} \quad (D-11)$$

Note that when $I_y = I_z$, the tip deflects in the plane of the applied force distribution, in the direction $\theta_F + \pi$. When the number of twists N , where

$$2\pi N = lT, \quad (D-12)$$

is large, the tip again deflects in the direction $\theta_F + \pi$. The magnitude of the tip deflection for large N is

$$\delta(l) = \frac{fl^4}{8E} \frac{I_y + I_z}{2I_y I_z} \quad (D-13)$$

This value is the tip deflection corresponding to an effective cross-sectional inertia of

$$I_{\text{eff}} = \frac{2I_y I_z}{I_y + I_z}. \quad (D-14)$$

Thus the reciprocal of I_{eff} is simply the average of the reciprocals of the principal inertias:

$$\frac{1}{I_{\text{eff}}} = \frac{1}{2} \left(\frac{1}{I_y} + \frac{1}{I_z} \right) \quad (D-15)$$

and the beam bending properties have been averaged.

To verify the averaging of antenna bending properties, evaluate the components $y_F(l)$ and $z_F(l)$ in the plane and normal to the plane of the applied force, respectively:

$$y_F(l) = y(l) \cos \theta_F - z(l) \sin \theta_F \quad (D-16)$$

$$z_F(l) = y(l) \sin \theta_F + z(l) \cos \theta_F \quad (D-17)$$

Substitution of equations (D-10) and (D-11) into (D-16) and (D-17) yields

$$\begin{aligned} y_F(l) = & \frac{fl^4}{16EI_z} \left\{ \left(1 + \frac{I_z}{I_y} \right) + \left(1 - \frac{I_z}{I_y} \right) \cos 2\theta_F \left[\frac{3}{l^2 T^2} \right. \right. \\ & \left. \left. + \frac{3}{2l^4 T^4} (\cos 2lT - 1) \right] + \left(1 - \frac{I_z}{I_y} \right) \sin 2\theta_F \left[\frac{2}{lT} - \frac{3}{l^3 T^3} + \frac{3}{2l^4 T^4} \sin 2lT \right] \right\} \\ z_F(l) = & \frac{fl^4}{16EI_z} \left\{ 1 - \frac{I_z}{I_y} \right\} \left\{ \sin 2\theta_F \left[\frac{3}{l^2 T^2} + \frac{3}{2l^4 T^4} (\cos 2lT - 1) \right] \right. \\ & \left. - \cos 2\theta_F \left[\frac{2}{lT} - \frac{3}{l^3 T^3} + \frac{3}{2l^4 T^4} \sin 2lT \right] \right\} \end{aligned} \quad (D-19)$$

It is clear that as the number of twists becomes large,

$$y_F(l) \rightarrow \frac{fl^4}{8E I_{eff}}$$

$$z_F(l) \rightarrow 0.$$

Figure D-2 shows the out-of-plane tip deflection $z_F(l)$ as a function of the total number of twists N and the angle of the applied force θ_F for the following case:

$$f = 10^{-7} \text{ lb/ft}$$

$$I_y = 1.070 \times 10^{-4} \text{ in.}^4$$

$$I_z = 1.382 \times 10^{-4} \text{ in.}^4$$

$$E = 19.0 \times 10^6 \text{ lb/in.}^2$$

$$l = 750 \text{ ft.}$$

For reference, the value of I_{eff} is

$$I_{eff} = 1.160 \times 10^{-4} \text{ in.}^4$$

and the averaged in-plane tip deflection is

$$y_F(l) = \frac{fl^4}{8E I_{eff}} = 258 \text{ ft.}$$

It is evident from figure D-2 that as few as five twists reduce out-of-plane deflection to relative insignificance -- less than 1 percent of the in-plane deflection.

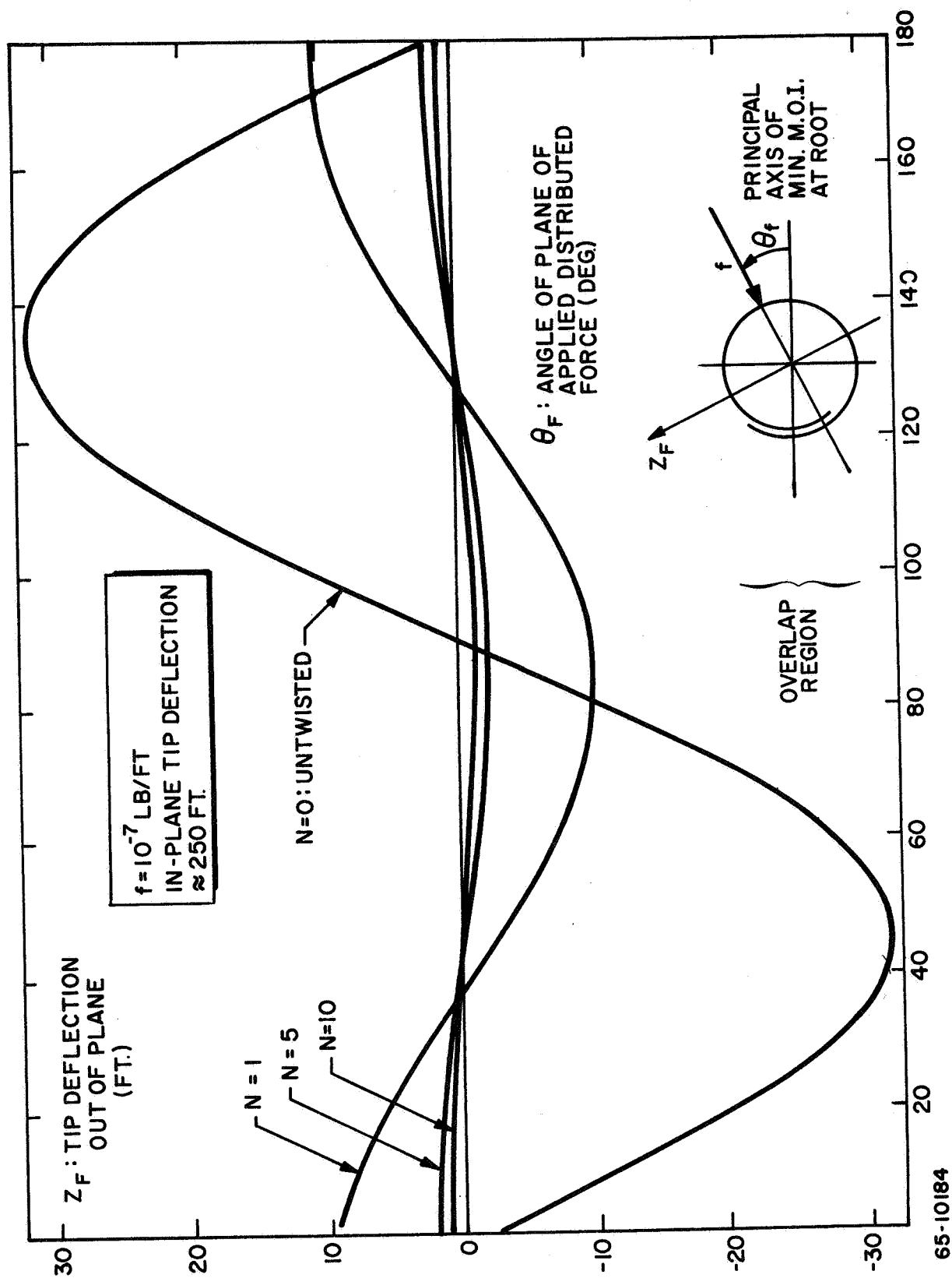
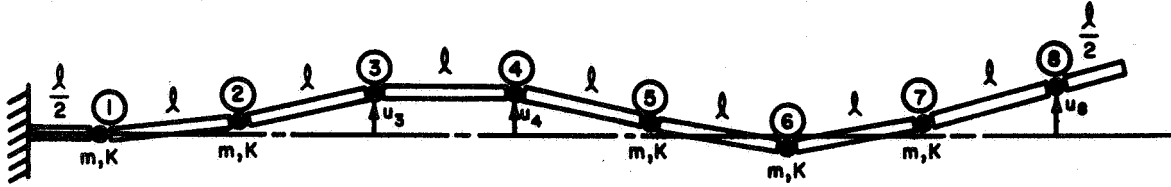


Figure D-2 EFFECT OF SPIRALING ON OUT-OF-PLANE TIP DEFLECTIONS

APPENDIX E

LINEAR EQUATIONS OF MOTION FOR ELEMENTIZED CANTILEVER BEAM

Consider a simple cantilever beam simulated by eight lumped mass and spring elements joined by rigid, massless sections:



$$\text{Mass elements are } m = \rho l \quad (\text{E-1})$$

$$\text{Spring constants are } K = \frac{EI}{l} \quad (\text{E-2})$$

$$\text{Section lengths are } l = \frac{1}{N} L \quad (\text{E-3})$$

$$\text{Number of elements is } N = 8. \quad (\text{E-4})$$

The equations of motion of the spring-mass simulation are derived from Lagrange's equation:

$$\frac{d}{dt} \frac{\partial (T - V)}{\partial \dot{q}_k} - \frac{\partial (T - V)}{\partial q_k} = Q_k \quad (\text{E-5})$$

where the generalized coordinates are the deflections u_k of each mass element normal to the undeformed baseline. T and V are the system kinetic and potential energies, respectively, and Q_k the generalized force associated with the k th coordinate.

The kinetic energy is simply

$$T = \frac{1}{2} m \sum_{k=2}^8 \dot{u}_k^2 \quad (\text{E-6})$$

(Note that u_1 is identically zero.) Then

$$\frac{d}{dt} \frac{\partial T}{\partial \dot{u}_k} = \frac{d}{dt} (m \dot{u}_k) = m \ddot{u}_k \quad (\text{E-7})$$

$$\frac{\partial T}{\partial u_k} = 0. \quad (\text{E-8})$$

The potential energy is the total stored energy in the spring elements,

$$V = \frac{1}{2} K \sum_{k=1}^7 \Delta \theta_k^2 \quad (\text{E-9})$$

where $\Delta \theta_k$ is the change of slope or bending angle at the k^{th} element. Note also that $\Delta \theta_8$ is zero since no forces act on the half section at the tip. The $\Delta \theta_k$'s are easily written in terms of the deflections u_k (assumed small):

$$\Delta \theta_k = \frac{1}{l} (u_{k+1} - 2u_k + u_{k-1}). \quad k = 3 \rightarrow 7 \quad (\text{E-10})$$

Because of the boundary constraints at the fixed end, $\Delta \theta_1$ and $\Delta \theta_2$ must be evaluated separately; they are

$$\Delta \theta_1 = \frac{1}{l} (u_2) \quad (\text{E-11})$$

$$\Delta \theta_2 = \frac{1}{l} (-2u_2 + u_3). \quad (\text{E-12})$$

These relations follow directly from the more general equation (E-10) for $\Delta \theta_k$ when u_1 and a hypothetical u_0 are taken identically to be zero. Including u_0 and u_1 for now, write

$$V = \frac{1}{2} \frac{K}{l^2} \sum_{k=1}^7 (u_{k+1} - 2u_k + u_{k-1})^2. \quad (\text{E-13})$$

Then

$$\frac{\partial V}{\partial \dot{u}_k} = 0 \quad (\text{E-14})$$

$$\begin{aligned}\frac{\partial V}{\partial u_k} &= \frac{K}{l^2} [(u_{k+2} - 2u_{k+1} + u_k) - 2(u_{k+1} - 2u_k + u_{k-1}) + (u_k - 2u_{k-1} + u_{k-2})] \\ &= \frac{K}{l^2} (u_{k+2} - 4u_{k+1} + 6u_k - 4u_{k-1} + u_{k-2}).\end{aligned}\quad (E-15)$$

Observe that for relation (E-15) to be valid for $k = 7$, one must determine a hypothetical u_9 by requiring $\Delta\theta_8$ to be zero from equation (E-10):

$$u_9 = 2u_8 - u_7. \quad (E-16)$$

For (E-15) to be valid for $k = 8$, a u_{10} must similarly be determined by requiring a hypothetical $\Delta\theta_9$ to be zero:

$$u_{10} = 3u_8 - 2u_7. \quad (E-17)$$

The generalized force Q_k is the incremental work done by outside forces during a virtual displacement δu_k of the k th mass, divided by δu_k . It is easily shown that:

$$\delta W_k = f_k \delta u_k \quad (E-18)$$

where f_k is the net external force acting on the k th mass element in the direction of u_k , from which

$$Q_k = f_k. \quad (E-19)$$

The equations of motion are obtained by substituting expressions (E-7), (E-8), (E-14), (E-15), and (E-19) into Lagrange's equation (E-5):

$$m\ddot{u}_k + \frac{EI}{l^3} (u_{k+2} - 4u_{k+1} + 6u_k - 4u_{k-1} + u_{k-2}) = f_k \quad (E-20)$$

k ranges from 2 to 8, with the constraints

$$\left. \begin{aligned} u_0 &= 0 \\ u_1 &= 0 \\ u_9 &= 2u_8 - u_7 \\ u_{10} &= 3u_8 - 2u_7 \end{aligned} \right\} \quad (E-21)$$

as before. The spring constant K has been replaced by EI/l according to relation (E-2). Note that equation (E-20) is simply the difference equation corresponding to the familiar Bernoulli equation for linearized beam dynamics:

$$EI \frac{\partial^4 u}{\partial z^4} + \rho \frac{\partial^2 u}{\partial t^2} = f(z,t) \quad (E-22)$$

where $f(z,t)$ is external force per unit length along the beam. Equations (E-21) are the difference equations corresponding to the boundary conditions on the cantilever beam:

$$\left. \begin{aligned} u(0) &= 0 \\ u'(0) &= 0 \\ u''(l) &= 0 \\ u'''(l) &= 0 \end{aligned} \right\} \quad (E-23)$$

Writing equations (E-20) in matrix form after substituting the constraint equations (E-21) yields

$$m \begin{Bmatrix} \ddot{u}_2 \\ \ddot{u}_3 \\ \ddot{u}_4 \\ \ddot{u}_5 \\ \ddot{u}_6 \\ \ddot{u}_7 \\ \ddot{u}_8 \end{Bmatrix} + \frac{EI}{l^3} \begin{bmatrix} 6 & -4 & 1 & 0 & 0 & 0 & 0 \\ -4 & 6 & -4 & 1 & 0 & 0 & 0 \\ 1 & -4 & 6 & 1 & 0 & 0 & 0 \\ 0 & 1 & -4 & 6 & -4 & 1 & 0 \\ 0 & 0 & 1 & -4 & 6 & -4 & 1 \\ 0 & 0 & 0 & 1 & -4 & 5 & -2 \\ 0 & 0 & 0 & 0 & 1 & -2 & 1 \end{bmatrix} \begin{Bmatrix} u_2 \\ u_3 \\ u_4 \\ u_5 \\ u_6 \\ u_7 \\ u_8 \end{Bmatrix} = \begin{Bmatrix} f_2 \\ f_3 \\ f_4 \\ f_5 \\ f_6 \\ f_7 \\ f_8 \end{Bmatrix} \quad (E-24)$$

To determine the natural modes and frequencies of the elementized cantilever beam, set the right-hand side of equation (E-24) equal to zero, and substitute for u_k as follows:

$$u_k = e^{i\omega t} \phi_k \quad (E-25)$$

The result is the homogeneous equation of motion:

$$\begin{bmatrix}
 6-\lambda & -4 & 1 & 0 & 0 & 0 & 0 \\
 -4 & 6-\lambda & -4 & 1 & 0 & 0 & 0 \\
 1 & -4 & 6-\lambda & -4 & 1 & 0 & 0 \\
 0 & 1 & -4 & 6-\lambda & -4 & 1 & 0 \\
 0 & 0 & 1 & -4 & 6-\lambda & -4 & 1 \\
 0 & 0 & 0 & 1 & -4 & 5-\lambda & -2 \\
 0 & 0 & 0 & 0 & 1 & -2 & 1-\lambda
 \end{bmatrix}
 \begin{Bmatrix}
 \phi_2 \\
 \phi_3 \\
 \phi_4 \\
 \phi_5 \\
 \phi_6 \\
 \phi_7 \\
 \phi_8
 \end{Bmatrix}
 = \underline{0} \quad (E-26)$$

where

$$\lambda = \frac{m l^3}{EI} \omega^2 \quad (E-27)$$

The eigenvalues λ_n ($n = 1$ to 7), obtained by setting the determinant of the above matrix equal to zero, determine the natural frequencies of the elementized beam:

$$\omega_n = \sqrt{\lambda_n \frac{EI}{m l^3} \frac{\text{rad}}{\text{sec}}} \quad (E-28)$$

The corresponding values $\phi_k^{(n)}$ are the natural mode shapes of the elementized beam. Recall that the natural frequencies of the continuous cantilever beam are

$$\omega_{n(\text{cont})} = c_n \sqrt{\frac{EI}{\rho l^4} \frac{\text{rad}}{\text{sec}}} \quad (E-29)$$

where $c_1 = 3.52$, $c_2 = 22.05$ etc. As the number of elements N is increased without bound, the values of λ_n must approach c_n^2/N^4 . The desired accuracy of ω_n and $\phi_k^{(n)}$ for the lower natural modes of the elementized beam determines the minimum number of elements that is acceptable.

The eigenvalues of matrix (E-26), calculated by digital computer, and the corresponding values of c_n^2/N^4 are as follows:

λ_n	c_n^2/N^4
0.0030685	0.0030175
0.12006	0.11853
0.88138	0.9294
2.9559	3.5693
6.5469	9.7514
10.920	21.763
14.573	42.449

The natural frequencies of the lumped-mass simulation and those of the continuous cantilever, evaluated for $EI = 13.85 \text{ slug-ft}^2$, $\rho = 0.000482 \text{ slug/ft}$, and $L = 750 \text{ feet}$, are then:

$\omega_n \times 10^3 \text{ (cps)}$	$\omega_{n(\text{cont})} \times 10^3 \text{ (cps)}$
0.1702	0.1688
1.065	1.058
2.888	2.962
5.284	5.804
7.86	9.59
10.15	14.33
11.73	20.02

It is clear that the eight-element lumped-mass simulation represents the first four natural frequencies with acceptable accuracy; the accuracy degenerates rapidly for the higher frequencies.

The natural modes shapes of the simulation, each normalized to a tip deflection of 1.0, are the eigenvectors of the matrix (E-26). Calculated by digital computer, these are as follows:

Element	$\phi_k(1)$	$\phi_k(2)$	$\phi_k(3)$	$\phi_k(4)$	$\phi_k(5)$	$\phi_k(6)$	$\phi_k(7)$
2	0.0506	-0.247	0.530	-0.777	0.961	-1.082	1.149
3	0.142	-0.541	0.773	-0.444	-0.314	1.200	-1.886
4	0.266	-0.712	0.376	0.588	-0.733	-0.524	2.314
5	0.412	-0.657	-0.328	0.595	0.738	-0.522	-2.311
6	0.573	-0.354	-0.680	-0.407	0.335	1.212	1.895
7	0.742	0.136	-0.307	-0.645	-0.874	-1.018	-1.096
8	0.914	0.712	0.565	0.452	0.375	0.327	0.301

The natural mode shapes are shown graphically in figure E-1. It is evident that the first four modes are well represented by the lumped-mass simulation, but that the accuracy degenerates with the fifth and is poor for the sixth and seventh. Figure E-2 compares the simulated mode shapes with the actual mode shapes for the first and second modes, and figure E-3, for the third and fifth modes. The discrepancy is essentially indistinguishable for the first two modes, and is of minor significance for the third; the fifth mode is simulated with noticeable inaccuracy, yet should be acceptable for most applications.

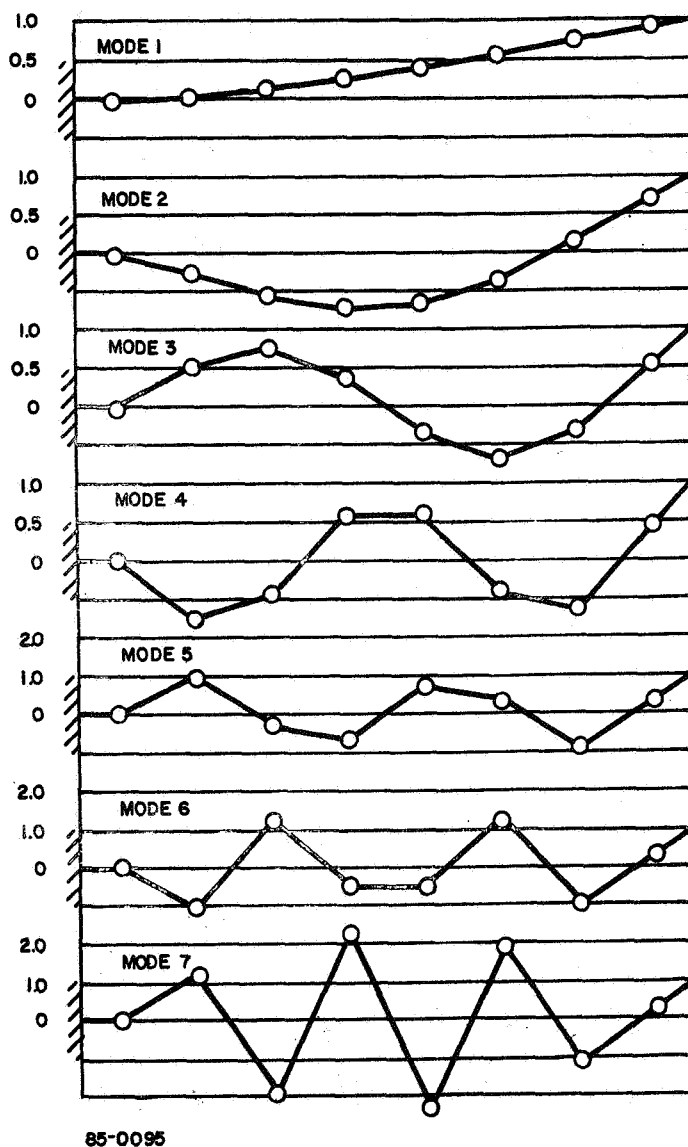


Figure E-1 NATURAL MODE SHAPES FOR EIGHT-SECTION, LUMPED-MASS CANTILEVER BEAM SIMULATION

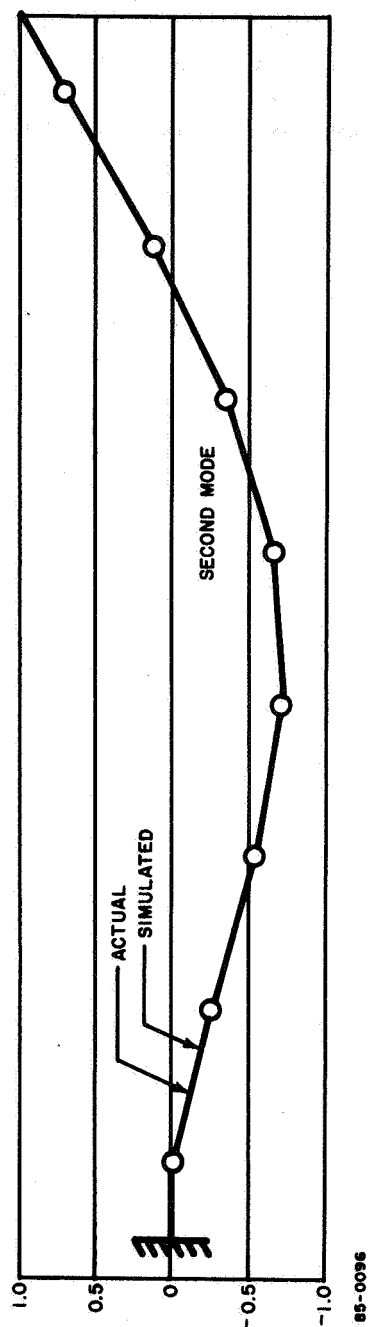
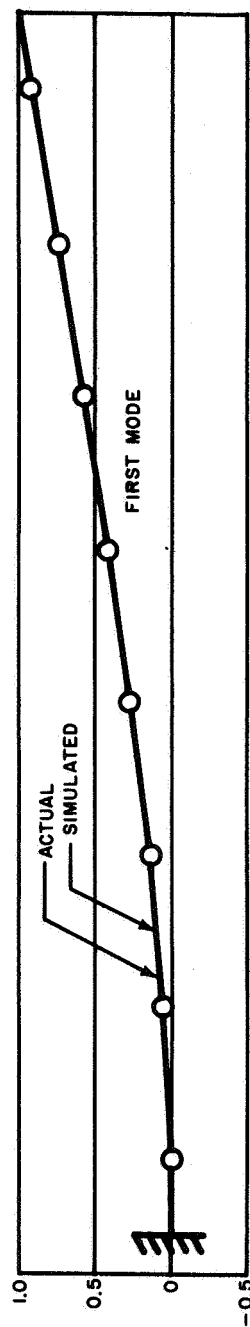


Figure E-2 COMPARISON OF ACTUAL AND SIMULATED MODE SHAPES FOR FIRST AND SECOND MODES

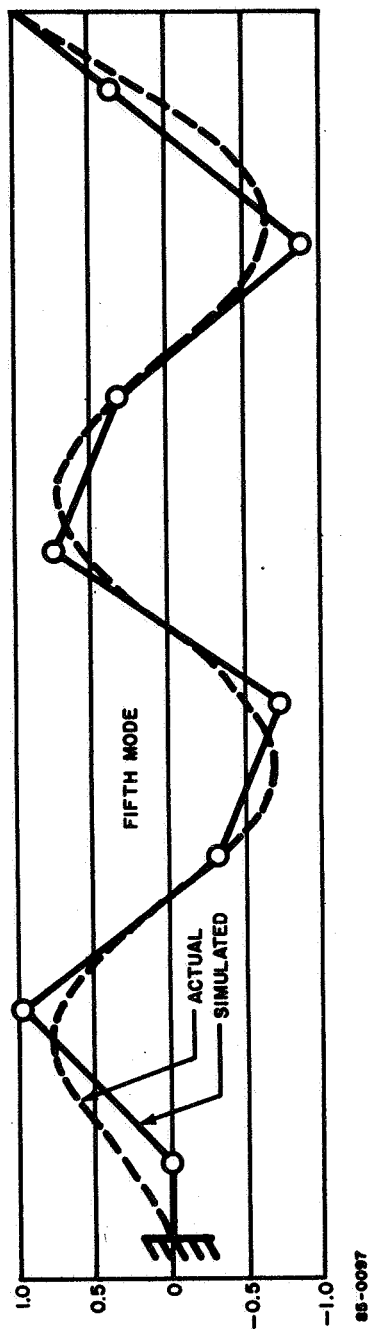
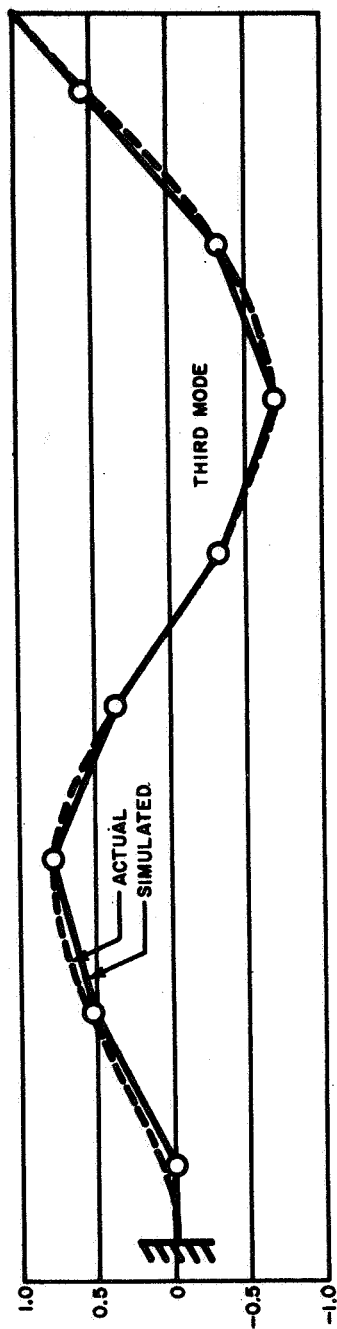


Figure E-3 COMPARISON OF ACTUAL AND SIMULATED MODE SHAPES FOR THIRD AND FIFTH MODES

APPENDIX F

DEAD BEAT CONTROL FOR THE DEPLOYMENT ACQUISITION PHASE

1. Summary

A boom deployment technique for the radio astronomy satellite is described which may be capable of reducing the oscillations in attitude induced by normal antenna deployment. Basically the technique requires control over the satellite rotational energy by means of modulation of the antenna deployment rate.

2. Introduction

After injection into the desired orbit, it is presently anticipated that a magnetic control system will align the satellite core (booms undeployed) to the local vertical. The magnetic control system is then deactivated and boom deployment is initiated.

The transition phase to the desired end conditions of fully deployed antennas and properly oriented body is referred to as the deployment/acquisition phase.

Several different techniques may be employed to effect attainment of these state conditions. Of primary interest is the technique designated "dead beat control"

3. Discussion

Let us consider the planar problem for a circular orbit. The satellite central body is initially aligned with the local vertical such that the x, y, z axes are: aligned with the velocity vector, normal to the plane of the orbit and colinear with the local vertical, respectively. For the satellite to maintain this alignment, there exists, with respect to an inertial reference, a rotation rate about the satellite y body axis equal to Ω , the orbital angular rate. Thus between the inertial system and the system rotating with the satellite there exists a relative angular rate, Ω , so that angular velocity expressed in the inertial system is the angular velocity expressed in the rotating system plus Ω .

Neglecting external forces, which are small during this phase, the inertial rotation rate of the satellite at the instant of full deployment, ω_D , becomes:

$$\omega_D = \frac{I_{y_0}}{I_{y_d}} \Omega$$

Since the pitch moment of inertia increases by several orders of magnitude during deployment, the satellite has virtually stopped rotating relative to inertial space. However, relative to the local vertical reference frame it has a rotating rate of $-\Omega$. The pitch attitude angle now tends to increase and would do so indefinitely if ω_D and the external forces were neglected. However, a "righting" torque due to the gravitational gradient is introduced and opposes this increase in the attitude angle. Expressed in the rotating system, this torque, T , is

$$T = \frac{3}{2} \Omega^2 (I_x - I_z) \sin 2\theta \quad (F-1)$$

where I_x , I_z are the roll and yaw moments of inertia, respectively, and the rotational kinetic energy, K.E., is:

$$\text{K.E.} = \frac{1}{2} I_{y_d} \Omega^2. \quad (F-2)$$

As the satellite slowly swings away from the local vertical at a rate $\dot{\theta}$, the attitude angle reaches a maximum value θ_{\max} . At this point the rotational angular velocity is zero; thus the inertial angular velocity is Ω .

The angle θ_{\max} is evaluated by equating the kinetic and potential energies;

$$\frac{1}{2} I_{y_d} \Omega^2 = \int_0^{\theta_{\max}} T d\theta \quad (F-3)$$

where T is obtained from equation (F-1). For the RAE satellite, the pitch, yaw and roll moments of inertia are:

$$I_y = \frac{4}{3} \rho l^3$$

$$I_z = \frac{4}{3} \rho l^3 \sin^2 a$$

$$I_x = \frac{4}{3} \rho l^3 \cos^2 a$$

where a is the antenna half angle and ρ = mass per unit length of each boom, l = length of booms. Although the boom mass constitutes less than 25 percent of the satellite mass, the booms contribute nearly all the inertia as significant boom deployment lengths, e. g., 100 feet, are attained. The solution¹ to equation (F-3) for an initial pitch attitude angle of zero is:

¹ RAD, A Proposal to Investigate the Dynamic Characteristics of a V-Antenna Radio Astronomy Satellite, Avco RAD B862D-264 (9 October 1964), Appendix III.

$$\theta_{\max} = \frac{1}{2} \cos^{-1} \left[1 - \frac{2}{3} \left(\frac{1}{\cos^2 \alpha - \sin^2 \alpha} \right) \right] \quad (\text{F-4})$$

From inspection of equation (F-4) it is clear that θ_{\max} is solely a function of the ratio of pitch moment of inertia to the difference between yaw and roll moment of inertia. Furthermore, this ratio is invariant with boom extension length.

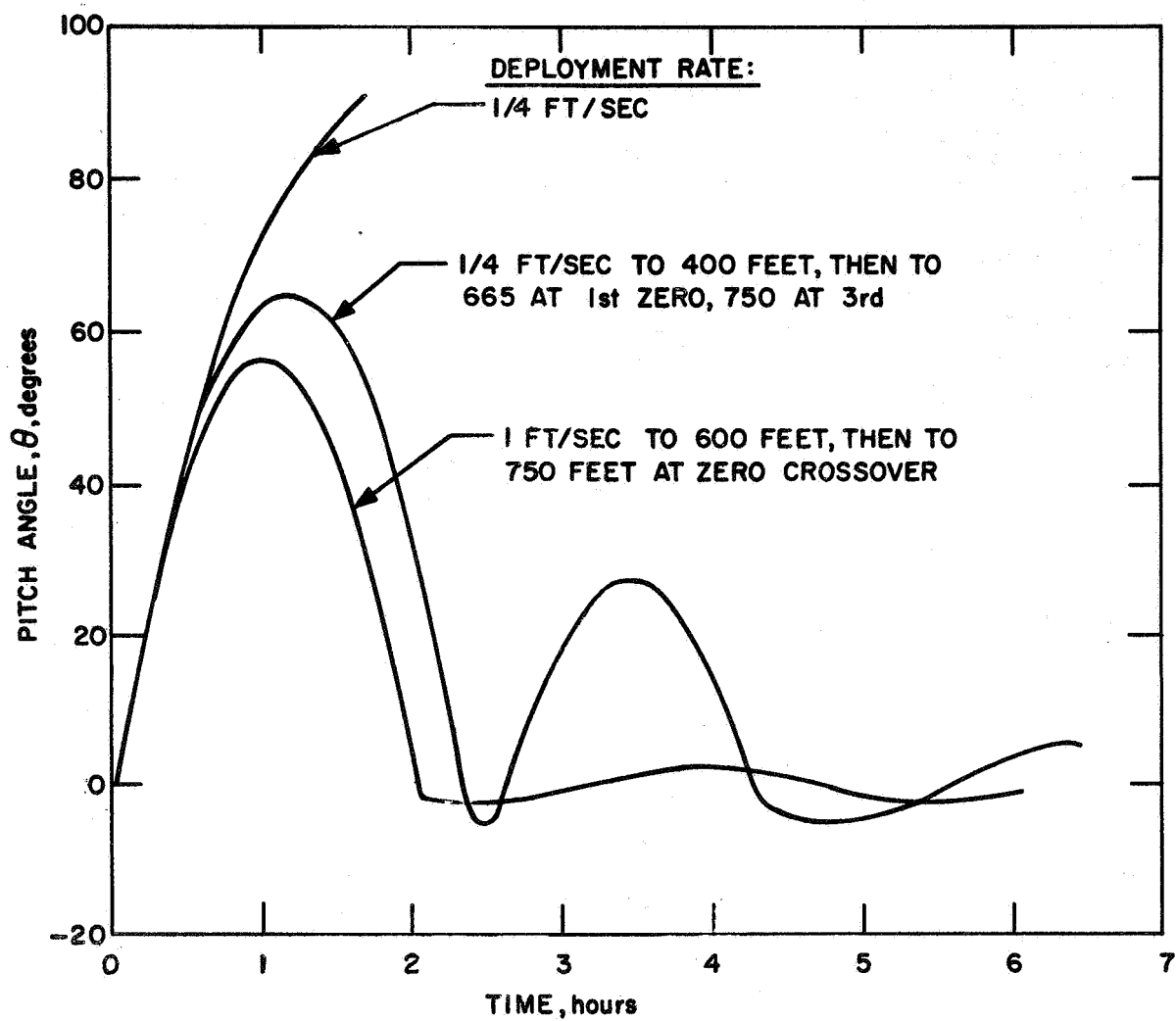
The ramifications of this condition are easily appreciated by considering two simple examples. Assume that the antennas are quickly deployed initially to approximately half the final value of their moment of inertia. The value of θ_{\max} attained is approximately 55 degrees; the inertial rate when $\theta = \theta_{\max}$ is Ω . Assume at this point that the deployment of the antennas to the full value is effected. The inertial rate is reduced to $\Omega/2$; thus the rate in the rotating system becomes $-\Omega/2$. The attitude angle θ will now increase to a value greater than 90 degrees and the satellite will "tumble." This mode of antenna deployment then effects a substantial increase in the amplitude of the oscillatory behavior of the satellite; clearly, its effect is destabilizing.

Consider next the following case: assume again that the antennas are initially quickly deployed to approximately half the final value of their moment of inertia. Now let the satellite attitude angle reach $\theta_{\max} \approx 55$ degrees and then begin decreasing. The attitude angle will pass through zero degrees when the angular velocity in the rotating system is Ω , and in the inertial system is 2Ω . At this point ($\theta = 0^\circ$) if the booms are fully deployed, the inertially measured angular velocity will be reduced to Ω . The rotational rate is thus reduced to zero, and the attitude motion in the rotating frame is effectively stopped. This mode of antenna deployment, then effects a decrease of the amplitude of the oscillatory behavior of the satellite; indeed the motion is stopped. Its effect is stabilizing.

4. Analog Simulation

A version of this technique was simulated on the analog computer, where the assumption was made that the antennas are rigid. The rate of deployment was varied, as well as the time of starting and stopping deployment, to identify the potential merits of the dead beat control.

In figure (F-1) the pitch attitude angle is shown as a function of time. For a constant deployment rate of 1/4 ft/sec, the satellite is clearly unstable. An attempt at dead beat control was made by deploying at 1/4 ft/sec until a length of 400 feet was reached, then stopping deployment. When the pitch attitude angle again reached zero, deployment was resumed until the antenna reached a length of 665 feet, and when the attitude angle reached zero the third time the antenna was deployed completely. This resulted in rather large oscillations as shown. Better results were obtained by deploying the antenna to a length of 600 feet using a rate of 1 ft/sec, then stopping, and completing deployment at the time

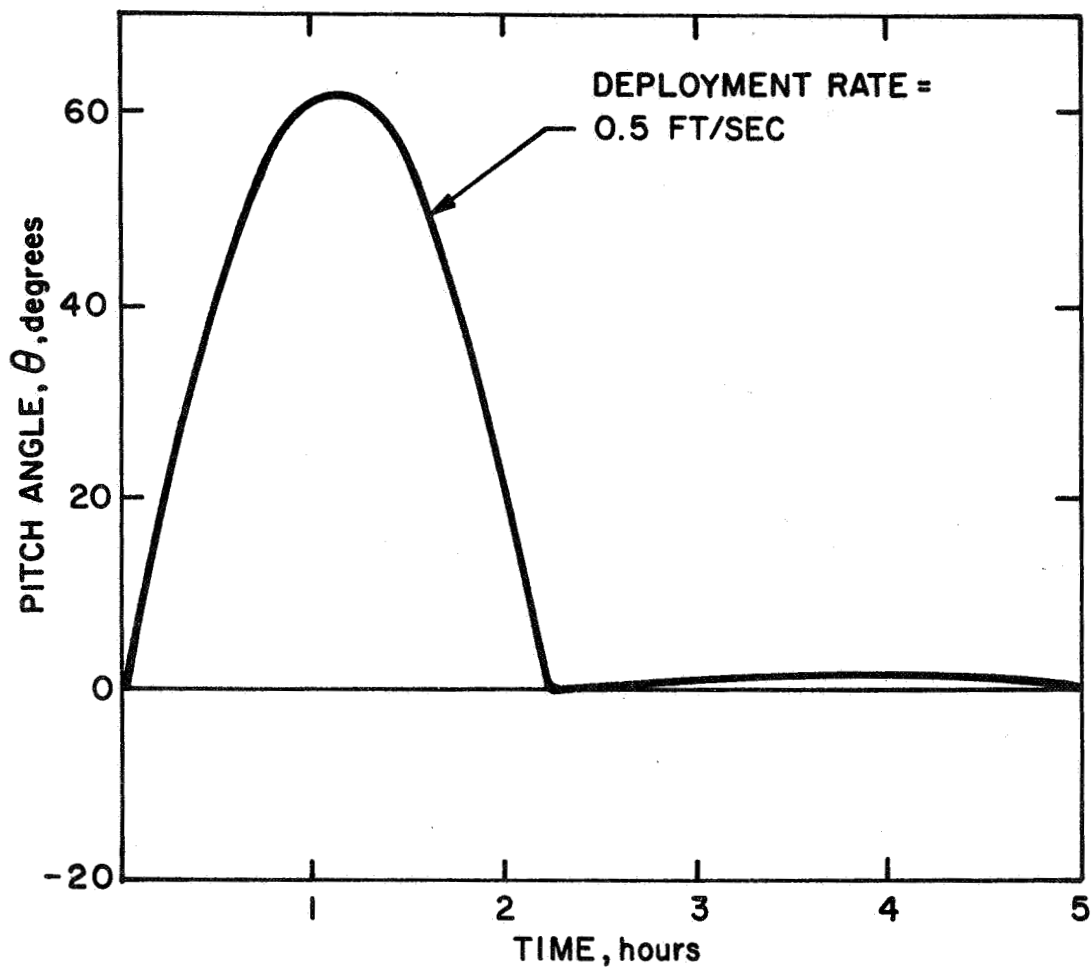


65-10186-A

Figure F-1 ANALOG SIMULATION OF RIGID BODY ANTENNA DEPLOYMENT

the pitch attitude angle is zero. Figure F-2 shows the results using a deployment rate of 0.5 ft/sec, with partial deployment followed by complete deployment after the first zero crossing.

It must be emphasized that these results are for a rigid body, and therefore caution must be used in attempting to draw conclusions about the method or results when applied to a flexible body.



65-10185-A

Figure F-2 ANALOG SIMULATION OF DEAD-BEAT ANTENNA DEPLOYMENT